LOCAL HEAT TRANSFER COEFFICIENTS

FOR

FALLING FILM EVAPORATION OUTSIDE A VERTICAL TUBE

M.J. MESSENGER, B.E.

A Thesis submitted for the Degree of Doctor of Philosophy in December 1964. The investigation reported was carried out in the Chemical Engineering Department of the University of Adelaide from April 1960 to November 1963.

22nd September, 1965

The Registrar,
The University of Adelaide.

Dear Sir,

I agree that the copies of my thesis, "Local Heat Transfer Coefficients for Falling Film Evaporation Outside A Vertical Tube", deposited in the Barr Smith Library, be available for loan or for photocopying.

Yours faithfully,

M. J. Messenger

CONTENTS

LIST OF FIGURES

APPENDIX V

SUMMARY

Local heat transfer coefficients have been studied for falling film evaporation outside a vertical 1 in. O.D. x 18 in. long electrically-heated tube, mounted within a $1\frac{1}{2}$ in. nominal bore pyrex glass jacket. The test liquids used were water, chloroform, methyl alcohol, ethyl alcohol and iso-propyl alcohol. Film flows with and without significant concurrent vapour flow were considered, the vapour flow being varied independently of the heat flux and of the liquid flow by the introduction to the test section of externally-generated saturated vapour.

Agreement has been shown with previous work for falling film evaporation, falling film condensation, and non-boiling falling film heat transfer, but the observed trend differs from that which has been observed for the climbing film evaporator, for which the nature of the liquid-vapour flow is significantly different. The experimental data differ from the theoretical analysis of Dukler in the transitional liquid flow regime, and an explanation is suggested in terms of a small uncertainty in the Deissler pipe velocity profile when applied to moderate Reynolds number flows. The observed effect of vapour flow rate ($h \propto (\text{flow rate})^{1.0}$) is in agreement with the experimental work of Carpenter and Colburn for condensation and with the theoretical analysis of Dukler for falling film evaporation and condensation. However, the

observation differs from the results of the analysis of Rohsenow et al. for condensation and also differs from some of the experimental data of Staker for falling film evaporation. Explanations for the deviations of these workers are suggested.

Correlations for the experimental data in terms of dimensionless mechanism ratios have been proposed by Mechanism Ratio Analysis. For liquid film flow, conventional correlations in terms of Reynolds number, Prandtl number and Nusselt number (based on film thickness) are proposed. For significant interfacial shear a Weber number term and a vapour Reynolds number term are introduced. This form differs from the previous analyses by Dukler, Rohsenow et al., and Carpenter and Colburn, in which a liquid surface tension term does not appear directly. A term similar to that used by these previous workers was checked for correlation, but the Weber number and Reynolds number combination was found to lead to a correlation which fits experimental data more closely.

Observations were also made of the nucleate boiling regime. However, with the variable nature of the heated surface, consistent data could not be obtained for the critical temperature difference or for the exponent in the observed relation, $h \propto (\Delta T)^n$. This surface variability for nucleation did not affect reproducibility for the falling film

evaporation regime.

The heat transfer mechanism for falling film evaporation is concluded to be transport by conduction and eddy turbulence for subcritical vapour flows. For supra-critical vapour flow, the dependence on liquid-induced turbulence decreases and the mechanism appears to be controlled by vapour-induced turbulence and by a liquid interface disruption mechanism. Previous analyses of heat transfer to films falling under the influence of significant interfacial shear have not included this disruption mechanism, and further work is required to check the effect of interfacial energy on the heat transfer mechanism.

DECLARATION

This thesis contains no material which has been accepted for the award of any other degree or diploma in any University and, to the best of the author's knowledge and belief, the thesis contains no material previously published or written by another person, except where due reference is made in the text.

ACKNOWLEDGEMENT

The author wishes to thank Professor R.W.F. Tait for his supervision of this work, the members of the Chemical Engineering Department of the University of Adelaide for their assistance, and the Australian Atomic Energy Commission for its financial support of the project.

Thanks are also due to Dr. K.R. Weller, who supplied tested preliminary programmes for use with a computer Regression Analysis of the experimental data, and to Mr. N. Stenhouse and other members of the C.S.I.R.O. Mathematical Statistics Department, Adelaide, who gave valuable help to minimise computation problems caused by correlation of some of the experimental variables.

1. INTRODUCTION

The advantages of the falling film evaporator (2,51) make the unit a useful method for the concentration of heat-labile liquids such as orange juice (26) or milk (53,54), or for the evaporation of sea water (79) and other liquids which tend to form scale.

The relatively low liquor operating temperature and the small retention time minimise the combination of conditions which promote degradation of the concentrate.

Recent work (27,64) has shown that the retention time is the more important factor affecting concentrate degradation, and the tendency is to use high vapour velocity, low retention time units which either have long tubes (27) or have a climbing film section before the falling film unit (64).

There is a lack of experimental data for the falling film evaporator, especially for these high vapour velocity conditions. However, work within the University of Adelaide by Staker (80) provided some basic data, and a recent analysis by Dukler (30,31,32) has given a theoretical basis against which experimental data may be compared.

This project was undertaken with the following aims:

1. to extend the work of Staker by the consideration of local heat transfer coefficients, larger diameter tubes, and high vapour velocities varied independently

of the liquid flow conditions,

2. to attempt a more satisfactory correlation of the data,
3. to elucidate the mechanisms which operate, and
4. to check whether comparison is possible with heat transfer data determined in other film apparatus.

2. DISCUSSION OF PREVIOUS WORK*

Investigations by previous workers of heat transfer in the falling film evaporator have been limited mainly to the measurement of average coefficients for industrial-scale equipment, or to theoretical prediction of heat transfer coefficients based on transport theory and on studies of falling film hydrodynamics. Few measurements have been made in laboratory-scale falling film evaporators, for which the operating conditions can be more closely controlled. Such measurements would allow a study of local coefficients, and hence give an insight into the mechanisms which act.

It is to be expected that the mechanisms which govern in the falling film evaporator may be similar to those which operate in film condensers and in selected regimes of the other forms of film apparatus. Much more investigational work has been carried out in these fields.

Therefore it is proposed to review the previous work of interest to a study of boiling heat transfer to falling liquid films under the following general headings:

1. Hydrodynamics of Falling Liquid Films.
2. Heat Transfer across Flowing Liquid Films (which will include non-boiling heat transfer to falling films, heat transfer for film condensation, and heat transfer in the falling film evaporator, in the wiped film evaporator, and in the climbing film evaporator).

*Nomenclature is given in Section 8 (i.e. pages 198-203).

2.1. HYDRODYNAMICS OF FALLING LIQUID FILMS

2.1.1. Flow Regimes and Critical Reynolds Numbers

For falling film flow the flow regime varies with flow rate from predominantly laminar to predominantly turbulent, with the laminar regime being modified by the occurrence of waves at the film surface for Reynolds numbers beyond a critical value, and with an extended transitional zone existing between the rippled laminar and the turbulent regimes.

A complete description of the nature of film flow was given by Brauer (12) who carried out a detailed investigation in which flow down the outside of a tube was studied using a micrometer probe to determine wave frequency, shadow photography to obtain film thickness and wave profiles, and the timing of small plastic particles carried by the flowing film to obtain the surface velocity.

Brauer found that up to a critical Reynolds number, Re_{w_1} (16 for water), flow remained non-rippled laminar. Above this critical value, waves approximating the form of pure sine waves appeared and became unstable at Re_i (40 for water). The experimental results for surface velocity showed their first deviation from the classical Nusselt theory (66) at this instability point, Re_i. At a higher Reynolds number, Re_{w_2} (80 for water), these regular waves were replaced by random surface waves although the bulk of the film remained

in laminar motion up to a further critical Reynolds number, Re_{cr} (1600 for water), at which point "capillary" waves first appeared. These capillary waves, which were waves of short wavelength, indicated the onset of turbulence. The nature of the turbulent flow varied at higher Reynolds numbers (about Re = 2400 to 3200) with the appearance of "ring" waves. These ring waves consisted of circumferential rings of fluid which transported a large proportion of the total flow and which appeared to fall down the surface rather than to flow. At this point the surface of the film became very coarse and the flow became more like a swell.

A set of dimensionless equations, from which each of the critical Reynolds numbers may be determined for any liquid, was presented by Brauer.

Tailby and Portalski (82) found fault with many of Brauer's measurement techniques, with his conclusion that a spectrum of wave frequencies exists, and with his observation that the increase in surface area due to rippling is only of the order of 3%. Tailby and Portalski observed an increase of 150%. However, recent work by Allen (1) supports a value much less than that observed by Tailby and Portalski, and Stirba and Hurt (81) estimated the increase to be less than 50%. Furthermore, support for the Brauer method of surface velocity measurement was provided by Asbjornsen (3) for Reynolds numbers up to Re = 400.

Other observers agree that the Reynolds number for the onset of wave formation lies within the range Re = 6 to 30, and that the critical Reynolds number for the onset of the predominance of turbulence lies within the range Re = 1000 to 4000. These ranges follow from the summaries of previous work which were presented by Brauer (12), by Zhivaikin and Volgin (91) and by Wilkes and Nedderman (87), and are based on the observations of eight and fifteen workers respectively. Subsequent values for the critical Reynolds number for the onset of turbulence are available (8,73), and these values also lie within the suggested range.

Theoretical predictions of the Reynolds number for the onset of waves have been made using mathematical instability analyses of the waves (9,48,77,82,88,89), but there is disagreement (82) regarding mathematical technique. These analyses are of interest here only because of their prediction of an effect on the wave motion of liquid properties, surface tension in particular.

Values of the critical Reynolds number for the onset of turbulence generally range from 1000 to 2000, but Zhivaikin and Volgin claimed that it is not until Re = 4000 that flow can be described as fully turbulent, whilst Jackson (46) extended his observations to Re = 5000 and claimed that the laminar flow equations adequately described the observed results, although an increase in scatter of the results was

noticed for Reynolds numbers above 2000.

This lack of agreement suggests that the onset of turbulence is a gradual phenomenon, and an attempt (30,31,32) has been made recently to consider a fresh approach to the onset of turbulence in the falling film.

The approach follows from the suggestion of Lin (59) that there exist damped turbulent fluctuations which commence at the wall. This means that neither true laminar nor fully-developed turbulent flow exists in the film, and any theory which studies transport within the falling film must consider combined mechanisms at all points in the film.

Such an analysis was presented by Dukler (30,31,32), as an improvement of earlier work by Dukler and Bergelin (29). As a preliminary to discussion of this analysis it will now be necessary to outline the work which has been carried out on the measurement and prediction of film thicknesses and velocity profiles, part of which serves as a basis.

2.1.2. Film Thickness and Velocity Profiles for Falling Films

The classical expression for the liquid layer thickness for the laminar flow region was developed by Nusselt (66) for flow of a liquid of constant viscosity and density down a vertical plate. Zero interfacial shear was assumed between the liquid and its bounding gas.

Measurements of local and average film thickness have been made at Reynolds numbers up to 20,000. Good summaries of the results are provided by Brauer (12), Belkin et al (8), Zhivaikin and Volgin (90,91), and Dukler (33).

The summaries of previous work show that the Nusselt theoretical equation, which can be rearranged in the simplified form,

$$t = \left(\frac{3\nu^2}{g}\right)^{1/3} \left(\frac{\Gamma}{\mu}\right)^{1/3} = \left(\frac{3\nu^2}{4g}\right)^{1/3} \left(\frac{4\Gamma}{\mu}\right)^{1/3} = 0.91\ (\nu^2/g)^{1/3}\ Re^{1/3},$$

adequately defines the film thickness for non-rippling laminar flow, and also gives the average film thickness for flow with rippling.

It is accepted that an equation of the same general form defines the film thickness for turbulent flow, but there is much less agreement (8,12,15,90,91) as to the values for the constant and for the Reynolds number exponent.

Zhivaikin and Volgin (90,91) showed that film thickness data measured by the various workers tend to superimpose, and suggested an equation,

$$t = 0.141\ (\nu^2/g)^{1/3}\ Re^{7/12},$$

whilst Brauer (12) suggested a Reynolds number exponent of 8/15, and values of 0.6 and 2/3 were suggested by Belkin et al (8) and by Brotz (15).

The initial work on velocity profiles for falling film flow was the theoretical analysis of Nusselt (66), which

predicted a parabolic velocity distribution for smooth laminar flow, with a value of 1.5 for the ratio of the film surface velocity to the average velocity of the film.

Subsequent experimental observation (12,37,41,46) showed that the value of 1.5 holds up to the onset of rippling at the Reynolds number, Re_i. Beyond this point the ratio increases to about 2.2 at Re = Re_{w_2}, and remains at this value until approximately Re = 1000. As the Reynolds number is increased further the ratio decreases until a constant value of 1.5 is attained again, with the onset of the predominance of turbulent flow.

Jackson (46), in particular, gave a good description and explanation of the increase in velocity ratio in terms of observed waves with crests of high surface velocity, which sweep downward with a velocity greater than that of the laminar sublayer, with the result that the film is disturbed and the increased shear causes the normal parabolic velocity gradient to become more nearly linear. Such observations explain the presence of the significant mixing action even though the basic flow is essentially streamline.

The other variations in the velocity ratio may be attributed to structural changes in the film as the large waves of high crest velocity, formed initially in the wave-free film, change eventually to the much smaller waves of low crest height observed with the onset of turbulence.

Wilkes and Nedderman (87) carried out checks that the velocity distribution in laminar flow is parabolic, as suggested by the theoretical analysis and by the surface velocity measurements. Use was made of stereoscopic photography of small air bubbles moving within the fluid film. It was found that the Nusselt analysis holds for wave-free flow. The results showed that the analysis also holds for laminar Reynolds numbers beyond the normal critical value for the onset of rippling, provided that the inception of waves is suppressed by the addition of surface active agents.

Little is known experimentally about the velocity distribution in turbulent falling films. The most significant work is the theoretical analysis of Dukler (30,31,32) which applies the universal velocity distributions observed in pipe flow to the case of film flow. Indirect checks of the applicability of the assumed velocity distributions are provided by comparison of experimental data with values for film thickness (33) and heat transfer coefficient (30,31,79) predicted on this basis. The observed agreement suggests that the Dukler analysis is essentially correct.

Dukler and Bergelin (34) were the first to apply this type of analysis, but in a simplified form.

Use was made of the universal velocity distribution equations, with the limits set by Nikuradse, i.e.

$$u^+ = y^+ \qquad \text{for } 0 < y^+ < 5$$

$$u^+ = -3.05 + 5.0 \ln y^+ \qquad \text{for } 5 < y^+ < 30$$

$$u^+ = 5.5 + 2.5 \ln y^+ \qquad \text{for } 30^+ < y < \eta$$

where u^+ = universal velocity parameter, defined in Section 8

y^+ = universal distance parameter, defined in Section 8

η = magnitude of the universal distance parameter at the liquid surface.

A relation between η and the film Reynolds number was obtained by integration of the expression

$$\frac{\Gamma}{\mu} = \frac{Re}{4} = \int_0^{\eta} u^+ \, dy^+ .$$

Integration gives

$$\frac{\Gamma}{\mu} = \left[\frac{(y^+)^2}{2}\right]_0^5 + \left[-8.05y^+ + 5y^+ \ln y^+\right]_5^{30} + \left[3.0y^+ + 2.5y^+ \ln y^+\right]_{30}^{\eta}$$

$$= 3.0\eta + 2.5\eta \ln\eta - 64, \quad \text{for } \eta > 30,$$

or alternatively the integration may be terminated at the relevant term for $\eta < 30$.

The relation between η, t, and wall shear stress, τ_o, is given by

$$\eta = \frac{\rho_L \, t \sqrt{\frac{\tau_o \, g_c}{\rho_L}}}{\mu_L} .$$

Dukler and Bergelin obtained an expression for the wall shear stress, τ_o, by a force balance analysis, but one which did not consider any variation of shear stress across the film.

The simplified result was

$$\tau_o \cdot \frac{g_c}{g} = \left(\rho_V - \frac{\Delta P}{Z} \cdot \frac{g_c}{g}\right) \frac{r}{2} + \rho_L t \ ,$$

where the first term on the right-hand side is the interfacial shear term for the presence of a flowing vapour core.

For interfacial shear, solution for t vs. Re by trial and error is necessary. However, for no interfacial shear,

$$\tau_o \cdot \frac{g_c}{g} = \rho_L t$$

$$\therefore \ \eta = \frac{\rho_L g^{\frac{1}{2}} t^{3/2}}{\mu_L} \ ,$$

and direct solution for t vs. Re is possible.

Dukler and Bergelin found good agreement between the resultant t vs. Re relation and film thicknesses determined by a capacitance probe method for the range Re = 500 to 3000.

Subsequent papers by Dukler (30,31,32) refined the analysis presented by Dukler and Bergelin.

In the outline given below only film thickness and velocity profiles will be considered. The heat transfer studies carried out concurrently by Dukler will be considered in Section 2.2.3.

Dukler used Deissler's expression (28) for the eddy viscosity for the region near the wall, and von Karman's

expression (50) for the flow field removed from the immediate vicinity of the wall.

The expressions which were used for eddy viscosity are

$$\epsilon = m^2 \, uy \, (1 - e^{-m^2 uy/\nu}), \quad \text{for } y \leqslant 20, \text{ and}$$

$$\epsilon = p \, \left(\frac{du}{dy}\right)^3 \Big/ \left(\frac{d^2u}{dy^2}\right)^2 , \quad \text{for } y > 20.$$

The differential equations which were used to describe the mechanics of flow are

$$\tau = \frac{1}{g_c} \left(\mu_L + \epsilon \rho_L\right) \frac{du}{dy} , \quad \text{and}$$

$$Re_L = \frac{4 \rho_L}{\mu_L} \int_0^t u \, dy .$$

Additional expressions to include the effect of interfacial shear were developed from a series of force balances on a fluid element. Substitution of the relevant values of eddy viscosity led to non-linear equations for which analytical solution was not possible.

A digital computer was used to solve these equations to give a modified universal velocity distribution, with interfacial shear and film thickness as parameters. By integration, an expression for film thickness as a function of Reynolds number was obtained. The expression predicted values in agreement with the Nusselt analysis at low Reynolds numbers.

A parameter,

$$\beta = \frac{\left(\frac{\Delta P}{Z}\right)_{TP} D\, g^{1/3}}{4\, \rho_L^{1/3}\, \mu_L^{2/3}},$$

which is a dimensionless grouping of variables representing the forces due to interfacial shear, was introduced for the graphical presentation of the results.

Subsequently, Dukler (33) used film thickness data obtained by other workers to check the theoretical film thicknesses over the whole flow range, and hence indirectly to check the assumed velocity profiles. Many of these data were obtained for large values of β, and very good agreement was found for flow both with and without significant interfacial shear.

Thus, it appears that the Dukler analyses could provide a sound basis for the study of transport across falling films. Detailed criticism will be made in Section 2.2.3, following a review of the Dukler falling film heat transfer analysis.

2.1.3. Conclusions

The following conclusions, derived from the review of falling film hydrodynamics, will be useful in subsequent discussion of heat transfer across falling films.

1. Hydrodynamic studies have differentiated between the various flow regimes for falling films and it has been shown that turbulence may be promoted either by increased eddy action at high flowrates or by the action of interfacial waves which change in form as the liquid flow is increased. There is some disagreement between workers on the factors which affect this wave motion, but much work has been done on the inception of waves.

2. The most suitable concept of turbulence in a falling film is that which considers that eddies are present at almost all Reynolds numbers and that their decay is governed by the presence of the solid boundary. This means that neither true laminar nor fully developed turbulent flow exists, and thus a study of transport across falling films must consider combined mechanisms. Such a concept leads to a continuous variation between the regime where laminar flow predominates and the regime for which turbulent flow predominates and explains much of the difficulty encountered with experimental attempts to fix a critical Reynolds number.

3. The basis for transport studies has been provided by the assumed similarity between turbulence in a falling film and turbulence in the boundary layer of a pipe

flow. This assumption has led to the development of the necessary relationships for velocity profiles and film thicknesses under most flow conditions. Satisfactory checks with experimental observations indicate that further similar development should allow analysis of heat transfer across a falling film.

2.2. HEAT TRANSFER ACROSS FLOWING FILMS

2.2.1. Introduction

Previous work on heat transfer to and from flowing films is of interest to the present study only for the case of fully-developed conditions.

This limits discussion of heat transfer in film apparatus to the following cases:

1. heat transfer for film condensation in the absence of subcooling of the condensate,
2. heat transfer for the film evaporation zone in the falling film evaporator, the wiped film evaporator, and the climbing film evaporator, and
3. non-boiling heat transfer to falling films in the zone beyond the thermal entry length region.

2.2.2. Heat Transfer for Film Condensation

Fully-developed heat transfer across a falling film of condensate should be similar to the equivalent case for falling film evaporation. In each case heat is transferred, under the influence of an overall temperature difference $\pm(T_{saturation} - T_{wall})$, across a film of given film thickness and hence of given turbulence.

Much more work on the effect of interfacial shear

caused by high velocity flow of the vapour has been carried out for film condensation than for film evaporation.

Therefore the results of the most important film condensation investigations will be discussed below to enable comparison with falling film evaporation work.

Only brief consideration will be given to results presented as average coefficients, because flow variations in film condensers are usually sufficient that the heat transfer mechanism may vary along the flow surface, so that these averaged coefficients will usually represent more than one mechanism.

2.2.2.1. Laminar Film Condensation

The classical analysis of film condensation is that of Nusselt (66), carried out in 1916, for non-rippling laminar flow of a condensate film in the absence of any effect of vapour velocity. The analysis has been presented in English by Jakob (47a), and it was rearranged in dimensionless form by Kirkbride (55).

A linear temperature gradient across the film was assumed, and heat transfer was considered to occur by conduction alone through a film of thickness, t. The film thickness was given by an equation developed in the same paper (see Section 2.1.2.).

In the simplified form, the analysis gave the local

coefficient as

$$h = \frac{k}{t}$$

i.e. $Nu = \frac{ht}{k} = 1$

It followed that

$$\frac{h\,(\frac{3\nu^2}{4g})^{1/3}\,Re^{1/3}}{k} = 1$$

i.e. $$\frac{h(\nu^2/g)^{1/3}}{k} = 1.10\,(\frac{4\Gamma}{\mu})^{-1/3} = 1.10\,Re^{-1/3}.$$

Subsequent checks against experimental observations showed that measured coefficients generally exceeded the theoretical values (60a). This increase was attributed to rippling, and it was suggested (60b) that a correction factor of 20% be added to the theoretical heat transfer coefficient, i.e. that Nu = 1.2 be used for rippled flow.

So far no theoretical analysis has considered the effect of waves on heat transfer across falling films. However, a basis has been supplied by Heartinger (42) who proposed an unsteady state diffusion model for rippling laminar layers in terms of a mixing frequency and a depth of disturbance. Such a model has been supported by the recent observations of Wilke (85), for non-boiling heat transfer to falling films, who found that for rippled flow there is definite evidence of a thermal boundary layer over which the temperature drops almost linearly up to a distance which corresponds very closely

with the "trough thickness" of the waves, and beyond which the temperature remains nearly constant. Wilke proposed that heat transfer across this boundary layer does not occur by molecular conduction alone but is aided by the mixing effect of the waves, even near to the wall.

Until a suitable theoretical description of wave motion in the falling film has been proposed it will be necessary to use the approximate empirical correction of 20%.

2.2.2.2. Turbulent Film Condensation

For the turbulent condensate flow region, Colburn (19) proposed an analogy between fluid friction and heat transfer based on the observation by Cooper, Drew, and McAdams (23) that the friction factor for turbulent flow in conduits may be used for the flow of liquid layers.

A value of film thickness was obtained from the friction factor equation, which was rearranged in the form

$$f/2 = \frac{t^3 \rho^2 g}{\Gamma^2}$$

and this value was substituted into the j-factor equations obtained previously (20) for turbulent flow in conduits, i.e.

$$j = \left(\frac{h}{cG}\right)\left(\frac{c\mu}{k}\right)^{2/3}$$

$$j = 0.027\left(\frac{4\Gamma}{\mu}\right)^{-0.2}$$

A substitution of $G = \Gamma/t$ was made for film flow, and use was made of the observation for flow in conduits that $f/2 = j$.

The final equation was

$$\frac{h(\nu^2/g)^{1/3}}{k} = 0.056 \left(\frac{c\mu}{k}\right)^{1/3} \left(\frac{4\Gamma}{\mu}\right)^{0.2}$$

This result will now be carried further than was done by Colburn by the introduction of an expression for film thickness derived from the equation for friction factor and j-factor.

$$\text{i.e.} \quad j = f/2 = \frac{t^3 \rho^2 g}{\Gamma^2} = 0.027 \left(\frac{4\Gamma}{\mu}\right)^{-0.2}$$

$$\text{Hence} \quad t = \left(\frac{0.027}{16}\right)^{1/3} \left(\frac{\mu^2}{\rho^2 g}\right)^{1/3} \left(\frac{4\Gamma}{\mu}\right)^{0.6}$$

$$= 0.12 \left(\nu^2/g\right)^{1/3} \left(\frac{4\Gamma}{\mu}\right)^{0.6} .$$

It is interesting to note that this result is close to the film thickness equation suggested by Zhivaikin and Volgin (91) as the most accurate for turbulent flow (see Section 2.1.2).

Multiplying throughout in Colburn's final equation leads to

$$Nu = \frac{ht}{k} = 0.0067 \left(\frac{c\mu}{k}\right)^{1/3} \left(\frac{4\Gamma}{\mu}\right)^{0.8}$$

It will be shown later that this expression is similar to an empirical correlating expression obtained by

Staker (80) for boiling heat transfer to turbulent falling films.

Care must be taken in the application of the Colburn analysis because the relation between the j-factor and the friction factor is approximate, and only holds for $Re > 10{,}000$. Furthermore, a constant of 0.023 is more commonly accepted (60c) in the equation relating j-factor to Reynolds number, so that the constant in the Colburn equation should be taken as 0.051.

Results which are in agreement with Colburn's empirical analysis were obtained by Seban (75), who applied the Prandtl-Nikuradse velocity distribution to predict film thickness and momentum eddy diffusivity for turbulent condensate layers. Thermal eddy diffusivity was assumed to be equal to momentum eddy diffusivity and, by integration over the film thickness using limits for the laminar sublayer and the buffer sublayer suggested by von Karman, the temperature difference across the film and hence the local heat transfer coefficient were obtained.

The final equation was

$$\frac{h(\nu^2/g)^{1/3}}{k} = \frac{Pr(\delta^+)^{1/3}}{F_2}$$

where $\delta^+ = \left(\frac{Re}{38.4}\right)^{0.9}$,

$$F_2 = 5Pr + 5\ln(5Pr + 1) + \frac{2.5}{B} \ln \left[\frac{1 + B}{1 - B} \cdot \frac{\frac{60}{\delta^+} - 1 - B}{\frac{60}{\delta^+} - 1 + B} \right],$$

$$B = \sqrt{1 + \frac{10}{Pr\ \delta^+}}\ .$$

Seban checked the results predicted by this expression against the Colburn correlation for Pr = 5. Colburn's results were about 10-20% higher. This difference would be reduced if the revised coefficient was introduced into the Colburn correlation.

2.2.2.3. Transitional flow

Colburn (19) and Kirkbride (55) assumed a sharp break in the variation of h with Re at about Re = 2000. Grigull (40) used a value of Re = 1400. Such sharp breaks are contrary to experimental observations (13,40).

Brauer (13) was the first to derive a more satisfactory series of equations, which defined a transition zone for falling film condensation, and which were based on his boundary layer observations for non-boiling falling film heat transfer (12). These equations showed a smooth transition from laminar flow at a Reynolds number corresponding to the onset of rippling, at which the Nusselt analysis no longer holds. Unfortunately, the complex Brauer equations are presented as averages.

This observation that a gradual transition, rather than a sharp break, occurs in the relationship between heat transfer coefficient and Reynolds number, is in agreement with the most universal analysis, that of Dukler, which will be outlined in Section 2.2.3.

The outline of the Dukler analysis will also consider the additive effect of vapour flows. To allow comparison with the work of Dukler, previous work on condensation in the presence of large vapour flows is reviewed below.

2.2.2.4. Effect of Interfacial Shear

Laminar falling film condensation in the presence of significant vapour velocity was considered by Nusselt (66), as an extension of his analysis of condensation.

Jakob (47b) presents the analysis in translation and claims to correct many typographical errors in the original paper. Jakob also introduces some modifications to the analysis.

The Nusselt extension changed the boundary condition of zero velocity gradient at the interface, assumed for the initial analysis, and replaced this by the slope of the velocity profile at the free surface of the condensate. The velocity profile at the interface followed from an analysis of the shear stress exerted on the film by the moving vapour.

This modified velocity profile was used to give the

value of film thickness determined by the combined effects of gravity and interfacial vapour friction.

Heat transfer coefficients followed as before.

For vapour flow conditions for which the gravity term affecting h_m could be neglected relative to the vapour friction term, the final equation was

$$h_m = {}^3/_2 \sqrt[3]{\frac{f\,\rho_L\,\lambda\,k^2}{3\,\mu\,H\,\Delta T} \cdot \frac{\rho_V\,v_V^2}{2}}\,.$$

To obtain this result it was necessary to consider that the friction factor, f, and the vapour velocity, v_V, remained constant, so that the necessary integration could be carried out. These assumptions should hold only for short lengths of tube. Thus h_m may be considered to approximate to a local coefficient, and inaccuracies in the predicted average coefficients for a long tube are to be expected. This is no problem for the present study, for which local coefficients are of interest.

Jakob (47c) incorrectly concluded that the above equation indicated that $h_m \propto v_V^{2/3}$, for Nusselt's assumption of constant f, or $h_m \propto v_V^{0.58}$ when he himself introduced a vapour flow dependent value of the friction factor.

However, the above form of the equation includes a hidden heat transfer coefficient factor because of the inclusion of the latent heat, condensation length, and temperature difference terms.

A simple heat balance shows that

$$h_m = \frac{q/A}{\Delta T} = \frac{\Gamma \lambda}{H} / \Delta T \quad .$$

Replacement of $\frac{\lambda}{H \Delta T}$ by $\frac{h_m}{\Gamma}$ in the above equation gives a more satisfactory form,

$$h_m^3 = (\text{constant}) \cdot f \cdot \frac{k^2 \rho_L}{\mu} \cdot \frac{h_m}{\Gamma} \cdot \rho_V v_V^2 \ ,$$

or $h_m^2 \propto f v_V^2$.

Introduction of the Blasius expression for friction factor, i.e. $f \propto v_V^{-\frac{1}{4}}$, as suggested by Jakob, leads to the conclusion that

$$h_m \propto v_V^{0.9} \text{ (approximately)}.$$

For turbulent film condensation, the most complete experimental consideration of the effect of vapour velocity is that of Carpenter and Colburn (16).

The experimental results of these workers indicated that at high values of vapour shear stress the onset of turbulence within the film occurs at values of liquid Reynolds number as low as 200, so that the Nusselt analysis apparently is valid only for a very narrow range.

The authors developed a semi-empirical correlation method to describe the turbulent zone by assuming that the total resistance to heat transfer was provided by the laminar boundary layer.

It was assumed that the velocity gradient across this boundary layer would be linear for the condition of high interfacial shear, and an expression was developed for the boundary layer thickness in terms of the total interfacial drag force.

An estimate was made of the limit of applicability of the Nusselt analysis (including the effect of vapour friction) by considering that the laminar boundary layer was maintained up to a dimensionless wall distance, $y^+ = 11$, based on velocity distribution studies. This assumed value of y^+ was confirmed by the observed value of the constant for the eventual correlation of the results, and it leads to $Re_L = 240$ as the limit beyond which the Nusselt analysis no longer applies.

The heat transfer coefficient was obtained as the ratio of the thermal conductivity and the boundary layer thickness. A further term, a Prandtl number to the one-half power, was arbitrarily introduced by analogy with pipe flow.

The resulting expression was

$$h = (\text{constant}) \left(\frac{c\mu}{k}\right)^{\frac{1}{2}} \frac{k(\rho F_T)^{\frac{1}{2}}}{\mu},$$

where F_T is the total force or drag per unit surface of the laminar layer. This total force was composed of the gravitational force (subsequently shown to be small in effect in accordance with initial assumption), the friction of the

vapour (the largest effect), and the force due to the momentum change of the vapour on condensation (subsequently shown to be significant, but not so large as the vapour friction).

This equation correlated the experimental results within approximately ±50% limits.

Thus, although the Carpenter and Colburn semi-empirical analysis is approximate and only holds at high vapour velocity above a non-specified limit, it has the advantages that it fits the observed results fairly well and it predicts the correct trends.

If it is assumed that F_T may be replaced by the most important term, the vapour friction, defined as $\frac{f\ G_V^2}{2\ \rho_V}$, the expression for the local coefficient becomes

$$h = (\text{constant})\ \left(\frac{g\ \rho\ k\ f}{2\ \mu\ \rho_V}\right)^{\frac{1}{3}}\ G_V\ .$$

Values of the friction factor for vapour flow through a wetted tube are available from the studies by Bergelin, Kegel, Carpenter, and Gazley (11) of the turbulent downward flow of a water film in the presence of a co-current air flow. It was found that beyond a certain vapour Reynolds number the f vs. Re_V lines are parallel to the dry-wall line, and offset according to the value of an empirical parameter $\frac{\sigma_{water}\ \Gamma}{\sigma_L\ \rho_L}$. A warning was given that the use of this parameter was only tentative. The results were obtained only for water, so that the postulated surface tension ratio appeared merely as the

ratio of the surface tension (at the boiling point) of water to that of the condensate. Also, since viscosity did not vary greatly, its supposed effect could not be included.

The Bergelin et al. results gave

$$f \propto Re_V^{-\frac{1}{4}} \cdot \phi \left[\frac{\sigma_{water} \Gamma}{\sigma_L \rho_L} \right].$$

Substitution in the Carpenter and Colburn point coefficient expression shows that, ignoring the effect of momentum change of the condensing vapour,

$$h \propto v_V^{0.9} \text{ (approximately)},$$

which is the same effect as was predicted by the Nusselt laminar analysis.

Rohsenow, Webber and Ling (71) attempted to produce a more refined analysis, by including the small resistance of the turbulent portion of the boundary layer by the introduction of the universal velocity distribution to the analysis to give the effect of shear stress at the vapour-liquid interface.

It was admitted that the assumed velocity distribution would very likely be in error in the highly turbulent region near the interface, but it was proposed that any deviation in this region would not have any great effect since this portion of the film is one of low resistance to heat transfer.

The derived results were presented as average coefficients, but are worth considering because of the number of points they raise for discussion.

Analysis of the laminar region was carried out first using a linear temperature profile and ignoring the momentum term introduced by Carpenter and Colburn. It was argued that the momentum transfer effect at the interface would be small since interfacial slip and hence relative velocity should be small.

The derived equation was

$$\frac{h_m(\nu^2/g)^{1/3}}{k} = \frac{4}{3}\frac{(x_{o_L}^*)^3}{z_L^*} + 2\tau_V^* \frac{(x_{o_L}^*)^2}{z_L^*} ,$$

where $x_{o_L}^*$ and z_L^* are a dimensionless film thickness and flow length respectively, and τ_V^* is a dimensionless shear stress.

These dimensionless variables are defined as

$$x_o^* = \frac{x_o}{(\nu^2/g)^{1/3}} ,$$

$$z^* = \frac{4\ z\ \Delta T}{Pr} \cdot \frac{c}{\lambda + \frac{1}{8}c\ \Delta T} \cdot (\nu^2/g)^{-1/3} \cdot \frac{1}{1-\rho_V/\rho_L} , \text{ and}$$

$$\tau_V^* = \frac{g_c\ \tau_V}{g(\rho_L-\rho_V)(\nu^2/g)^{1/3}} .$$

Physical interpretation of these complex expressions was considerably simplified by the presentation of plots, for constant Pr, of $\frac{h_m(\nu^2/g)^{1/3}}{k}$ vs. Re_L with τ_V^* as a parameter.

It was proposed that at high τ_V^* the above expression would hold up to a transition Reynolds number of 72, which was a value obtained from an arbitrarily chosen value of six for the dimensionless laminar sublayer thickness.

The universal velocity profile of Prandtl-Nikuradse was introduced for the consideration of turbulent liquid flow. This was as used previously by Dukler and Bergelin (see Section 2.1.2) and by Seban (see Section 2.2.2.2). The Martinelli procedure (71A) was used to predict eddy diffusivities. The method of derivation of the heat transfer coefficient was the same as used by Dukler, whose analysis will be outlined in detail in the next Section, but who derived diffusivities from different sources.

The expression for local heat transfer coefficient for the turbulent zone was

$$\frac{h(\nu^2/g)^{1/3}}{k} = \frac{Pr\ (x_o^+)^{1/3}}{F_2} \cdot \left[\frac{(1 - \rho_V/\rho_L)}{M}\right]^{1/3},$$

where x_o^+ is the dimensionless film thickness, and F_2 and M are complex combinations of the terms Pr, x_o^+, τ_V^* and x_o^*.

Finally an expression for the overall average coefficient was derived. This again consisted of a complex multi-term expression.

However, as mentioned above, the expressions reduce to the form

$$\frac{h_m (\nu^2/g)^{1/3}}{k} = \phi \ (Re, \ Pr, \ \tau_V^{*}) \ ,$$

which is the form in which the results were presented graphically, and the form in which the authors made comparisons with the experimental results of Carpenter and Colburn.

Rohsenow et al. showed that the Carpenter and Colburn semiempirical expression, which may be expressed as

$$\frac{h_m \mu}{k \rho^{\frac{1}{2}}} = (\text{constant}) \ Pr^{\frac{1}{2}} \tau_V^{\frac{1}{2}} \ ,$$

could be readily converted to the dimensionless form,

$$\frac{h_m (\nu^2/g)^{1/3}}{k} = (\text{constant}) \ Pr^{\frac{1}{2}} \tau_V^{*\frac{1}{2}} \ .$$

The authors presented their final expression and that of Carpenter and Colburn graphically in two plots of $\frac{h_m (\nu^2/g)^{1/3}}{k}$ vs. τ_V^{*} using arithmetic axes: one plot was for Re = 5000 with Pr = 1-10 as parameter (their Figure 9), the other was for Pr = 2 with Re = 10^3 - 10^5 as parameter (their Figure 10). It was claimed that the Carpenter and Colburn expression "agrees very well with the results of the present analysis in the Prandtl number range of 2-3 and the τ_V^{*} range of 5-50."

Although this appears to be the case for the arithmetic plots, replots on logarithmic axes of data from these two graphs (replots are shown in Appendix V, Figures A1-A5) indicate that the Rohsenow expression gives $h_m \propto \tau_V^{*0.3}$ (cf. Carpenter and Colburn exponent of 0.5) for Re = 5000, with

Prandtl numbers of 1, 2, 5 and 10 as parameters. A similar replot (Figure A5) gives $h_m \propto Pr^{1/3}$, with τ_V^* of 10, 30 and 50 as parameters.

Further checks (Appendix V, Figures A3 and A4) which involve logarithmic replots of data from the authors' Figures 6 and 8 $\left[\frac{h_m(\nu^2/g)^{1/3}}{k}\right.$ vs. $\left.\frac{4\Gamma}{\mu}, \tau_V^*\right.$ as parameter, Prandtl numbers fixed at Pr = 1 (Figure 6), and at Pr = 10 (Figure 8)] give the following exponents for the relation

$$\frac{h_m\,(\nu^2/g)^{1/3}}{k} \propto \tau_V^{*n} .$$

	Exponent n (approx.)	
Re	Pr = 1	Pr = 10
10	0.50	0.53
100	0.47	0.46
1000	0.38	0.44
10000	0.30	0.27
100000	0.15	0.15

It is concluded that the analysis of Rohsenow et al. agrees with the Carpenter and Colburn semi-empirical correlation of experimental results only at small liquid Reynolds numbers, and the agreement extends only partly into the liquid flow range for which the Prandtl-Nikuradse velocity

distribution and the Martinelli analogy have been applied.

A comment by Seban (75), in the discussion attached to the paper, suggested a reason for the observed deviation. Seban pointed out that Rohsenow et al. neglected the pressure variation in the direction of vapour flow, and he suggested a liquid and vapour flow-dependent correction which should be applied to the heat transfer coefficient.

The occurrence of further error, caused by any inapplicability of the Prandtl-Nikuradse velocity distribution for large interfacial shear, is uncertain.

With the doubts which have been raised it remains to check the applicability of the other major application of eddy diffusivity and universal velocity distribution observations to falling films, that of Dukler, which will be considered in the next Section.

2.2.3. Heat Transfer for Falling Film Evaporation

Dukler (30,31,32) analysed heat transfer in the falling film evaporator as a continuation of the derivation for film thickness and velocity distribution which was outlined in Section 2.1.2.

A heat transfer equation,

$$q = - (k + \epsilon_H \, c \, \rho) \frac{dT}{dy}$$

was introduced, and values for the eddy thermal conductivity

were obtained from the previous expressions for eddy viscosity by assuming that $\epsilon_H = \epsilon$, which is found to be a reasonably good assumption for the region near the wall for pipe flow, and therefore should apply over the whole falling film.

Solution of the above equation was carried out simultaneously with the previous computer solutions for velocity distribution and film thickness. It was assumed that the heat flux is constant over the film and equal to the wall flux, which is a reasonable assumption for thin films, so that the problem reduced to one of finding the film temperature difference from the temperature profile and film thickness computed for fixed flow rate and vapour shear.

The results were presented, for fixed Prandtl number, as plots of $\frac{h\,(\nu^2/g)^{1/3}}{k}$ vs. Re, with β as a parameter. Both local and average values were given.

An assumption was made in the derivation that physical properties do not change significantly in the direction of heat transfer, so that the results should apply to both film condensation and film evaporation.

This assumption is satisfactory for moderate temperature differences. The only property which varies significantly with temperature is the viscosity of the liquid. The variation of the viscosity of the five test liquids which were used for the present investigation has been checked, by

the use of McAdams' nomogram (60f), for liquid temperatures of (T_{sat} + 20F°) and (T_{sat} - 20 F°). The viscosities at these temperatures vary by less than 25% from the values at saturation temperatures. A viscosity correction of $(\frac{\mu_{wall}}{\mu})^{0.14}$ is commonly accepted (60c). Thus the assumption should lead to deviations of less than $(1.25^{0.14} - 1) \times 100\% = 3\%$.

Dukler checked his analysis by comparison with experimental results for the average heat transfer coefficient for the condensation of water, toluene, trichlorethylene and mercury, obtained for conditions of moderate interfacial shear. Other comparisons were made with the variation of the local heat transfer coefficient along the length of a condenser tube for the condensation of methyl alcohol and of water, again for the case of significant interfacial shear. In all cases the correct trend was shown and agreement was found to be very good.

This agreement suggests that the assumptions which were made are valid and also suggests that the use of the equation of Deissler to give the eddy viscosity near a solid boundary is valid.

In the same way as was done for the results of Rohsenow et al., replots of the Dukler results have been carried out for comparison purposes (see Appendix V, Figures A6-A9). For Prandtl numbers of 1, 5 and 10, the replots show that beyond a liquid flow dependent value of β, the

relation between heat transfer coefficient and the vapour velocity is given by

$$\frac{h\,(\nu^2/g)^{1/3}}{k} \propto \beta^{0.5} ,$$

for a liquid Reynolds number range of 100 to 100,000.

By definition (30,31,32)

$$\beta = \frac{\left(\frac{\Delta P}{Z}\right)_{TP} r\, g^{1/3}}{2\,\rho_L^{1/3}\,\mu_L^{2/3}} = \frac{\left(\frac{\Delta P}{Z}\right)_{TP} D}{4\rho} \Big/ (\nu^2/g)^{1/3}$$

Also, from definition of friction factor,

$$\frac{\Delta P}{\rho_V} \propto \frac{f\,Z\,v_V^2}{g_c\,D}$$

$$\therefore \quad \frac{\Delta P}{Z} \propto \frac{f\,\rho_V\,v_V^2}{g_c\,D} .$$

Thus $\beta \propto f\,v_V^2$.

It follows that the Dukler analysis gives $h \propto v_V^{0.9}$ (approximately), over the whole range of liquid flowrates, which is in agreement with the experimental observations of Carpenter and Colburn, but which disagrees with predictions of the analysis of Rohsenow et al.

Thus, the universal velocity distribution approach is justified by the results of the analysis of Dukler, and it would appear that the errors observed with the analysis of Rohsenow et al. follow from the omission of the pressure drop term, as pointed out by Seban (Section 2.2.2), rather

than from any inapplicability of the universal velocity distribution for conditions of large interfacial shear.

The Dukler analysis appears to be suitable for the range for which checks have been carried out. However the following points of criticism should be considered.

1. The analysis ignores the presence of the free interface, the overall effect of which cannot be predicted yet. It has been suggested in Section 2.2.2.1 that the occurrence of wave motion at the interface aids in the development of turbulence in the film. However, it is also possible that the action of surface tension forces at the interface could tend to damp out the effect of turbulent eddies near the interface.
2. As pointed out by Dukler and Bergelin (34), the use of the velocity profile determined for pipe flow and the use of the same constants as for pipe flow may be of limited applicability when large interfacial shear forces act. For such a case very large velocity gradients would exist, whereas, for pipes flowing full, the velocity gradients in the turbulent core would not be large.

However, the work of Hershman (43) on the interaction between a turbulent air stream and a flowing liquid film has led to the conclusion that the results "seemed to verify that a turbulent film flowing under

the influence of a high interfacial shear can be described by the u^+ vs. y^+ relationship for the wall layer of a single phase flow".

3. The assumption of the limit of $y^+ = 20$ for transfer from the use of the Deissler expression to the use of the von Karman expression differs from the commonly accepted limit of $y^+ = 26$. However, the error introduced by the use of the von Karman expression for the range $y^+ = 20$-26 should be small despite the fact that the Deissler expression is more accurate for the region near to the wall.

4. The expression for eddy viscosity presented by Deissler for the region near to the wall, which was based on wind tunnel investigations with air at Reynolds numbers greater than 20,000, may be in error for part of its range of applicability.

It was recognized by Dukler (30,31) that application of these results to falling film flow would be a "severe test". For film flow it is possible for the dimensionless film thickness to be less than 20 ($y^+ = 20$ corresponds to Re = 600 for zero interfacial shear), and the Deissler equation would have to apply over the whole field.

It was claimed that the observed agreement with experiment was a "powerful confirmation" of the Deissler

equation. However, the checks were carried out almost exclusively for turbulent liquid flow with significant interfacial shear.

Corcoran and Sage (24) present a comparison of experimentally measured velocity distributions and show that deviation from the Deissler results is encountered with velocity profiles derived for Reynolds numbers in the range 7000 to 20,000, which corresponds much more closely with the intended range of application of y^+. If these lower-velocity results be more correct, the Deissler results would indicate a greater deviation from the laminar ($u^+ = y^+$) profile than is the case. Thus, in the range $5 < y^+ < 20$ the Deissler equation would indicate a greater degree of eddy action than is the case, and it would be expected that application of the Deissler relation would lead to heat transfer coefficients for the transition region which are too high. It will be shown later that such a deviation has been encountered for the present investigation.

A recent paper by Vieth, Porter and Sherwood (83) shows that this inadequacy of the empirical expressions for $y^+ < 30$ is appreciated. These authors suggested the use of a universal velocity distribution which relates u^+ to y^{++}, where $y^{++} = \phi\ (y^+, f)$. This approach led to satisfactory prediction of mass transfer in a turbulent boundary layer.

The only application of the Dukler analysis to falling film evaporation which has come to notice is that of Sinek and Young (78,79). These authors used the analysis to predict theoretical liquor-side coefficients for an investigation of overall coefficients for a falling film steam-heated LTV evaporator fitted with tubes 24 ft. long and operating with sea water and sea water concentrates.

From this theoretical liquor-side coefficient a theoretical film temperature difference was calculated for a given heat flux. This temperature drop was corrected for the longitudinal pressure drop, for the boiling point rise due to solutes, and for the boiling point rise due to the presence of bubbles. The need to introduce these latter corrections shows that it is very unlikely that Dukler's assumption that the liquid properties do not vary across the film will hold even approximately.

It was not possible to measure either wall temperature or vapour temperature to check the calculated temperature difference.

The corrected liquor-side temperature difference was used to obtain an overall coefficient by the further introduction of an average steam-side temperature drop based on a condensation coefficient, assumed to be 1.28 times the Nusselt predicted value, and by the introduction of a wall temperature drop based on a coefficient calculated as an

average for the mixed tube bundle consisting of tubes of six different metals, the variation of conductivity of which was claimed to be insufficient to cause uneven distribution of heat flow.

It was found that the proposed model correlated overall coefficients within ±10% and liquid-side coefficients within ±20%, for runs with zero superheat.

However, because of the many shell-side, tube wall, and superheat assumptions and approximations, the results cannot be taken as complete confirmation of the Dukler analysis.

Sinek and Young also found limited agreement of their test results with an equation suggested by Drew (60d) for non-boiling heat transfer, i.e.

$$\frac{h\,(\nu^2/g)^{1/3}}{k} = 0.01\ Re^{1/3}\ Pr^{1/3}.$$

Agreement was found for conditions of high flow rates and temperatures above 150°F and also for low flow rates and temperatures below 130°F.

Empirical correlations for the falling film evaporator have been presented by Keville (53,54), who considered the concentration of milk and milk concentrates in a commercial falling film evaporator containing ten tubes, each 3 in. O.D. x 10 ft. long.

The correlations were presented for whole milk only, and were based on practically constant values of ρ_L, k_L, c_L

and σ_L, and on a limited range of liquid flow rates, mainly in the transition regime. Further, v_V was varied only over a 2:1 range.

Only pressure and concentrate viscosity were varied over a wide range. Thus the observed correlations between the groups

$$\frac{Nu}{Pr^{0.3}\left(\frac{PZ}{\sigma}\right)^{0.9}} \quad \text{and} \quad \left(\frac{D\, v_V\, \rho_L}{\mu_L}\right)^{0.35 \text{ or } 0.5},$$

in which Nu is based on tube diameter, are essentially correlations between

$$h\,\mu_L^{-0.3}\,p^{-0.9} \quad \text{and} \quad \left(\frac{v_V}{\mu_L}\right)^{0.35 \text{ or } 0.5}.$$

Rowe (72) has pointed out recently that such an introduction of the same "strong" term to both sides of a correlation can result in a very large apparent reduction of scatter of data.

A more suitable approach was taken by Staker (80), who obtained a correlating equation for average heat transfer coefficients based on a wide range of variables for the falling film evaporation of six pure liquids at normal and reduced pressures. The liquids were water, methanol, ethanol, iso-propanol, n-butanol and ethyl acetate. Other work was done with sucrose solutions and with glycerol solutions.

Many of Staker's heat transfer coefficients were

determined for short lengths of tube (tube lengths of 4 in., 17 in., 30 in., and 63 in., diameters $\frac{3}{8}$ in. and $\frac{5}{8}$ in.), and therefore approximate to local coefficients.

It was not possible to obtain sufficiently small flow rates that the laminar flow regime could be studied fully.

The following empirical equation, which correlated experimental results for pure liquids within ±30%, was proposed for turbulent flow

$$\frac{h_m\, t}{k} = (\text{constant})\ Re^{0.8} \cdot Pr^{0.5} \cdot \mu/\mu_f \cdot \frac{D}{(0.016 + 0.48D)}$$

$$\text{for } Re^{0.8}\ Pr^{0.5} > 1000.$$

The last two terms on the right-hand side of this equation vary over a much smaller range than the others, and it is doubtful whether their inclusion is warranted. If they are omitted it is seen that the form of the Staker equation could have been predicted closely by the equation proposed by Colburn for condensation (see Section 2.2.2.2).

The form of the above equation again introduces the problem of duplication of terms, which can lead to an apparent improvement of correlation. The film thickness, t, on the left-hand side, may be expressed as a function of Reynolds number, as shown previously in Section 2.1.2. Staker's justification of the inclusion of the film thickness, by the claim that rearrangement leads to a poorer correlation,

indicates that scatter is probably being reduced in this way. Such a correlation method is misleading, and cannot be justified by the suggestion that inclusion of the film thickness draws attention to its role in affecting heat transfer rates.

The correlating equation applied up to a critical vapour velocity, defined by an empirical correlation,

$$v_{V_{crit}} = \phi \left(P^{0.5} . f_{D/\sigma}\right) ,$$

beyond which it was found that $h \propto v_V^{\,n}$. Experimental values of n were approximately 0.5 for seven levels of liquid properties, and 0.7 for two others. These values do not agree with the exponent of 0.9 which was predicted by Dukler and observed by Carpenter and Colburn. An empirical correlation for the exponent was presented,

$$n = \phi \left(P\, \rho_L\, \mu_V / \sigma\, \rho_V\, \mu_L\right) ,$$

but cannot be said to be satisfactory, because of the observed scatter.

Staker's basic correlation applied up to the point of onset of nucleate boiling at a critical temperature difference which was dependent on the liquid in use (25F° for water).

With the onset of nucleation a much greater increase in rate of heat transfer was observed. It was found that $h \propto (\Delta T)^5$ (approximately). This increase is to be expected because of the additive effects of additional turbulence

induced by the bubbles, bubble pumping action of superheated liquid away from the surface due to the alternate growth and collapse of bubbles (35), and latent heat transport through the growing bubbles (4).

Data which indicate the onset of nucleation for the falling film evaporation of water at a temperature difference of approximately 20F° have been presented by Norman and McIntyre (65). These results have been shown by Collier (22) to merge with the submerged nucleate boiling curve at a temperature difference dependent on the liquid flow rate.

Detailed visual observations of the onset of nucleation for falling film evaporation of water on a steam-heated vertical steel plate have been presented by Leidenfrost (58). The water was introduced subcooled at a temperature of about 200°F. It was found that, for temperature differences as low as 3½ F° above the boiling point, small bubbles were observed which had little disturbing effect and which either collapsed because of insufficient superheat or were swept away. The rate of initiation of these bubbles became greater for a temperature difference of 7 F°, until, at a difference of 9 F°, the bubbles formed and burst so rapidly over the whole surface that the entire film was violently stirred up.

This critical temperature difference appears to be low, but may be due to the nature of the heated surface.

Bankoff (5) pointed out that the critical superheat for bubbles to continue to grow, which corresponds to the true critical temperature difference, may be affected considerably by surface roughness. Leidenfrost gave no details of his surface preparation.

With the onset of the Leidenfrost-type violent boiling, stable foamy clumps of bubbles were found to run down the surface like soap foam, even when anti-foaming agents were added.

Similar observations by Russian workers (49,70) for films flowing down the outside of internally heated tubes were reported by Sinek and Young (79).

Leidenfrost observed no further change in the boiling process until, at a temperature difference of approximately 70 F°, intense bubble turbulence occurred, followed by throwoff of the liquid from the heated wall. This led to splitting of the film flow and dry patches on the heated surface. Backward inclination of the plate did not reduce the throw-off.

Bressler (14) carried out similar observations as part of a comparison of a flat plate falling film evaporator with a wiped film evaporator.

It was also observed by Bressler that flow of vapour over the film appeared to stop bubble formation, and evaporation appeared to occur then from the liquid surface. Cine-

films showed that under such circumstances small bubbles were still formed at the wall, but disappeared in the liquid film.

Bressler compared results for a 300 mm. wide flat-plate falling film evaporator with those for a Sambay wiped film evaporator, of the same wetted perimeter. Agreement was found when correction was made for the actual utilization of the heated area. This correction is necessary because the flat plate evaporator suffers from film splitting difficulties, whereas, with the wiped film evaporator, the wipers respread the film after splitting has occurred and allow greater utilization of the heated surface.

In addition, it was shown that application of the Nusselt theoretical analysis for condensation gave results 30% lower than the experimental results. This is very close to the discrepancy which has been observed between the Nusselt analysis and experimental condensation results (see Section 2.2.2.1).

Thus, for the laminar regime, it is to be expected that coefficients for wiped film evaporation and falling film evaporation may be predicted from condensation equations, for temperature differences below the point of onset of nucleation and for rotor speeds which are sufficient to maintain film spreading for the case of the wiped film evaporator.

This is in agreement with the observations of Staker,

who found that his equation for the falling film evaporator correlated the experimental results of Kramers et al. (56) for the Muller wiped film evaporator.

Thus, interrelation between heat transfer coefficients for vertical film processes is found to be extended further. It is also possible, but less likely, that agreement with correlations for the climbing film evaporator may be found.

2.2.4. Heat Transfer for Climbing Film Evaporation

The mode of operation of a climbing film evaporator requires that the climbing film zone should be preceded by a nucleate boiling zone and a slug flow zone.

For comparison with falling film evaporation only studies of the actual climbing film zone will be suitable. Also, because of the necessity for large vapour flows to generate the climbing film, climbing film correlations should be comparable only with falling film correlations obtained for conditions of high vapour shear. Furthermore, vapour flow conditions will have to be sufficient in both cases that the effect of gravity on the film flow may be neglected, but not sufficient, for the climbing film case, that considerable carryover of entrainment from the slug zone should occur.

The summary of Lacey et al. (57) of the climbing film flow work carried out at Harwell shows that it is

unlikely that this last condition will be met. The flow condition in the vapour space for climbing film flow is nearly always partially dispersed flow.

The effects of this flow dispersion, and of the additional ring waves generated by the high velocity vapour flows, are indicated by the lack of consistent agreement between experimental results (39) and the results for an attempted application by Hewitt (44) of the Dukler downward-flow analysis to upward flow. This lack of agreement occurred despite refinements which were introduced into the modified analysis to correct the shear stress distribution. Lacey et al. concluded that it is likely that there exists for the climbing film zone "gross distortion of the film by waves and the entrainment phenomenon".

Recent experimental work by Penman (68) led to a correlation for the variation of the local heat transfer coefficient in the climbing film region, based on the results for five liquids and four tube sizes. Agreement or prediction of the correct trend was found with the few workers (29,62) whose results could be analysed to give local data for the climbing film zone. The correct trends were also predicted for the extreme case of heat transfer to sprays, which was studied by Bennett, Collier, Pratt and Thornton (10,69).

The final equation was

$$\frac{h\, D^{\frac{1}{2}}}{c_L \sqrt{\rho_L \sigma g_c}} = (\text{constant}) \left[v_B \sqrt{\frac{\rho_V D}{\sigma g_c}} \right]^{0.5}$$

An important conclusion from this correlation is that $h \propto v_B^{0.5}$, where v_B is a bulk velocity which approximates to the vapour velocity for the high vapour flow rate conditions of climbing film flow.

This basic disagreement with the exponent of 0.9, the vapour velocity exponent predicted by the theoretical analyses and experimental observations for falling film heat transfer, indicates that it will not be possible to compare climbing film results with normal falling film results, as would be expected from the conclusions of Lacey et al. reported above.

However, it still remains to explain why many of Staker's vapour velocity exponent determinations agree with the values obtained for climbing film results, and only a few approach the value of 0.9 obtained for other falling film work. Further reference will be made to this when the results of the present investigation are discussed in Section 4.4.3.

One more film heat transfer process - non-boiling falling film heat transfer - remains to be considered for possible comparison with falling film evaporation heat transfer.

2.2.5. Non-boiling Heat Transfer to Falling Liquid Films

For non-boiling heat transfer the mean temperature of the liquid film tends to the wall temperature, and all of the heat transferred is accumulated by the film, there being assumed no heat transfer from the film surface either as losses or by evaporation. The temperature difference is defined as $(T_{wall} - T_{liquid,mean})$, and tends to zero.

This is a different case to that for film evaporation for which all of the heat transferred to the falling film is lost by evaporation and there is no accumulation within the film. For the same case of constant wall temperature as considered above, the temperature difference, $(T_{wall} - T_{interface})$ i.e. $(T_{wall} - T_{saturation})$, remains constant.

However, Wilke (85,86) has pointed out that analysis of non-boiling heat transfer to falling liquid films predicts that, beyond a certain thermal entry length, the heat transfer coefficient for laminar flow is given by

$$\overline{Nu} = \frac{h't}{k} = 1.88.$$

This relation is similar in form to the result presented by Nusselt for condensation (Section 2.2.2.1).

The heat transfer coefficient h' is defined as a mean value for the whole tube length. However, for conditions of short thermal entry length, and for negligible

evaporation and hence negligible variation in the liquid flow rate, the mean coefficient is equivalent to a local coefficient, i.e. $\overline{Nu} = Nu$.

The heat transfer coefficient is designated here as h' because it is based on $\Delta T = (T_{wall} - T_{liquid,mean})$, and also to distinguish it from the coefficient, h, presented previously for evaporation and condensation. For the same overall temperature difference, $h' > h$. However, for the fully-developed flow regime it should be possible to compare h' and h provided that the ratio $\frac{T_{wall} - T_{liquid,mean}}{T_{wall} - T_{interface}}$ can be determined. This will be discussed later.

Wilke's analysis followed from the original analysis of non-boiling heat transfer to falling liquid films in laminar flow, which was carried out by Nusselt (67) in 1923. Jakob (47d) presented the Nusselt analysis in English translation, and with some slight modifications to the technique.

The velocity profile used was that derived previously by Nusselt (66), and temperature profiles were obtained from the solution of a heat balance over a liquid element by integration using the method of finite differences.

The final equation of Nusselt contained two parts. The first part expressed the influence of the thermal entry regime, the other gave the relationship for fully-developed flow.

By introducing the Nusselt expression for film thickness, Wilke showed that the final equation could be presented as

$$Nu = 0.0942 \cdot \frac{Re}{4} \cdot Pr \cdot \frac{t}{Z} + 1.88$$

for $\frac{1}{3} \cdot \frac{4}{Re.Pr} \cdot \frac{Z}{t} > 0.05$,

where Nu is the value for the tube length, Z.

The first term usually is negligible because the analysis holds only for small Reynolds numbers (for which the film thickness, t, also is small), and thus the term can only be large for the cases of large Prandtl numbers or small Z (i.e. short tubes).

Wilke also obtained experimental data for heat transfer to films flowing down the outside of a tube 2.4 metres long x 42 mm. diameter. The ranges of variables considered were Γ/μ = 12 to 3000, and Pr = 5.4 to 210. The test liquids used were water, diethylene-glycol, and mixtures of these two liquids.

The data were correlated by the equations

$Nu = 1.88$, for $\Gamma/\mu < Re_u$

where $Re_u = 615\ Pr^{-0.646}$, for $Pr > 5$

($Re_u \simeq 200$ for water, for which Pr = 5.4),

$Nu = 0.0614\ (\Gamma/\mu)^{8/15}\ Pr^{0.344}$, for $Re_u < \Gamma/\mu < 400$,

$Nu = 0.00112\ (\Gamma/\mu)^{6/5}\ Pr^{0.344}$, for $400 < \Gamma/\mu < 800$, and

$Nu = 0.0066\ (\Gamma/\mu)^{14/15}\ Pr^{0.344}$, for $\Gamma/\mu > 800$.

The expression which was used for the film thickness term in Nu was that derived by Nusselt for the laminar regimes, or that observed by Brauer for the turbulent regime ($\Gamma/\mu > 400$).

The critical Γ/μ values had the following significance:

$\Gamma/\mu = Re_u$: the limit of applicability of the Nusselt analysis in the presence of waves. Note that there was no apparent change in the nature of flow at this point.

$\Gamma/\mu = 400$: the critical flowrate at which the film flow became turbulent, which corresponded with the onset of Brauer's "capillary" waves.

$\Gamma/\mu = 800$: the flowrate at which the formation of circumferential ring waves was observed.

Fair agreement was found with previous experimental data of Bays and McAdams (7) for the laminar regime (approximately ±30% deviation), and with the experimental data of Sexauer (76), Garwin and Kelly (38), and McAdams, Drew and Bays (61) (whose results were subsequently correlated by Drew (60d)) for the turbulent regime. Compared with the data of these authors Wilke's data were respectively about 40%, 20% and 50% higher.

Wilke explained much of the deviation between his results and those of Sexauer and of Garwin and Kelly by the

failure of these authors to correct for the temperature drop across the wall for their "buried" thermocouples. A suggestion was also made that the results of McAdams, Drew, and Bays were low because of an effect of the thermal entry zone on the results. However, it appears that this latter criticism is unwarranted because, in addition to the data obtained for short tubes, McAdams et al. also presented other consistent data obtained with tubes six feet long (i.e. approximately the same length as the test section of Wilke. Furthermore falling film evaporation results of Sinek and Young (79), for tubes twenty-four feet long, agree with the correlation of Drew (60d) of the results of McAdams, Drew, and Bays (see Section 2.2.3).

Wilke found that his experimental data for the laminar regime were correlated by the predicted relation, $Nu = 1.88$, only for the solutions. The results for water were defined by $Nu = 1.6$. The author attributed this deviation from the Nusselt expression to the effects of significant evaporation and hence to the reduction of film thickness from the theoretical value used for the calculation of Nu. This explanation is difficult to accept because the operating temperature of the water film was only 20-30°C. Furthermore Nusselt (reported by Jakob (47e)) demonstrated that "the evaporation of water in a film cooler of ordinary size remains below 1% of the total flow and therefore is negligible".

An alternative explanation, not considered by Wilke, is that $\frac{h'(\nu^2/g)^{1/3}}{k}$ is a function of both Pr and Re below Re_u, as well as above. This would be in agreement with the results at small Reynolds numbers of the theoretical analysis of Dukler (discussed previously in Section 2.2.3). A replot of the data of Dukler in Appendix V, Figure A9, shows a $Pr^{0.14}$ dependence at $\Gamma/\mu = 50$, and Dukler's original plot leads to a Prandtl number term of $Pr^{0.10}$ even at $\Gamma/\mu = 25$. In Section 6 of this thesis, Wilke's observations of Nu = 1.6, for Pr = 5.4 (water), and Nu = 1.88, for Pr = 9.4 and above (solutions), will be tested against experimental data for the present investigation.

Wilke also presented film temperature profiles which will be used now to provide a basis for comparison of his non-boiling data with evaporation and condensation results.

Profiles measured at a distance of 2.2 metres from the liquid inlet (85) showed a linear temperature drop from the wall to a distance approximately equal to the film "trough thickness", beyond which the temperature across the remainder of the film remained approximately constant (see sketch plot below).

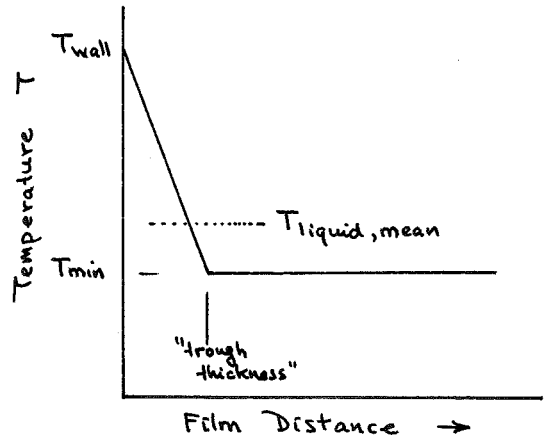

For $Re_u < \Gamma/\mu < 400$ it was found that

$$\frac{T_{wall} - T_{min.}}{T_{wall} - T_{L,mean}} = 1.15 \text{ (approximately).}$$

Inspection of the presented profiles shows that this relation also holds to a limited extent in the range $\Gamma/\mu < Re_u$.

A linear temperature profile across the entire film was not encountered until the Reynolds number was reduced to a value approaching the point of onset of waves.

For comparison with previous condensation and evaporation work,

$$\frac{T_{wall} - T_{min.}}{T_{wall} - T_{L,mean}} = \frac{T_{wall} - T_{interface}}{T_{wall} - T_{L,mean}} = \frac{(\Delta T)_{evap. \text{ or } condens.}}{(\Delta T)_{non\text{-}boiling}}$$

It follows that $h' = 1.15\ h$ (approximately) for flow rates near $\Gamma/\mu = Re_u$.

In an analysis for the case of linear temperature profile, Wilke (85) also showed that

$T_{L,mean} = T_{wall} - \frac{5}{8}$ (temperature gradient) x (film thickness).

This is now rearranged to give

$$\frac{T_{wall} - T_{L,mean}}{T_{wall} - T_{interface}} = \frac{5}{8}$$

$$\text{i.e.} \quad \frac{(\Delta T)_{evapn.\ or\ condens.}}{(\Delta T)_{non\text{-}boiling}} = 1.6 \ .$$

Thus, for comparison with film evaporation or condensation,

$Nu = 1.6$ or 1.88, for non-boiling,

when corrected for the different temperature difference bases, is equivalent to

$Nu = \frac{1.6}{1.6} = 1$ or $= \frac{1.88}{1.6} = 1.18$, near the point of onset of rippling, and

$Nu = \frac{1.6}{1.15} = 1.39$ or $= \frac{1.88}{1.15} = 1.64$, near Re_u.

For turbulent flow the effect of eddy action will be such that $T_{L,mean}$ approaches $T_{interface}$. Thus $(T_{wall} - T_{interface}) \simeq (T_{wall} - T_{L,mean})$. However Wilke's data for the most dilute diethylene glycol-water solution (Figure 36 in Reference (85)) show that the generalized temperature profile observed for $Re_u < \Gamma/\mu < 400$ is also followed at least up to $4\Gamma/\mu = 3800$. Thus, for comparison with turbulent film heat transfer,

$(\Delta T)_{non\text{-}boiling} \leqslant (\Delta T)_{condens.\ or\ evapn.} \leqslant 1.15(\Delta T)_{non\text{-}boiling}$.

This suggests that turbulent film evaporation and condensation

heat transfer data should lie between the values predicted by Wilke's correlations and values $\left[\left(1 - \frac{1}{1.15}\right) \times 100\%\right] = 13\%$ lower than these.

Detailed comparison with Wilke's data will be deferred until Section 6. However, it is apparent at this stage that the correlations presented by Wilke, suitably corrected, are close in form and value to others presented previously for falling film condensation and evaporation.

2.2.6. Conclusions

Discussion of previous work of interest to falling film evaporation leads to the following conclusions.

1. Sufficient is known about the hydrodynamics of the falling film process for simple analyses to be developed, and for observed deviations from these analyses to be explained approximately.

2. It is recognized that wave motion may have an important effect on transport in the falling film. However, as yet, the process is not sufficiently understood for analyses to be made in terms of wave parameters.

3. An advanced theoretical analysis, based on universal velocity profiles observed for pipe flow, has been presented for falling film evaporation. The analysis

appears to have promise, but its applicability remains to be checked over the full range of flow conditions.

4. A general similarity has been shown between coefficients and correlation methods for heat transfer in falling film evaporation, heat transfer in falling film condensation, and heat transfer to non-boiling falling films, although in many cases it was necessary to extend or reanalyse the presented results.

3. APPARATUS

Staker (80) carried out work with externally-heated tubes of $\frac{3}{8}$ in. and $\frac{5}{8}$ in. diameter. The aim of the present apparatus was to extend this work to large diameter tubes and to provide a more detailed study. More precise temperature measurements were to be made, and, if possible, fluxes up to 100,000 Btu/hr ft^2 F^o were to be used. In contrast to the apparatus of Staker, vapour flow rates were to be varied independently of liquid flow rate and of surface heat flux by the introduction to the test section of externally-generated vapour. In addition, it was required that the heated surface could be observed so that the nature of the evaporation process and of the liquid-vapour flow could be determined.

A flowsheet of the apparatus is given as Figure 3, and individual details are shown in Figures 1-6 (pages 81-88).

3.1. Heating method

An electrical heating method was chosen because of the ease of control and the simplicity of accurate direct heat flux measurement. It was not intended that the nucleate boiling regime should be studied into the dry-wall regime so that the possibility of burnout was not considered to be a problem for normal operation.

Pyrotenax heating cable was favoured as an electrical heat source because of the minimum requirement for ancillary equipment not already available, the advantage of operating at normal power voltages and currents, and the relative simplicity of measuring surface temperatures by direct attachment of thermocouples to or within the heated surface.

3.2. The preliminary test section

Initially a flat plate was considered to be ideal because it represented the extreme case of a large diameter tube. Use of a flat plate also had advantages for the removal of the leads of surface temperature measuring thermocouples.

A test section (Figure 6) was made which consisted of a length of copper waveguide clamped to a heating "sandwich" which contained six parallel lengths of Pyrotenax, each rated at 2 kW, and each supplied by an autotransformer. The heated length was 4 ft. and the internal dimensions of the waveguide were 2.000 in. ± 0.003 in. by 0.667 in. ± 0.003 in. Waveguide was chosen as the flow channel because this was the simplest method of obtaining a section with closely toleranced dimensions.

At the limit of safe working for the autotransformers the rated maximum heat flux input was 80,000 Btu/hr ft^2.

Viewing windows were fitted to the section, wall thermocouples were located in grooves cut across the back of the test section at the clamped interface, and traversing thermocouples were introduced into the vapour stream through glands in the side wall.

Liquid was fed in over a shrouded weir to prevent excessive disturbance to the intial liquid flow by the flow of vapour introduced at the top of the section.

Runs were carried out with uniform lateral heat flux input, and any adjustment necessary was detected by progressively switching a wattmeter from one parallel circuit to the next.

However, operation under boiling conditions led to uneven distributions of temperature and liquid, which occurred despite observations that the liquid flow had appeared to be even for non-boiling flow, and that the transverse temperatures (indicated by groups of thermocouples located at the quarter-, half-, and three quarter-way marks along the heated length) had been approximately even for zero flow conditions. Furthermore, at high liquid flow rates and heat fluxes, the liquid film spread completely around the rectangular test section. Thus, accurate measurements of local Reynolds number and local heat flux were impossible for the major part of the experimental range. The test section would have been of use only for low flow rates under conditions of small heat loads, and further work on it was abandoned.

3.3. The final test section

3.3.1. Introduction

An unbounded flow surface was chosen for the final apparatus to eliminate the problems encountered with the initial test section.

The use of an externally-heated tube was rejected because of difficulties for visual observation. Also, the use of a wide plate (i.e. effectively an unbounded surface) was rejected because of problems for the even distribution of liquid and of heat flux.

An internally-heated tube mounted within an insulated but transparent jacket appeared to satisfy requirements, provided that the heating method did not interfere with the liquid and vapour entry and exit.

The dimensions chosen for this technique were a tube diameter of 1 in. and a jacket diameter of 1½ in. This combination gave a reasonably large wetted perimeter, ensured satisfactory vapour velocities for the installed vapour generation capacity, and gave an annular flow area close to that of a 1 in. I.D. externally-heated tube.

A length to diameter ratio of about 20:1 was considered to be a satisfactory compromise to ensure even flow distribution, and to allow operation at a satisfactorily high heat flux for the amount of controlled power available.

Because of installation difficulties for the distribution of thermocouples along the wall, it was necessary to accept location of thermocouples only at the main test "point" (a circumferential zone three diameters from the bottom of the heated tube), and at a few control points at each end of the tube.

3.3.2. The heated tube

The test section on which results for the present work were obtained consisted of an 18 in. length of 1 in. O.D. 10 gauge ($\frac{1}{8}$ in. wall) brass tube inside which was inserted and soldered a Pyrotenax winding double-wound on a copper former (Figure 5A). The Pyrotenax cable used was Type 104/1K which has a conductor of Kumanal alloy, an alloy which has a negligible variation of electrical resistance with temperature. A winding fabricated from this constant-resistance cable generates a uniform heat flux over its whole length, despite any imposed temperature gradient.

The winding was fabricated with an outer dimension sufficient to ensure a light interference fit into the tube (Figure 5B). Before insertion into the tube the winding was coated with a thick layer of Fryolux solder paint. Application of a low voltage to the winding led to melting of this self-fluxing solder, and with the tube assembly mounted vertically, unfluxed solder was fed in at the top until the

flow out the bottom was seen to be flux-free. Thus, in the final assembly, all voids between the Pyrotenax winding, the brass tube, and the copper former were filled with solder, which itself was in intimate fluxed contact with each of the metal surfaces.

3.3.3. The flow surface

To prevent imposing any roughness which could affect the boiling process, the outer surface of the brass tube was not machined. Instead, the as-drawn surface was polished progressively down to Number 0000 abrasive paper, then with cloth and a mixture of Brasso and carborundum powder, and finally with cloth and Brasso. A mirror surface resulted, with only a few nicks which could not be polished out.

Thin brass extension pieces (thin to minimise conduction losses from the main heated surface), of length equal to four tube diameters, were press-fitted to the tube at the inlet and the outlet to provide non-heated smooth entry and exit for the liquid film. These extension pieces also enabled removal of thermocouple leads and power leads without interference to liquid flow (see Figure 4). The feed end extension piece, suitably profiled at the upper end, also served as an inlet reservoir and as a feed weir.

The test section assembly was supported in the

vertical position by the pipe, perforated at its bottom, which introduced the feed liquid. This pipe also allowed removal of the upper thermocouple leads. Screwed connection of the pipe to the test section was made through teflon spacers so that axial conduction would be minimised.

3.3.4. The glass jacket

The test section was suspended inside a jacket which consisted of a length of 1½ in. nominal bore Q.V.F. pyrex glass pipeline. The actual bore dimensions were 1.480 in. near the entry, and 1.487 in. near the exit. Slight internal shouldering of the glass was apparent near the ends of the pipeline. To avoid any effects due to this shouldering the tube was suspended in a position such that the main measurement "point" near the bottom of the heated tube was located near the centre of the pipe section.

Location within the jacket at the top was provided by the feed pipe. Screws tapped in teflon plugs, which in turn were press-fitted into holes drilled through the jacket, provided means of adjustment for the tube at the bottom. Contact of the locating screws was made only with the non-heated extension piece and any interference to flow occurred well beyond the test point.

Exact vertical location of the test section and of the jacket were checked by the use of a theodolite because

Friedman and Miller (37) had reported that an inclination of a tube from the vertical of as little as 0.020 inches per foot was sufficient to cause the local liquid velocity around the tube periphery to differ by up to 200%.

The theodolite was also used to check the centering of the test section within the jacket. Adjustment was continued until concentricity to within 1/100 of an inch was obtained. This limit was set by the twenty seconds of arc reading limit of the theodolite.

At the liquid and vapour feed end the 1½ in. Q.V.F. pyrex flow channel opened through a transition piece to connect to a 2 in. Q.V.F. glass tee which served to introduce externally-produced saturated vapour.

A circular baffle prevented direct impingement of the vapour on to the flow surface and thus eliminated any interference with the initial development of a steady liquid film.

Smooth development of cocurrent flow of liquid and vapour was provided by the geometry of the glass outer jacket assembly. Interaction of the two phases commenced at a point of enlarged cross-section of the annular vapour space, after which the gradual reduction of annular area in the region of the glass transition piece allowed an approach to flow equilibrium at the entry to the parallel jacket section.

At the lower end of the jacket, connection was made

to a 1½ in. Q.V.F. glass tee which in turn was bolted directly to a total condenser. Pyrotenax power leads and bottom surface thermocouple leads were removed through a gland housing fitted to the sidearm of this tee.

Heat losses from the lower part of the jacket were eliminated by means of a compensating heating winding. The glass jacket was surrounded by a thin glass tube on which was open-wound a variac-controlled nichrome winding. A thermometer was supported between the two glass tubes and the temperature inside the compensating jacket was maintained at the boiling temperature of the test liquid under consideration.

Convection heat losses were eliminated because of the adjustment to give $\Delta T = T_{vapour} - T_{jacket} = 0$. Radiation losses were minimised because $T_{film} \simeq T_{jacket}$ and $emissivity_{film} \simeq emissivity_{jacket}$ (the emissivity of a metal surface covered by a thick fluid film is large, approximately 0.8-0.9 (60g), and it is close to the value, emissivity = 0.9, for glass (60g)). Thus heat losses were balanced while still allowing observation of the heated surface. The upper part of the glass jacket was wound with variac-controlled non-transparent heating tapes, also to minimise heat losses.

3.3.5. Surface temperature measurement

Surface temperature measurement by means of thermocouples inserted in holes drilled along the tube wall (see Figure 4 and the Figure on page A73 in Appendix IV) was chosen as the most satisfactory method for the accurate determination of local temperatures for the present apparatus.

This method eliminated the interference to the flow and nucleation characteristics of the evaporation surface, and the uncertainty in the value of the local surface heat flux, which would have been encountered if thermocouples were sealed in longitudinal external grooves in the heated surface.

The method also eliminated the interference to liquid film flow, and the lead conduction errors, which would have been encountered for the removal of exit thermocouple leads across the liquid film and through the vapour space. However, the technique resulted in greatly reduced flexibility in the location of the thermocouples.

Removal of thermocouple leads along a groove cut in the internal face of the tube would have been promising but for the practical difficulties of locating and attaching the thermocouple hot junctions, and of obtaining a longitudinal penetration much greater than that possible by drilling along the wall.

The thermocouples used were ½ mm. (0.020 in.) Philips Thermocoax stainless steel sheathed, magnesia insulated, chromel-alumel thermocouples (wire diameter approximately 0.00¼ in.) which were sufficiently small to present negligible interference to heat flow to the surface.

The thermocouples were prepared with bare hot junctions which protruded from the end of the sheath a distance equal to the bead diameter.

Drilling of a hole along the tube wall of the same diameter as the sheathed thermocouple was impractical because the length of a standard 0.020 in. drill is only about one inch, and it was considered that a thermocouple penetration of about three inches would be required to eliminate errors due to end effects.

However, Long Series drills were available, the smallest being 3/64 in. and 1/16 in., with drill lengths of 2½ in. and 3 in. respectively.

Therefore the use of a 1/16 in. Long Series drill followed by the insertion of a copper sleeve was adopted, and for this purpose precision copper capillary tube was drawn to a specification of 0.020 in. I.D., 1/16 in. (0.062 in.) O.D.

Six holes were drilled at each end of the test section - three to the limit of the drill (2⅞ in.) and spaced 120° apart, the remaining three to a depth of 1½ in.

spaced 120° apart and offset 60° from the three "deep" thermocouples. Very careful preliminary setting up was required so that the holes would be drilled down the centre of the tube wall.

The ½ mm. Thermocoax thermocouples were fitted inside lengths of the capillary tube, each length being a half-inch longer than the drilled holes. The bare beads were allowed to protrude slightly from the ends of the copper sleeves. The thermocouple-tube assemblies were then press-fitted into the drilled holes. Litharge-glycerine cement, which was applied to the hot junction before insertion, provided good thermal contact with the brass wall and eliminated any air space at the hot junction.

Thus, at the top and bottom of the test section, local temperatures could be determined at two circumferential zones each of three points.

The three lower surface thermocouples located farther ($2\frac{7}{8}$ in.) from the lower end of the test section were adopted as the test "point" to minimise end effects. However, with nucleate boiling, for which localised patches of nucleation could occur, it was necessary sometimes to consider all six lower points to obtain a more representative surface temperature.

The thermocouple e.m.f.s were measured using a multi-point switch and a Tinsley portable potentiometer.

The reference point was provided by a common cold junction immersed in ice in a vacuum flask.

Capillary tube of copper was used for thermocouple sleeving in the brass section only because a large quantity had been drawn for a copper test section of identical dimensions, on which initial tests were carried out. However, deep-drilling of copper proved to be extremely difficult because of excessive drill "wander", and brass was chosen as the material for the final tube.

The effect of the presence of the copper sleeve within the brass wall was checked by means of an approximate flux plot which predicted a distortion of the surface heat flux of less than 6% (difference between peak heat flux and the undisturbed heat flux) in the region of the exit sleeves. This error would be much reduced at the test zone, which corresponds with the tips of the longer sleeves, where the flux pattern would be nearer to the normal undisturbed configuration.

Some distortion of the isothermals across the brass wall also was to be expected. However, with the location of the thermocouple and sleeve assembly at the centre of the wall, the distorted isothermals would be symmetrical about the midpoint of the tube wall cross-section (except for a small effect due to tube curvature). Thus, a thermocouple bead located at the centre of the tube wall would lie on an

undistorted isothermal, and would measure the true mid-wall temperature.

The flux plot estimate showed that the surface temperature above the thermocouple should differ from the undistorted temperature by only a small percentage (of the order of 5%) of the temperature drop across the wall. The wall temperature drop usually is small compared with the film temperature drop (Appendix IV). Therefore surface temperature variations caused by the presence of the thermocouples can be ignored.

3.3.6. Vapour temperature measurement

Vapour temperature measurement at the main surface test point was provided by three Thermocoax thermocouples with bare hot junctions. These thermocouples were introduced through teflon plugs press-fitted into holes drilled through the glass jacket (Figures 4, 5A) downstream of the measurement point. Availability of three thermocouples, 120° apart, allowed a check of any discrepancies, and ensured that the reading of any thermocouple obviously affected by contact with a spray of superheated liquid could be ignored.

3.4. Power supply

Power was supplied to the Pyrotenax winding by

operation across two phases of a three-phase Variac assembly which consisted of three 7.5 kVA autotransformers ganged in star (i.e. two "arms" of the star were used as two series-operated variacs).

The maximum heat flux available with the Pyrotenax winding and variac combination was 95,000 Btu/hr ft^2.

For safety of the heating winding the power supply to the variac was interlocked with the power supply to the test liquid recirculation pump and with a test section burn-out prevention device. This overload detector consisted of an Ether Transitrol on-off controller actuated by a Thermo-coax thermocouple embedded in the lower end of the brass heated surface. This latter safety device also operated an alarm, and was installed after the copper version of the final test section had burned out, and the flow surface of the final brass version had been blackened on two occasions while operating near the point of onset of dry wall conditions.

3.5. Heat flux measurement

The power input to the test section was measured by a calibrated A.J. William Precision Wattmeter, Model PW9, correct to within 0.2% full scale reading. This instrument has three ranges (50/100/250 volts, 2.5/5/10 amps) and at power inputs above its maximum reading it was used with a precision current transformer (class AL, ratio 40:5, limit of

error ±0.15%) and a precision potential transformer (class AL, ratio 440:110, limit of error ±0.25%).

End heat losses through the exit Pyrotenax tails and through the support pipe were negligible, because of the small area of the conductors in the tails, and because of the teflon insulation introduced at the feed end. In addition, heat losses through the jacket were eliminated by adjustment of the compensating winding.

Therefore the heat flux could be calculated directly from the measured power input and the dimensions of the heated surface (length 18 in. ± 1/64 in., diameter 1.000 in. ±0.001 in.).

3.6. The liquid flow circuit

The test liquid was contained in a lagged 12-gallon overhead stainless steel tank and its temperature was maintained about 2F° below the boiling point by a 3kW immersion heater, 1.5kW controlled by a variac, the other 1.5kW controlled by a sensitive mercury contact thermometer and a relay. The tank was vented to atmosphere through a reflux condenser.

Feed to the test section was by gravity flow through a calibrated rotameter and a Pyrotenax-wound preheater. The feed temperature was measured by a Thermocoax thermocouple at the entry to the test section. Generally it was necessary to

limit the liquid preheat to give a bulk liquid temperature 3-10 F^{o} below the saturation temperature to prevent vapour generation in the preheater and subsequent surging flow of the liquid over the feed weir.

The smoothness of flow over the distribution weir was observed through slots cut in the circular baffle and the range of liquid flowrate which was considered for each liquid (see Figure 3⁴) was limited by the observation of the onset of unstable liquid flow over the weir, or by the occurrence of incomplete wetting of the surface.

Provisions to allow subsequent smooth interaction of the liquid flow with any cocurrent vapour flow were described in Section 3.3.4.

Lighting was provided to aid visual observation of the nature of the liquid-vapour flow and of the boiling mechanism in the region of the test zone. The lights were turned off to eliminate local radiant heating effects before vapour thermocouple readings were taken.

The liquid and vapour discharged from the test section passed to a total condenser (which was vented to atmosphere through a small reflux condenser), and then to a condensate receiver. A recirculation pump, manually controlled to maintain a constant level in the condensate receiver, returned the liquid through the calibrated "total flow" rotameter to the head tank. This system enabled the feed

rate of externally-produced vapour to be obtained as the difference between the flow rate indicated by the total flow rotameter and that indicated by the liquid feed rotameter.

Control of recirculation rate was provided by partial bypass of the pump, and by speed control through a four-step pulley drive system. Flow pulsations at the pump discharge were reduced by the installation of an air bell. In addition, a fine wire mesh filter was fitted to the pump discharge to collect scale, and also to remove rubber and metal chips formed in the pump.

A number of types of recirculation pump was tried. The difficulty was that the pump had to be operated unlubricated to prevent contamination of the test liquid, and was required to pump hot organics usually at temperatures well above the recommended operating temperature of the rotor.

Satisfactory recirculation of all of the test liquids except chloroform was provided by a special model Jabsco pump which was rendered lubricant-free by the provision of ball bearing housings to support the drive shaft. The neoprene flexible-vaned impellers considerably reduced flow oscillation and proved to be wear-resistant in the high temperature version.

With chloroform, excessive swelling of the neoprene impellers occurred quickly, and it was necessary to replace the Jabsco pump with a gear pump to complete the series of tests.

3.7. The vapour flow circuit

External generation of saturated vapour of each of the test liquids was provided by a small version of an LTV evaporator (Figure 2B) which consisted of four vertically-mounted 4 ft. x 1 in. I.D. pyrex tubes inside each of which was suspended a former wound with two 2kW stainless steel Pyrotenax windings. One of these windings was operated on-off, the other was controlled by a variac.

Liquid-vapour separation was effected by feeding the discharge from each tube through a stainless steel header into an entrainment separator. Direct impingement on to deflector caps, followed by passage through a bed of ½ in. glass helices, provided satisfactory separation. The lower level of the bed was also contacted by feed liquid delivered from the main head tank through a rotameter. This liquid-vapour contact ensured that the exit vapour was not super-heated, and that the feed liquid was given a slight preheat.

Vapour was delivered to the test section by a 2 in. Q.V.F. glass pipeline continuously traced with heating tapes, and provision was made for the collection of any small amount of condensate at an elbow immediately before the delivery point.

Subsequent vapour flow is described in Sections 3.3.4 and 3.6.

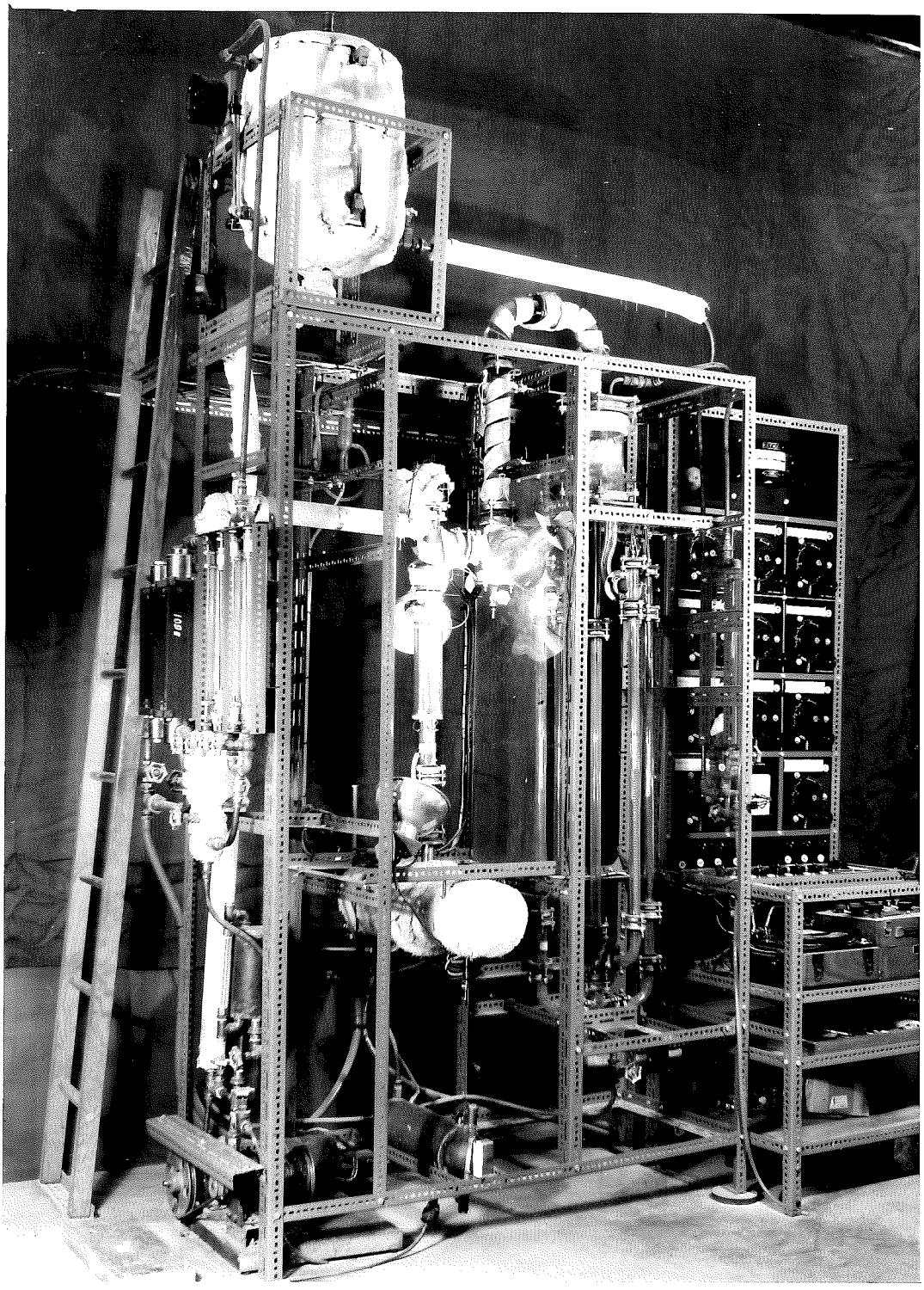

Figure 1 FALLING FILM APPARATUS

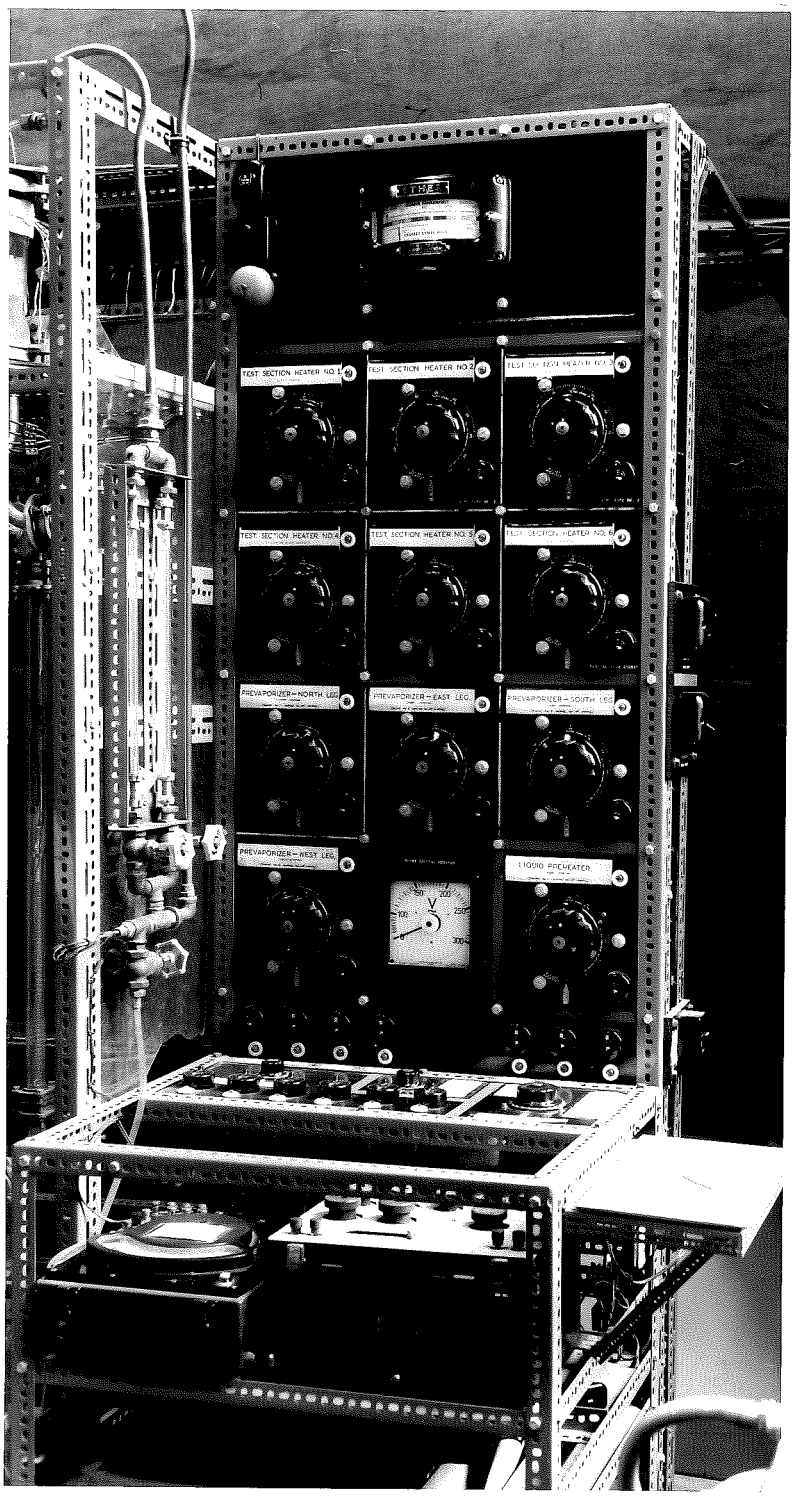

Figure 2A MAIN CONTROL PANEL

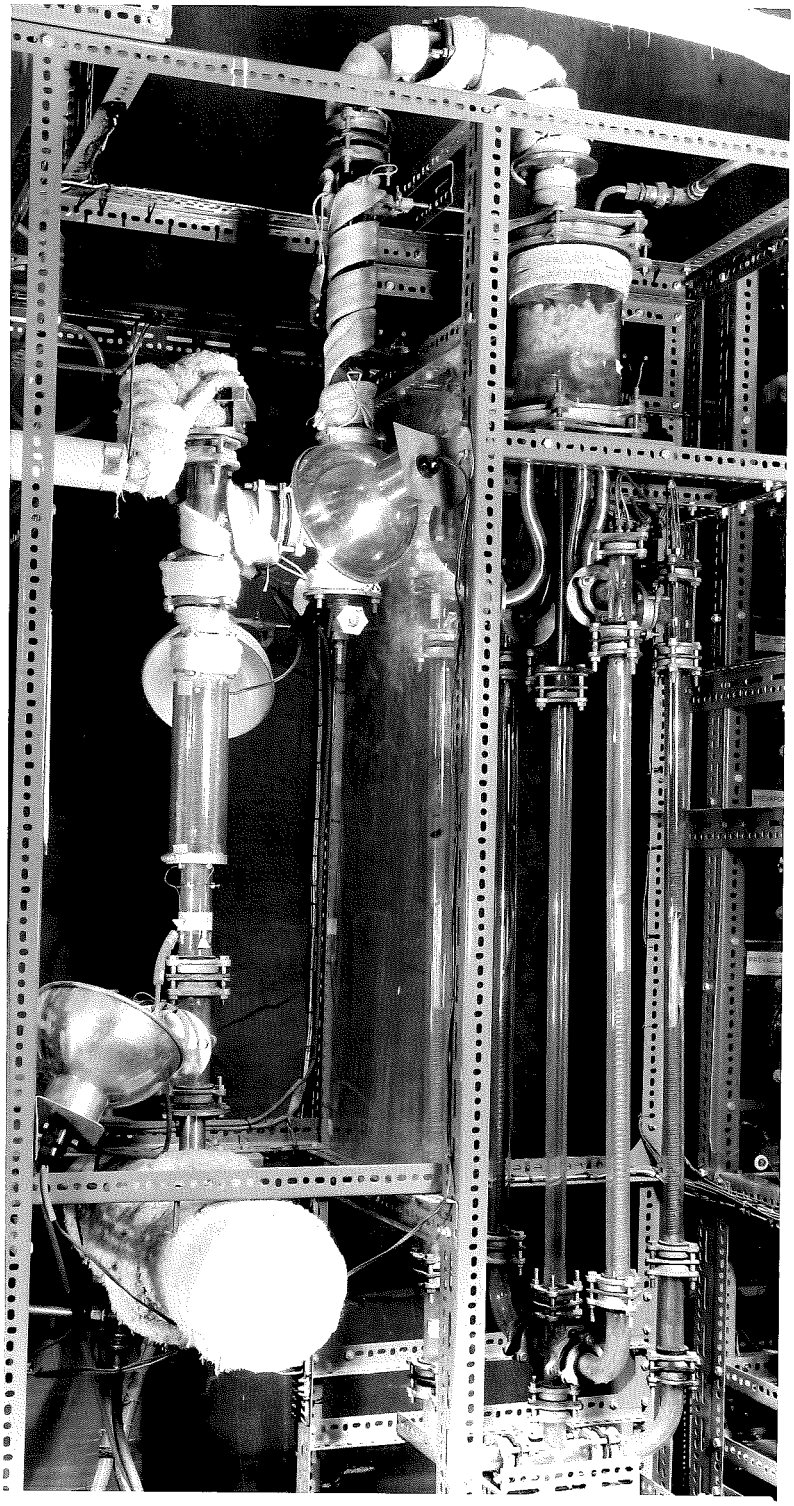

Figure 2B TEST SECTION AND PREVAPORIZER

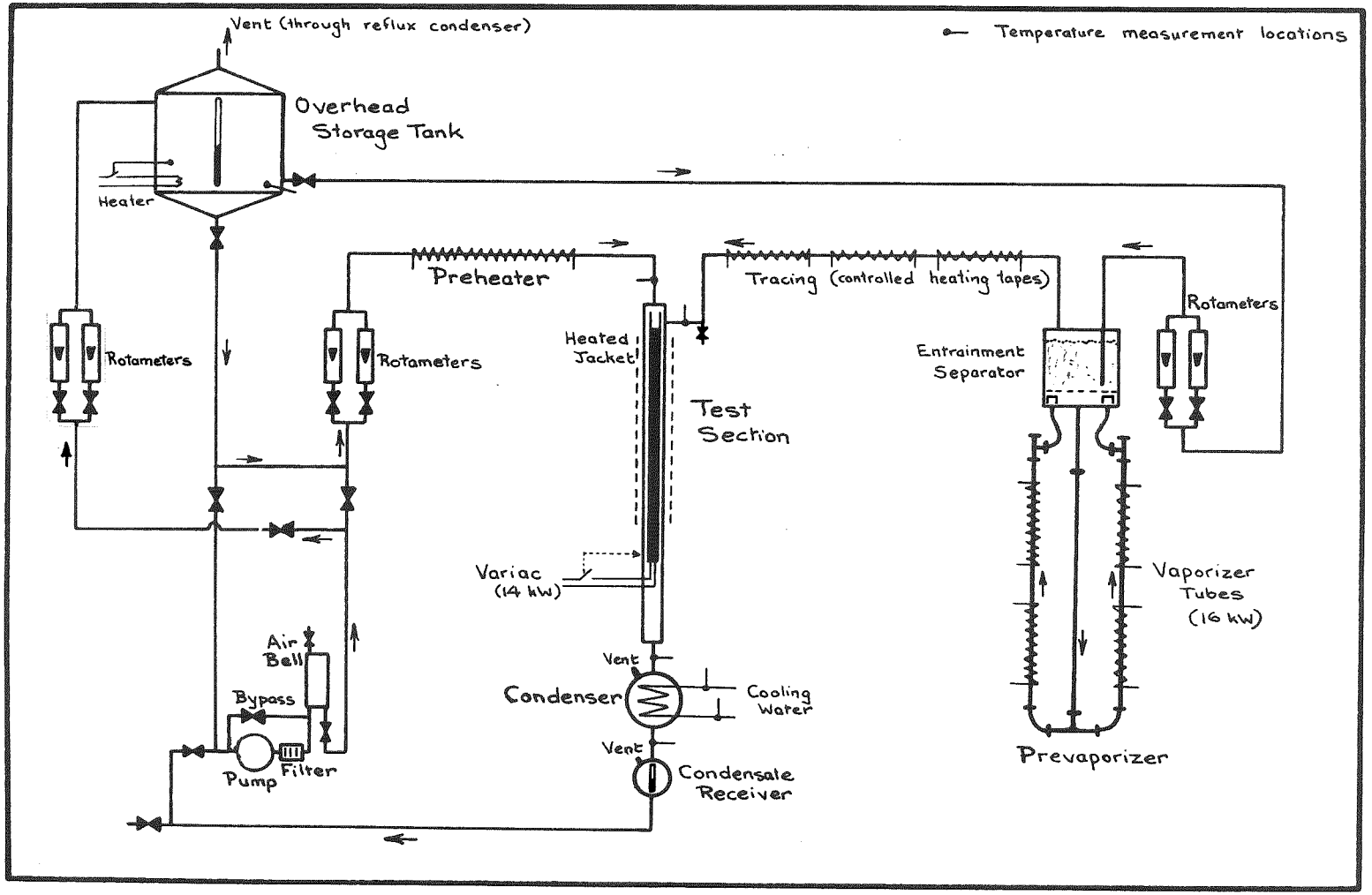

Figure 3 FLOWSHEET : FALLING FILM EVAPORATOR

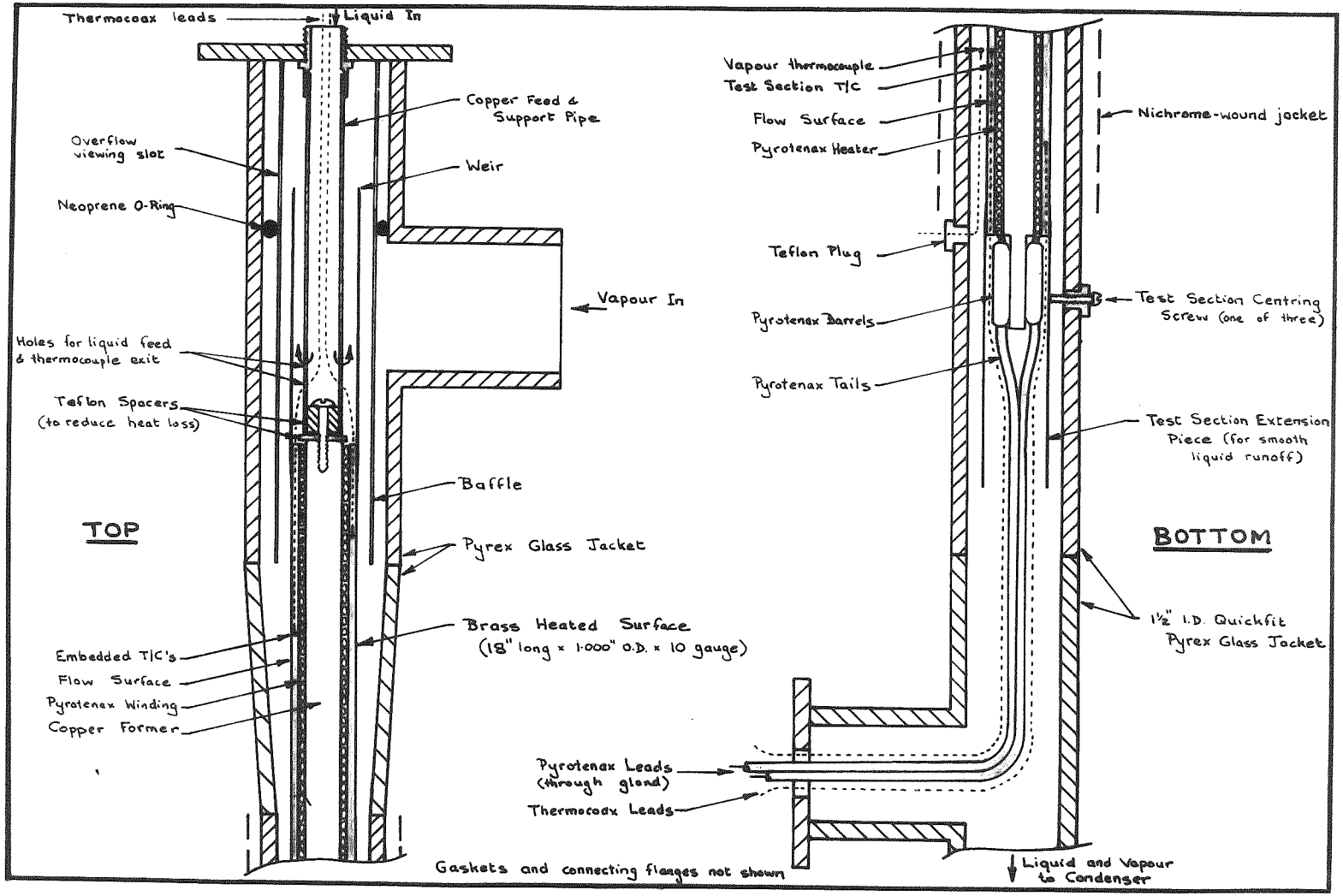

Figure 4

CROSS-SECTION OF FALLING FILM TEST SECTION

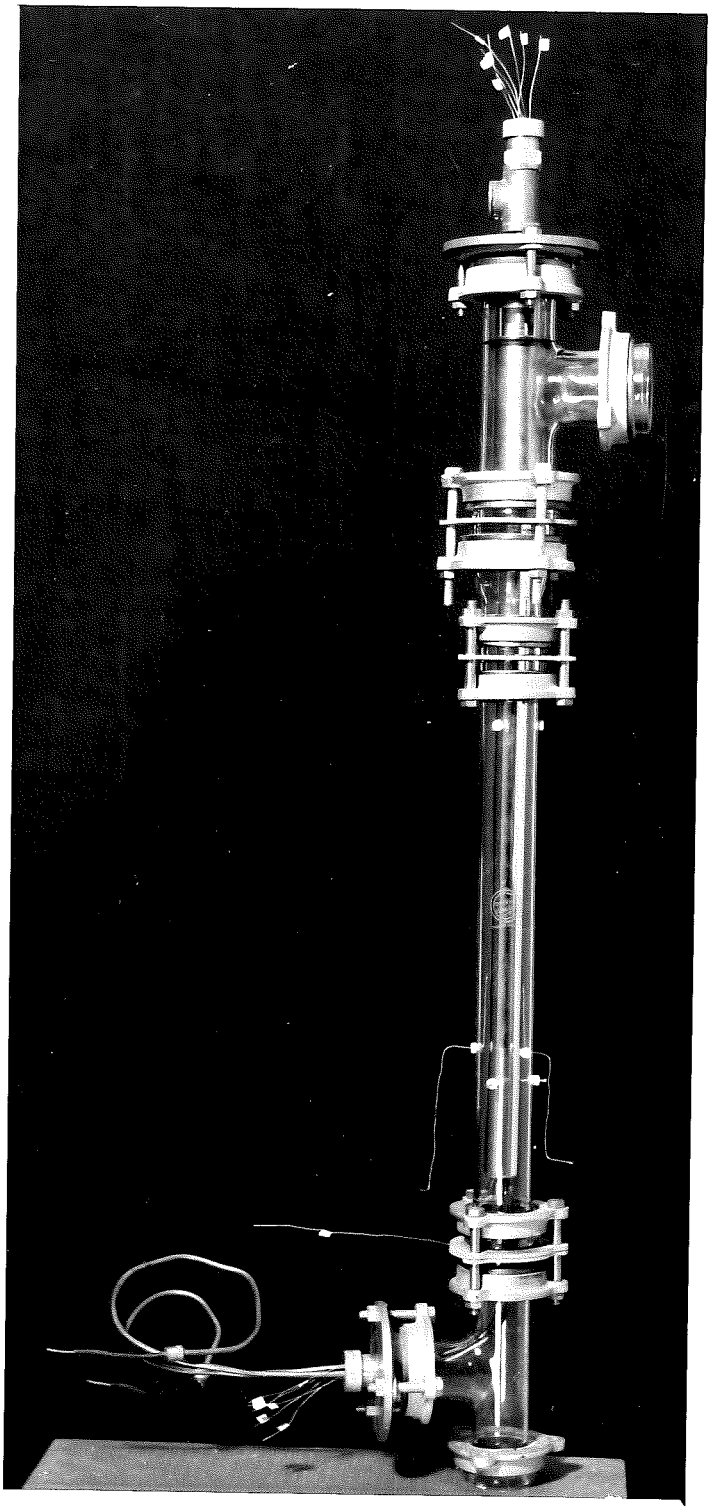

Figure 5A THE TEST SECTION

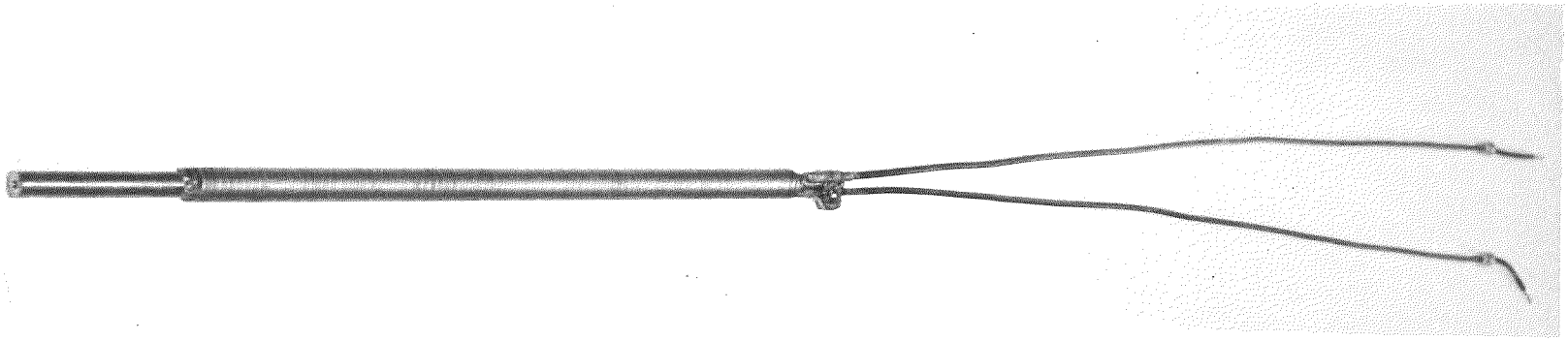

Pyrotenax-wound former

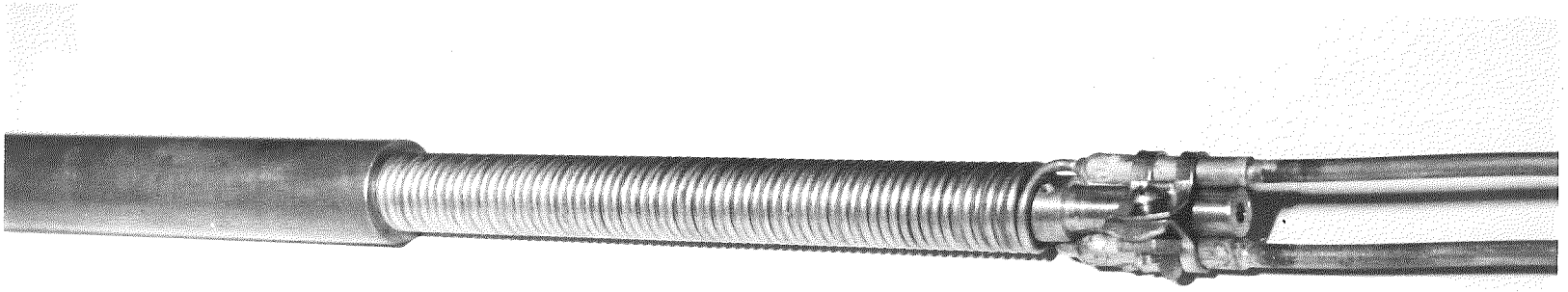

Pyrotenax winding partly inserted in brass tube

Figure 5B DETAILS OF ASSEMBLY OF TEST SECTION

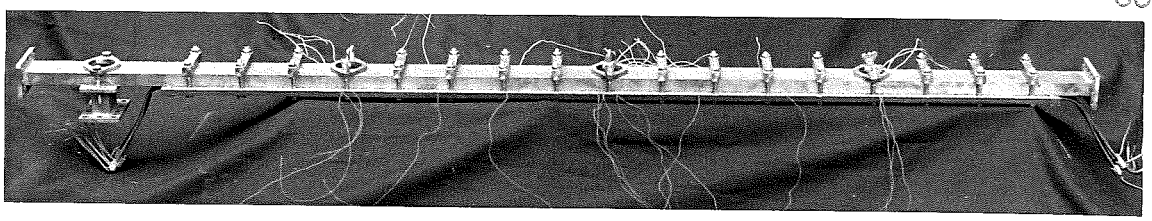

Overall view

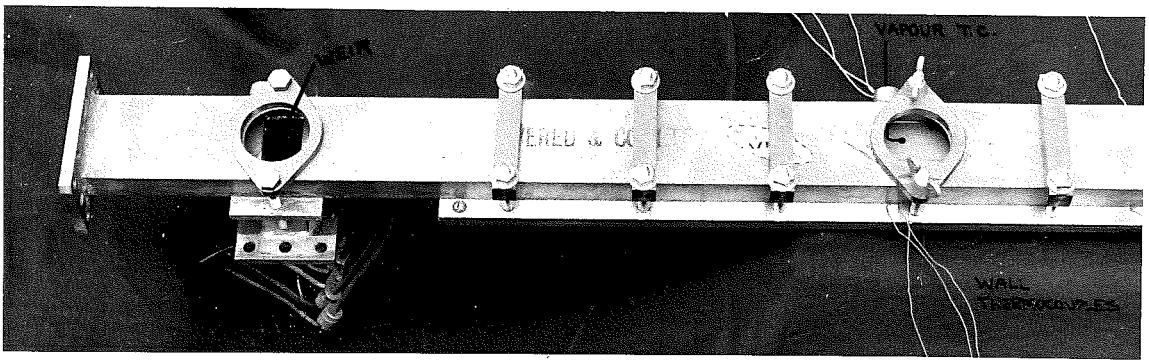

Details of windows, heating plate and thermocouples

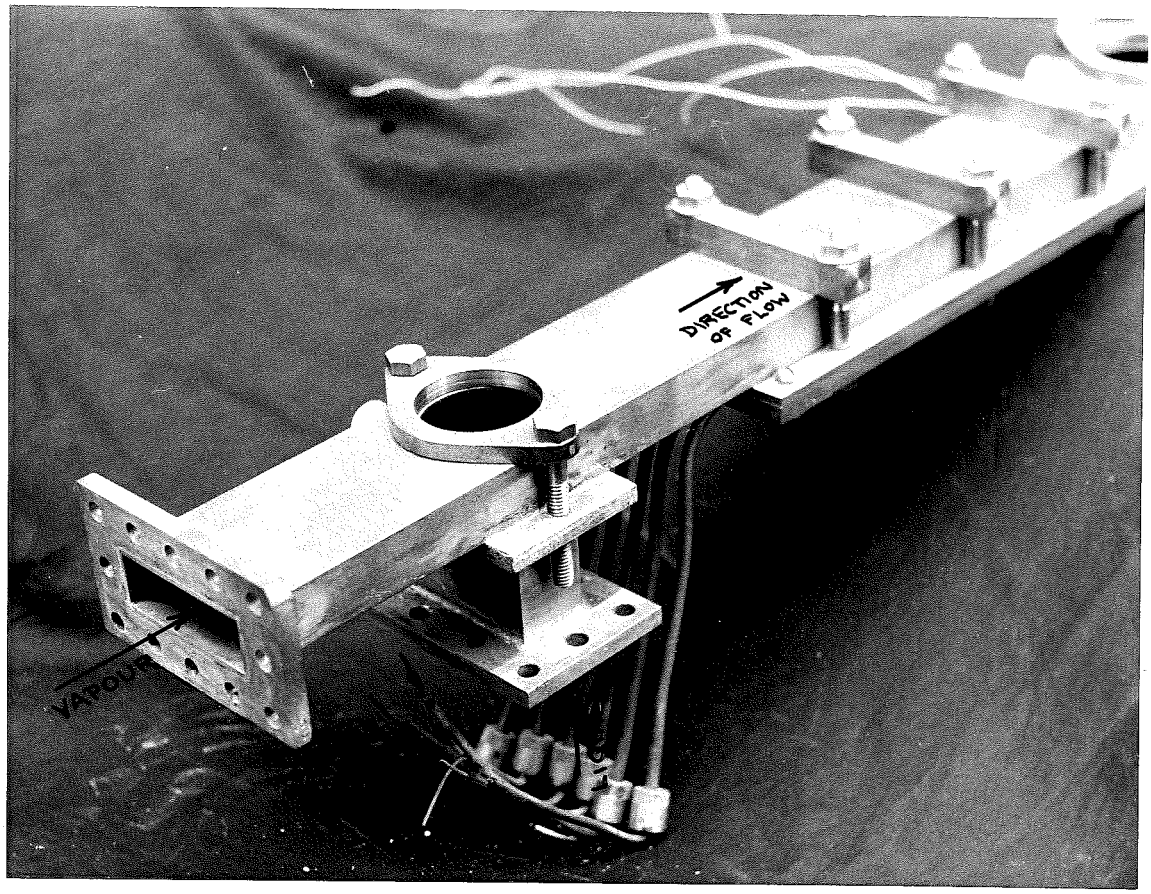

Closeup — Feed end of test section

Figure 6 INITIAL TEST SECTION

4. EXPERIMENTAL WORK

A series of 336 experimental runs was carried out with the brass test section for five test liquids. Each run consisted of a number of readings at various heat flux inputs for a particular combination of liquid and vapour flow rates. In all, 1723 experimental determinations were made, and these results are tabulated in Appendix I.

4.1. Test Liquids

The five test liquids which were used are ethyl alcohol, methyl alcohol, iso-propyl alcohol, water and chloroform.

Details of the purities and sources of the test liquids are given in the following table.

Test liquid	Source	Specification	Purity
Ethyl Alcohol	C.S.R. Chemicals	-	99.8%, remainder 0.2% water, trace of benzene
Methyl Alcohol	I.C.I.A.N.Z.	B.S.506:1958	98.5%
iso-Propyl Alcohol	Shell Chemicals	B.S.1595:1957	99.5%
Water	Laboratory still	-	Pure
Chloroform	May and Baker	British Pharmacopoeia	98-99%, remainder 1-2% ethyl alcohol

The physical properties of the pure test liquids at their boiling points are tabulated in Appendix II. Any departure from these values for the properties of the slightly impure test liquids should be negligible for calculation and correlation purposes. The liquid properties were evaluated at the saturation temperature for simplicity, and because the difference between the properties at the wall temperature and at the saturation temperature is small for moderate temperature differences (see Section 2.2.3).

Agreement between sources of physical data was satisfactory for all data except the thermal conductivities of ethyl alcohol and iso-propyl alcohol. The quoted sources for these two liquids are in good agreement, but deviations from these quoted values of up to 20% were apparent with some of the other published conductivity values (Reference 6 for ethyl alcohol, Reference 45 for chloroform).

From quoted accuracies and from observed agreement between sources it is estimated that all of the physical data are accurate to within ±3%, except for the thermal conductivity data, which should be accurate to within ±5%.

4.2. Experimental Procedure

Before each series of runs with each of the test liquids the main rotameters and thermocouples were recalibrated for the operating temperature conditions.

The liquid feed rotameter and the total flow rotameter were calibrated by weighing timed flows of test liquid preheated to the normal feed and recycle temperatures of about 5-10 F° below the boiling point.

Calibration of feed and surface thermocouples relative to the vapour thermocouples was carried out at the boiling point of the test liquid by the introduction to the test section of saturated vapour generated in the prevaporizer. For these calibrations the liquid feed thermocouple was removed from its inlet location and was inserted into the jacket in the region of the vapour thermocouples.

For each run operating conditions were attained as follow:

(1) preheat of the test liquid in the storage tank was attained,

(2) the liquid flow was set, and its preheat was adjusted to the limit fixed by the necessity to avoid bubble generation in the preheater,

(3) the liquid and power inputs to the prevaporizer were set, and the power was adjusted until the vapour flow as indicated by the difference between total flow and feed rotameters was as required,

(4) the condenser cooling water was set to give a condensate subcooling of about 10 F°,

(5) the heating tapes on the vapour delivery line were

adjusted,

(6) the power input to the nichrome jacket winding was adjusted to maintain the jacket space at the boiling temperature,

(7) the set point of the surface over-temperature cutout was adjusted to about 20 F^{o} above the maximum expected surface temperature,

(8) heat fluxes were then set progressively. The minimum heat flux which was used was fixed at least equivalent to the heat input required to raise the subcooled liquid to its boiling point at the test zone.

After a time for stabilization, readings were made of rotameters for feed liquid, total flow, and condenser cooling water, the wattmeter, the feed thermocouple, the twelve surface thermocouples, the three vapour thermocouples, and the condenser cooling water control temperatures. Variac settings for the jacket heater, the preheater, and the prevaporizer, and also the mains voltage, and the ambient temperature, were recorded as a guide for settings with subsequent runs.

Stabilization times of about an hour at start up, and about a quarter to half an hour between flux settings were adequate for non-nucleation runs. Both visual observation and monitoring of thermocouples were used to detect stability. For runs which extended into the nucleation

regime further stabilization times at the onset of nucleation of about 1½-2½ hours were required for a steady nucleation pattern to be attained, and for surface temperature drift to cease. With subsequent settings in the established nucleation regime about an hour was satisfactory to ensure stability.

From the readings, vaporization within the test section was calculated, and the liquid and vapour flows at the test zone were corrected for this vaporization. In addition, the potentiometer and wattmeter readings were corrected and converted to temperature difference and heat flux values. Hence the local heat transfer coefficient corresponding to the local liquid and vapour flow rates was calculated. The calculated heat transfer coefficients were rounded to the nearest 5 for $h < 500$, and to the nearest 10 for $h \geqslant 500$. Typical calculations are presented in Appendix III.

4.3. Presentation of Results

The experimental data are tabulated fully in Appendix I. Most of these data are presented or summarised in Figures 7-36 (Pages 113-134).

The results for ethyl alcohol and chloroform, which were the main test liquids used to study the nucleate regime and the effect of vapour flow respectively, are

presented in full to show the method of plotting which was adopted.

Ethyl alcohol results are shown in Figures 7-10, as heat transfer coefficient versus temperature difference, for fixed liquid feed rate with vapour feed rate as a parameter. The effects of short-term and long-term variations in the nature of the brass surface also are included.

Distinction must be made between the term "feed rate", as used above, which is the rate of flow at the entry to the test section, and "flow rate", which will be introduced below, which is the local rate of flow at the test location (i.e. "feed rate" corrected for vapour generation up to the test location).

In Figures 11-14 the results from Figures 7-10 for low temperature differences have been replotted to clarify the effect of vapour flow rate on the heat transfer coefficient. To facilitate comparison by reducing the plots to the same axes, the measured heat transfer coefficient, h_{LV}, which corresponds to a local liquid and vapour flow rate of L lb/hr and V lb/hr respectively, was divided by h_L, the coefficient which would have been encountered for liquid flow, L, with negligible vapour flow. For comparison Figures 11-14 have been summarised as a composite plot, Figure 15.

The data for h_L were obtained from Figure 16, in which the heat transfer coefficient, measured for low temp-

erature differences and negligible vapour flows, has been replotted versus the liquid flow rate using the data presented in Figures 7-10. Additional fill-in results obtained at intermediate flow rates, and tabulated fully in Appendix I, are also included in Figure 16.

Similar plots of data for chloroform are presented in Figures 17-27. Runs were not extended into the nucleate boiling regime for chloroform. The results for the effect of liquid and vapour flow rates are summarised in Figures 26 (composite plot of Figures 17B-25B) and 27, respectively.

For the remaining test liquids, methyl alcohol, iso-propyl alcohol and water, summary plots for the effect of liquid and vapour flow rates are presented as Figures 28-33.

4.4. Discussion of Results

Inspection of Figures 7-16, which present a complete set of results for ethyl alcohol, and comparison with the results for the other test liquids, show that a number of regimes may be observed in the falling film evaporator. In general, agreement with previous workers is found.

At low temperature differences the heat transfer coefficient is dependent almost entirely on the liquid and vapour flow rates and properties. As would be expected from the results of previous workers, laminar, transitional, and

turbulent flow regimes are encountered for liquid flow, and the transition occurs as a continuous variation. Also, it is found that there is a critical vapour velocity, below which the effect of interfacial shear on the film coefficient is small, but beyond which the coefficient increases approximately proportionally with vapour flow rate. Thus the flow effects are identical to those which have been observed for condensation, but differ in some respects from the observations of Staker for falling film evaporation.

For higher temperature differences, beyond a critical value which is dependent on the liquid properties and on the condition of the surface, nucleate boiling occurs, and becomes the predominant heat transfer mechanism.

4.4.1. Nucleate Boiling

4.4.1.1. Variability of the Surface

At the start of the series of tests the brass flow surface was still essentially in the as-polished state (Section 3.3.3.), although some ageing by prolonged boiling during preliminary trials had been carried out, and close agreement of nucleate boiling results at various vapour feed rates for a particular liquid feed rate was obtained (see Figures 7, 8). The surface became slightly blackened due to overheating when the results for the nucleate boiling regime

were almost complete, and a shift of the group of nucleate boiling lines along the temperature axis occurred (compare e.g. Figures 8A and 8B). A subsequent overheat resulted in considerable blackening of the surface and again the critical temperature difference decreased (e.g. see Figures 7 and 8).

With this variability of the surface it was apparent that only qualitative observations for the nucleation regime were justified. This conclusion was confirmed by reproducibility checks carried out nine months after the original tests (see Figure 8), which showed an increase in the critical temperature difference.

The period of nine months after the commencement of the tests corresponded to the following number of actual operating hours:

(1) approximately 1100 hours after start up with the polished surface, i.e.

(2) approximately 1000 hours after the occurrence of the slight surface blackening, i.e.

(3) approximately 850 hours after the surface was fully blackened (due to severe overheating).

Results obtained for ethyl alcohol during the short series with the copper version of the final test section, which subsequently burned out, showed an increase of critical temperature difference after extreme surface oxidation of the already aged surface. The degree of this surface blackening

was visibly much worse than for the accidentally-oxidised brass surface.

The observation of an initial decrease of the required superheat is contrary to the conclusions of previous workers (25, 47f, 84) who observed only that an increase of superheat was required as ageing progressed.

It is proposed that the initial decrease may be explained by Bankoff's nucleation analysis (5), which predicted that the air or vapour bubbles which would be entrapped in surfaces with cavities would be substantially larger than those which would be entrapped in grooved surfaces. Thus it would be expected that lower superheats would be required for surfaces with cavities.

The method of preparation of the heat transfer surface for the present investigation (polishing by rotary action in a lathe) resulted in fine circumferential grooves. This surface finish is contrary to the pattern of intersecting grooves (an approximate pit or cavity distribution) which results from normal polishing of a flat surface.

Bankoff also suggested that oxidised surfaces may contain cavities rather than grooves. This would follow because any local surface depositions of oxide must tend to reduce the length of grooves formed during fabrication.

Thus it would be expected that initial oxidation for the special case of the tube polished in the circumfer-

ential direction would result at first in improved nucleation conditions. However, once conditions of pit distribution were approximated, subsequent oxidation would be expected to result in a reduction of the size of the pits and the deposition of a general surface oxide film across which a temperature difference would exist. Both of these effects would require greater surface temperatures for bubble nucleation, which is as was encountered for the severely oxidised copper surface and for the moderately oxidised and the aged brass surface. These latter observations are in agreement with those of Corty and Foust (25).

4.4.1.2. Visual Observation

Visual observation showed that for the polished surface the distribution of the nucleation sites was approximately uniform, and the experimental results (e.g. Figures 7A, 8A) indicated that the onset of nucleation occurred at a sharply-defined critical temperature difference.

However, as surface ageing progressed, nucleation tended to occur in patches, and temperature differences well beyond the "normal" critical temperature difference were required to initiate these nucleation areas (compare Figures 7A and 7B, at the lower vapour feed rates).

For this extended transition regime the nucleation areas tended to be longitudinally elongated in shape, rather

than circumferential, and extended periods were required (see Section 4.2) for the size of the patches to stabilize, and for surface temperature drift to cease.

Generally the definite straight-line relationship between heat transfer coefficient and temperature difference on the logarithmic plot was not attained until heat flux had been increased sufficiently for nucleation to become approximately evenly distributed around the flow surface.

The range over which the nucleate regime could be studied was limited by this necessity to overshoot the critical heat flux for a stable nucleation pattern to be achieved. Upon nucleation, this overshoot resulted in stabilization at conditions well beyond the lower part of the nucleate boiling line. An upper limit to the usable heat flux also was set by the tendency for the liquid film to be lifted from the wall at the boiling patches, and to lead to dry spots similar to the effect observed by Leidenfrost (58). With this limited nucleate boiling regime the value of the ΔT exponent (given by the slope of the shortened nucleation line) became less certain.

For small or nil vapour feed rate, often a uniform nucleation pattern could not be attained before the upper flux limit was reached. Thus it was possible to have intense nucleation patches which affected one or two of the surface thermocouples, yet which were not truly representative.

Higher vapour flow rates generally respread the liquid film when dry wall conditions tended to occur with the Leidenfrost-type effect, and it was possible to work with higher heat fluxes and truer nucleation patterns at the higher vapour feed rates.

Despite the uncertainties, the observed critical temperature differences for both ethyl alcohol and methyl alcohol were about 20-30 F°, which are in general agreement with Staker's values of 25 F° and 23 F° respectively. However the observed slopes for the aged surface are about twice Staker's observed values of 4-5, although the slopes for the fresh surface do lie in the range 4½-7½.

Visual observation by means of the transparent jacket also proved useful during hysteresis runs carried out with the copper tube surface. Agreement was found with Staker's observation that higher heat transfer coefficients were obtained for a given temperature difference in the nucleation regime when the final heat flux was approached from above. Visual observation showed that overheating led to initiation of nucleation sites which remained as sites upon reduction of heat flux. Approach to final flux from below was observed to produce neither the number nor the uniformity of distribution of sites. This is as was proposed by Staker, but in his case visual confirmation was not possible.

4.4.1.3. Effect of Feed Rates on Nucleate Boiling

Comparison of nucleate boiling lines for the fresh surface in Figures 7A, 8A and 10A, and comparison of the clusters of lines for the blackened surface in Figures 7B-10B, show no apparent effect of liquid feed rate upon the critical temperature difference for the onset of nucleation, within the limit of uncertainty of these lines.

The distribution of individual nucleation lines within the clusters of lines for various vapour feed rates in Figures 7B-10B might suggest some effect of vapour feed rate. However closer examination shows that some of the lines are located out of "order" (particularly for the lower vapour feed rates), and reproducibility is not good (e.g. lines for approximately 40 lb/hr in Figure 8B, and lines for approximately 20 lb/hr in Figure 9B).

The results for the blackened surface presented in Figures 7B and 8B suggest that the nucleation lines for various vapour feed rates tend to converge at high heat fluxes, for which visual observations showed an increase in the uniformity of nucleation distribution. Extension to sufficiently high heat fluxes to check this convergence was not possible due to the onset of Leidenfrost-type partial dry wall conditions. This lack of dependence on the vapour flow rate is also seen with the results for the fresh surface (e.g. Figures 7A, 8A and, to a lesser extent, Figure 10A),

for which nucleation was uniform.

Norman and McIntyre (65) also observed this convergence of results for falling film boiling heat transfer to give a common line independent of liquid flow rates at the higher temperature differences, and Collier (22) showed the converged results of Norman and McIntyre to be in good agreement with a submerged surface nucleate boiling curve.

It is concluded that at supra-critical temperature differences in the falling film evaporator the contribution to heat transfer by the nucleate boiling mechanism (e.g. the vapour-liquid exchange mechanism of Forster and Greif (35), i.e. the pumping of superheated liquid by the growing bubbles) considerably predominates over the effect of eddy transport induced by turbulence caused by liquid and vapour flow.

4.4.2. Effect of Liquid Flow Rate

Figures 16, 27, 29, 31 and 33 show the effect of liquid flow rate on the falling film heat transfer coefficient for the five test liquids. The best fit for the data generally was obtained with a smooth curve which terminated in straight lines. For the case of small flows with ethyl alcohol (Figure 16), for which scatter of the data was encountered, a mean squares line was fitted. The calculated slope of this mean squares line is in good agreement with the average of the slopes for the straight lines obtained with

the four other test liquids. The curves are compared in Figure 34.

The data were obtained at sub-critical temperature differences for conditions of liquid feed alone, with the only flow of vapour being that generated within the test section. Inspection of results plotted as Figures 7-10 shows that small vapour feed rates have little effect on the observed heat transfer coefficient, and this is emphasized in Figures 11-14 replotted from these results. Therefore the plots indicate the separated effect of liquid flow rate.

Reproducibility checks were carried out for the fresh surface and for the blackened surface, and repeats were made on the surface aged after nine months. The results are superimposed on the original data in Figures 7-10. It can be seen that reproducibility is usually well within ±10%. This agreement shows that the experimental technique was satisfactory. The reproducibility also indicates that the surface variation which occurred with ageing, which was indicated by visual observation and by the considerable variation in the results for the nucleate boiling regime, was small enough to lie within the laminar sublayer, and hence to cause no effect on the results for turbulence-controlled falling film heat transfer.

The curves show laminar, transitional and turbulent regimes. The slope of the lines in the laminar regime is

approximately $-1/3$ as predicted by Nusselt. The slope for the turbulent regime is less definite because of the short turbulent flow rate range which could be studied. In an attempt to extend the liquid flow rate range, flows up to the limit which would remain on the tube were used, provided that the film turbulence (apparently) introduced by flow over the weir was not gross. The observed trends and the scatter at the highest flow rates (Figures 16, 29, 31, 33) show that the heat transfer results obtained under these conditions are suspect. Further discussion will be deferred until Section 5.2.

Visual observation showed rippling of the liquid film over the whole flow range down to the lowest Reynolds number, Re = 200, which could be studied. This is as would be expected from predictions for the onset of rippling (Section 2.1.1.). Also, as would be expected, no nucleation was apparent, so that evaporation appeared to occur from the surface of the falling film alone.

Contrary to the conclusion of Staker it was not found to be necessary to correct the results for temperature difference, provided that the liquid feed rate was corrected for vaporization. The apparent temperature difference effect for the h vs. ΔT data in the surface evaporation regime results from a decrease in liquid flow caused by the increased vaporization at the higher heat fluxes and temperature

differences. This leads to an increase of coefficient with temperature difference for the laminar regime, and a decrease for the turbulent regime, which is very well shown with the results for chloroform (Figures 17A-25A), for which vaporizations were large because of the lower latent heat of vaporization of chloroform.

The observed variation of heat transfer coefficient with liquid flow rate holds only for low vapour flow rates. At higher vapour flow rates the slopes and the critical liquid flow rate change because of the varying vapour-liquid interaction. This is shown in Figures 35 and 36, replotted from the experimental data, and it will be discussed further in the next Section.

4.4.3. Effect of Vapour Flow Rate

The vapour flow data for the five test liquids are summarised in Figures 15, 26, 30, and 32, which are replotted from the relevant h vs. ΔT data.

It is seen that vapour flow has little effect until a critical flow rate is exceeded beyond which a power law relation, with exponents between 0.83 and 1.1, is found. The usual value of the exponents is about 1.0, which is in good agreement with the value of 0.9 predicted by Carpenter and Colburn.

A reason for the lack of agreement between the vapour velocity exponent found for climbing film flow (0.5, as for spray flow) and that found for condensation (0.9) is provided by the results at high vapour flow rate and liquid feed rate for chloroform in Figures 23B-25B, in which it is seen that a sudden change in slope from about 1.0 to about 0.5-0.6 is found. Visual observation showed that this transition point coincided with the onset of significant entrainment to give misty vapour-liquid flow in the annulus. It would appear that Staker's exponent values of 0.5-0.7 for the falling film evaporator may have been obtained under conditions of uneven liquid distribution around the tube, such that considerable entrainment existed for most of the vapour runs.

The technique of plotting $\frac{h_{LV}}{h_L}$ vs. V does not lead to a common line at supracritical vapour flow rates, nor is there a unidirectional trend with liquid feed rate, thus indicating that there is a significant and variable effect of vapour-liquid interaction.

This variable interaction is shown in Figures 35 and 36, in which the heat transfer coefficient is replotted as a function of liquid and vapour flow rates. The vapour flow rate levels were chosen as those for which most experimental data were available. However in some cases it has been necessary to include fill-in data (labelled "interpolated

data") derived using the plotted $\frac{h_{LV}}{h_L}$ curves.

It is seen that as vapour flow rate increases, the dependence on liquid flow rate decreases, and the onset of turbulence occurs at lower values of the critical liquid flow rate. This latter observation is in agreement with the results of Carpenter and Colburn (16) for condensation with high vapour velocities, but contradicts the calculated curves of Dukler (30, 31, 32), although Dukler's curves do agree with the observed decrease of the effect of liquid flow rate at the higher vapour velocities.

4.5. Estimation of Experimental Accuracy

The accuracy of the experimental results may be estimated by analysis of the observed reproducibility data, by summation of maximum individual errors, and by comparison with other workers.

The first two methods will be considered in this Section. Comparison with previous workers will be deferred until Section 6.1.

Reproducibility data for zero vapour feed conditions for ethyl alcohol are tabulated below. The data are those plotted in Figures 7-10. The results for the whole falling film evaporation regime are tabulated, and the slight effects of vaporization will be ignored.

REPRODUCIBILITY DATA - ETHYL ALCOHOL

Liquid Feed Rate	Run No.	h	$\bar{h}$	R.M.S. Devn. = $\sqrt{\frac{\Sigma(h-\bar{h})^2}{n}}$
30	1 8 33 69 244	200,190,190,195 180,195,195 195,185,185,190 180,180,185,185 175,180,185,185	187	$\pm 6\frac{1}{2}$ ∴ 95% confidence limits approx. $\pm 13\frac{1}{2}$ i.e. $\pm 7\%$
50	9 15 26 54 63 243	180,170,170 165,165,170 175,165,165,170,170 165,165,170,170 165,165,165 165,165,165	168	± 4 ∴ 95% confidence limits* approx. ± 8 i.e. $\pm 5\%$
100	18 27 58 242	170,170,165,165,165,170 170,185,170,170,170 170,170,170,170 175,175,175	171	$\pm 3\frac{1}{2}$ ∴ 95% confidence limits approx. ± 7 i.e. $\pm 4\%$
200	25 71 241	280,270,265,265 265,260,250,260,265 265,265,260,260	264	$\pm 6\frac{1}{2}$ ∴ 95% confidence limits approx. ± 14 i.e. $\pm 5\%$

*Note that experimental h data for this feed rate appear not to follow a normal distribution, apparently because of rounding errors.

The reproducibility results indicate a relative error of well within ±10% for low vapour flow rates.

Few reproducibility checks were carried out at high vapour flow rates, because of the difficulty of setting an exact vapour generation rate. However, repeat runs at

intermediate flow rates were performed for the various surface conditions. Figures 12 and 13, in particular, show the very good consistency which was obtained. Reproducibility again within ±10% is indicated.

The maximum possible absolute error can be estimated by summation of the estimates of error for the individual measurements.

The wattmeter was accurate to ±0.2% full scale deflection, and range selection allowed it to be used at not less than 15% full scale reading. Thus maximum error was ±1.3%. Total error, including reading error, was probably ±2%.

Current and potential transformers were used at the higher heat flux inputs. Class AL instrument transformers were used. This grade is intended to be used as a substandard, and contrary to the performance of industrial instrument transformers the absolute error in the specified ratio does not increase for operation at normal levels below the maximum rating. Thus the maximum error which could be contributed by the instrument transformers was ±0.25% + ±0.15% = ±0.4%.

Errors in the local value of the heat flux could be introduced by longitudinal conduction along the test section, and by heat flux pattern distortion due to the presence of the copper thermocouple sleeves within the brass wall. These errors are estimated to be $< -4\%$ for the longitudinal error

(Appendix IV), and $<+6\%$ for the circumferential distortion error (Section 3.3.5). An overall error of $\pm 6\%$ will be assumed.

The error in the area over which the heat flux is distributed is negligible. However an uncertainty of $\pm \frac{1}{2}\%$ will be allowed to compensate for any uneven distribution of the winding within the tube.

Calibration errors and reading errors for temperature differences each should be within $\pm 5\ \mu V$ for non-nucleation conditions. For the temperature differences given for the falling film regime in the typical calculations (Appendix III) this total error of $\pm 10\ \mu V$ corresponds to $\pm 16\%$ and $\pm 2\%$ respectively. The reading error increases considerably for nucleate boiling conditions, because of the fluctuating surface temperatures, and errors of about $\pm 5\%$ are likely.

A further small error in temperature difference may be introduced by temperature distortion due to the presence of the sleeved thermocouples within the wall, and also by error in the calculated correction to surface temperature for the temperature drop between the thermocouple and the surface. However the wall correction is usually less than 10% of the measured temperature difference for non-nucleation conditions, and the distortion error is unlikely to be more than 5% of this correction (Section 3.3.5), so that the error introduced

into the temperature difference is unlikely to be more than ±½%, even at high heat fluxes.

These error estimates will be summed below to give the maximum expected percentage error in the calculated heat transfer coefficient (63).

ERROR ESTIMATE - FALLING FILM CONDITIONS

Error Contribution	Low Heat Flux	Moderate Heat Flux
Wattmeter error	±2%	±1%
Transformer error	Nil (not used)	±0.4%
Flux distribution error	±6%	±6%
Area uncertainty	±½%	±½%
Temperature difference measurement and calibration error	±16%	±2%
Error in wall correction	Nil	±½%
Total error	approx. ±25%	approx. ±10%

For any run, practically the same value of the heat transfer coefficient is found for low and moderate heat fluxes, particularly if the effect of vaporization is considered. This would suggest that the error estimate of ±25% for low heat fluxes is excessive. However, the value of ±10% appears to be reasonable and this will be checked by comparison with previous workers in Section 6.1.

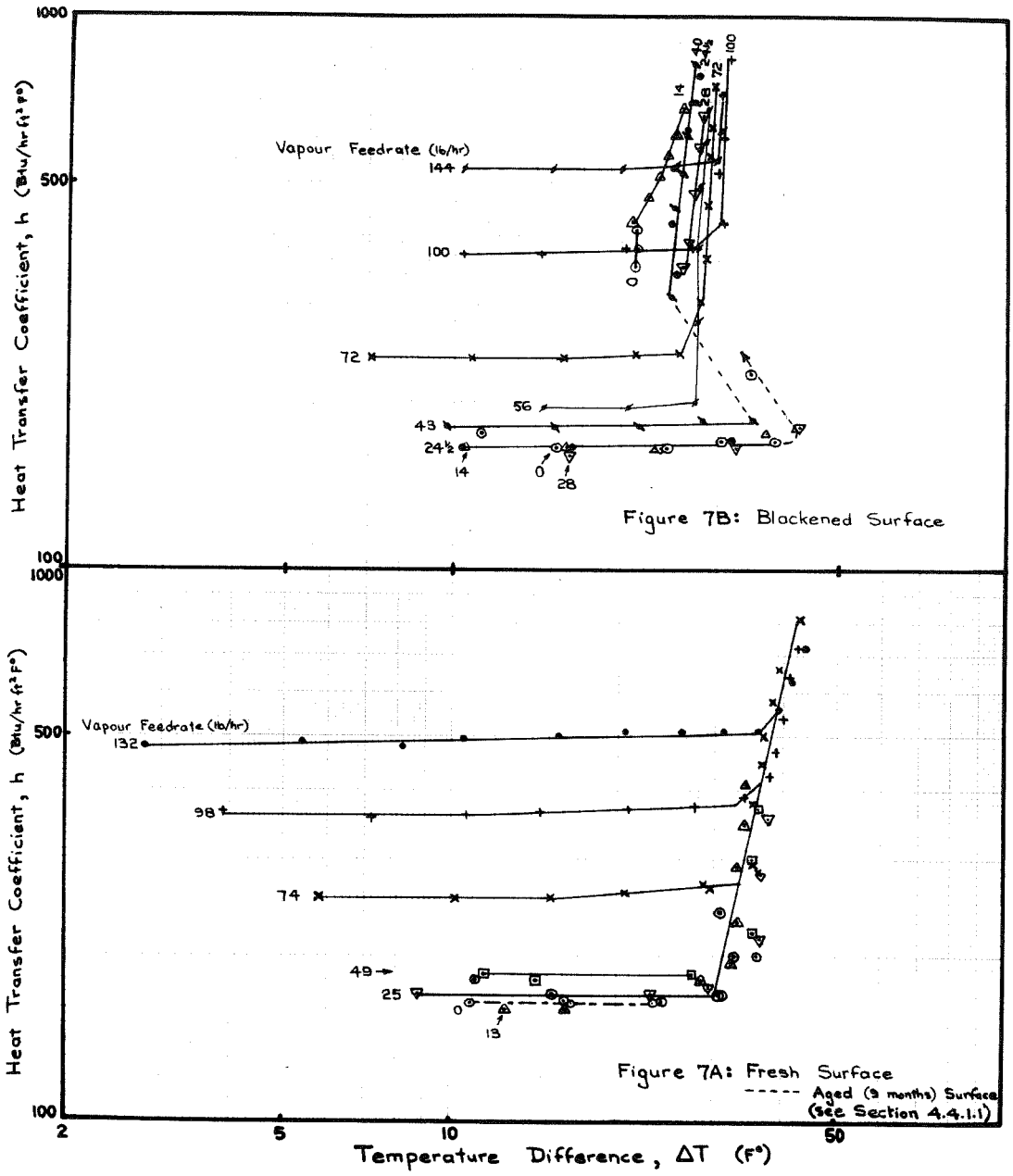

Figure 7 EXPERIMENTAL DATA ETHYL ALCOHOL 50 LB/HR

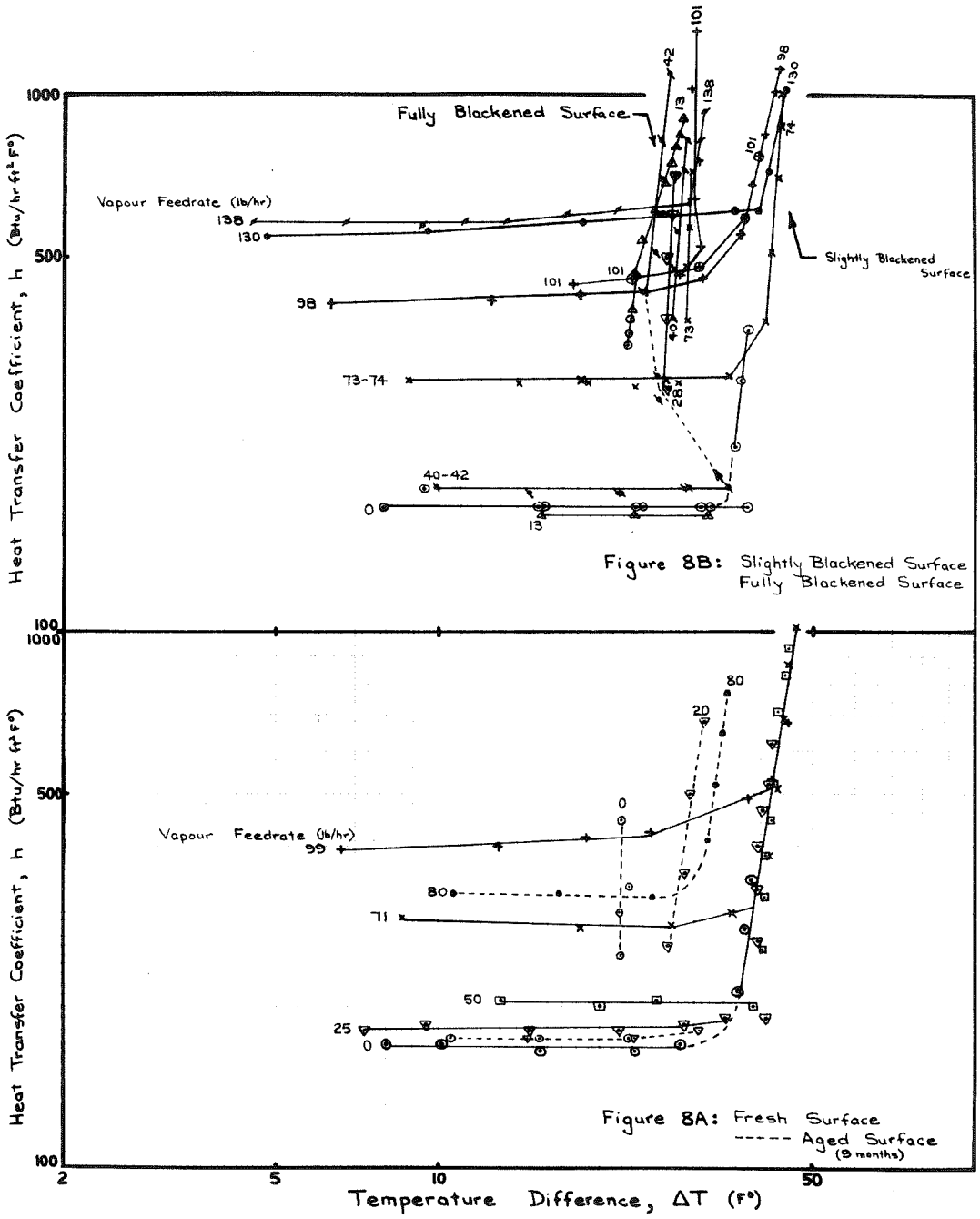

Figure 8 EXPERIMENTAL DATA ETHYL ALCOHOL 100 LB/HR

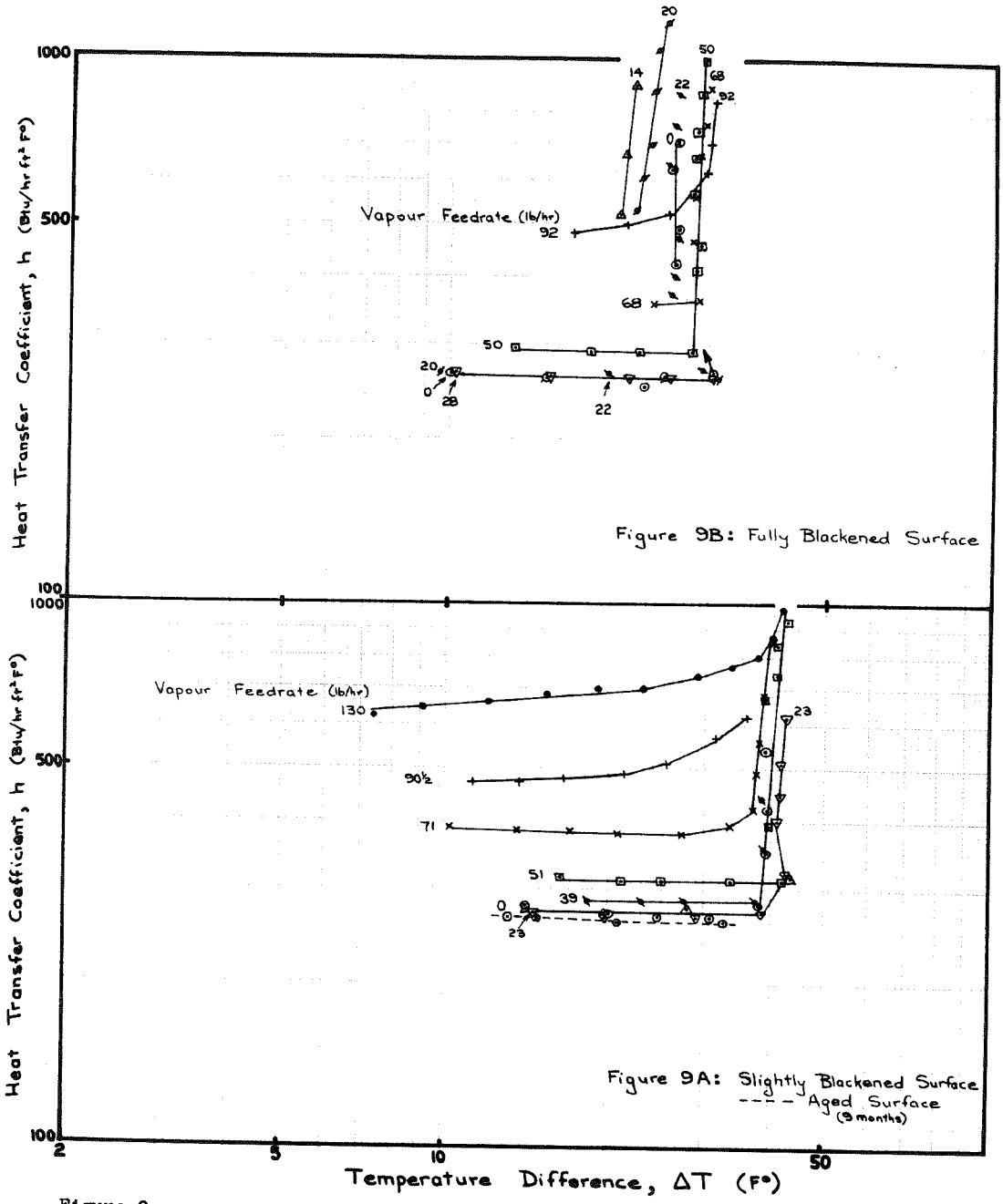

Figure 9 EXPERIMENTAL DATA ETHYL ALCOHOL 200 LB/HR

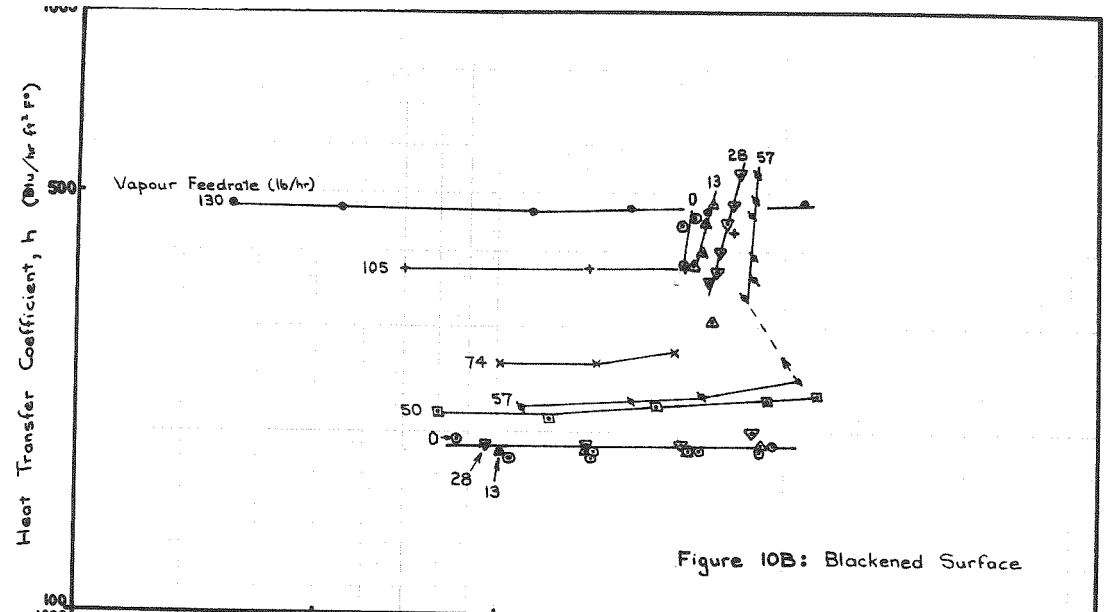

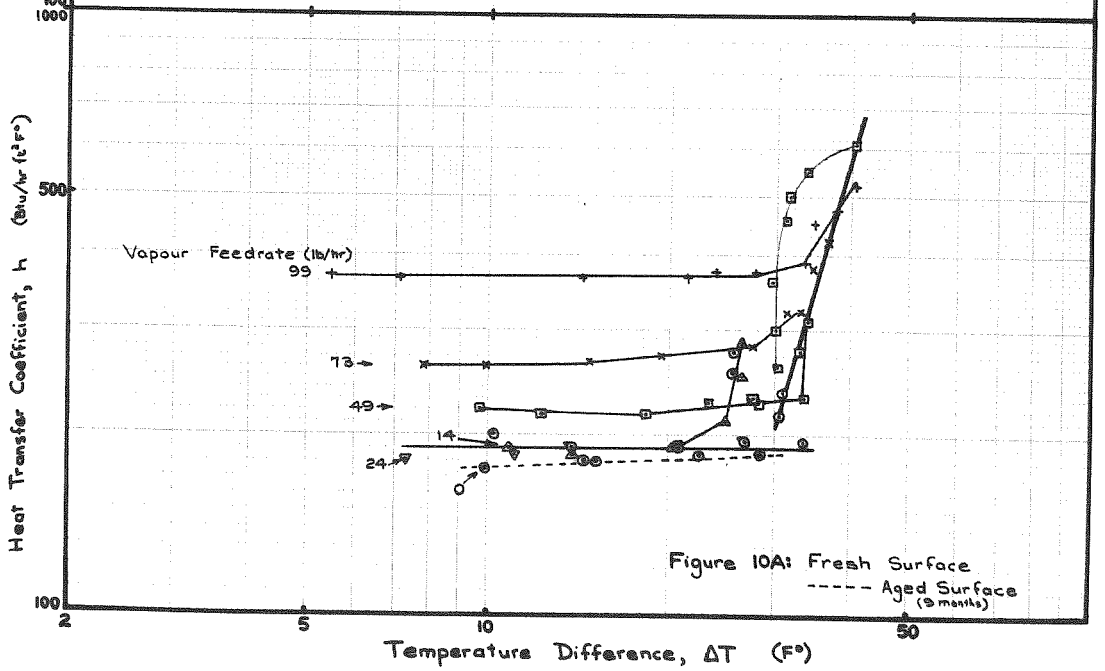

Figure 10 EXPERIMENTAL DATA ETHYL ALCOHOL 30 LB/HR

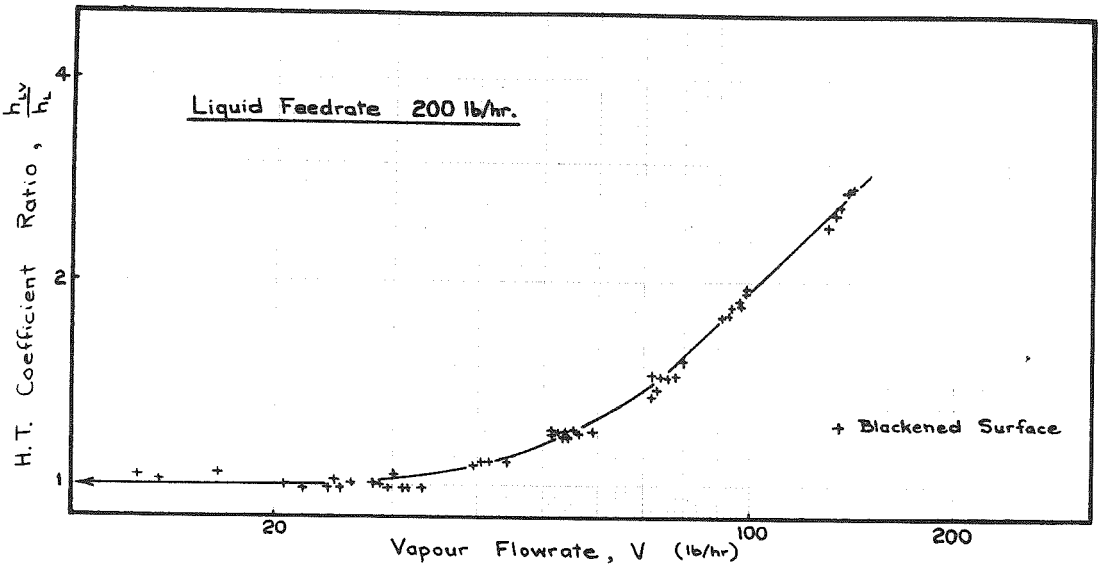

Figure 11 EFFECT OF VAPOUR FLOWRATE ETHYL ALCOHOL 200 LB/HR

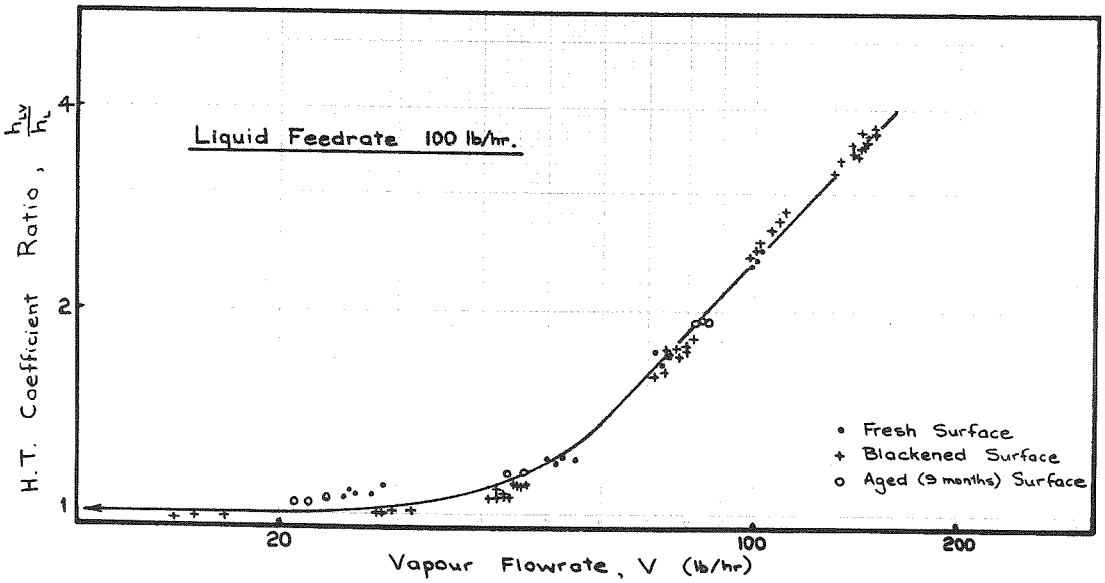

Figure 12 EFFECT OF VAPOUR FLOWRATE ETHYL ALCOHOL 100 LB/HR

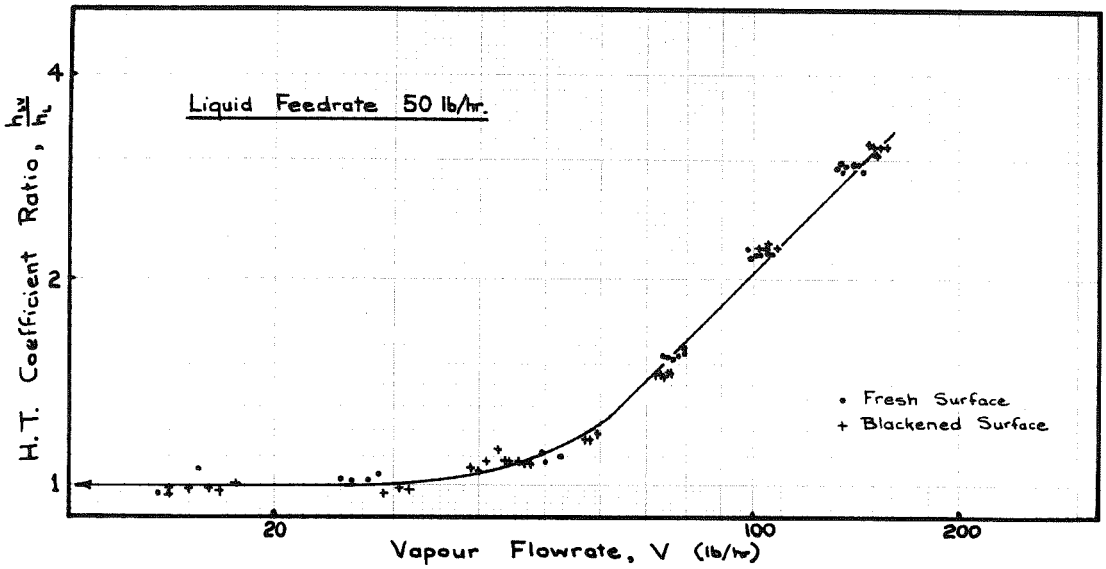

Figure 13 EFFECT OF VAPOUR FLOWRATE ETHYL ALCOHOL 50 LB/HR

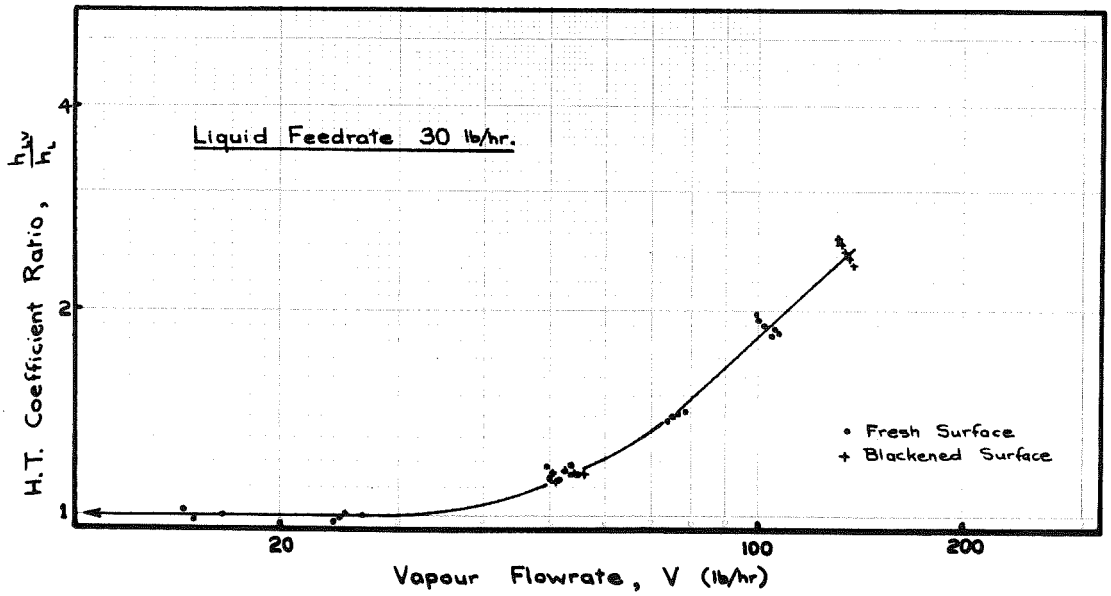

Figure 14 EFFECT OF VAPOUR FLOWRATE ETHYL ALCOHOL 30 LB/HR

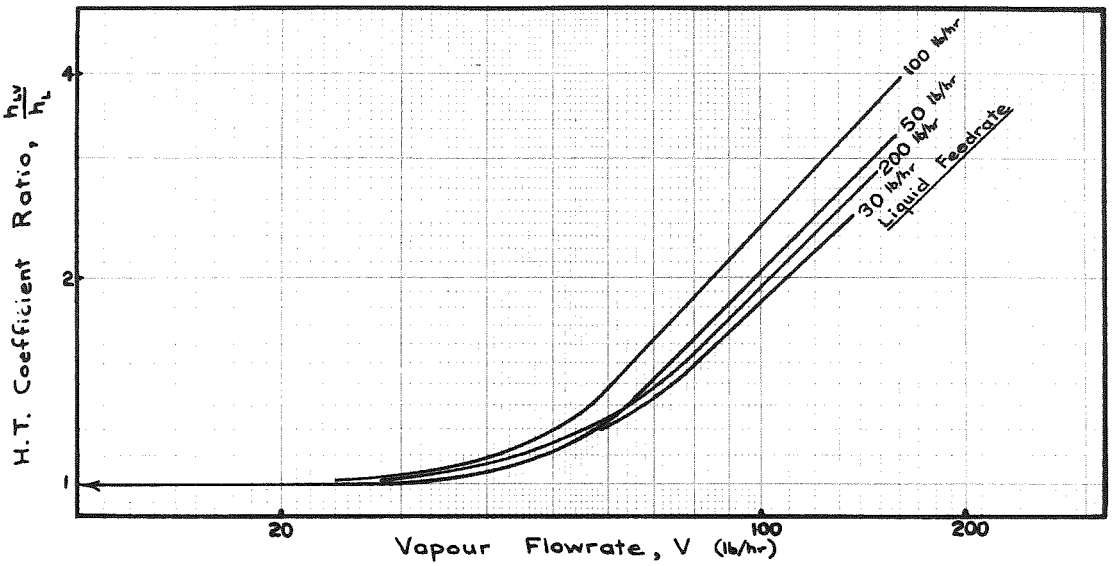

Figure 15 COMPARISON OF EFFECT OF VAPOUR FLOWRATE ETHYL ALCOHOL

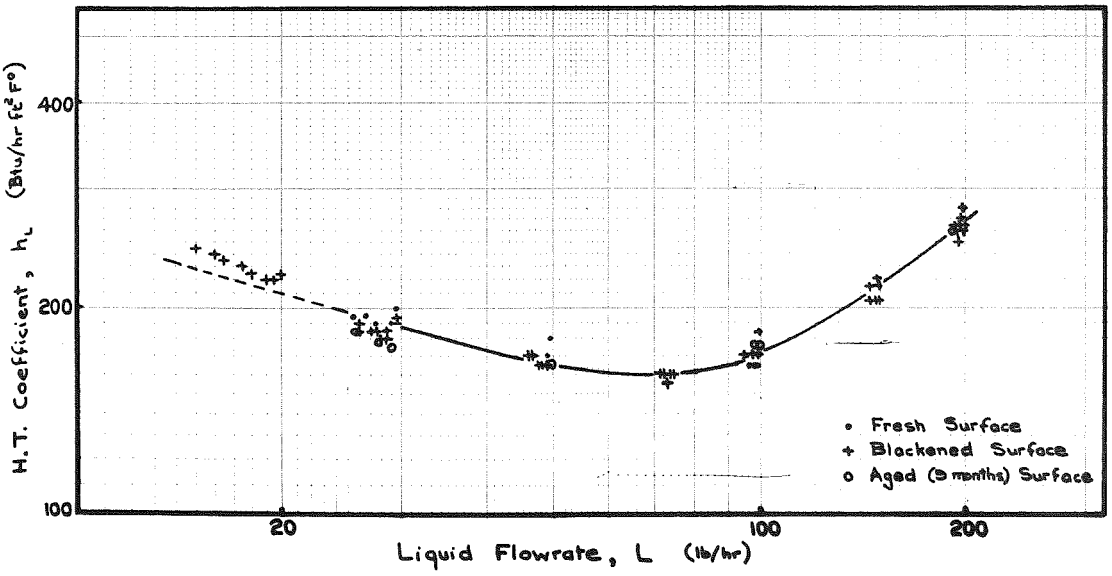

Figure 16 EFFECT OF LIQUID FLOWRATE ETHYL ALCOHOL

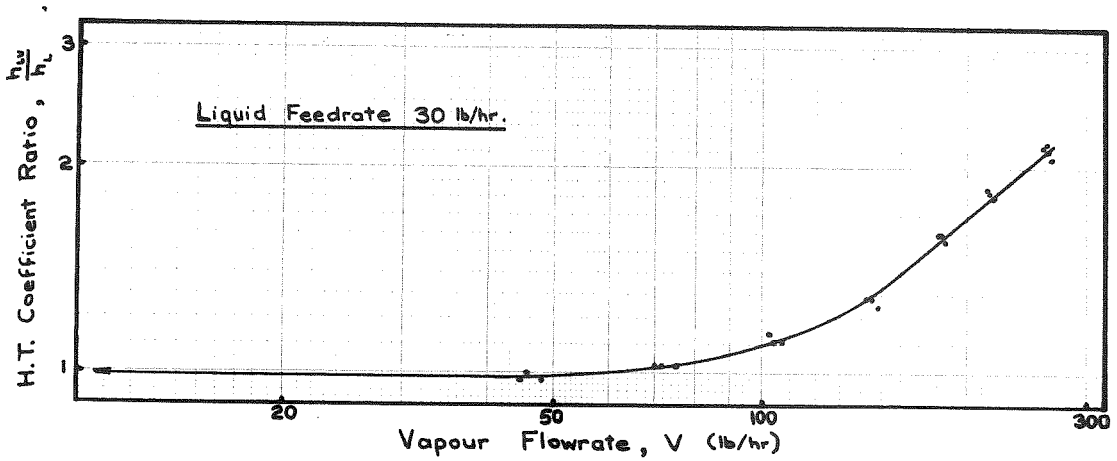

Figure 17B EFFECT OF VAPOUR FLOWRATE CHLOROFORM 30 LB/HR

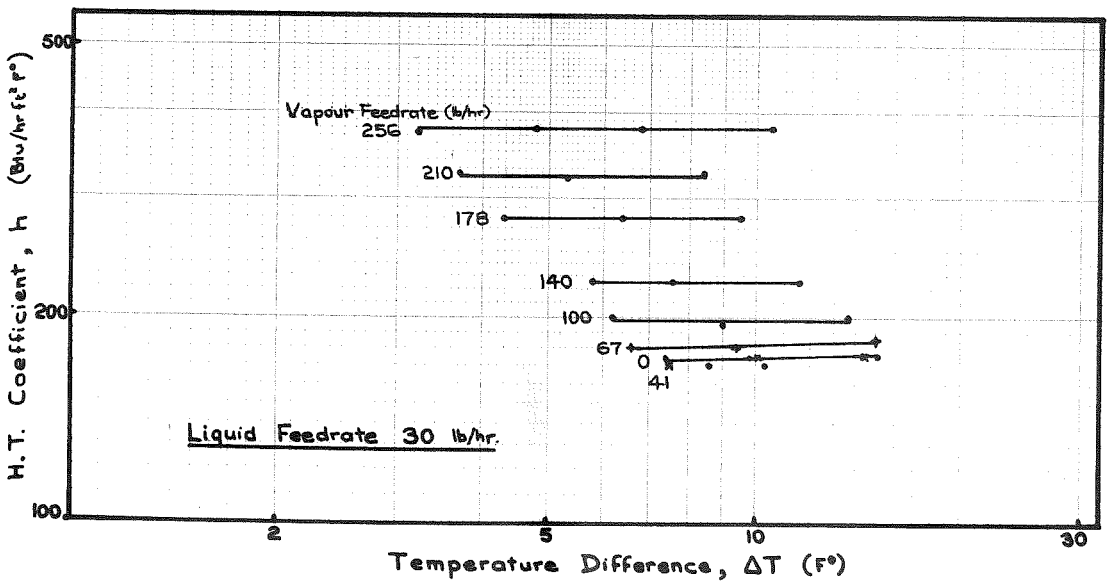

Figure 17A EXPERIMENTAL DATA CHLOROFORM 30 LB/HR

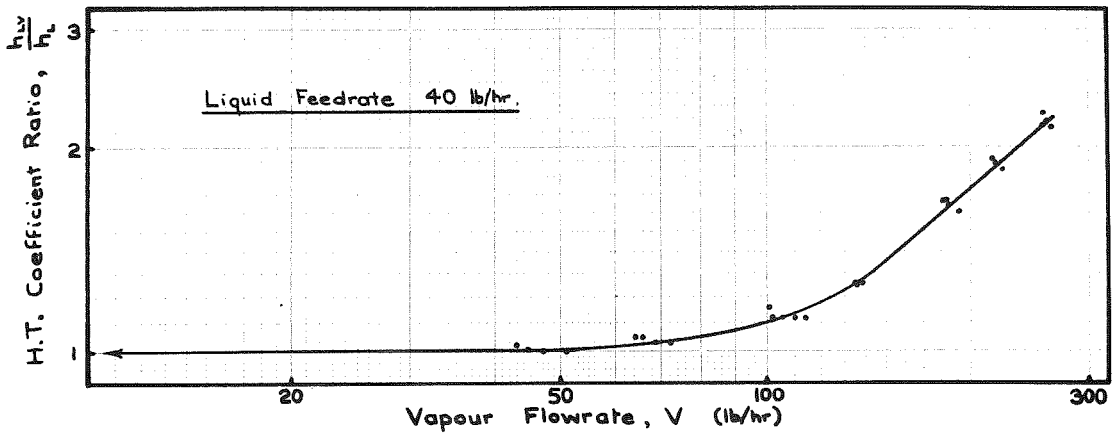

Figure 18B EFFECT OF VAPOUR FLOWRATE CHLOROFORM 40 LB/HR

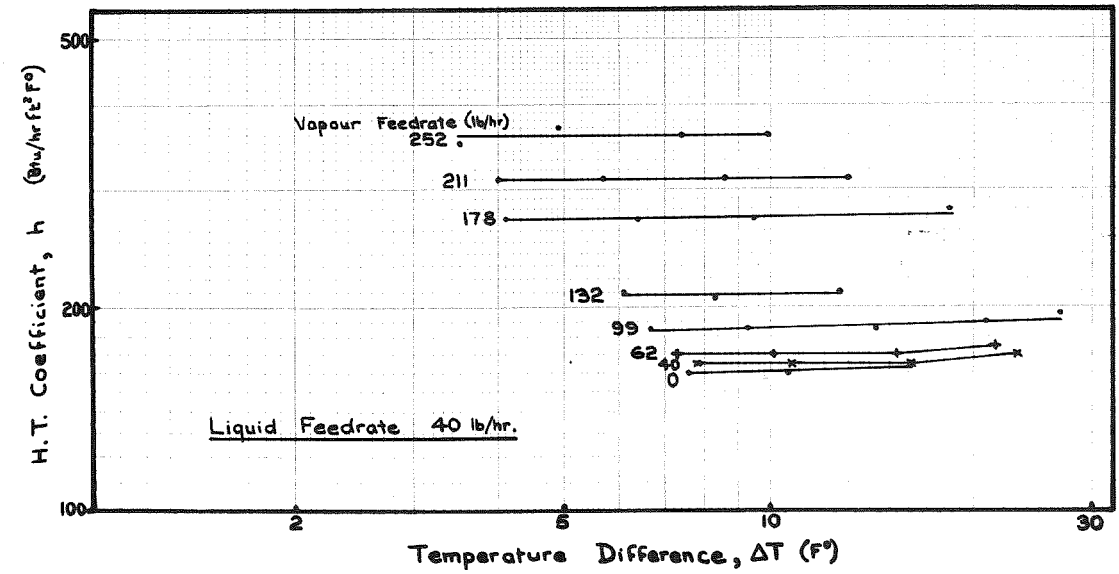

Figure 18A EXPERIMENTAL DATA CHLOROFORM 40 LB/HR

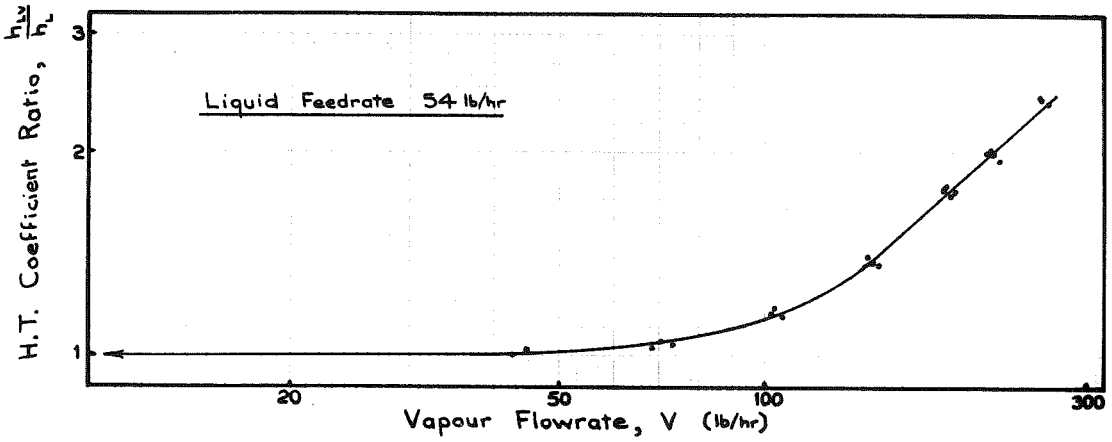

Figure 19B EFFECT OF VAPOUR FLOWRATE CHLOROFORM 54 LB/HR

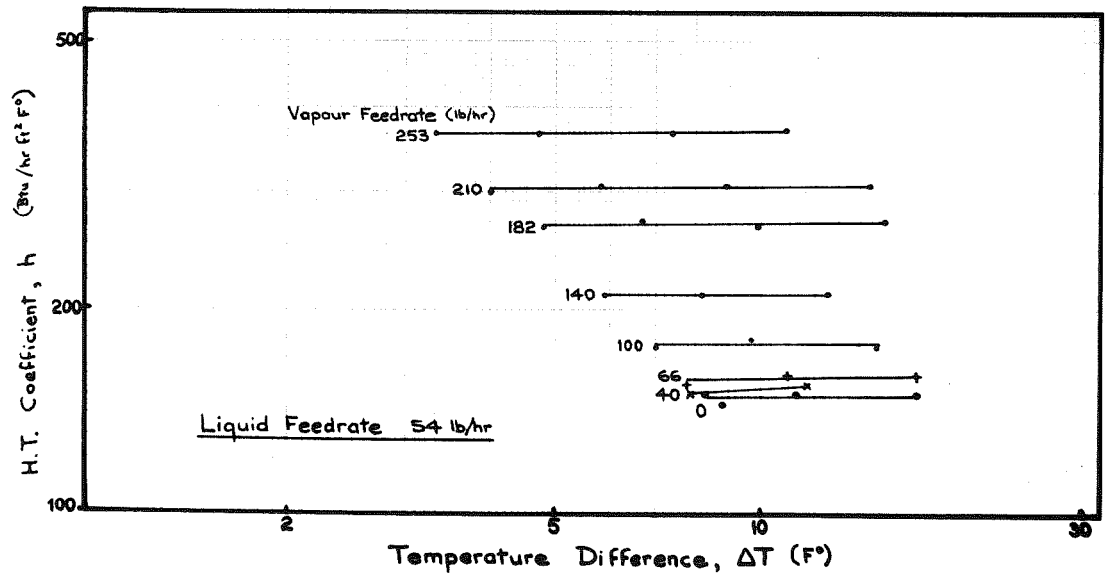

Figure 19A EXPERIMENTAL DATA CHLOROFORM 54 LB/HR

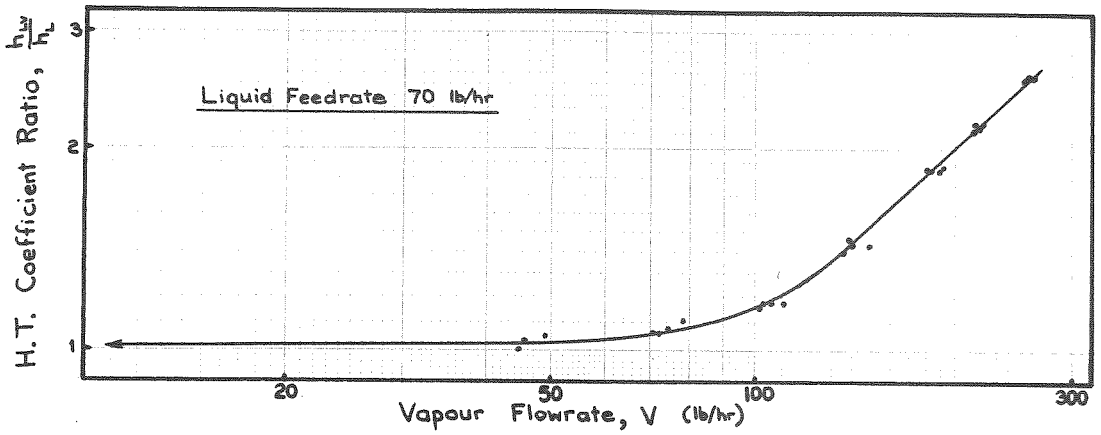

Figure 20B EFFECT OF VAPOUR FLOWRATE CHLOROFORM 70 LB/HR

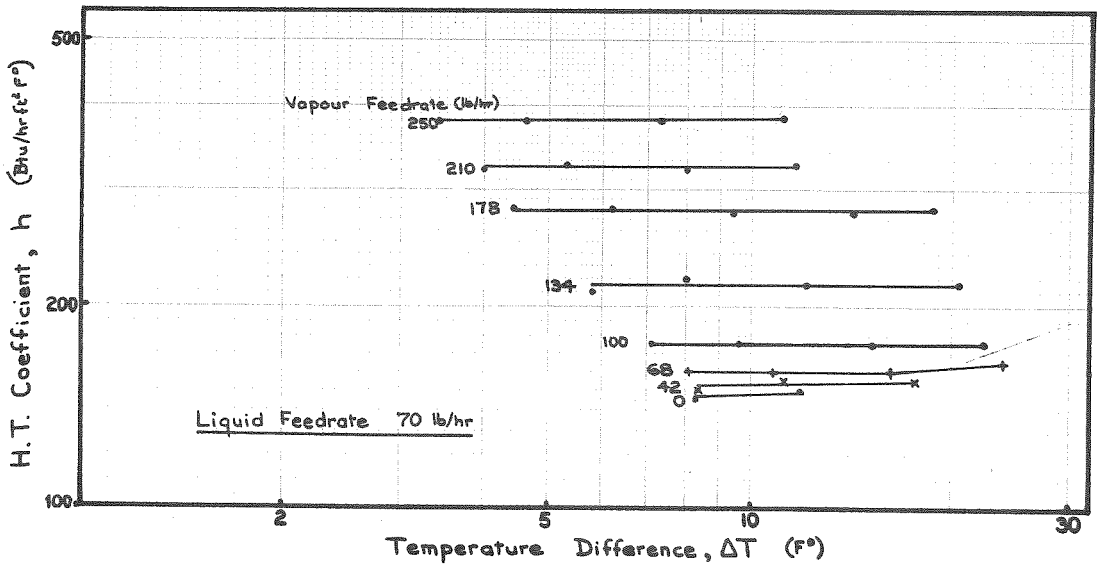

Figure 20A EXPERIMENTAL DATA CHLOROFORM 70 LB/HR

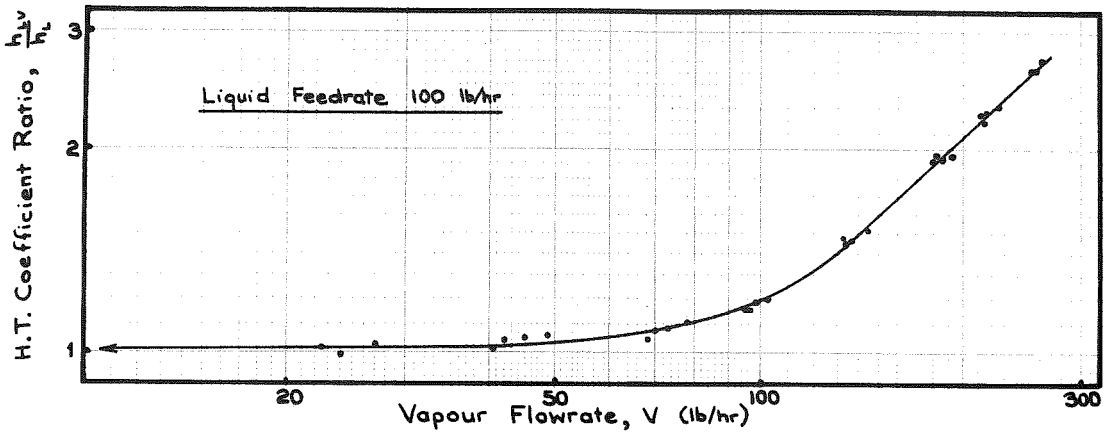

Figure 21B EFFECT OF VAPOUR FLOWRATE CHLOROFORM 100 LB/HR

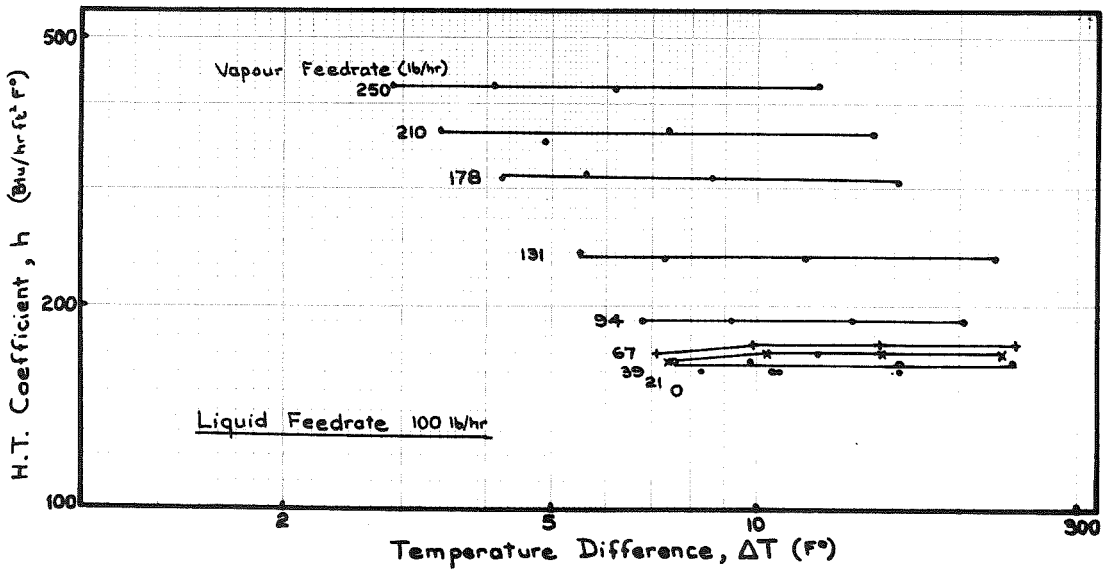

Figure 21A EXPERIMENTAL DATA CHLOROFORM 100 LB/HR

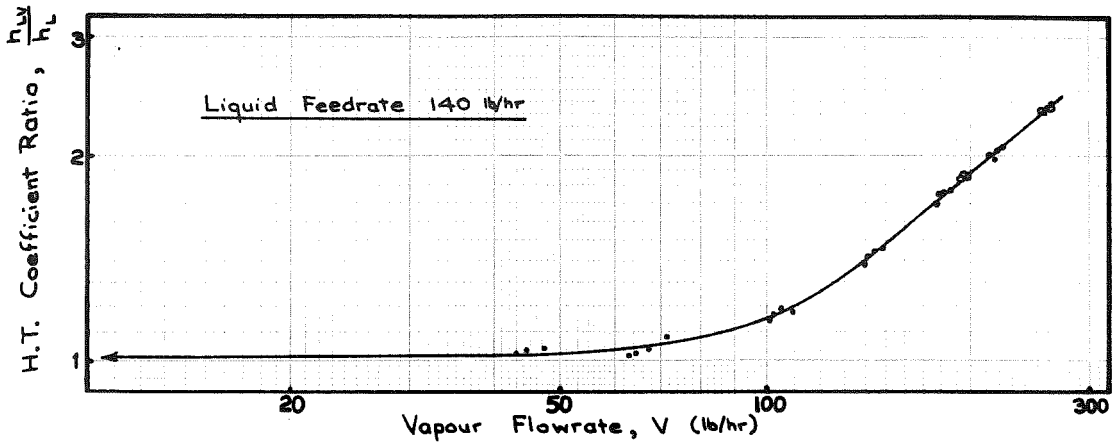

Figure 22B EFFECT OF VAPOUR FLOWRATE CHLOROFORM 140 LB/HR

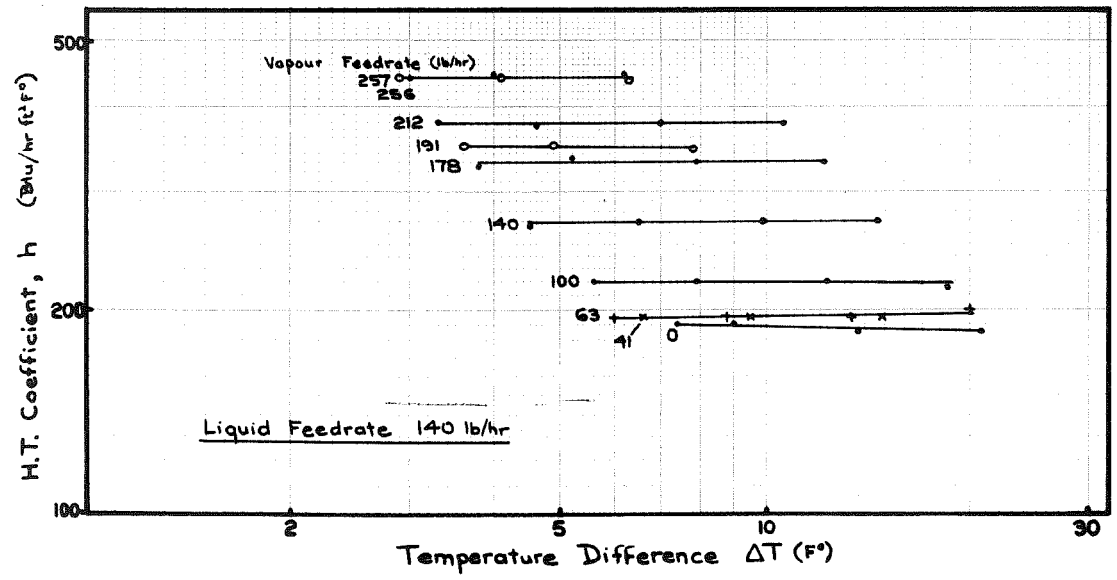

Figure 22A EXPERIMENTAL DATA CHLOROFORM 140 LB/HR

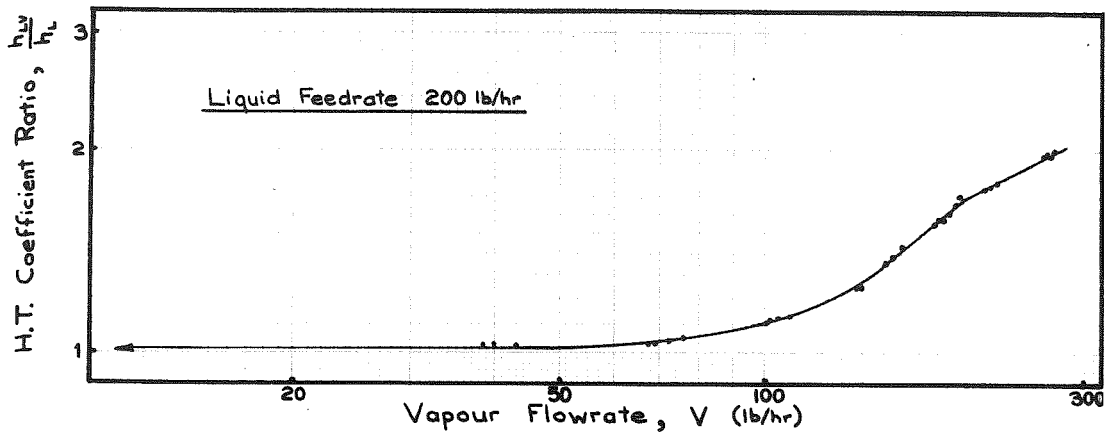

Figure 23B EFFECT OF VAPOUR FLOWRATE CHLOROFORM 200 LB/HR

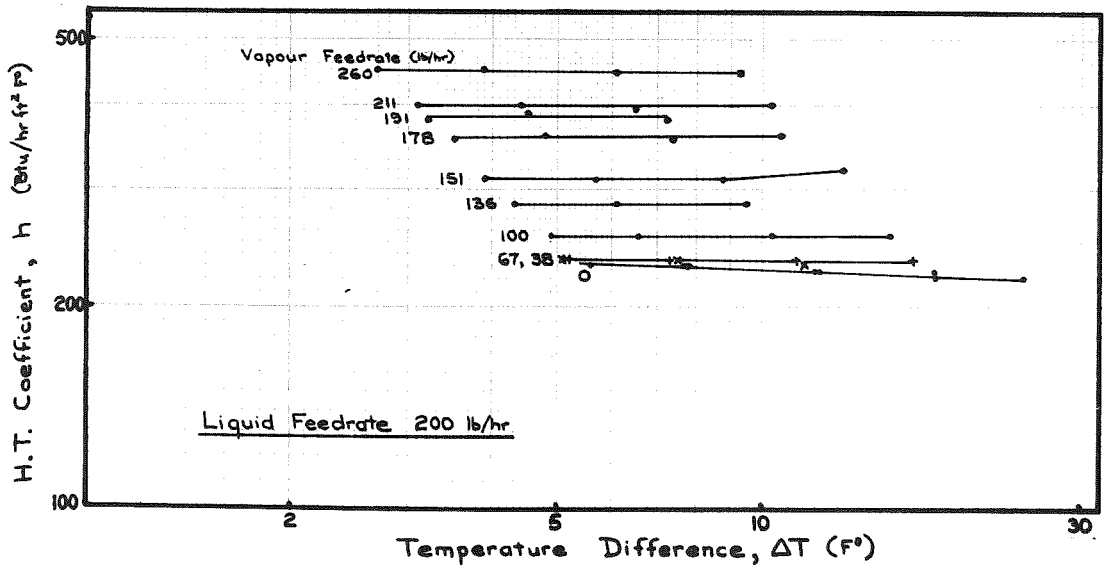

Figure 23A EXPERIMENTAL DATA CHLOROFORM 200 LB/HR

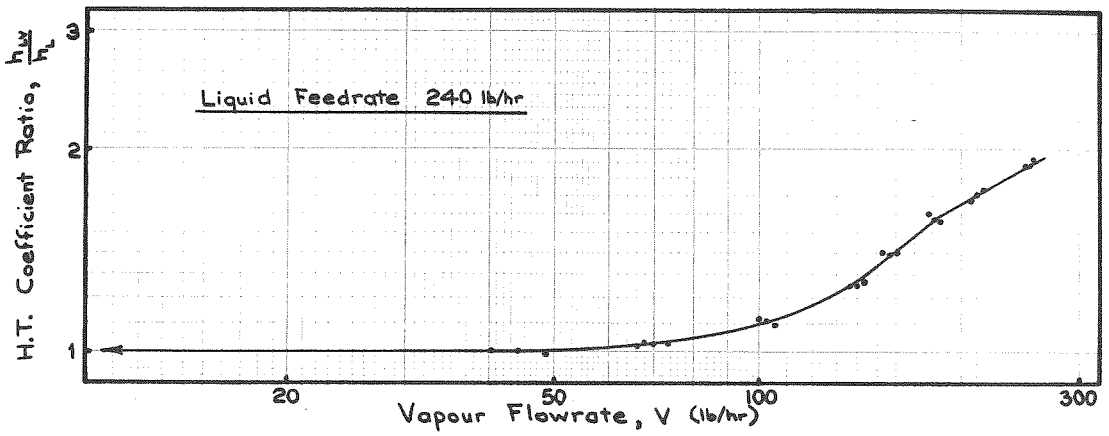

Figure 24B EFFECT OF VAPOUR FLOWRATE CHLOROFORM 240 LB/HR

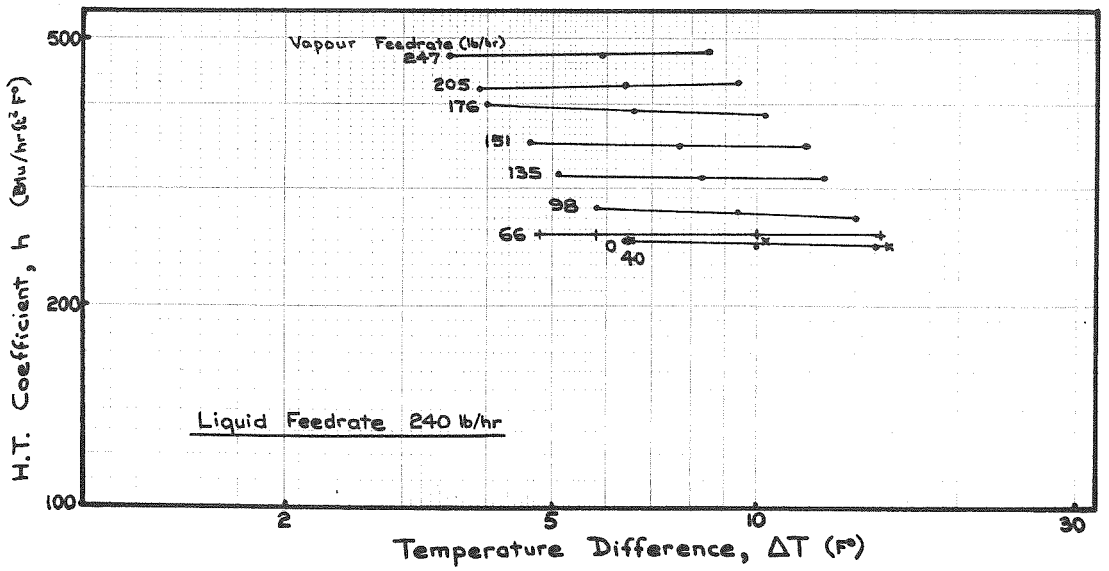

Figure 24A EXPERIMENTAL DATA CHLOROFORM 240 LB/HR

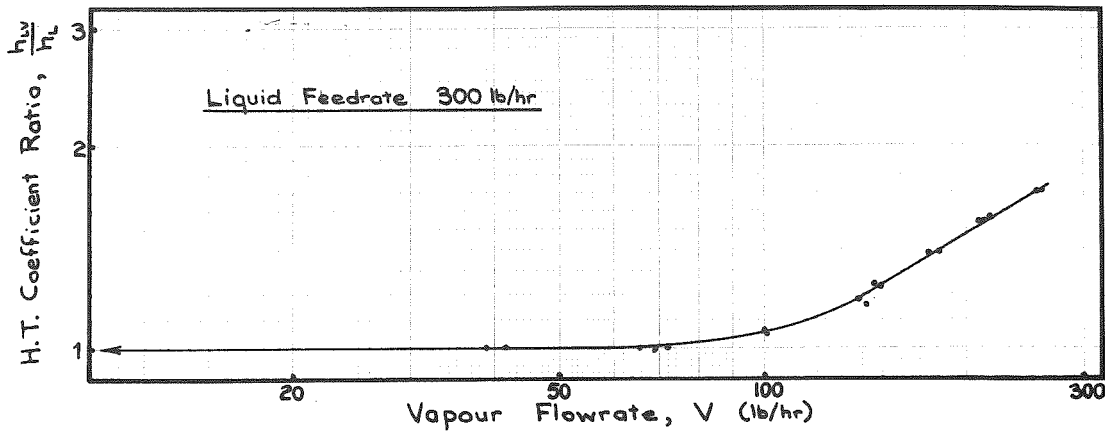

Figure 25B EFFECT OF VAPOUR FLOWRATE CHLOROFORM 300 LB/HR

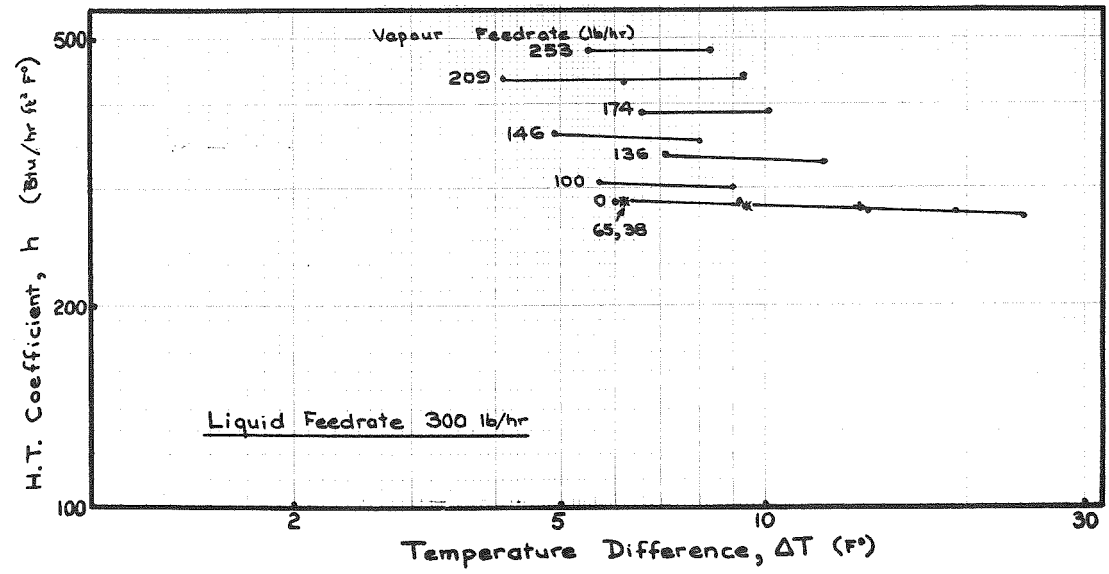

Figure 25A EXPERIMENTAL DATA CHLOROFORM 300 LB/HR

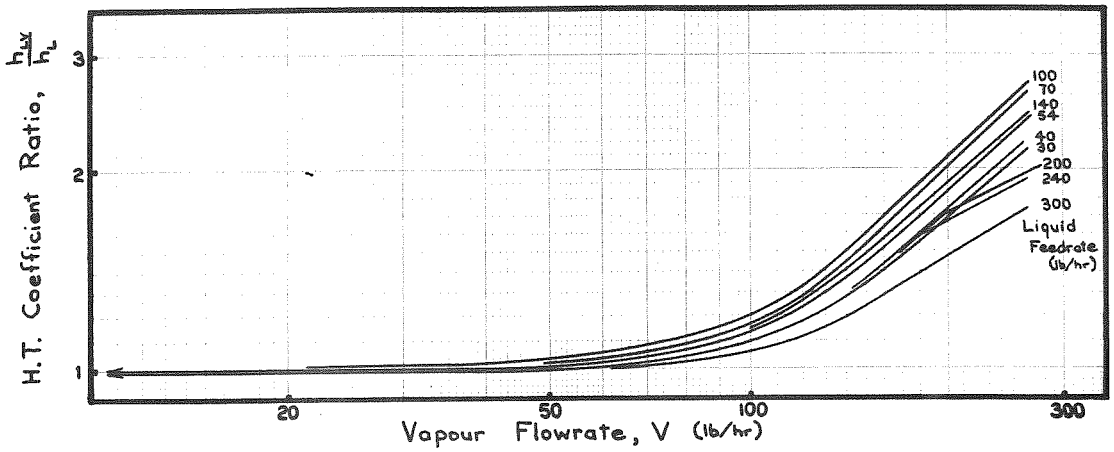

Figure 26 COMPARISON OF EFFECT OF VAPOUR FLOWRATE CHLOROFORM

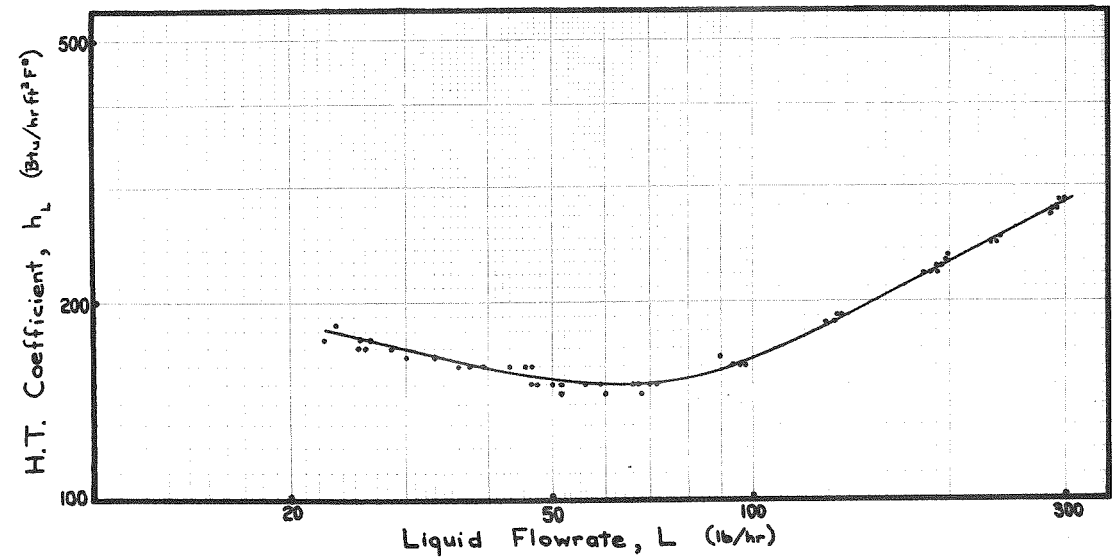

Figure 27 EFFECT OF LIQUID FLOWRATE CHLOROFORM

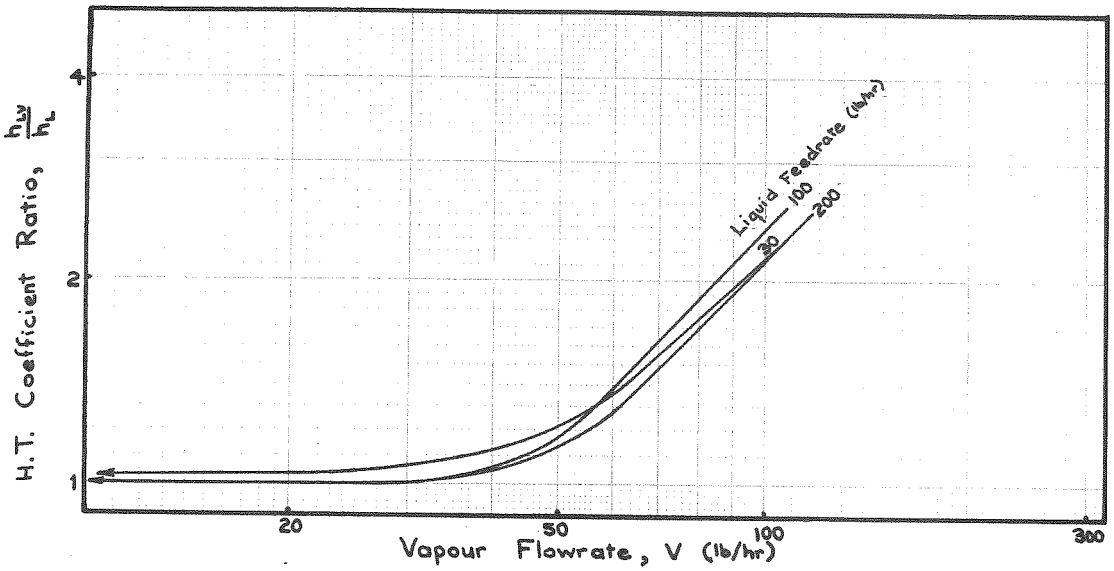

Figure 28 COMPARISON OF EFFECT OF VAPOUR FLOWRATE METHYL ALCOHOL

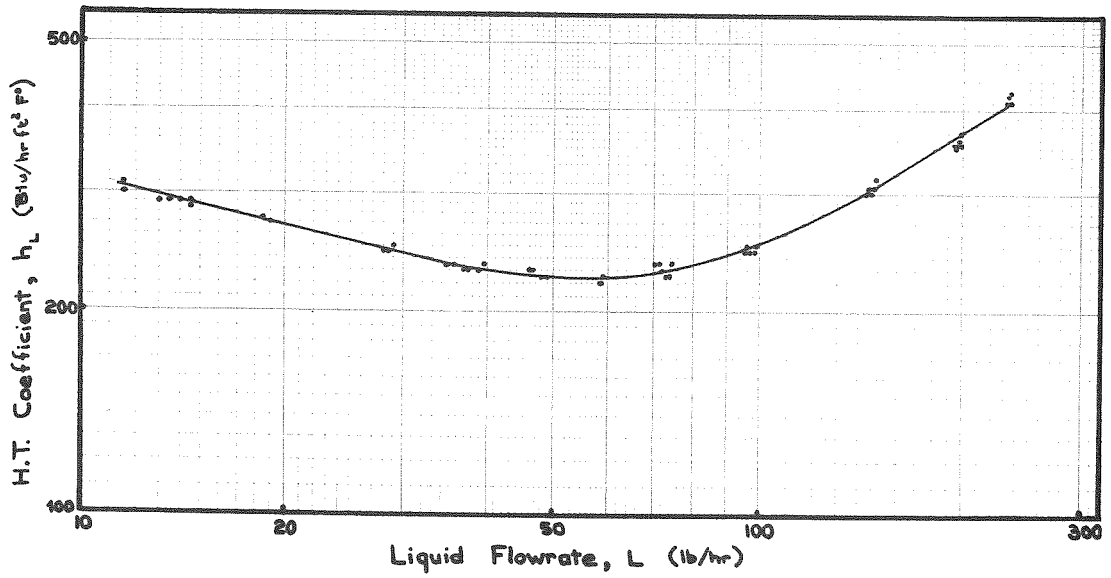

Figure 29 EFFECT OF LIQUID FLOWRATE METHYL ALCOHOL

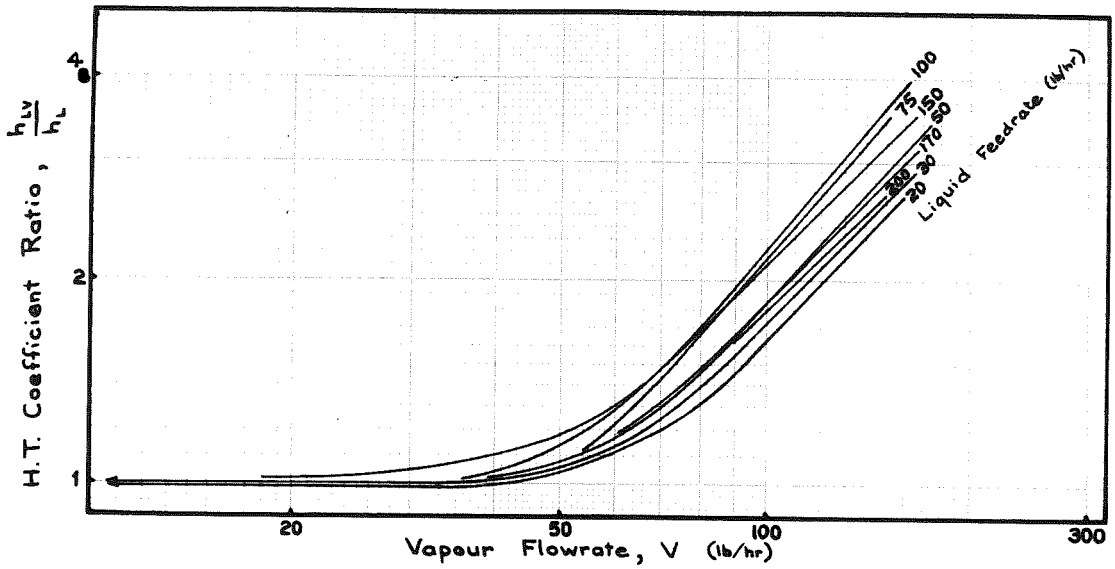

Figure 30 COMPARISON OF EFFECT OF VAPOUR FLOWRATE iso-PROPYL ALCOHOL

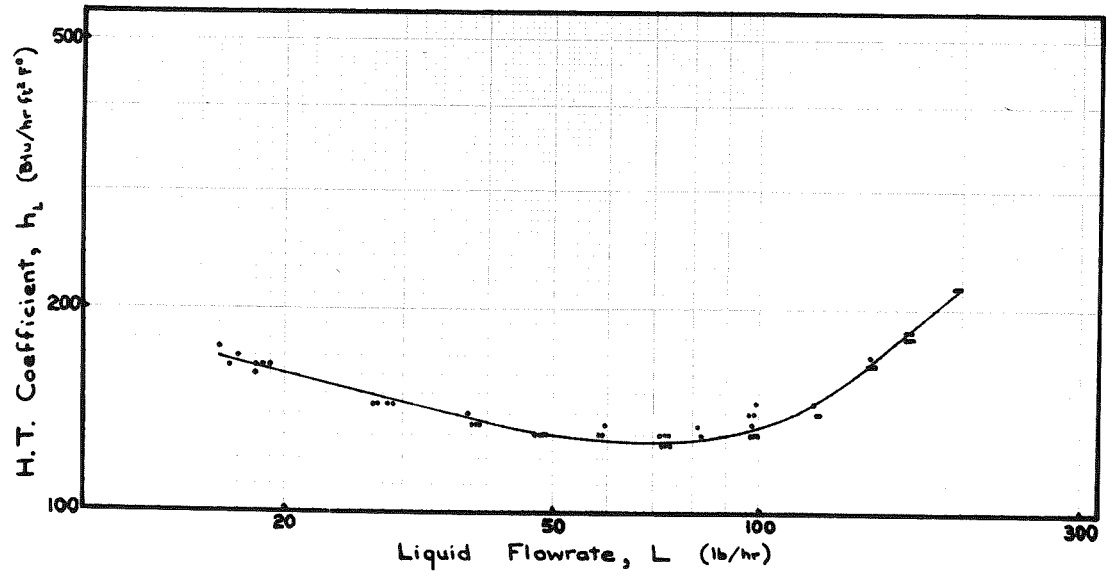

Figure 31 EFFECT OF LIQUID FLOWRATE iso-PROPYL ALCOHOL

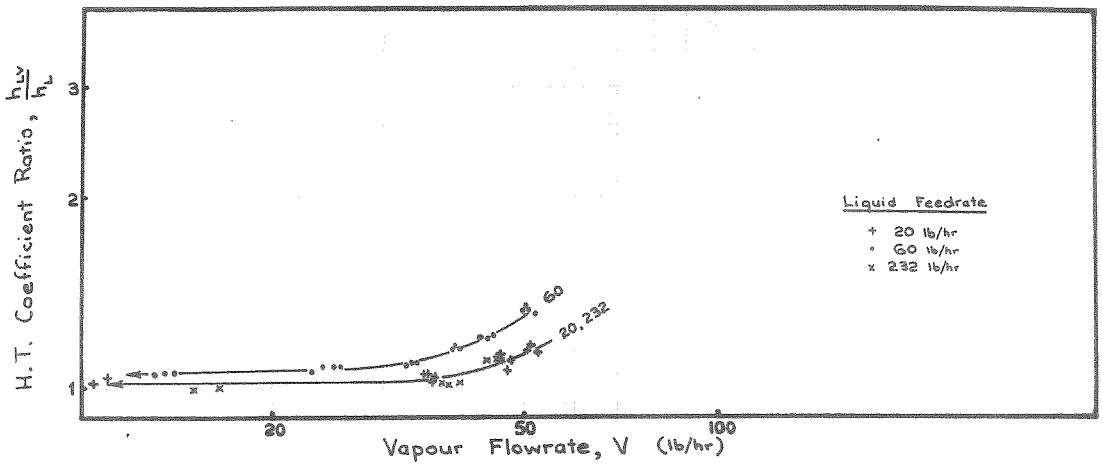

Figure 32 COMPARISON OF EFFECT OF VAPOUR FLOWRATE WATER

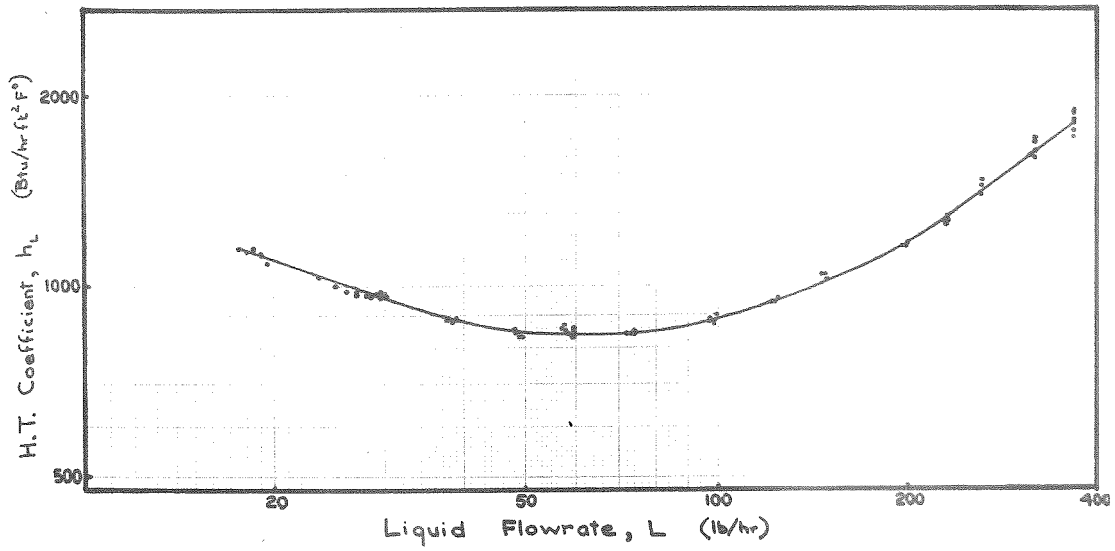

Figure 33 EFFECT OF LIQUID FLOWRATE WATER

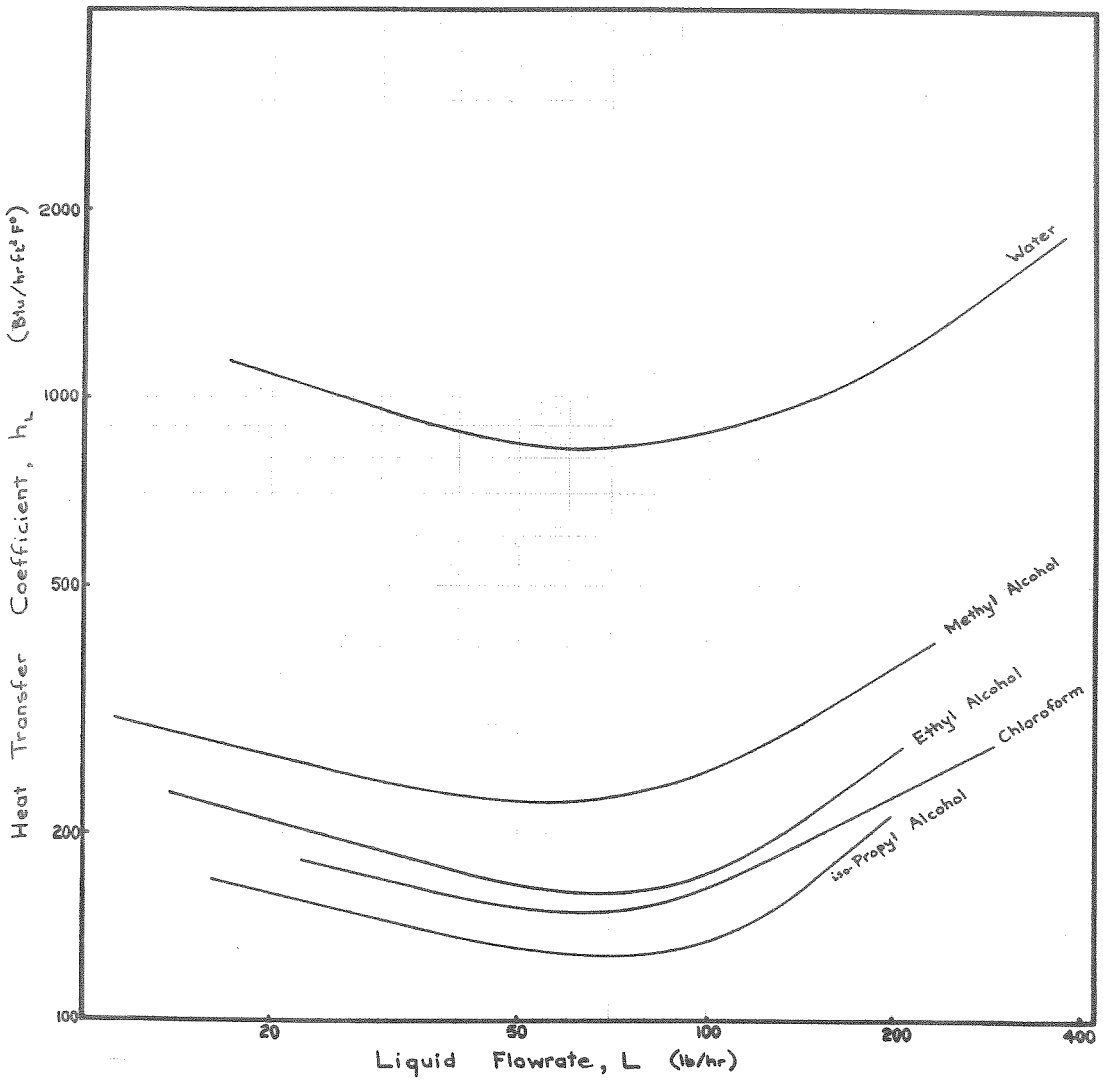

Figure 34 COMPARISON OF EFFECT OF LIQUID FLOWRATE

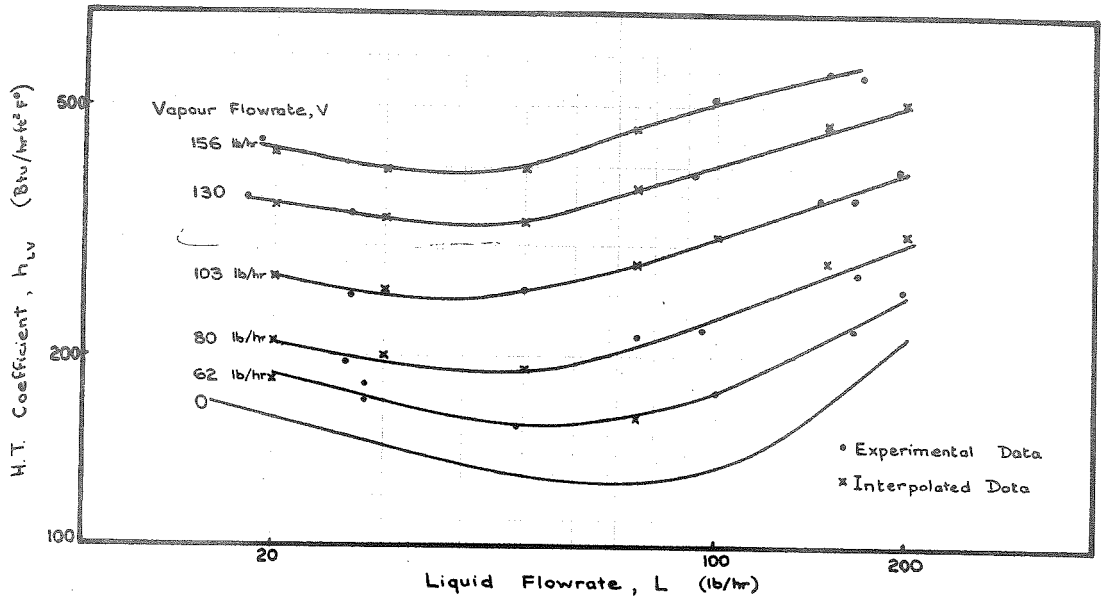

Figure 35 EFFECT OF LIQUID FLOWRATE, VARIABLE INTERFACIAL SHEAR ISO-PROPANOL

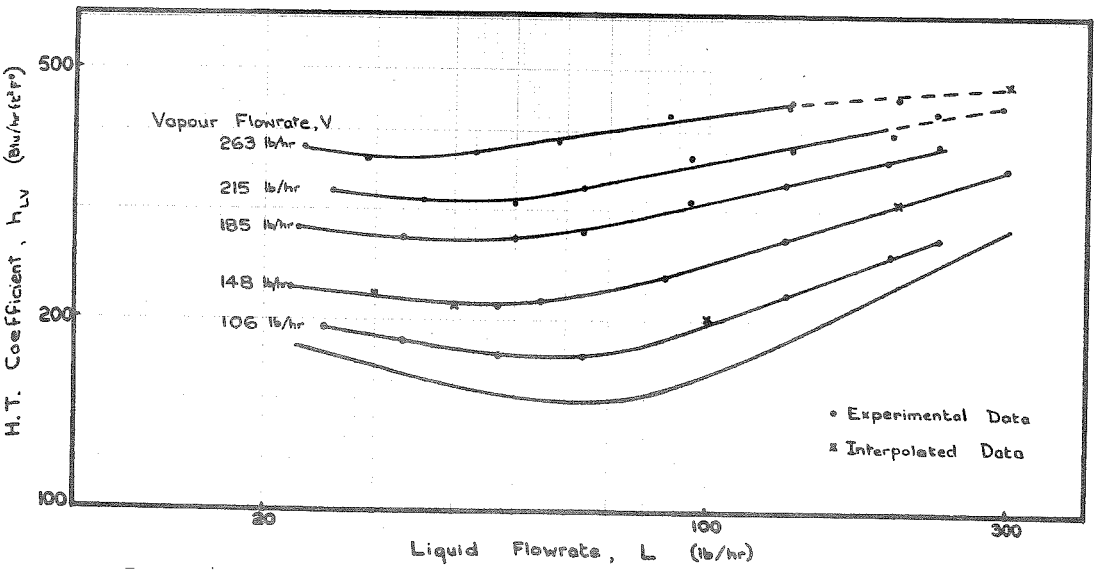

Figure 36 EFFECT OF LIQUID FLOWRATE, VARIABLE INTERFACIAL SHEAR CHLOROFORM

5. CORRELATION OF RESULTS

The similarity between film evaporation and film condensation was shown in Section 2, and correlation by analogy would appear to be possible.

However, rather than assume correlating expressions, it is intended to consider the mechanisms which should predominate in the respective regimes of the falling film evaporator, and then to attempt to justify correlation methods, either by simple analysis, or by the method of Mechanism Ratio Analysis (36) for the more complex cases of large liquid and vapour flow.

The more direct method of Mechanism Ratio Analysis is to be preferred to Dimensional Analysis.

The effect of the variables on the heat transfer coefficient in the falling film evaporator could be expressed as a function of the form,

$$h = \phi\ (D,\ D',\ \Gamma,\ v_V,\ \rho_L,\ \rho_V,\ \mu_L,\ \mu_V,\ \Delta T,\ \lambda,\ k,\ c,\ \sigma,\ g)\ ,$$

which could be used as the basis for a Dimensional Analysis. However, suitable arrangement of the factors into significant dimensionless groups would require considerable assumption regarding mechanisms, since there are fifteen factors to be expressed in terms of five dimensions. Such assumption of interacting mechanisms is the basis of Mechanism Ratio Analysis.

Mechanism analysis is aided by the fact that the particular flow effects can be separated relatively easily for the falling film evaporator. This case should be contrasted with the somewhat similar case of the climbing film evaporator, for which film flow cannot be generated without the coexistence of appreciable vapour flow.

No attempt will be made to correlate the nucleate boiling results because of their variability due to the indefinite surface effects which have been encountered. If the nucleate boiling regime is not to be considered, the variables ΔT and λ may be omitted from the correlation, provided that local liquid and vapour flow rates are considered. This omission follows because h for the falling film regime is independent of ΔT (see Section 4.4.2) if the effect of the λ-dependent variation of L and V is first accounted for.

5.1. Development of Correlation Methods

5.1.1. Film flow with subcritical vapour flow

In the absence of appreciable vapour shear the overall mechanism will probably be made up of the following individual forces or mechanisms:

(1) total heat transfer (sum of turbulent and molecular transport),

(2) heat transfer by molecular conduction,

(3) driving force for flow, a gravitational force,

(4) turbulent momentum transport, and

(5) momentum transport by molecular diffusion.

From basic transport theory it can be shown that the standard dimensionless groups, the Nusselt number, the Reynolds number, and the Prandtl number, represent the following ratios of four of the above mechanisms:

$$Nu = \frac{(1)}{(2)} = \frac{\text{total heat flux}}{\text{molecular heat flux}}$$

$$Re = \frac{(4)}{(5)} = \frac{\text{turbulent momentum flux}}{\text{molecular momentum flux}} = \frac{\text{liquid inertial forces}}{\text{liquid viscous forces}}$$

$$Pr = \frac{(5)}{(2)} = \frac{\text{molecular momentum flux}}{\text{molecular heat flux}}$$

5.1.1.1. Laminar film flow with subcritical vapour flow

For the simple case of laminar flow, mechanisms (1) and (2) are equal, i.e.

$$\frac{(1)}{(2)} = Nu = \frac{ht}{k} = \frac{h(\text{constant})\ (\nu^2/g)^{1/3}\ Re^{1/3}}{k} = 1 \ .$$

The expression introduced for film thickness follows from the Nusselt analysis, the basis of which was to equate mechanisms (3) and (5).

The above expression may be simplified by noting that the group $(\nu^2/g)^{1/3}$ has dimensions of length.

This allows definition of another Nusselt number as

$$Nu' = \frac{h\,(\nu^2/g)^{1/3}}{k} .$$

Thus, the correlating expression simplifies to the form

$$Nu' \propto Re^{-1/3} .$$

5.1.1.2. Turbulent film flow with subcritical vapour flow

For turbulent flow, mechanisms (1), (2), (3), (4) and (5) are operative. With five mechanisms, Mechanism Ratio Analysis requires that four dimensionless groups be used to define the system.

It is evident that the three groups, $Nu = \frac{(1)}{(2)}$, $Re = \frac{(4)}{(5)}$ and $Pr = \frac{(5)}{(2)}$ should be important.

It will be necessary to define a further group which includes mechanism (3), the gravitational driving force for flow.

This may be done either in terms of liquid inertial pressure, into which the gravitational driving force is converted, or in terms of the wall shear stress, which opposes the driving force.

A force balance over an element of fluid of film thickness, t, flowing with a mean velocity, v, gives:

Gravitational driving force per unit of wall area

$$= (\rho_L - \rho_V)\, g\, t$$

$$= \text{wall shear stress}$$

$$= \tau_0 g_c$$

Also, friction factor, $f = \dfrac{\tau_0 g_c}{\rho_L v^2} = \dfrac{\text{wall shear stress}}{\text{liquid inertial pressure}}$

$$\therefore f = \frac{\tau_0 g_c}{\rho_L v^2} = \frac{(\rho_L - \rho_V)\, g\, t}{\rho_L\, v^2} = \frac{(3)}{(4)} = \frac{\text{gravitational "pressure"}}{\text{liquid inertial pressure}}$$

Assuming $(\rho_L - \rho_V) \simeq \rho_L$ (i.e. neglecting the small buoyancy effect of the vapour) the ratio becomes

$$\frac{(3)}{(4)} = \frac{g\, t}{v^2},$$

i.e. the term has the form of the inverse of a Froude number. Eliminating v, by the introduction of $vt\rho = \Gamma$, the flow per wetted perimeter,

$$\frac{(3)}{(4)} = \frac{g\, t}{\dfrac{\Gamma^2}{\rho^2 t^2}} = \frac{g\, t}{\dfrac{\mu^2}{\rho^2 t^2} \cdot \left(\dfrac{\Gamma}{\mu}\right)^2} = (\text{constant})\, \frac{t^3}{\dfrac{\nu^2}{g} \cdot Re^2}.$$

The proposed form of the correlation is

$$\frac{(1)}{(2)} = \phi \left[\frac{(3)}{(4)}, \frac{(4)}{(5)}, \frac{(5)}{(2)} \right]$$

$$\text{i.e.} \quad Nu = \phi \left[\frac{t^3}{\dfrac{\nu^2}{g} \cdot Re^2}, Re, Pr \right]$$

This four-group expression may be simplified: film thickness can be eliminated by use of the relation, $t = \phi(\nu^2/g, Re)$. The form in which the expression was found to apply for

turbulent film condensation was

$$Nu' = \frac{h\,(\nu^2/g)^{1/3}}{k} = \phi\,(Re,\ Pr)\ .$$

So far Mechanism Ratio Analysis has merely confirmed accepted condensation correlation methods. The technique becomes of more use for the complex case of film flow with supracritical vapour flow.

5.1.2. Effect of supracritical vapour flow

The observed increase in the heat transfer coefficient for supracritical vapour flow could be caused by an induced increase in turbulence of the falling liquid film, by a thinning of the film and hence a reduction in the heat transfer path, by the promotion of wave motion, or by the entrainment of superheated liquid from the film.

It is probable that the following mechanisms become important for supracritical vapour flow:

(6) surface forces of the liquid,

(7) momentum transfer to the film by molecular transport (represented by viscous forces of the vapour), and

(8) momentum transfer to the liquid film by turbulent transport (represented by inertial forces of the vapour).

Thus for turbulent liquid film flow, eight mechanisms will be operative, and seven groups will be necessary to

define the system. Therefore three additional groups will be required. This additional requirement will also hold for laminar film flow with supracritical vapour flow.

The Weber group, which can be interpreted as the tendency for the vapour stream kinetic energy to convert to new liquid surface energy, should be one of the required groups, i.e.

$$We = \frac{\text{vapour inertial pressure}}{\text{surface tension pressure}} = \frac{(8)}{(6)} = \frac{\rho_V v_V^2}{\sigma/(D+2t)} \quad \frac{D v_V^2 \rho_V}{\sigma} .$$

The Weber group should be significant for the whole range of flow regimes. The surface tension term represents the resistance to disruption of the surface for conditions of liquid entrainment, which are to be expected at high vapour flow rates for the supracritical zone. The term also represents the resistance to the creation of new liquid-vapour interfacial area caused by rippling, by spreading of the film, or by the promotion of interfacial turbulence, and as such indirectly represents the mechanisms more likely to be important at the lower vapour flow rates for the supracritical vapour flow regime.

Two more groups remain to be predicted by Mechanism Ratio Analysis. At least one of these groups should relate one of the two newly introduced mechanisms to one of the previously proposed mechanisms, and should further represent the interaction of vapour and liquid.

A more direct indication of the extent of the vapour-liquid interaction should be provided by the use of the second proposed group, which compares the vapour inertial forces with the gravitational driving force for film flow,

i.e. $\frac{\text{vapour inertial pressure}}{\text{gravitational driving force per unit of flow area}} = \frac{\rho_V v_V^2}{\rho_L g t} = \frac{(8)}{(3)}$.

This group may be considered to be a modified or two-phase Froude number, Fr'. It will not have the same meaning as does the Froude number for the horizontal flow of a single phase because, for vertical flow, gravity does not act as a restoring force opposing any disturbance of the film. However, for vertical flow the group can be taken to represent the relative motive effect of the vapour flow on the flow of the falling film when compared with the basic driving force for film flow, the gravitational effect. Therefore, the magnitude of this group should indicate the tendency for deviation to occur from the simple (negligible vapour flow) film heat transfer analyses of Nusselt and Colburn.

At very high vapour velocities, when $\frac{\rho_V v_V^2}{\rho_L g t}$ would become large (and also when liquid entrainment should become important), it is probable that the effect of gravity may become insignificant and the gravity mechanism could be neglected. These extreme conditions will not be considered here.

For the two groups which have been proposed, inter-

action of vapour inertial forces with forces acting in the falling film has been considered. However, it must be recognized that the vapour inertial forces can act on the liquid-vapour interface only through the medium of the viscous forces of the vapour.

Therefore it would appear that a vapour Reynolds number term,

$$Re_V = \frac{\text{inertial forces vapour}}{\text{viscous forces vapour}} = \frac{\text{mechanism (8)}}{\text{mechanism (7)}},$$

should be included in the correlation if either a Weber or a modified Froude group is to be used.

Thus, three groups are proposed, the use of which should allow for the additive effect of vapour velocity over the full range of supracritical vapour flows up to the point at which significant entrainment occurs.

5.2. Correlation of Results: Film flow with subcritical vapour flow

The experimental data, obtained for conditions of no introduction of externally-produced vapour, are plotted as h vs. Re in Figure 37, and as $\frac{h\,(\nu^2/g)^{1/3}}{k}$ vs. Re in Figure 38. It can be seen that a maximum deviation of about 700% among the heat transfer coefficient data for the various liquids for the laminar regime (Figure 37) is reduced to about 50% for the correlated data (Figure 38).

Plots at constant Reynolds number (Figure 39)

indicate that Prandtl number terms, $Pr^{0.15}$ for the laminar regime, and $Pr^{0.5}$ or $Pr^{0.33}$ for the turbulent regime, are required.

The final correlations are:

Laminar: $$\frac{h_L (\nu^2/g)^{1/3}}{k} = 0.84\ Re^{-0.27}\ Pr^{0.15}$$

Turbulent: (1) $$\frac{h_L (\nu^2/g)^{1/3}}{k} = 0.00042\ Re^{0.7}\ Pr^{0.5}$$

(for all data), or

(2) $$\frac{h_L (\nu^2/g)^{1/3}}{k} = 0.0027\ Re^{0.5}\ Pr^{1/3}$$

(for data after omission of suspect high flow rate data).

The laminar equation correlates the experimental data (Figure 40A) within ±10% up to Re = 600, and within -20% at Re = 1000.

Correlating equation (1), for all of the turbulent data, represents the line to which the experimental data converge within ±10% for Re > 4000. Deviation from the common line occurs in the transition region, but correlation within ±20% is still found at Re = 2500.

The alternative turbulent correlating equation, equation (2), which is shown at the left-hand side in Figure 40, correlates the experimental data within ±10% from Re = 1600. Equation (2) was obtained after the elimination of heat transfer data which were obtained at the highest liquid flow rates, for which flow over the weir was observed

to be erratic and surgy (see Section 4.4.2). Quantitative reasons for the preference of equation (2) will also be presented when correlation of supracritical vapour flow rate data is considered in the next section.

No equation is developed for the transition regime. However, smooth curves drawn by eye to fit between Re = 600 and Re = 2000 for each liquid agree with the smoothed experimental data within ±15%.

5.3. Correlation of Results: Supracritical Vapour Flow

Plots of experimental data (e.g. Figure 26 for chloroform) show the effect of vapour flow rate ($h \propto V$, approx.), and also show a secondary liquid flow effect, which is not accounted for by the use of $\frac{h_{LV}}{h_L}$, and which is due to the interaction between vapour and liquid flows.

Because of the difficulty of graphically obtaining a relation of the form

$$\frac{h_{LV}}{h_L} = \phi \left[\frac{\rho_V v_V^2}{\sigma/D}, \frac{\rho_V v_V^2}{\rho_L g t}, Re_V, Re_L \right],$$

multiple linear regression by means of an I.B.M. 1620 computer was attempted.

Data from the fully-developed supracritical vapour flow regime (i.e. the region of unity slope, e.g. in Figure 26) were divided into those for which the liquid flow was

laminar, and those for which the liquid flow was turbulent, in each case taking into account the action of the vapour flow in promoting turbulence at lower than normal critical liquid flow rates (e.g. Figures 35, 36). Supracritical vapour flow data for transitional liquid flow were eliminated.

The computer was supplied with or formed the terms $\frac{h_{LV}}{h_L}$, $\frac{V^2}{\rho_V \sigma}$, $\frac{V^2}{\rho_V \rho_L (\nu^2/g)^{1/3}}$, $\frac{V}{\mu_V}$, and Re_L, for the two groups of data. Length terms were omitted from the vapour flow terms for simplicity, and because only one apparatus geometry was considered.

The number of data points used as the basis for each regression is tabulated below.

NUMBER OF DATA POINTS FOR THE COMPUTER REGRESSIONS

Test liquid	Laminar Liquid Flow	Turbulent Liquid Flow
Ethyl Alcohol	57	58
Methyl Alcohol	14	28
iso-Propyl Alcohol	37	75
Chloroform	28	83
Total supracritical vapour data	136	244

No supracritical data for water could be included because the installed vapour generation capacity was insufficient to allow the critical vapour flow rate to be exceeded. Those data will be supplied by Clegg (17).

The final relations were:

Laminar

$$\frac{h_{LV}}{h_L} = 0.0000245 \left(\frac{V^2}{\rho_V \sigma}\right)^{1.28} \left(\frac{V^2}{\rho_V \rho_L (\nu^2/g)^{1/3}}\right)^{-0.58} \left(\frac{V}{\mu_V}\right)^{-0.38} Re_L^{0.14}$$

Turbulent

$$\frac{h_{LV}}{h_L} = 0.000227 \left(\frac{V^2}{\rho_V \sigma}\right)^{1.31} \left(\frac{V^2}{\rho_V \rho_L (\nu^2/g)^{1/3}}\right)^{-0.59} \left(\frac{V}{\mu_V}\right)^{-0.42} Re_L^{-0.16}$$

Analysis of variance calculations, which are summarised below, were carried out as part of the programme to calculate regression coefficients. The results show that each coefficient is highly significant and that both regressions are highly significant.

ANALYSIS OF VARIANCE - COMPUTER REGRESSIONS

Group	Turbulent Correlation			Laminar Correlation		
	Expo-nent	Std. Error	Student's t	Expo-nent	Std. Error	Student's t
$\frac{V^2}{\rho_V \sigma}$	1.31	0.039	34	1.28	0.042	30
$\frac{V^2}{\rho_V \rho_L (\nu^2/g)^{1/3}}$	-0.59	0.035	17	-0.58	0.039	15
$\frac{V}{\mu_V}$	-0.42	0.017	24	-0.38	0.019	20
Re_L	-0.16	0.010	16	0.14	0.013	11
Variance Ratio for Correlation	1340			1140		

The reliability of the correlations is reduced by the observation that, although the groups $\rho_V \sigma$ and $\rho_V \rho_L (\nu^2/g)^{1/3}$ were varied over a normally acceptable range, each group was dominated by the term ρ_V. The terms σ, $\rho_L (\nu^2/g)^{1/3}$ and μ_V each vary by little more than 20% for the four test liquids. The effects of this small variation are worsened when logarithms are taken for the regression analysis.

To find whether the correlation based on mechanism ratios was justified, a regression in terms of the individual

variables was attempted, i.e.

$$\frac{h_{LV}}{h_L} = \phi \left[V,\ \rho_V,\ \sigma,\ \rho_L(\nu^2/g)^{1/3},\ \mu_V,\ Re_L \right]$$

Considerable difficulty was encountered at the matrix inversion stage of the computer regression programmes. The matrices were found to be very ill-conditioned, due largely to the apparent close correlation between log μ_V and log σ (correlation coefficient approximately 0.9) and between log ρ_V and log $\rho_L(\nu^2/g)^{1/3}$ (correlation coefficient approximately 0.8). This ill-conditioning resulted in almost complete loss of significant figures during the computation. The results, and that of a laborious check repeat carried out by hand by the C.S.I.R.O. Mathematical Statistics Department for the laminar data, suggested that only V and Re_L could be relied upon to be significant.

The C.S.I.R.O. result was

$$\frac{h_{LV}}{h_L} \propto V^{1.02}\ Re_L^{0.22},$$

for the laminar liquid flow regime. The standard deviation of each exponent was calculated to be ± 0.01.

The individual variables multiple regressions were inconclusive because of the uncertainty caused by the loss of significant figures, and a greater range of liquid and vapour properties data is required to overcome the apparent close correlation between the properties groups.

A more conclusive check, and an extension of the proposed correlation method, is provided by the inclusion of data obtained by Staker for falling film evaporation within $\frac{3}{8}$ in. and $\frac{5}{8}$ in. externally-heated tubes.

Although it was stated in Section 2 that there are inconsistencies in Staker's vapour velocity exponents of 0.45-0.73, which disagree with the results of Carpenter and Colburn and with the results of the present investigation, there is no initial reason to assume that the observed critical vapour flow rates are incorrect.

The data tabulated below were taken or calculated from Tables VII and VIII of Staker. The critical vapour velocities which were presented by Staker were based on the tube cross-sectional area, and no allowance was made for the effect of the liquid film thickness on the vapour flow area. These data have been recalculated to allow for the effect of the liquid film thickness, and the corrected values are included in the tabulation below. The film thickness which was used for this correction was given by $t/(\nu^2/g)^{1/3} = 12$. This value was obtained from Figure 1 of Dukler (33), for $\beta = 20$ and $Re_L = 3000$. The value $\beta = 20$ for the dimensionless interfacial shear group was chosen because replots of previous Dukler data (presented as Figures A6-A8 in Appendix V) show this to be the order of the critical value. The film thickness of $12(\nu^2/g)^{1/3}$ ft. for $\beta = 20$ compares with an

expected film thickness of $17(\nu^2/g)^{1/3}$ ft. for zero interfacial shear, i.e. $\beta = 0$.

CRITICAL VAPOUR FLOW DATA OF STAKER (80)

Test Liquid	Tube Diameter	Approximate Re_L	V_{crit} (lb/hr)	$v_{V_{crit}}$ (ft/hr)	
				Staker calculation	Corrected for L
Water 212°F	3/8	2980	3.0	10.2×10^4	10.8×10^4
	5/8	2940	11	13.5	13.9
Water 150°F	3/8	2960	1.5	19	20.5
Methanol	3/8	3060	2.7	4.7	5.1
Ethanol	3/8	2910	2.6	3.3	3.6
iso-Propanol	3/8	3080	3.4	3.4	3.8
	5/8	2940	11	3.9	4.1
n-Butanol	3/8	3190	2.9	2.6	2.8
Ethyl Acetate	3/8	3750	4.7	3.2	3.4

The physical properties of the additional test liquids used by Staker (i.e. water 150°F, n-Butanol, and Ethyl Acetate) are listed in Appendix IIA, and were taken from Appendix X of Reference (80).

Critical vapour flow rates for $Re_L = 3000$ for the present investigation are tabulated below. These data were

taken from figures 15, 26, 28, 30, and were inferred for water from Figure 32. The value for water was confirmed approximately by preliminary data of Clegg (18).

CRITICAL VAPOUR FLOW DATA FOR THE PRESENT INVESTIGATION

Test Liquid	V_{crit} (lb/hr)	$v_{V_{crit}}$ (ft/hr)	
		Based on annular area	Corrected for L
Ethyl Alcohol	50	7.3×10^4	7.7×10^4
Chloroform	100	5.4	5.6
Methyl Alcohol	45	9.0	9.4
iso-Propyl Alcohol	55	6.2	6.6
Water	about 50	20.3	21.2

Inclusion of the results of Staker is made as follows. By the definition of V_{crit} as the flow rate obtained by extrapolation of the vapour flow line of slope approximately unity to meet the liquid flow line, boundary conditions for the supracritical vapour flow rate correlation are

$$\frac{h_{LV}}{h_L} = 1 \quad \text{at} \quad V = V_{crit}, \quad \text{i.e.}$$

$$1 = (\text{constant}) \left(\frac{v_{crit}^2}{\rho_V \sigma}\right)^{1.3} \left(\frac{v_{crit}^2}{\rho_V \rho_L (\nu^2/g)^{1/3}}\right)^{-0.6} \left(\frac{V_{crit}}{\mu_V}\right)^{-0.4} Re_L^{\,n}$$

Thus, a correlation of V_{crit} in terms of $1/\rho_V\sigma$, $1/\rho_V\rho_L(\nu^2/g)^{1/3}$ and $1/\mu_V$ is to be expected.

Initial plots (e.g. Figure 41) show that the $\sigma^{1.3}$ exponent is too high and suggest that the exponent is nearer 0.6 to 0.7. This difference may be explained by the observation of a very good apparent correlation between $1/\rho_V\sigma$ and $1/\rho_V\rho_L(\nu^2/g)^{1/3}$ for the four test liquids on which the computer regression is based. The apparent correlation disappears when properties data for other test liquids, e.g. water, and the additional test liquids used by Staker, are checked for correlation. Thus there is justification for elimination of the $(1/\rho_V\rho_L(\nu^2/g)^{1/3})^{0.6}$ term such that the exponent on the $\frac{V^2}{\rho_V\sigma}$ group becomes $(1.3-0.6) = 0.7$ and the proposed correlating expression becomes

$$\frac{h_{LV}}{h_L} \propto \left(\frac{V^2}{\rho_V\sigma}\right)^{0.7} \left(\frac{V}{\mu_v}\right)^{-0.4} Re_L^{\,n} .$$

By the same reasoning $1/\rho_V\sigma$ could be eliminated in favour of $1/\rho_V\rho_L(\nu^2/g)^{1/3}$. However the extended range of experimental data obtained by Staker suggests that only the former approach is justified. Plots of V_{crit} versus both groups of variables are shown in Figure 41, and the results of regression analyses for the data for the annulus and the $\frac{3}{8}$ in. tube are summarised in the following Table.

RESULTS OF REGRESSION ANALYSES FOR DATA PRESENTED IN FIGURE 41

Regression Considered	Regression Coefficient	Standard Error	Variance Ratio for Regression
Annulus			
$\log V_{crit}$ vs. $\log \frac{1}{\rho_V \rho_L (\nu^2/g)^{1/3}}$	-0.29	0.13	5
$\log V_{crit}$ vs. $\log \frac{1}{\rho_V \sigma}$	-0.58	0.06	93
$\frac{3}{8}$ in. Tube (Staker)			
$\log V_{crit}$ vs. $\log \frac{1}{\rho_V \rho_L (\nu^2/g)^{1/3}}$	-0.30	0.08	15
$\log V_{crit}$ vs. $\log \frac{1}{\rho_V \sigma}$	-0.65	0.09	51

The calculated Variance Ratios for the individual regressions indicate that both regressions of $\log V_{crit}$ vs. $\log 1/\rho_V \sigma$ are highly significant, and that the regression of $\log V_{crit}$ vs. $\log 1/\rho_V \rho_L (\nu^2/g)^{1/3}$ for the $\frac{3}{8}$ in. tube is significant. However, the regression of $\log V_{crit}$ vs. $\log 1/\rho_V \rho_L (\nu^2/g)^{1/3}$ for the annulus is of lower significance, and for the $\frac{5}{8}$ in. tube the two V_{crit} data available are independent of $1/\rho_V \rho_L (\nu^2/g)^{1/3}$. The observed lower significance and the large standard errors in the regression coefficients for the correlation of $\log V_{crit}$ vs. $\log 1/\rho_V \rho_L (\nu^2/g)^{1/3}$ justify the attempt to correlate in terms of $1/\rho_V \sigma$ only.

The few comparative data available at constant $1/\rho_V\sigma$ in Figure 41 indicate that the inclusion of the $\mu_V^{0.4}$ term suggested by the computer regression is warranted. The data are replotted in Figure 42. The exponent on log $1/\rho_V\sigma$ becomes approximately -0.7 with the introduction of this vapour viscosity term.

Length terms are introduced into the correlation in Figure 43, and V_{crit} is converted to $v_{V_{crit}}$ (based on reduced flow area).

The liquid flow "perimeter", D_p, where

$D_p = (D_{tube} + 2 \times \text{film thickness})$,

for the present investigation, and

$= (D_{tube} - 2 \times \text{film thickness})$,

for the data of Staker,

is introduced into the Weber number term, and the equivalent diameter for flow, D_{e_F}, where

$$D_{e_F} = \frac{4 \times \text{flow area}}{\text{drag perimeter}} = \frac{4 \times \frac{\pi}{4}(D_{tube} - 2t)^2}{\pi(D_{tube} - 2t)}$$

$$= (D_{tube} - 2t), \text{ for a tube, and}$$

$$= \frac{4 \times \frac{\pi}{4}\left[D^2_{jacket} - (D_{tube} + 2t)^2\right]}{\pi\left[D_{jacket} + (D_{tube} + 2t)\right]}$$

$$= D_{jacket} - D_{tube} - 2t, \text{ for an annulus,}$$

is introduced into the vapour Reynolds number term.

Figure 43 shows that

$$v_{V_{crit}} \propto \left[\left(\frac{D_p \rho_V}{\sigma g_c} \right)^{0.7} \left(\frac{D_{e_F} \rho_V}{\mu_V} \right)^{-0.4} \right]^{-1} ,$$

and the lines which represent the results for the three apparatus geometries are offset by an amount proportional to $D_{e_{HT}}$, the equivalent diameter for heat transfer, where

$$D_{e_{HT}} = \frac{4 \times \text{flow area}}{\text{heat transfer perimeter}}$$

$$= \frac{4 \times \frac{\pi}{4} (D_{tube} - 2t)^2}{\pi D_{tube}} , \quad \text{for the tube, and}$$

$$= \frac{4 \times \frac{\pi}{4} \left[D^2_{jacket} - (D_{tube} + 2t)^2 \right]}{\pi D_{tube}} , \quad \text{for the annulus.}$$

The equivalent diameters for heat transfer and flow are discussed further by Kern (52).

The experimental data are replotted in Figure 44, and the final critical vapour velocity correlation is

$$\frac{v_{V_{crit}}}{D_{e_{HT}}} = 5.4 \left[\left(\frac{D_p \rho_V}{\sigma g_c} \right)^{0.7} \left(\frac{D_{e_F} \rho_V}{\mu_V} \right)^{-0.4} \right]^{-1}$$

$$\text{i.e.} \left(\frac{\rho_V v^2_{V_{crit}}}{\sigma g_{c/D_p}} \right)^{0.7} \left(\frac{D_{e_F} v_{V_{crit}} \rho_V}{\mu_V} \right)^{-0.4} = 5.4 D_{e_{HT}} ,$$

for fixed Re_L.

Introducing Re_L terms from the computer correlation gives

$$\frac{h_{LV}}{h_L} = (\text{constant}) \left(\frac{\rho_V v_V^2}{\sigma \varepsilon_c / D_p}\right)^{0.7} \left(\frac{D_{e_F} v_V \rho_V}{\mu_V}\right)^{-0.4} \frac{Re_L^{\,n}}{D_{e_{HT}}}$$

where $n = 0.14$ (or 0.22), for laminar liquid flow

$n = -0.16$, for turbulent liquid flow.

The constant for turbulent liquid flow may be evaluated as follows.

At $Re_L = 3000$,

$$\frac{v_{V_{crit}}}{D_{e_{HT}}} \left(\frac{D_p \rho_V}{\sigma \varepsilon_c}\right)^{0.7} \left(\frac{D_{e_F} \rho_V}{\mu_V}\right)^{-0.4} = 5.4$$

$$\therefore \left(\frac{h_{LV}}{h_L}\right)_{crit} = 1 = (\text{constant})_{Turb.} \times 5.4 \times 3000^{-0.16}$$

$$\therefore (\text{constant})_{Turb.} = \frac{3.6}{5.4} = 0.67 .$$

The approximate value of the constant for laminar liquid flow may be obtained by scaling down the turbulent value by the ratio of the constants obtained for the computer regression,

$$\text{i.e. } (\text{constant})_{Lam.} = 0.67 \times \frac{0.0000245}{0.000227} = 0.072 .$$

The supracritical vapour flow correlations are plotted against experimental data in Figure 45. The predicted values of the correlation constants are satisfactory, and the data points, including those for which the liquid flow is near transitional, lie within lines representing ±15% scatter.

For subcritical vapour flow, i.e. for

$$(\text{constant})\ We^{0.7}\ Re_V^{-0.4}\ \frac{Re_L^{\,n}}{D_{e_{HT}}} < 1\ ,$$

$\frac{h_{LV}}{h_L}$ tends to unity. Inspection of Figures 15, 26, 28 and 30 shows that an assumption of $\frac{h_{LV}}{h_L} = 1$ for $v_V < v_{V_{crit}}$ would generally lead to an error of $< -15\%$ for $\frac{1}{2}v_{V_{crit}} < v_V < v_{V_{crit}}$, and the error involved would be negligible for $v_V < \frac{1}{2}v_{V_{crit}}$.

Combinations of the supracritical vapour velocity correlations with the previous correlations for liquid flow alone give

<u>Turbulent liquid flow, supracritical vapour flow</u>

$$\frac{h_{LV}\ (\nu^2/g)^{1/3}}{k} = 0.0027 \times 0.67\ Re_L^{0.5}\ Pr^{0.33}\ We^{0.7}\ Re_V^{-0.4}\ \frac{Re_L^{-0.16}}{D_{e_{HT}}}$$

<u>Laminar liquid flow, supracritical vapour flow</u>

$$\frac{h_{LV}(\nu^2/g)^{1/3}}{k} = 0.84 \times 0.072\ Re_L^{-0.27}\ Pr^{0.15}\ We^{0.7}\ Re_V^{-0.4}\ \frac{Re_L^{0.14\ (\text{or } 0.22)}}{D_{e_{HT}}}$$

which can be rearranged to give

<u>Turbulent liquid flow, supracritical vapour flow</u>

$$\frac{h_{LV}\ D_{e_{HT}}}{k} = 0.0018\ Re_L^{0.34}\ Pr^{0.33}\ We^{0.7}\ Re_V^{-0.4}\ /(\nu^2/g)^{1/3}$$

Laminar liquid flow, supracritical vapour flow

$$\frac{h_{LV}\, D_{e_{HT}}}{k} = 0.060\ Re_L^{-0.13(\text{or } -0.05)}\ Pr^{0.15}\ We^{0.7}\ Re_V^{-0.4}/(\nu^2/g)^{1/3}$$

The agreement of the above Re_L exponent of 0.34, for turbulent liquid flow and supracritical vapour flow, with the slopes observed for these conditions with iso-propyl alcohol and chloroform in Figures 35 and 36, confirms the preference expressed in Section 5.2 for the turbulent liquid flow correlation based on data from which suspect high flow rate data had been omitted.

The following Table summarises the results of the correlation work outlined above.

CORRELATIONS FOR FALLING FILM EVAPORATION

FLOW CONDITIONS	PLOT OF CORRELN.	RESULT GIVEN	RANGE OF APPLICABILITY
Laminar liquid flow	Fig.40A	h_L	$200 < Re_L < 1000$
Turbulent liquid flow	Fig.40	h_L	$1600 < Re_L < 6000$
Subcritical vapour flow	Figs. 40, 40A	$h_{LV} = h_L$	$(\text{const.})\ We^{0.7}\ Re^{-0.4}\ \frac{Re_L^{\,n}}{D_{e_{HT}}} < 1$
Supracrit. vapour flow	Fig.45	$\frac{h_{LV}}{h_L}$	$1 < (\text{const.}) We^{0.7} Re^{-0.4}\ \frac{Re_L^{\,n}}{D_{e_{HT}}} < 3.6$

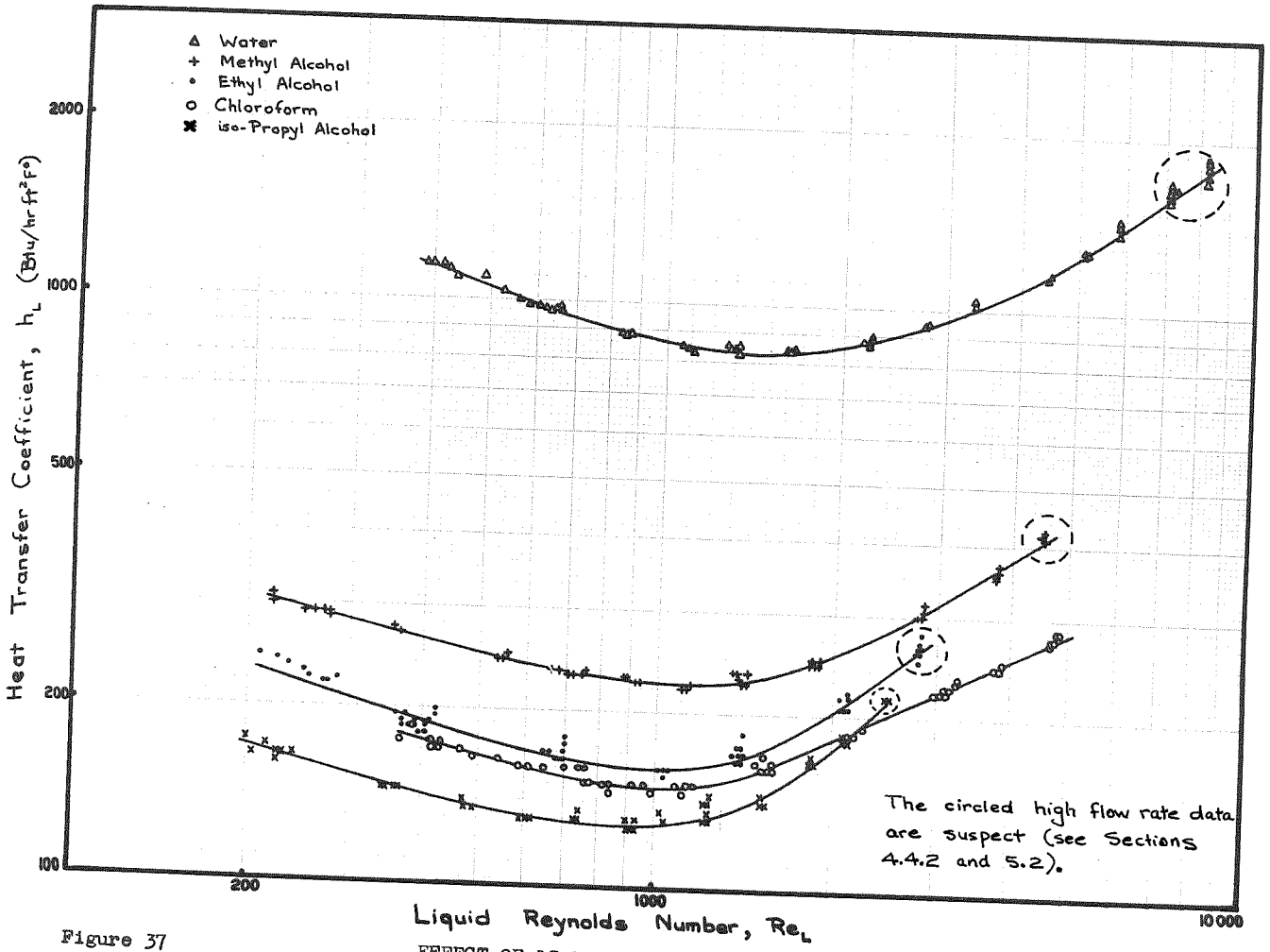

Figure 37

EFFECT OF LIQUID REYNOLDS NUMBER

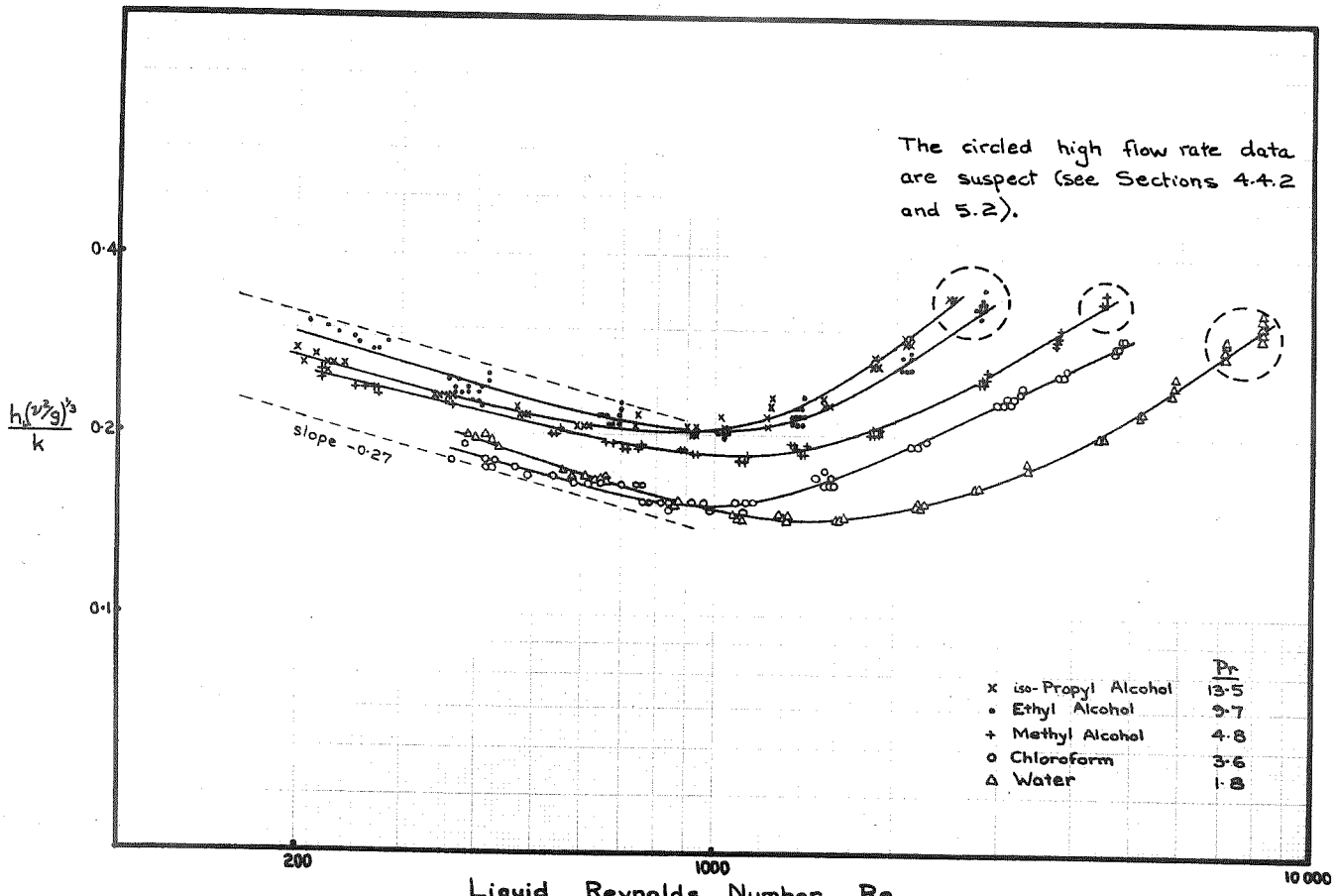

Figure 38

PARTIAL CORRELATION OF EXPERIMENTAL DATA

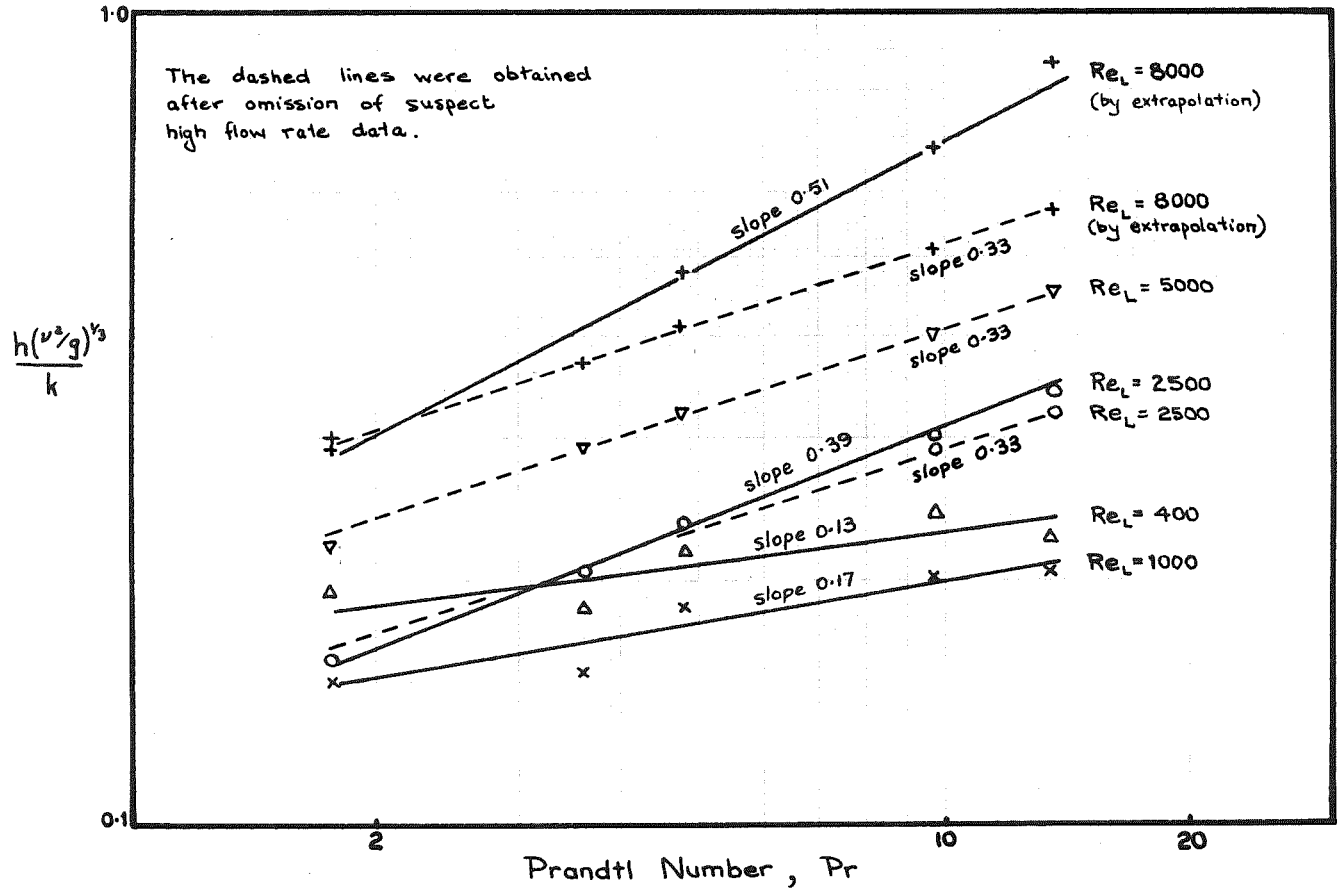

Figure 39 EFFECT OF PRANDTL NUMBER

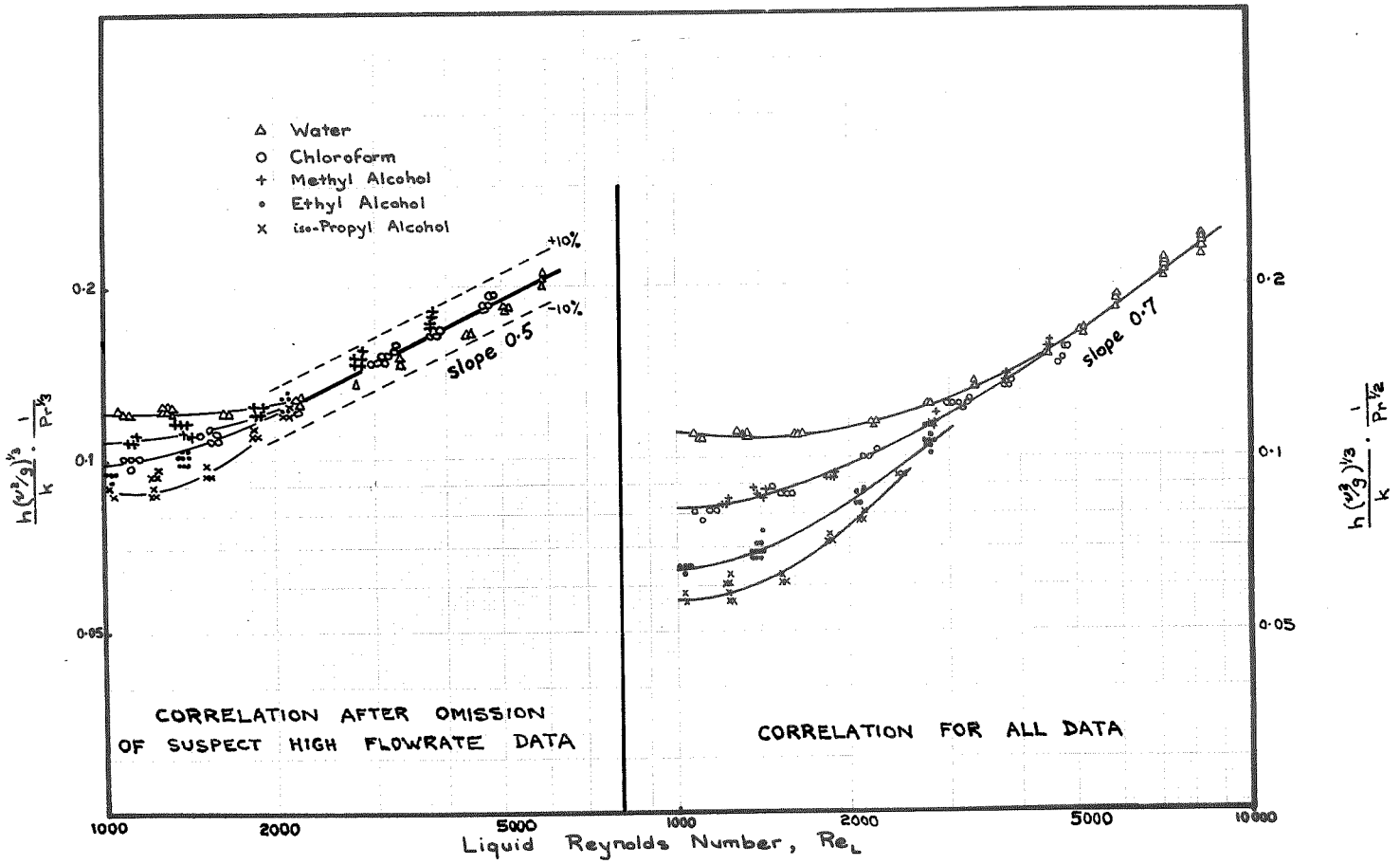

Figure 40 CORRELATION OF TURBULENT DATA

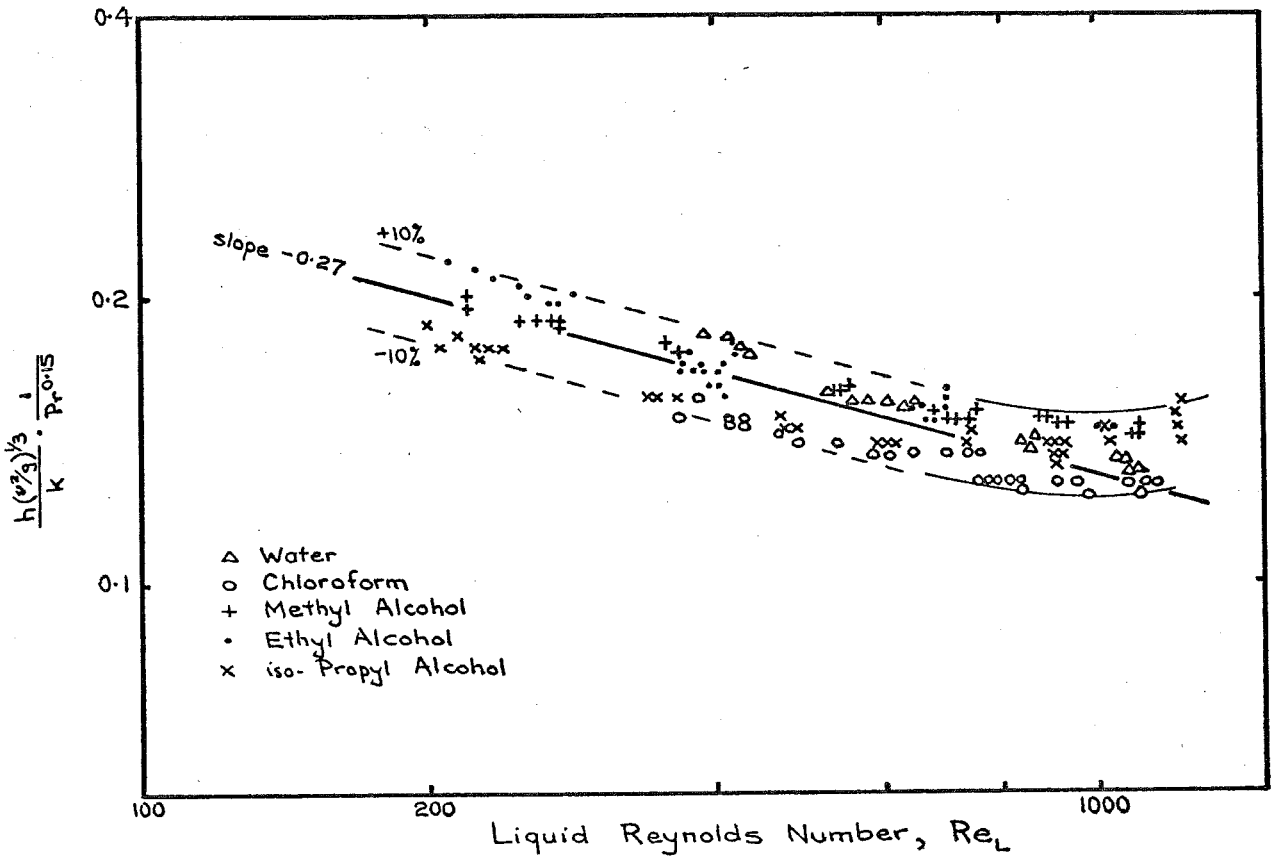

Figure 40A CORRELATION OF LAMINAR DATA

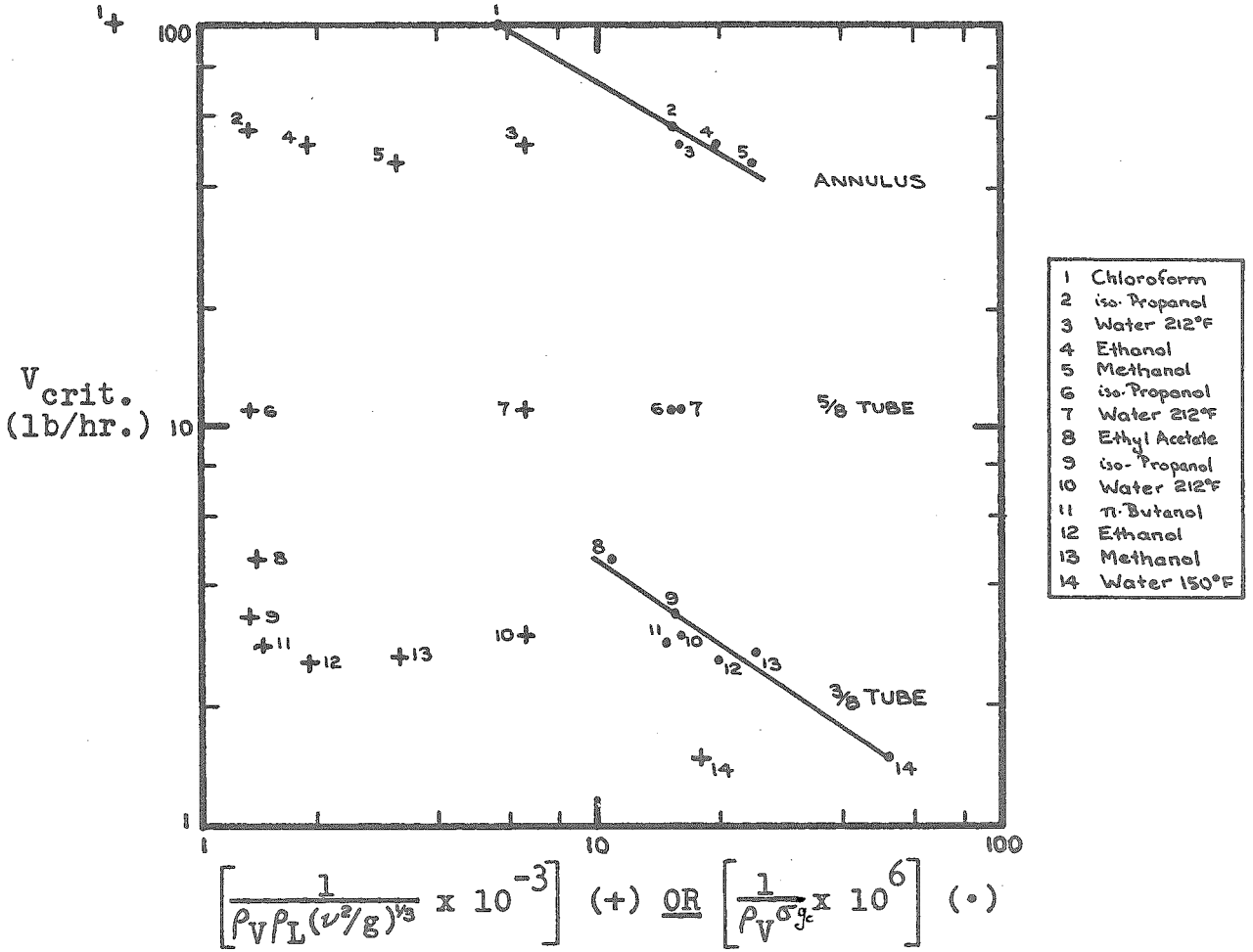

Figure 41 CRITICAL VAPOUR FLOWRATE DATA

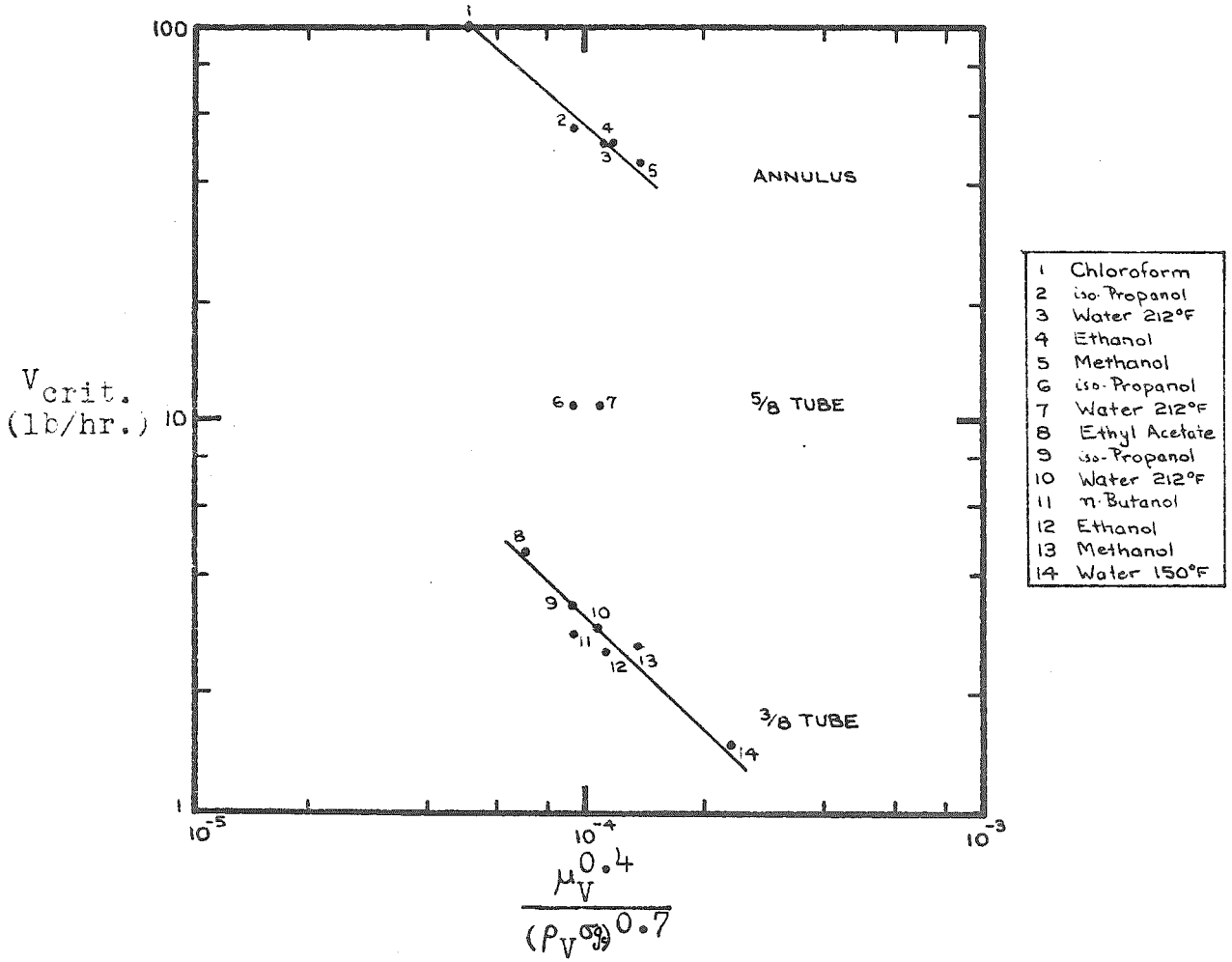

Figure 42 PARTIAL CORRELATION OF CRITICAL VAPOUR FLOWRATE DATA

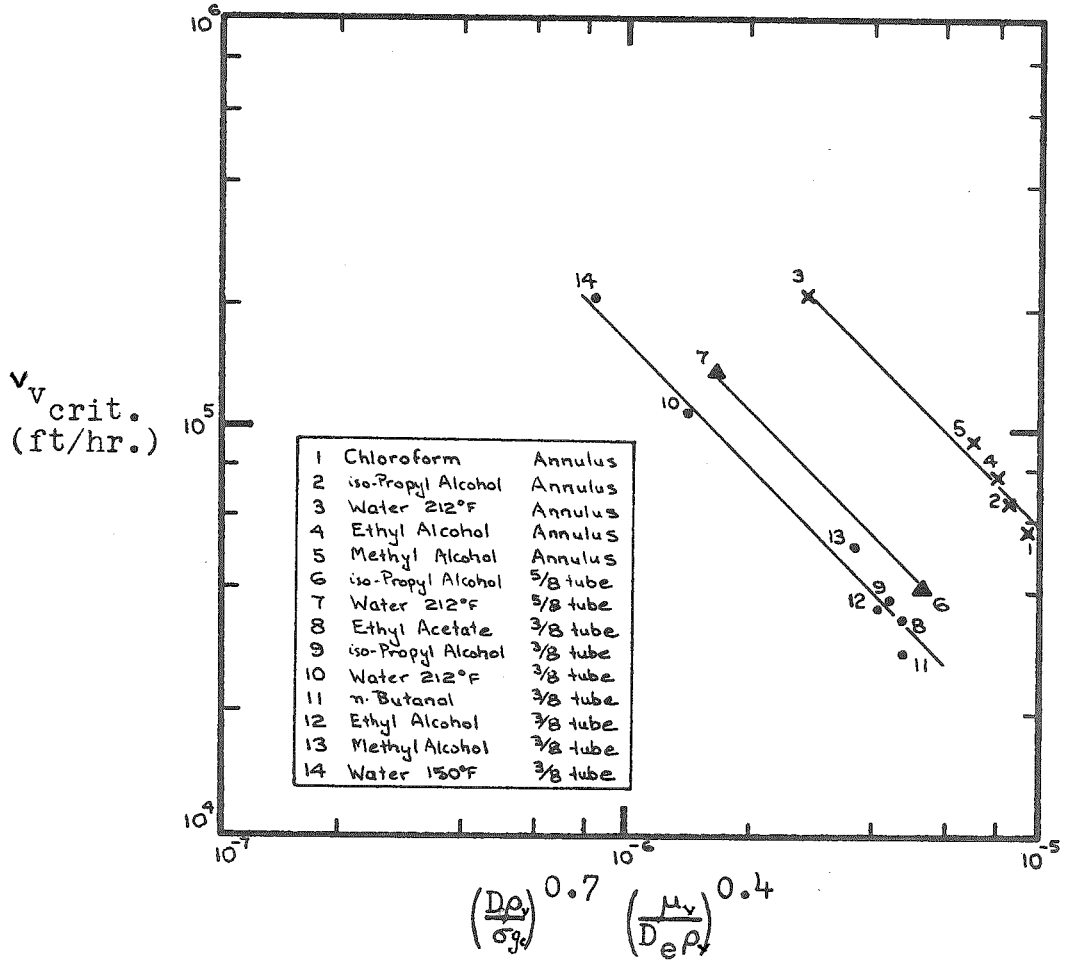

Figure 43 PARTIAL CORRELATION OF CRITICAL VAPOUR VELOCITY DATA

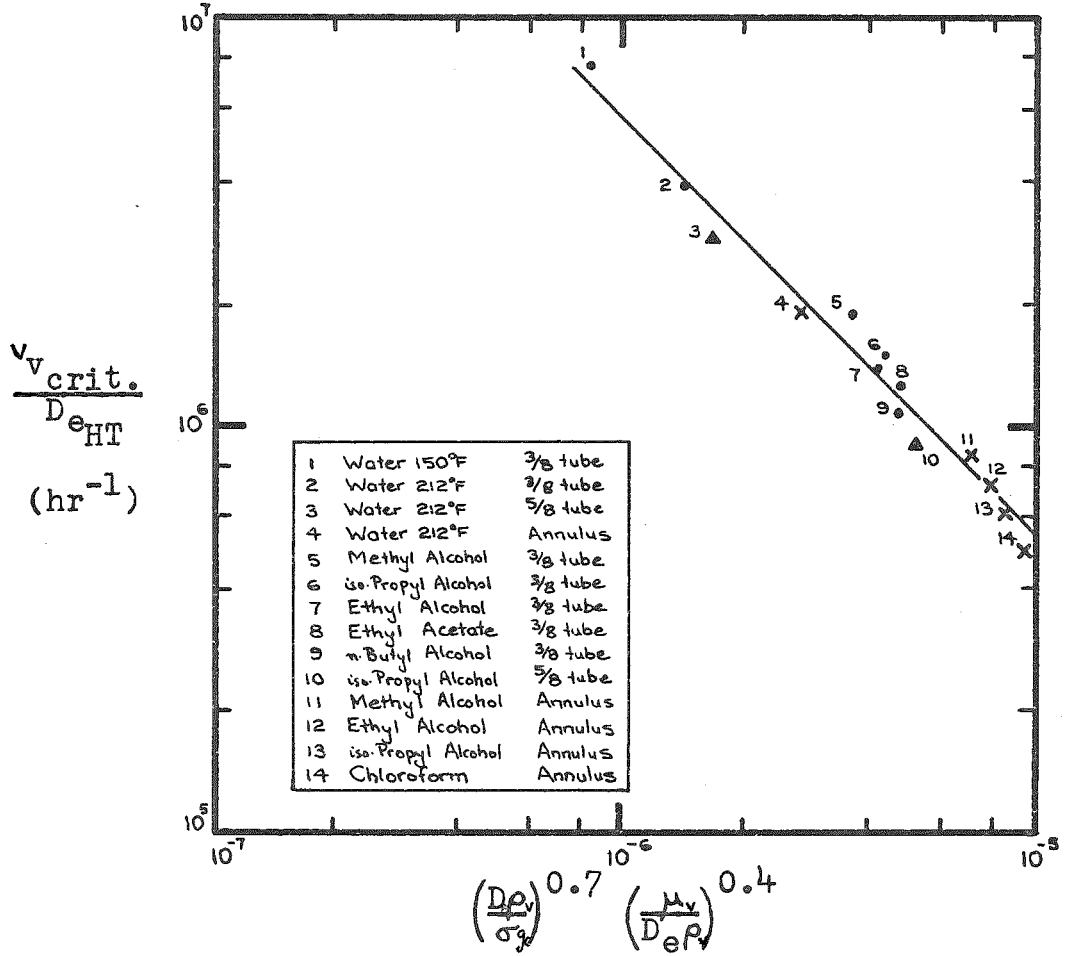

Figure 44 CORRELATION OF CRITICAL VAPOUR VELOCITY DATA

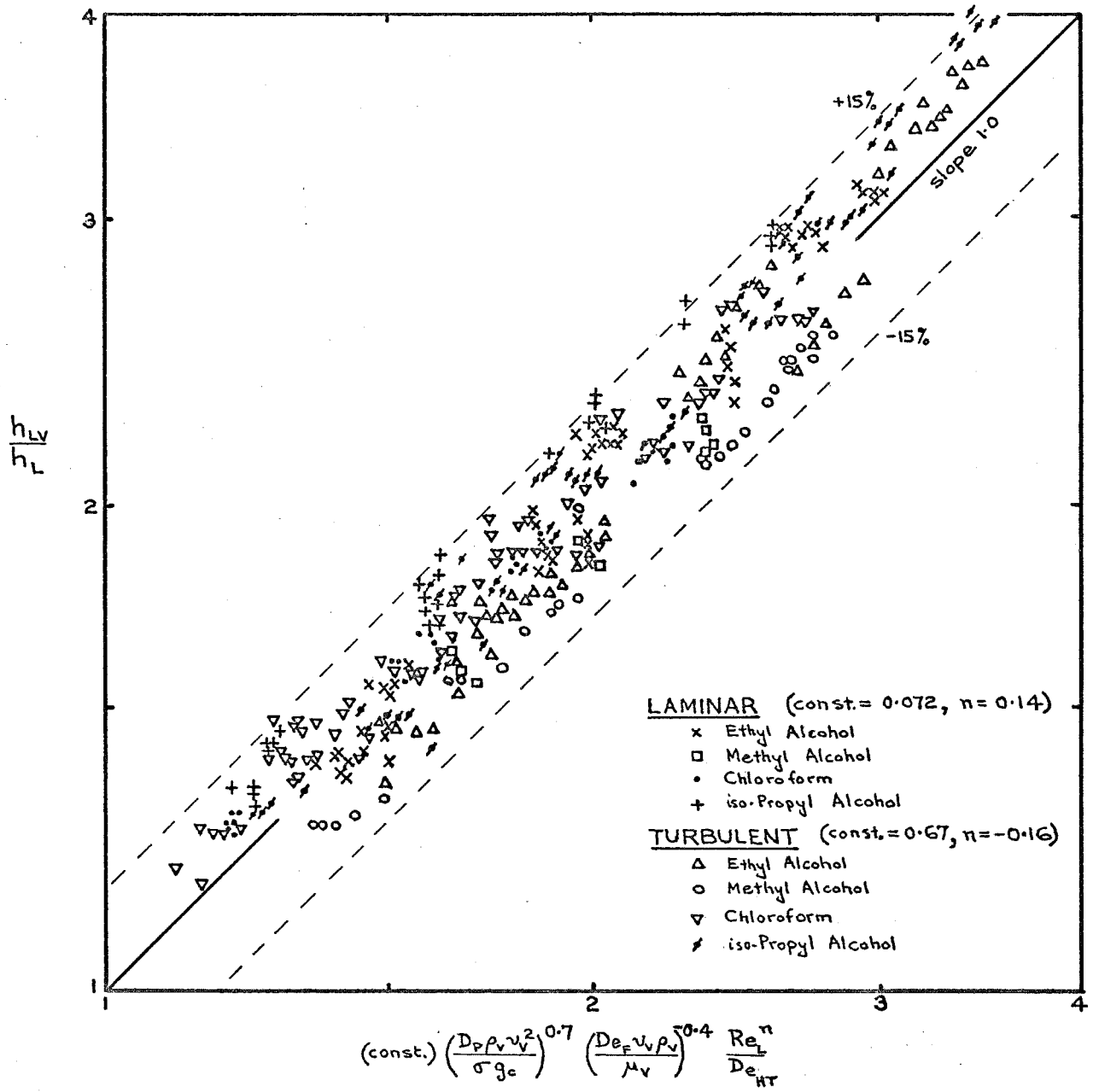

Figure 45 CORRELATION OF HEAT TRANSFER DATA FOR SUPRACRITICAL VAPOUR FLOW

6. DISCUSSION

Previous work has been discussed in Section 2. In this Section the proposed correlations will be compared with the results of previous workers, any discrepancies will be discussed, and the significance of the correlation methods will be examined.

6.1. Comparison with Previous Workers

In Figures 46 to 48 (Pages 189-191) experimental data obtained for conditions of negligible interfacial shear are compared with the following correlations, analyses, or experimental data of previous workers:

(1) Nusselt (laminar condensation):

$$Nu = 1$$

$$\text{i.e. } Nu' = \frac{h(\nu^2/g)^{1/3}}{k} = 1.10\ Re^{-1/3}.$$

(2) Nusselt (laminar condensation), recommended:

$$Nu'_{rec.} = 1.2\ Nu' .$$

(3) Wilke (laminar non-boiling heat transfer) - Low Pr (water, Pr = 5.4):

For $Re < 800$

$$Nu = \frac{1.6}{1.15} = 1.39$$

$$\text{i.e. } Nu'_{W_1} = 1.39\ (1.10\ Re^{-1/3}) = 1.53\ Re^{-1/3}.$$

(4) Wilke (laminar non-boiling heat transfer) - Higher Pr (9.4 and above):

For $Re < 600$

$$Nu = \frac{1.88}{1.15} = 1.64$$

i.e. $$Nu'_{W_2} = 1.64\ (1.10\ Re^{-1/3}) = 1.80\ Re^{-1/3}.$$

(5) Wilke (turbulent non-boiling heat transfer):

(a) For $400 < \Gamma/\mu < 800$ (i.e. $1600 < Re < 3200$)

$$Nu = \frac{h't}{k} = 0.00112\ (\Gamma/\mu)^{6/5}\ Pr^{0.344}$$

Substitute, $t = 0.302\ (3\nu^2/g)^{1/3}\ (\Gamma/\mu)^{8/15}$

(Brauer (12) film thickness equation)

$$\therefore \quad \frac{h'(\nu^2/g)}{k} = \frac{0.00112}{0.302 \times 3^{1/3}}\ (\Gamma/\mu)^{2/3}\ Pr^{0.344}$$

$$= \frac{0.00112}{0.302 \times 3^{1/3} \times 4^{2/3}}\ \left(\frac{4\Gamma}{\mu}\right)^{2/3}\ Pr^{0.344}$$

$$= 0.00102\ \left(\frac{4\Gamma}{\mu}\right)^{2/3}\ Pr^{0.344}.$$

(b) For $800 < \Gamma/\mu$ (i.e. $3200 < Re$)

$$Nu = 0.0066\ (\Gamma/\mu)^{14/15}\ Pr^{0.344}$$

$$\therefore \quad \frac{h'(\nu^2/g)^{1/3}}{k} = \frac{0.0066}{0.302 \times 3^{1/3} \times 4^{0.4}}\ \left(\frac{4\Gamma}{\mu}\right)^{0.4}\ Pr^{0.344}$$

$$0.00873\ \left(\frac{4\Gamma}{\mu}\right)^{0.4}\ Pr^{0.344}.$$

(6) Colburn (turbulent condensation), reliable only for $Re > 10000$:

$$\frac{h(\nu^2/g)^{1/3}}{k} = 0.056\ Re^{0.2}\ Pr^{1/3}.$$

(7) Colburn (turbulent condensation), recommended, based on revised constant:

$$\frac{h(\nu^2/g)^{1/3}}{k} = 0.051\ Re^{0.2}\ Pr^{1/3}.$$

(8) Drew (turbulent non-boiling heat transfer), with whom fair agreement was found by Sinek and Young for falling film evaporation:

$$\frac{h(\nu^2/g)^{1/3}}{k} = 0.01\ Re^{1/3}\ Pr^{1/3}.$$

(9) Dukler (general analysis of falling film heat transfer):

$\frac{h(\nu^2/g)^{1/3}}{k}$ vs. Re data, for Pr = 2, 5 and 10, taken from Figures 4, 5 and 6 of Reference (32).

(10) Staker (falling film evaporation inside $\frac{3}{8}$ in. I.D. tube, 17 in. long):

Experimental data, for water at 212°F, Pr = 1.76, taken from Figure 32 of Reference (80).

(11) Clegg (falling film evaporation outside 1 in. O.D. tube, 40 in. long, 38 in. heated length):

Experimental data, for water at 212°F, Pr = 1.76, personal communication (18).

The work of most of the above authors was discussed previously in Section 2.2.

6.1.1. Comparison of data obtained for conditions of negligible interfacial shear

Figures 46 to 48 show that there are significant differences among the results of some of the previous workers. However it can be seen that there is a general consensus of opinion among the workers. The results of the present investigation are in good agreement with this consensus of opinion. The agreement is even better if the suspect high-flow rate data be omitted (the broad lines in Figures 46 to 48 represent the correlation for all of the experimental data, the shorter dotted lines represent the correlation after the omission of the maximum-flow rate data).

Comparison with two of the major workers - Dukler and Wilke - will now be made. This will be followed by a general comparison.

6.1.1.1. Comparison with the analysis of Dukler

The Dukler analysis predicts a flatter overall trend of heat transfer coefficient with liquid Reynolds number than that which has been observed with the experimental results.

The analysis predicts approximately the correct trend for turbulent flow, particularly for Re >10000.

However, for the laminar regime, Dukler predicts a coefficient which varies only slightly over the range Re =100 to 1000. This prediction is not in agreement with the observed trend. The analysis tends towards the Nusselt theoretical line (which corresponds to the condition $u^+ = y^+$) as Re is decreased, and merges with the line at small Reynolds numbers. The experimental data also tend to converge with the Nusselt line but the rate of convergence is much greater for the Dukler analysis than for the observed results. With this different rate of convergence, at the upper limit of the laminar regime the Dukler analysis predicts neither the correct trend for h vs. Re nor the correct magnitude of the coefficient.

For the transition regime there are differences of up to 90% between the analysis and the experimental results. In Section 2.2.3 the possibility of such a disagreement was predicted on the basis of an observed difference, for $y^+ > 5$, between the Deissler universal velocity distribution and experimental profiles measured for Re $< 20{,}000$. It was suggested that the observed uncertainty should lead to the prediction of high heat transfer coefficients for the transition flow regime and for the lower part of the turbulent regime. This would explain the observed deviation of the Dukler analysis from the experimental results.

Thus, the Dukler analysis is applicable at small and

at large Reynolds numbers. These conditions correspond to the cases for which observers agree on the velocity distributions, on which prediction of the eddy diffusivities depends.

6.1.1.2. Comparison with the data of Wilke

The experimental data for the laminar regime tend toward or lie between the limits of Nu = 1.63 to 1.2 for Pr = 9.4, or Nu = 1.39 to 1.0 for the liquids of lower Prandtl number. These are the limits which were suggested in Section 2.2.5., in which the results of Wilke were corrected for his different definition of film temperature difference.

For the turbulent regime, close agreement between the observed trends of heat transfer coefficient with liquid Reynolds number is found, but the data of Wilke are about 50% higher than the data for the present investigation. Only part of this difference can be explained by the different basis for temperature difference (at most, 13% of the Wilke values, see Section 2.2.5). Wilke previously explained his high results by the suggestion that the results of other workers included the effect of the thermal entry zone. However, in Figures 46 to 48 it can be seen that the results for the present investigation (18 in. heated section) are in good agreement with the correlation of Drew (based on results for sections up to 6 ft. long). In Section 2.2.3 the Drew correlation was reported to be in agreement with the results

of Sinek and Young (falling film evaporator tubes 24 ft. long). These agreements suggest that the results of the present investigation have not been affected seriously by thermal entry zone effects.

6.1.1.3. General comparison of falling film evaporation, condensation and non-boiling results

The plots in Figures 46 to 48 indicate that the analysis of Dukler, the empirical analysis of Colburn, and the wide-range non-boiling correlation of Drew, tend to converge at large Reynolds numbers.

In addition, the experimental data for the present investigation are seen to be in good agreement with the correlation of Drew for the non-boiling turbulent regime. The slope of the experimental $\frac{h(\nu^2/g)^{1/3}}{k}$ vs. Re line is greater, but it is in good agreement with the slopes observed by Wilke, especially if the suspect high flow rate data be omitted from the present experimental data.

The differences among the observed slopes for the turbulent regime (Colburn 0.2, Drew $1/3$, Dukler 0.2 to 0.25, Wilke 0.4 to $2/3$, present investigation 0.5) require that further work should be done at large Reynolds numbers if detailed conclusions are to be drawn regarding mechanism.

Differences among the predicted and the observed Prandtl number exponents for the turbulent regime (Colburn $1/3$, Drew $1/3$, Dukler 0.5 to 0.6 (Appendix V, Figure A9), Wilke 0.344,

present investigation $^{1}/_{3}$) also are apparent.

For the laminar regime the experimental data are in good agreement with the Wilke correlation (suitably modified), and are in fair agreement with the corrected Nusselt line.

It can be concluded, from inspection of Figures 46 to 48, that a general trend line with ±30% limits could be drawn which would include all of the plotted correlations and analyses for the range of applicability of each. Thus, for the ranges of Reynolds numbers and Prandtl numbers which have been considered, there is general agreement between the results for falling film evaporation, falling film condensation, and non-boiling falling film heat transfer, despite the observed differences among the Re and Pr exponents.

6.1.2. Comparison of Correlations obtained for supracritical vapour flow

The supracritical vapour flow correlations of Dukler, Rohsenow et al., and Carpenter and Colburn were discussed in Sections 2.2.2. and 2.2.3.

Quantitative comparison of the correlation method proposed in Section 5 with these previous correlations would require that pressure drop or friction factor data be available. These data, which would be required for the calculation of the interfacial shear variables β, $\tau_V^{\pm}$ and F_V, were not measured for the present investigation, but will be

supplied by Clegg (17).

Therefore, rather than assume the applicability or accuracy of previously published correlations of ΔP or f, discussion will be limited to a qualitative comparison. This will suffice as a basis for the discussion of mechanisms.

The interrelation among the various interfacial shear variables will be considered initially. This will be followed by a discussion of the observed effect of liquid surface tension.

6.1.2.1. The equivalence of the interfacial shear terms

Mechanism Ratio Analysis predicted that the terms Fr', We and Re_V would be required in order to correlate supracritical vapour flow data.

Consider the Dukler term, β, the dimensionless interfacial shear.

$$\beta = \frac{F.r.g^{1/3}.\rho_L^{2/3}}{2\mu_L^{2/3}} = \frac{F.r}{2} \Big/ (\nu^2/g)^{1/3}$$

where $F = \frac{\text{frictional pressure gradient}}{\text{liquid density}}$, and is dimensionless.

For $F = \frac{(\frac{\Delta P}{Z})_{TP}}{\rho_L}$ to be dimensionless, the pressure gradient must be defined to include g/g_c.

Introducing Carpenter and Colburn nomenclature,

$$F_V = \frac{\Delta P \; g_c \; D}{4 \; Z} = \frac{f \; G_V^2}{2 \; \rho_V}$$

Thus, for comparison between Dukler and Carpenter and Colburn,

$$\left(\frac{\Delta P}{Z}\right)_{TP} g/g_c = \frac{\Delta P}{Z}$$

$$\therefore \quad F = \frac{\left(\frac{\Delta P}{Z}\right)_{TP}}{\rho_L} = \frac{\frac{\Delta P}{Z} \cdot \frac{g_c}{g}}{\rho_L} = \left(\frac{4}{\rho_L \; g \; D}\right) \left(\frac{f \; G_V^2}{2 \; \rho_V}\right)$$

where $G_V = \rho_V \; v_V$

Substituting into the Dukler equation,

$$\beta = (\text{constant}) \cdot f \cdot \frac{\rho_V \; v_V^2}{\rho_L \; g \; (\nu^2/g)^{1/3}}$$

Multiplying throughout by $\left(\frac{Re_L}{Re_L}\right)^n$, where n is dependent upon the flow regime,

$$\beta = (\text{constant}) \cdot f \cdot \frac{\rho_V \; v_V^2}{\rho_L \; g \; (\nu^2/g)^{1/3} Re^n} \cdot Re^n$$

$$= (\text{constant}) \cdot f \cdot (Fr') \cdot Re^n$$

Also, Bergelin et al (11) showed that

$$f = \phi \left[Re_V, \frac{\sigma_{water} \; \Gamma}{\sigma_L \; \rho_L} \right]$$

$$\therefore \beta = \phi' \left[Fr', Re_V, Re_L, \frac{\sigma_{water} \; \Gamma}{\sigma_L \; \rho_L} \right]$$

This function is of similar form to that predicted by Mechanism Ratio Analysis. The Weber group does not appear, but basis

for it is supplied by the appearance of liquid surface tension in the denominator of the group $\frac{\sigma_{water}\,\Gamma}{\sigma_L\,\rho_L}$.

Consider also the τ_V^* term of Rohsenow et al.

$$\tau_V^* = \frac{g_c\,\tau_V}{g\,(\rho_L - \rho_V)\,(\nu^2/g)^{1/3}}$$

Rohsenow et al gave τ_V (using Carpenter and Colburn nomenclature) as

$$\tau_V = \frac{f\,G_V^2}{2\,g_c\,\rho_V}$$

$$\therefore\ \tau_V^* = \frac{g_c \cdot \frac{f\,G_V^2}{2\,g_c\,\rho_V}}{g\,(\rho_L - \rho_V)\,(\nu^2/g)^{1/3}}$$

$$= (\text{constant}) \cdot f \cdot \frac{\rho_V\,v_V^2}{g\,(\rho_L - \rho_V)\,(\nu^2/g)^{1/3}}$$

But $(\rho_L - \rho_V) \simeq \rho_L$

Thus τ_V^* reduces to the reduced form of Dukler's β. Furthermore, Rohsenow et al showed that the correlation method of Carpenter and Colburn may be reduced to a form identical to that of their own.

Thus, the supracritical vapour flow correlation methods of Dukler, Rohsenow et al, and Carpenter and Colburn are equivalent, and are similar in form to the function proposed by Mechanism Ratio Analysis in Section 5.1.

6.1.2.2. The effect of liquid surface tension

The main difference between the correlation method for the present investigation and the methods of the previous workers is in the different forms taken by the major vapour velocity term, although agreement is found for the value of the overall vapour velocity exponent (see Sections 2.2.2.4, 2.2.3 and 4.4.3).

The analyses predict the use of an Fr'-type term, as shown in Section 6.1.2.1, and the liquid surface tension does not appear directly in the correlation. However, for the present investigation, the Weber group is found to be highly significant (Figure 41), and the use of Fr' is rejected because of the considerable scatter observed with results plotted in Figure 41 using this group.

With the rejection of the use of Fr' for the present investigation, the correlation presented for supracritical vapour flow has one too few mechanism ratios for the number of mechanisms which are presumed to act. Considering the satisfactory use of the equivalent of Fr' shown in Section 6.1.2.1, the use of the term cannot be eliminated definitely. However, the results for the present investigation would suggest an emphasis on the various vapour velocity terms significantly different to that predicted by previous workers.

Thus, previous workers suggest little or no effect of surface tension, whereas the present results suggest that

$h \propto \sigma^{-0.7}$ for falling film heat transfer under supracritical vapour flow conditions.

The significance of this observation will be discussed further in Section 6.3, after consideration has been given to the range of experimental variables for which this and other observations are valid.

6.2. The Ranges of the Experimental Variables

The ranges of the major experimental variables, including the additional data of Staker, are summarised in the following Table.

RANGES OF THE EXPERIMENTAL VARIABLES

Variable	Units	Range for Present Investigation	Range including Data of Staker	Overall Variation
Re_L	-	200-8500 (effective upper limit is 6000)		30:1
Pr_L	-	1.8, 3.6, 4.8, 9.7, 13.5		7.5:1
$\frac{h_L(\nu^2/g)^{1/3}}{k}$	-	0.143-0.35		2.5:1
$\frac{h_{LV}}{h_L}$	-	0.96-4.02		4.2:1
G_V	$lb/hr ft^2$	up to 40900		
v_V	ft/hr	up to 233000		
We	-	up to 940		
Re_V	-	up to 59800		
σ	$\frac{lb\ force}{ft}$	0.00115-0.00403	0.00113-0.0045	4.0:1
$\frac{1}{\rho_V \sigma\ g_c}$	$\left(\frac{lb^2}{ft^3 hr^2}\right)^{-1}$	0.58×10^{-5}-2.42×10^{-5}	0.58×10^{-5}-5.17×10^{-5}	8.9:1

RANGES OF THE EXPERIMENTAL VARIABLES

Variable	Units	Range for Present Investigation	Range including Data of Staker	Overall Variation
$\frac{1}{\rho_V \rho_L (\nu^2/g)^{1/3}}$	$\frac{ft^5}{lb^2}$	620-6600	620-17800	29:1
V_{crit}	lb/hr	45-100	1.5-100	67:1
$v_{V_{crit}}$	ft/hr	5.6×10^4-21.2×10^4	2.8×10^4-21.2×10^4	7.6:1
We_{crit}	-	85.5-122	6.3-122	19.4:1
$Re_{V_{crit}}$	-	10000-22000	2300-22000	9.6:1
D_P *	in.	1.000	0.375, 0.625, 1.000	2.7:1
D_{e_F} *	in.	0.487	0.375, 0.487, 0.625	1.7:1
$D_{e_{HT}}$ *	in.	1.21	0.375, 0.625, 1.21	3.2:1
$v_{V_{crit}}/D_{e_{HT}}$	hr^{-1}	4.9×10^5-18.9×10^5	4.9×10^5-75.3×10^5	15:1

*dry wall basis

6.2.1. Comments on Ranges, and Recommendations for Future Work

1. The variation of liquid flowrates is satisfactory, considering the simple design of the liquid distribution system.

The laminar and the transitional flow regimes are covered adequately. However, further work at higher flowrates will be necessary to obtain a more reliable trend of $\frac{h(\nu^2/g)^{1/3}}{k}$ vs. Re for the turbulent regime, and also to test agreement with the suggested convergence (for $Re > 10^4$) of the results of previous workers.

2. The range of Prandtl numbers is limited, but it includes the values for most of the common organics at their normal boiling points (e.g. the range Pr = 1.8 to 13.5 includes the Prandtl numbers at the boiling points of each of the 29 pure liquids considered by McAdams (60e) in his nomogram for liquid Prandtl numbers).

3. The range of vapour flow rates is sufficient for the critical vapour flow rate to be considered satisfactorily, but further work at higher flow rates will be required to check the trend of $\frac{h_{LV}}{h_L}$ vs. V at the point of onset of significant entrainment.

4. The 4:1 variation of liquid surface tension is greater than the variation of 3.3:1 (for test liquids water,

ethanol, methanol, toluene and trichlorethylene) considered by Carpenter and Colburn, whose experimental data were used as bases for the checks of the theoretical analyses of Dukler and of Rohsenow et al.

The ranges of $\frac{1}{\rho_V \sigma}$ and $\frac{1}{\rho_V \rho_L (\nu^2/g)^{1/3}}$ are satisfactory for the rejection of the Fr'-type term suggested by Dukler and by Rohsenow et al, and for its replacement by a Weber number term.

Additional work, including pressure drop measurements, will be required to check whether surface tension must be introduced into the theoretical interfacial shear analyses.

The comments given above indicate that sufficient ranges of the most important variables have been considered for reliable conclusions regarding mechanisms to be drawn from the experimental data and from the mechanism ratio correlations.

6.3. The Significance of the Correlations

For film flow alone, the correlations are similar to the common form for heat transfer in closed conduits, $Nu = \frac{hD}{k} = \phi\,(Re, Pr)$, except that for the present case the equivalent of film thickness is used as the characteristic length term for the Nusselt number. This use indicates the

importance of the film thickness in determining heat transport across the falling film.

At small liquid Reynolds numbers, the tendency of the experimental results to converge with the Nusselt analysis indicates that the heat transfer mechanism tends to one of simple conduction across the film. However, with increase of the liquid Reynolds number, deviation from the Nusselt analysis is encountered. This deviation corresponds to the onset of significant eddy transport in the outer layers of the falling film, and possibly also to a small eddy contribution to transport across the laminar sublayer.

These observations are consistent with the conclusions of previous workers.

For supracritical vapour flow, the variation in the form of the correlation indicates the occurrence of significant changes in the overall mechanism.

It is found that vapour-induced liquid turbulence predominates over the eddy action induced by the liquid flow. This predominance is indicated by the observed necessity to introduce $D_{e_{HT}}$ into the Nusselt group to replace the film thickness term, and also by the observed decrease in the dependence on L as V is increased, and by the observed onset of turbulence at smaller L as V is increased.

Further, the observation of a significant effect of liquid surface tension suggests that disruption of the film,

either as entrainment of superheated liquid or as the promotion of rippling and of interfacial turbulence, predominates over the simple interfacial shear effect which would be suggested by the use of an Fr'-type group.

A further change in mechanism is encountered at the point of occurrence of significant entrainment. The observed large change in the slope of the h vs. V relation corresponds with the predominance of the liquid film disruption mechanism.

Thus, the mechanism for the observed increase of heat transfer for supracritical vapour flow appears to be a combination of increased transport across the film by eddy action generated at the interface, and increased transport from the film surface promoted by interfacial disruption. This latter effect has not been considered in the analyses of previous workers.

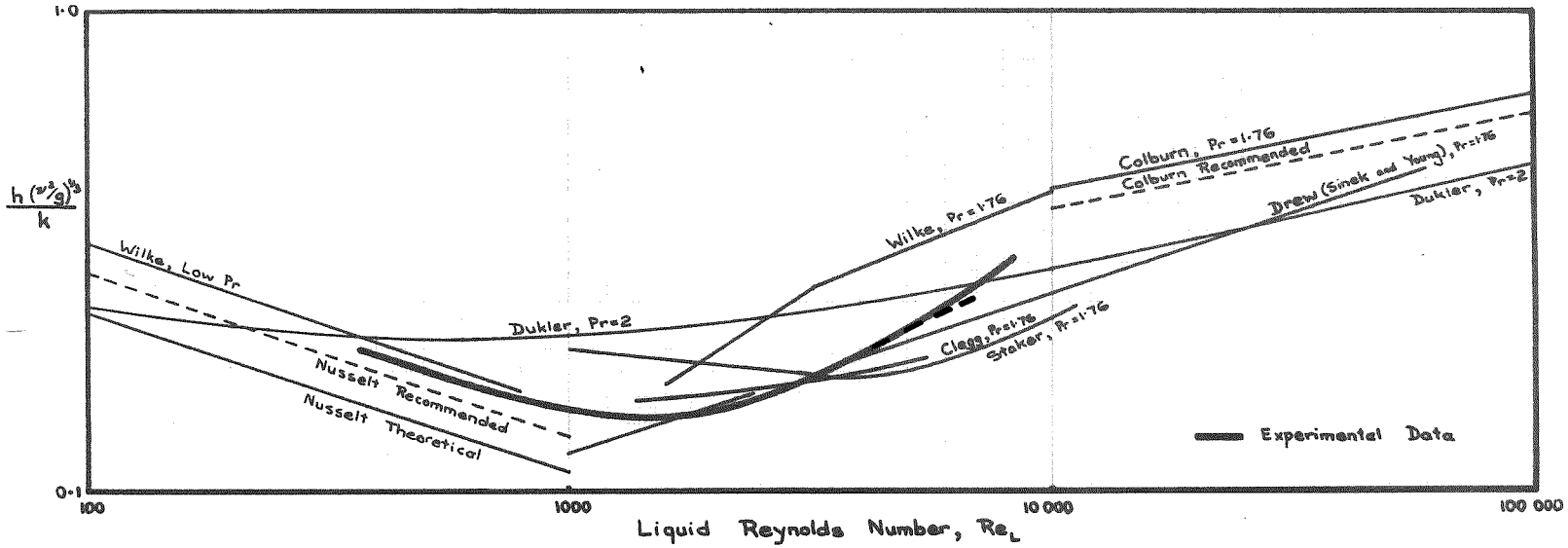

Figure 46 COMPARISON WITH PREVIOUS WORKERS WATER Pr = 1.76

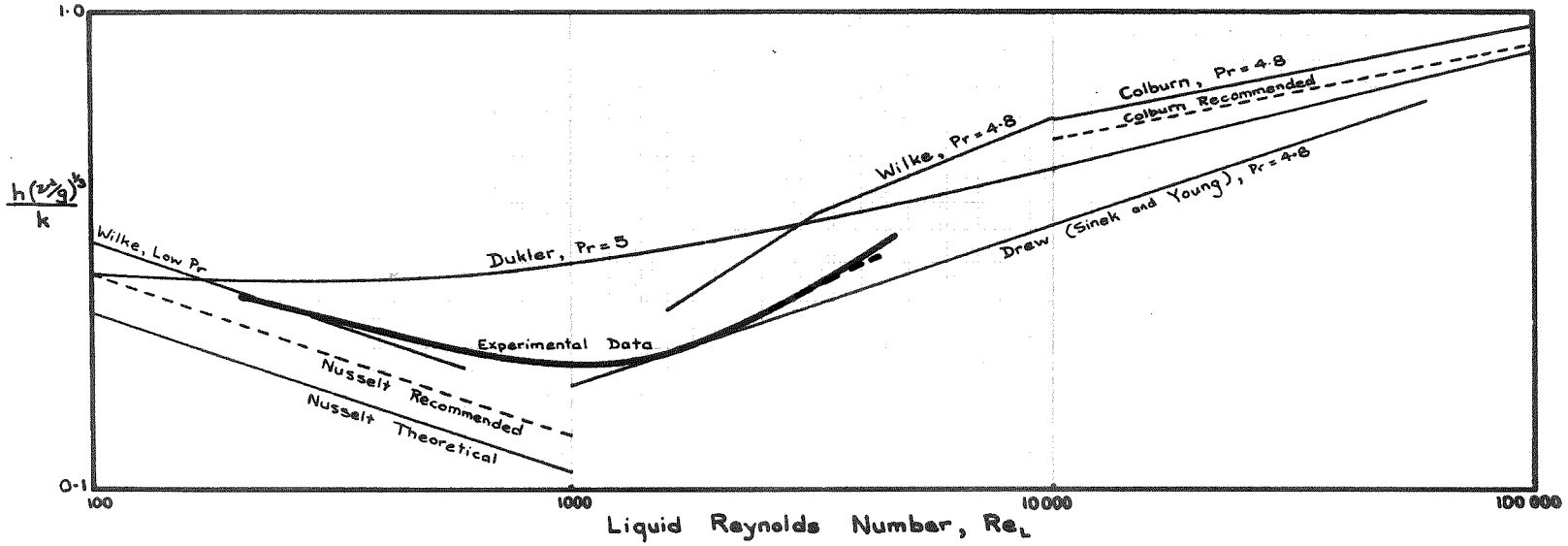

Figure 47 COMPARISON WITH PREVIOUS WORKERS METHYL ALCOHOL Pr = 4.8

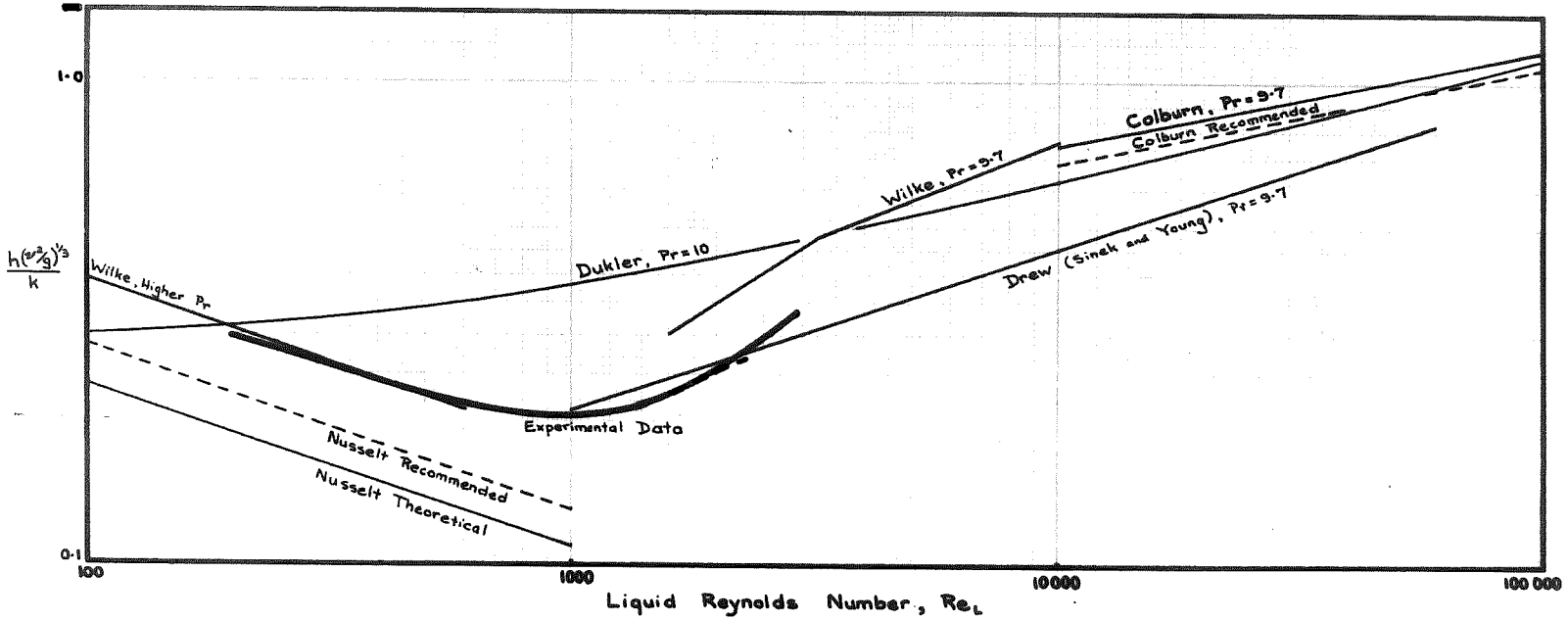

Figure 48 COMPARISON WITH PREVIOUS WORKERS ETHYL ALCOHOL Pr = 9.7

7. CONCLUSIONS

Falling film evaporation mechanisms

Consideration of local heat transfer coefficients and local liquid and vapour flow rates has enabled the individual effects of temperature difference, liquid flow rate, and vapour flow rate, to be separated for falling film evaporation.

For small temperature differences and subcritical vapour flows, heat transfer across the film occurs by a combination of conduction and eddy turbulence mechanisms, and heat transport from the film occurs by evaporation at the liquid-vapour interface. The heat transfer coefficient is practically independent of temperature difference, provided that the liquid and vapour feed rates are corrected for vaporization to give local flow rates.

A gradual transition from the predominantly laminar to the predominantly turbulent flow regime is observed. This observation agrees with the theoretical prediction of Dukler, but differs from early condensation correlations which suggested a sharp transition despite the gradual transition shown by experimental data.

For temperature differences greater than a critical value, nucleate boiling commences and predominates as the heat transfer mechanism. Beyond ΔT_{crit} it is found that

$h \propto (\Delta T)^n$, where n is large (approximately 5 to 10), and is determined by the nature of the heat transfer surface and by the duration of its ageing. The critical temperature difference is also dependent upon these factors. Data for the nucleate boiling regime were not consistently reproducible because of the stages of surface ageing which were encountered, and satisfactory data for n, ΔT_{crit}, and for any slight effect of liquid and vapour flowrate, could not be obtained. It is significant that for the same aged-surface runs for which reproducibility could not be obtained for the nucleate boiling regime, good reproducibility was found for the falling film regime.

As the concurrent flow of vapour increases, the heat transfer mechanism for the falling film evaporation regime is not affected significantly until a critical vapour flow rate is exceeded. Beyond the critical vapour flow rate it is found that $h \propto V^{1.0}$. The exponent is in satisfactory agreement with the work of Carpenter and Colburn for condensation, and with the prediction of the theoretical analysis of Dukler. The mechanism becomes decreasingly liquid flow dependent with increasing vapour flow, and the mechanism appears to be controlled by vapour-induced turbulence and by a liquid interface disruption mechanism. Previous workers for falling films with interfacial shear, with the exception of Staker, have not directly included a surface tension term in their analyses.

At higher vapour flow rates significant entrainment occurs and the flow becomes dispersed. At this point there is a sudden break in the h vs. V relation, which becomes $h \propto V^{0.5-0.6}$, which is in agreement with previous work on heat transfer in the climbing film evaporator and heat transfer to mist flow. This observation suggests an explanation for exponents of 0.5, within a range 0.5 to 0.7, which were observed by Staker for the falling film evaporator. The observation also emphasizes the differences between the mechanisms which are presumed to operate in the falling film evaporator and in the climbing film evaporator.

For large-scale falling film evaporators, the longitudinal variation of liquid-vapour conditions may be sufficient not only to cause the observed variation with flow of heat transfer coefficients within a particular regime but also to lead to the observed changes of heat transfer mechanism at points along the flow surface. Therefore, for practical evaporator design, account will have to be taken of the regimes which have been observed. Only few critical data are presented in the text for the onset of nucleate boiling or for the onset of significant entrainment. However, the critical flow rate data which are presented should enable the prevailing combination of the conditions of laminar or turbulent liquid flow with concurrent subcritical or supracritical vapour flow to be determined for successive

design increments of flow surface. The relevant heat transfer correlating expressions (of those given below) can then be applied for calculations over each increment.

Falling film heat transfer correlations

Correlations in terms of mechanism ratios have been derived by Mechanism Ratio Analysis, and general similarity with previous correlations for falling film condensation, falling film evaporation, and non-boiling falling film heat transfer, has been shown.

The experimental data for the 1 in. I.D. x 1½ in. O.D. annulus are correlated by the following expressions, which are applicable for the given flow ranges.

Laminar liquid flow

$$\frac{h_L (\nu^2/g)^{1/3}}{k} = 0.84\ Re_L^{-0.27}\ Pr^{0.15}$$

(Flow range, $200 < Re_L < 1000$. The expression correlates within ±10% up to Re = 600, and within -20% at Re = 1000.)

Turbulent liquid flow

$$\frac{h_L (\nu^2/g)^{1/3}}{k} = 0.0027\ Re_L^{0.5}\ Pr^{1/3}$$

(Flow range, $1600 < Re_L < 6000$. The expression correlates within ±10%.)

Laminar liquid flow with supracritical vapour flow

$$\frac{h_{LV}}{h_L} = 0.072\ We^{0.7}\ Re_V^{-0.4}\ \frac{Re_L^{0.14}}{D_{e_{HT}}}$$

Turbulent liquid flow with supracritical vapour flow

$$\frac{h_{LV}}{h_L} = 0.67\ We^{0.7}\ Re_V^{-0.4}\ \frac{Re_L^{-0.16}}{D_{e_{HT}}}$$

(Flow ranges, $1 < (\text{const.})\ We^{0.7}\ Re_V^{-0.4}\ \frac{Re_L^{n}}{D_{e_{HT}}} < 3.6.$ The expressions correlate within ±15%.)

The critical vapour velocity, below which $\frac{h_{LV}}{h_L} \simeq 1$, is given by

$$(\text{const.})\ We^{0.7}\ Re_V^{-0.4}\ \frac{Re_L^{n}}{D_{e_{HT}}} = 1.$$

This correlation is also applicable to data obtained by Staker for falling film evaporation inside $\frac{3}{8}$ in. and $\frac{5}{8}$ in. diameter tubes.

The film flow correlations agree with the most satisfactory previous analysis, that of Dukler, at small laminar Reynolds numbers and large turbulent Reynolds numbers. An explanation of the observed deviation in the transitional regime is proposed in terms of an uncertainty in the Deissler expression for the buffer regime.

For the supracritical vapour flow correlations, an important difference is apparent between the present

correlations and the analyses proposed by Dukler, Rohsenow et al., and Carpenter and Colburn. The previous workers predict the use of a Fr'-type term, whereas, for the present investigation, the use of this term was checked and rejected in favour of the use of a Weber group term. Further work is required to check the necessity to introduce liquid surface tension into the correlation.

8. NOMENCLATURE

A	heat transfer area, ft^2
B	dimensionless grouping used by Seban, defined in Section 2.2.2.2
c	specific heat of liquid, Btu/lb F^o
D	tube diameter, ft
D'	a characteristic dimension for an annulus, ft
D_{e_F}	equivalent diameter for flow, defined in Section 5.3
$D_{e_{HT}}$	equivalent diameter for heat transfer, defined in Section 5.3
D_p	liquid flow "perimeter", defined in Section 5.3
f	friction factor, dimensionless
f_D	tube diameter term used by Staker, $f_D = \frac{D}{0.016+0.48D}$
F	Dukler's term, frictional pressure gradient divided by liquid density, dimensionless
F_T	Carpenter and Colburn's term, total force or drag per unit surface of the laminar sublayer, $\frac{\text{lb mass}.\text{ft}}{ft^2 \quad hr^2}$
F_v	"force" due to vapour friction, $\frac{\text{lb mass}}{ft^2}.\frac{ft}{hr^2}$
F_2	term used by Seban, dimensionless, defined in Section 2.2.2.2
g	acceleration due to gravity, 4.17×10^8 ft/hr^2
g_c	conversion factor, $4.17 \times 10^8 \frac{\text{lb mass}.\text{ft}}{\text{lb force} \quad hr^2}$
G	liquid mass velocity, lb/hr ft^2
G_v	vapour mass velocity, lb/hr ft^2

h	local heat transfer coefficient, Btu/hr ft^2 F^o, based on $\Delta T = (T_{wall} - T_{saturation})$
h'	local heat transfer coefficient, Btu/hr ft^2 F^o, based on $\Delta T = (T_{wall} - T_{liquid,mean})$
h_L	local heat transfer coefficient, Btu/hr ft^2 F^o, for liquid flow L lb/hr alone
h_{LV}	local heat transfer coefficient, Btu/hr ft^2 F^o, for liquid flow L lb/hr and vapour flow V lb/hr
h_m	mean heat transfer coefficient, Btu/hr ft^2 F^o
H	height of condensation surface, ft, used by Jakob
j	Colburn j-factor, dimensionless, defined in Section 2.2.2.2
k	thermal conductivity of liquid, Btu/hr ft F^o
L	liquid mass flow rate, lb/hr
M	dimensionless term used by Rohsenow et al, $\dfrac{1}{\dfrac{\tau_y g_c}{g(\rho_L - \rho_V)x_o} + 1}$
m	numerical constant in Deissler's expression for eddy viscosity
n	miscellaneous exponents
p	numerical constant in Von Karman's expression for eddy viscosity
P	absolute pressure, lb force/ft^2
ΔP	pressure drop over length Z, lb force/ft^2
$\left(\dfrac{\Delta P}{Z}\right)_{TP}$	two-phase frictional pressure gradient, Dukler nomenclature, $\dfrac{\text{lb force}}{\text{ft}^2 \cdot \text{ft}} \cdot \dfrac{\text{lb mass}}{\text{lb force}}$
q	heat flux, Btu/hr
r	tube radius, ft

t	film thickness, ft
T	temperature, ^{o}F
ΔT	temperature difference, F^{o}, defined as $(T_{wall} - T_{saturation})$ for film evaporation, and $(T_{saturation} - T_{wall})$ for film condensation
u	local velocity in the direction of flow, ft/hr
u^{+}	universal velocity parameter, dimensionless, $u^{+} = \frac{u}{\sqrt{\frac{\tau_o g_c}{\rho}}}$
v	mean velocity of liquid, ft/hr
v_B	Penman's liquid-vapour bulk velocity, ft/hr, defined as $v_B = (\frac{L}{\rho_L} + \frac{V}{\rho_V}) \cdot \frac{1}{\text{flow area}}$
v_V	vapour velocity, ft/hr
$v_{V_{crit}}$	critical vapour velocity, ft/hr
V	vapour mass flow rate, lb/hr
V_{crit}	critical vapour mass flow rate, lb/hr
x_o	film thickness, ft, Rohsenow et al nomenclature
x_o^{+}	dimensionless liquid film thickness, Rohsenow et al nomenclature
$x_{o_L}^{*}$	film thickness term used by Rohsenow et al, dimensionless, defined as $x_{o_L}^{*} = \frac{x_o}{(\nu^2/g)^{1/3}}$
y	distance from wall, ft
y^{+}	universal distance parameter, dimensionless, defined as $y^{+} = \frac{y}{\nu}\sqrt{\frac{\tau_o g_c}{\rho}} = \frac{yu}{\nu} \cdot \sqrt{\frac{f}{2}}$

y^{++} modified universal distance parameter, dimensionless, defined as $y^{++} = \frac{yu}{\nu} \cdot \frac{f}{2} = y^{+} \cdot \sqrt{\frac{f}{2}}$

z condensation linear distance, ft, Rohsenow nomenclature

z_L^{**} complex linear distance, ft, Rohsenow nomenclature, defined in Section 2.2.4

Z length of flow surface or distance from entrance, ft

Fr' "modified" Froude number, dimensionless, defined as

$$Fr' = \frac{\rho_V v_V^2}{\rho_L g t} = \frac{\rho_V v_V^2}{\rho_L g (\nu^2/g)^{1/3} Re^n}$$

Nu local Nusselt number, dimensionless, $Nu = \frac{ht}{k}$

$\overline{Nu}$ mean Nusselt number, dimensionless, $\overline{Nu} = \frac{h_m t}{k}$

Nu' "modified" Nusselt number, dimensionless, $Nu' = \frac{h (\nu^2/g)^{1/3}}{k}$

Nu'_{W_1} Nu' for non-boiling heat transfer, given by Wilke correlation for $800 < Re$, $Pr = 5.4$

Nu'_{W_2} Nu' for non-boiling heat transfer, given by Wilke correlation for $600 < Re$, $Pr \geq 9.4$

Pr Prandtl number for liquid, dimensionless, $Pr = \frac{c\mu}{k}$

Re, Re_L local liquid Reynolds number, dimensionless, $Re = \frac{4\Gamma}{\mu}$

Re_{cr} Reynolds number given by Brauer for onset of turbulence and capillary waves

Re_i Brauer's Reynolds number for instability of ripples

Re_u Reynolds number given by Wilke as the limit of applicability of the Nusselt non-boiling analysis in the presence of waves

Re_V vapour Reynolds number, dimensionless, defined as

$$Re_V = \frac{D_{e_F} v_V \rho_V}{\mu_V}$$

Re_{w_1} Brauer's Reynolds number for the onset of rippling

Re_{w_2} Brauer's Reynolds number for the onset of random surface waves

We Weber number, dimensionless, $We = \frac{\rho_V v_V^2}{\sigma g_c / D_p}$

β Dukler's dimensionless interfacial shear,

$$\beta = \frac{F \cdot r \cdot g^{1/3} \cdot \rho_L^{2/3}}{2 \mu_L^{2/3}} = \frac{\left(\frac{\Delta P}{Z}\right)_{TP} D g^{1/3}}{4 \rho_L^{1/3} \mu_L^{2/3}}$$

Γ liquid mass flowrate per unit wetted perimeter, lb/hr ft

δ^+ Seban's generalized layer thickness, dimensionless

ϵ eddy viscosity, ft^2/hr

ϵ_H eddy thermal conductivity, ft^2/hr

η magnitude of y^+ at the liquid film surface, dimensionless

λ latent heat of vaporization of the liquid, Btu/hr

μ, μ_L viscosity of liquid, lb/hr ft

μ_V viscosity of vapour, lb/hr ft

ν kinematic viscosity of liquid, $\nu = \mu/\rho$, ft^2/hr

ρ, ρ_L density of liquid, lb/ft^3

σ surface tension of liquid, lb force/ft

τ shear stress, lb force/ft^2

τ_o shear stress at wall, lb force/ft^2

τ_V interfacial shear due to vapour flow, lb force/ft^2,

$$\tau_V = \frac{f\, G_V^2}{2\, g_c\, \rho_V}$$

τ_V^* Rohsenow's vapour interfacial shear term, dimensionless, defined in Section 2.2.2.4

ϕ a function of ....

SUBSCRIPTS

crit critical value, corresponding to point at which a change of mechanism occurs

rec. recommended value

APPENDIX I

TABULATION OF EXPERIMENTAL RESULTS

The runs are arranged in the order in which they were carried out over a period of approximately thirteen months.

The test liquids which were used are as follow.

Runs	Liquid	Boiling Point
1 - 80	ETHYL ALCOHOL	173°F
81 - 116	METHYL ALCOHOL	148°F
117 - 203	iso-PROPYL ALCOHOL	180°F
204 - 240	WATER	212°F
241 - 248	ETHYL ALCOHOL (Reproducibility Check)	173°F
249 - 336	CHLOROFORM	143°F

ETHYL ALCOHOL

Test No.	Feed Rates		q/A	Vaporization	ΔT		h
	Liquid	Vapour			Measured	Corrected	
	lb/hr	lb/hr	Btu/hrft^2	lb/hr	F°	F°	Btu/hrft^{2}F°
1	30	0	2060	0.5	10.5	10.3	200
			2600	1.0	14.0	13.8	190
			3960	2.5	21.0	20.7	190
			5220	3.5	27.3	26.8	195
			6460	4.5	26.1	25.5	255
			7020	5.0	26.2	25.6	275
2	30	14	2080	0.5	11.1	10.9	190
			2590	1.0	14.1	13.9	185
			3910	2.5	20.7	20.4	190
			5230	3.5	25.4	24.9	210
			6520	4.5	27.0	26.4	250
			7440	5.5	26.9	26.3	285
3	30	24	1320	0	7.4	7.3	180
			2070	0.5	11.3	11.1	185
			2590	1.0	14.0	13.8	190
			3960	2.5	21.0	20.7	190
			5220	3.5	27.0	26.5	195
			6430	4.5	28.3	27.7	230
4	30	49	6430	4.5	28.2	27.6	230
			7750	5.5	30.8	30.1	260
			9040	7.0	30.8	30.0	300
			10600	8.0	30.4	29.5	360
			14200	11.5	32.3	31.1	455
			15800	13.0	32.9	31.5	500
			18400	15.0	35.2	33.6	550
			21200	17.5	37.8	36.0	590
			24500	20.5	42.6	40.5	610
5	30	49	2150	0.5	9.9	9.7	220
			2640	1.0	12.6	12.4	215
			3940	2.5	18.5	18.2	215
			5250	3.5	23.6	23.1	225
			6390	4.5	28.7	28.1	225
			7730	6.0	34.0	33.3	230
			8970	7.0	33.6	32.8	275
			10500	8.5	34.8	33.9	310

ETHYL ALCOHOL

Test No.	Feed Rates		q/A	Vaporization	ΔT		h
	Liquid	Vapour			Measured	Corrected	
	lb/hr	lb/hr	Btu/hrft^2	lb/hr	F^o	F^o	Btu/hrft^{2}F^o
6	30	73	2020	1.0	8.0	7.8	260
			2570	1.0	10.1	9.9	260
			3870	2.0	15.0	14.7	265
			5180	3.5	19.6	19.2	270
			7640	5.5	28.0	27.3	280
			9890	7.5	32.0	31.1	320
			10500	8.0	33.7	32.8	320
			13100	10.5	35.4	34.3	380
			15400	13.0	38.0	36.7	420
7	30	99	2020	0.5	5.7	5.5	370
			2590	1.0	7.3	7.1	365
			5200	3.5	14.8	14.3	365
			7780	6.0	21.9	21.2	365
			9030	7.0	24.7	23.9	375
			10400	8.0	28.6	27.7	375
			13000	10.5	34.5	33.4	390
			15600	12.5	36.0	34.6	450
			18100	15.0	39.6	38.0	475
			21200	17.5	42.4	40.6	520
8	30	0	2610	1.5	14.6	14.4	180
			5250	3.5	27.5	27.0	195
			6520	4.5	33.9	33.3	195
			6610	5.0	31.2	30.6	215
			7230	5.5	31.5	30.9	235
9	50	0	2050	0.5	11.4	11.2	180
			2590	1.0	15.6	15.4	170
			5200	3.5	31.3	30.8	170
			6450	4.5	33.2	32.6	200
			7470	5.5	31.5	30.9	240
10	50	13	2040	0.5	12.8	12.6	160
			2610	1.0	16.3	16.1	160
			5190	3.5	29.1	28.6	180
			6340	4.5	32.7	32.1	195
			7510	5.5	33.7	33.0	230
			9560	7.5	33.7	32.9	290
			11700	9.5	34.9	33.9	345
			13900	11.0	35.2	34.0	410

ETHYL ALCOHOL

Test No.	Feed Rates		q/A	Vaporization	ΔT		h
	Liquid	Vapour			Measured	Corrected	
	lb/hr	lb/hr	Btu/hrft^2	lb/hr	F°	F°	Btu/hrft^{2}F°
11	50	49	2100	0.5	11.7	11.5	185
			2570	1.0	14.5	14.3	180
			5130	3.5	27.8	27.4	185
			7750	5.5	35.9	35.2	220
			10500	8.0	36.0	35.1	300
			13200	10.5	37.1	36.0	370
12	50	74	1480	0	5.9	5.8	255
			2620	1.0	10.4	10.2	255
			3870	2.5	15.6	15.3	255
			5320	3.5	21.1	20.6	260
			7810	5.5	29.5	28.8	270
			10300	8.0	36.0	35.1	295
13	50	74	7790	5.5	30.2	29.5	265
			10300	8.0	36.9	36.0	285
			13300	10.5	36.3	35.1	380
			16200	13.5	37.8	36.4	445
			18300	15.0	38.4	36.8	500
			22200	19.0	40.1	38.2	580
			25900	22.0	41.4	39.2	660
			34400	29.0	45.6	42.6	810
14	50	25	1470	0	8.9	8.8	170
			2620	1.0	15.6	15.4	170
			3960	2.5	23.3	23.0	170
			5180	3.5	30.0	29.6	175
			7830	6.0	37.0	36.3	215
			10300	8.0	37.4	36.5	280
			13300	10.5	38.8	37.6	355
15	50	0	2660	1.0	16.3	16.1	165
			4000	2.5	24.4	24.1	165
			5290	3.5	31.5	31.0	170
			7120	5.0	36.5	35.9	200

ETHYL ALCOHOL

Test No.	Feed Rates		q/A	Vaporization	ΔT		h
	Liquid	Vapour			Measured	Corrected	
	lb/hr	lb/hr	Btu/hrft^2	lb/hr	F^o	F^o	Btu/hrft^{2}F^o
16	50	98	1430	0	4.0	3.9	365
			2560	1.0	7.4	7.2	355
			3870	2.5	11.0	10.7	360
			5230	3.5	14.8	14.4	365
			7780	6.0	21.6	20.9	370
			10300	8.0	28.4	27.5	375
			13200	10.5	34.9	33.8	390
			16000	13.0	39.1	37.7	425
			18200	15.0	40.3	38.7	470
			21800	18.0	41.9	40.0	540
			26000	22.0	43.3	41.0	640
			30300	26.0	44.8	42.2	720
17	50	132	1340	0	2.9	2.8	480
			2640	1.0	5.6	5.4	490
			3930	2.5	8.5	8.2	480
			5180	3.5	10.9	10.5	495
			7820	5.5	16.4	15.7	500
			10400	8.0	21.5	20.6	510
			13200	10.5	27.2	26.1	510
			15900	13.0	32.5	31.1	510
			18400	15.0	37.5	35.9	510
			21800	18.5	41.1	39.2	560
			26000	22.0	43.4	41.1	630
			31300	27.0	46.1	43.4	720
18	100	0	1370	0.5	8.1	8.0	170
			1740	0.5	10.3	10.2	170
			2570	1.0	15.7	15.5	165
			3840	2.0	23.6	23.3	165
			5150	3.5	31.2	30.8	165
			6500	4.5	39.0	38.4	170
			7750	5.5	36.8	36.1	215
			10400	8.0	38.0	37.1	280
			13200	10.5	39.5	38.4	345

ETHYL ALCOHOL

Test No.	Feed Rates		q/A	Vaporization	ΔT		h
	Liquid	Vapour			Measured	Corrected	
	lb/hr	lb/hr	Btu/hrft^2	lb/hr	F^o	F^o	Btu/hrft^{2}F^o
19	100	25	1330	0	7.4	7.3	180
			1760	0.5	9.7	9.5	185
			2640	1.0	15.1	14.9	180
			3910	2.5	22.0	21.7	180
			5280	3.5	29.4	28.9	185
			6510	4.5	34.8	34.2	190
			7860	6.0	41.7	41.0	190
			10400	8.0	40.4	39.5	265
			13200	10.5	40.5	39.4	335
			15700	13.0	40.8	39.4	400
			18700	16.0	41.8	40.2	465
			22200	19.0	43.2	41.3	540
			26100	22.5	44.1	41.8	620
20	100	50	2660	0	13.3	13.1	205
			4000	1.5	20.3	20.0	200
			5320	2.5	26.2	25.7	205
			7840	5.0	39.5	38.8	200
			10300	7.5	41.2	40.3	255
			13000	10.0	41.8	40.7	320
			15700	12.5	42.3	40.9	385
			18500	14.5	43.3	41.7	445
			21800	17.5	44.0	42.1	520
			26500	22.0	45.0	42.7	620
			30600	25.5	45.6	42.9	710
			36600	31.0	47.3	44.1	830
			41600	35.5	48.5	44.9	930
21	100	71	2550	0.5	8.8	8.6	295
			5140	2.5	18.7	18.3	280
			7760	4.5	27.8	27.1	285
			10600	7.0	36.0	35.1	300
			15800	11.5	42.5	41.1	385
			21800	17.0	44.6	42.7	510
			30100	25.5	46.5	43.9	690
			39000	33.0	48.3	44.9	870
			47800	41.0	50.6	46.4	1030

ETHYL ALCOHOL

Test No.	Feed Rates		q/A	Vaporization	ΔT		h
	Liquid	Vapour			Measured	Corrected	
	lb/hr	lb/hr	Btu/hrft^2	lb/hr	F^o	F^o	Btu/hrft^{2}F^o
22	100	99	2610	0	6.8	6.6	395
			5190	2.5	13.3	12.9	400
			7760	4.5	19.3	18.6	415
			10500	7.0	25.6	24.7	425
			18500	14.0	39.4	37.8	490
			21900	17.0	43.6	41.7	530
			30300	24.0	47.2	44.6	680
SURFACE SLIGHTLY BLACKENED DUE TO ACCIDENTAL OVERHEATING							
23	100	101	10400	7.5	23.8	22.9	455
			14600	11.0	31.8	30.5	480
			21700	17.5	39.0	37.1	590
			30400	25.0	42.3	39.7	770
24	100	98	2590	0.5	6.5	6.3	410
			5200	2.5	13.0	12.5	415
			7700	4.5	18.9	18.2	425
			10500	7.5	25.2	24.3	430
			14300	10.5	32.4	31.2	455
			20200	16.0	38.5	36.7	550
			21600	17.5	39.0	37.1	580
			26100	21.0	40.7	38.4	680
			34800	29.0	43.9	40.9	850
			43500	36.5	46.6	42.8	1020
			47500	40.5	47.6	43.5	1100
25	200	0	3980	1.5	14.5	14.2	280
			5450	2.5	20.6	20.1	270
			6560	4.0	25.3	24.7	265
			8240	6.0	31.6	30.9	265
			10600	7.5	38.9	38.0	280
			13600	10.5	40.3	39.1	350
			16500	13.5	40.8	39.4	420
			21200	17.5	40.7	38.9	540

ETHYL ALCOHOL

Test No.	Feed Rates		q/A	Vaporization	ΔT		h
	Liquid	Vapour			Measured	Corrected	
	lb/hr	lb/hr	Btu/hrft^2	lb/hr	F^o	F^o	Btu/hrft^{2}F^o
26	50	0	2020	0.5	11.6	11.4	175
			2550	1.0	15.6	15.4	165
			4000	2.5	24.4	24.1	165
			5110	3.5	30.9	30.5	170
			6520	4.5	38.7	38.1	170
			7650	5.5	34.8	34.1	225
27	100	0	1360	0.5	8.0	7.9	170
			1740	0.5	9.5	9.4	185
			2630	0.5	15.5	15.3	170
			3910	2.0	23.4	23.1	170
			5230	3.0	31.3	30.8	170
			7850	5.5	36.6	35.9	220
			10800	8.0	37.6	36.7	295
			13900	10.5	39.1	37.9	365
28	100	130	2620	0.5	5.0	4.8	545
			5290	3.0	10.0	9.5	560
			10600	8.0	19.3	18.4	580
			15600	12.5	27.3	26.0	600
			21600	17.5	37.4	35.5	610
			24400	21.5	42.0	39.9	610
			29600	25.0	43.9	41.3	720
			38500	33.0	46.8	43.4	890
			45300	39.0	48.3	44.3	1020
29	100	74	2590	0.5	9.0	8.8	295
			5390	3.0	18.9	18.4	295
			7770	5.5	27.1	26.4	295
			10400	7.5	35.6	34.7	300
			15600	12.5	42.2	40.8	380
			21500	17.5	43.7	41.8	510
			30100	25.0	45.6	43.0	700
			38900	33.5	46.9	43.5	890
			44400	38.0	47.7	43.8	1010

ETHYL ALCOHOL

Test No.	Feed Rates		q/A	Vaporization	ΔT		h
	Liquid	Vapour			Measured	Corrected	
	lb/hr	lb/hr	Btu/hrft^2	lb/hr	F^o	F^o	Btu/hrft^{2}F^o
30	30	50	1730	0.5	8.2	8.0	215
			2600	1.0	12.5	12.3	210
			3980	2.5	18.6	18.3	220
			6260	4.5	28.5	28.0	225
			7840	6.0	34.6	33.9	230
31	30	130	1720	0.5	3.7	3.6	480
			2590	1.0	5.7	5.5	470
			5280	3.5	11.9	11.4	465
			7720	5.5	17.2	16.5	470
			10300	7.5	23.0	22.1	465
			15600	13.0	33.5	32.1	485
32	30	74	5390	3.5	20.6	20.1	270
33	30	0	1660	0.5	8.7	8.6	195
			2670	1.5	14.8	14.6	185
			4010	2.5	21.9	21.6	185
			5560	4.0	29.4	28.9	190
34	150	0	3980	1.5	18.8	18.5	215
			5280	3.0	26.1	25.6	205
			6520	4.5	32.4	31.8	205
			7840	5.0	37.0	36.3	215
35	200	23	3910	1.5	14.9	14.6	270
			5250	3.0	20.4	19.9	265
			7650	5.0	29.8	29.1	265
			10400	7.5	39.4	38.5	270
			13600	10.5	43.5	42.3	320
			16400	12.0	42.4	41.0	400
			18300	13.0	42.9	41.3	445
			21400	16.0	43.5	41.6	510
			26300	21.0	44.6	42.3	620
36	75	0	2160	0.5	13.8	13.6	160
			2650	1.0	17.0	16.8	160
			3870	2.0	25.1	24.8	155
			5280	3.5	33.6	33.1	160

ETHYL ALCOHOL

Test No.	Feed Rates		q/A	Vaporization	ΔT		h
	Liquid	Vapour			Measured	Corrected	
	lb/hr	lb/hr	Btu/hrft^2	lb/hr	F^o	F^o	Btu/hrft^{2}F^o
37	200	51	5140	0.5	16.8	16.4	315
			6510	2.5	21.7	21.1	310
			7740	3.5	25.7	25.0	310
			10400	5.5	34.4	33.5	310
			13000	8.0	42.9	41.8	310
			15600	10.5	40.9	39.6	395
			20700	15.5	40.3	38.5	540
			25900	20.0	40.8	38.6	670
			30100	23.5	43.3	40.7	740
			34200	27.0	43.6	40.6	840
			39400	32.0	45.6	42.2	930
38	200	130	3980	0	6.5	6.2	640
			5230	0.5	8.6	8.1	640
			7920	3.0	12.7	12.0	660
			10400	5.5	16.3	15.4	680
			13200	8.0	20.2	19.0	700
			16200	11.0	24.4	23.0	700
			21500	15.5	30.9	29.0	740
			25800	19.5	35.7	33.4	770
			30000	23.0	40.0	37.4	800
			34800	27.5	42.9	39.9	870
			41200	33.0	45.0	41.4	990
39	200	71	4000	1.0	10.5	10.2	390
			5210	1.5	14.1	13.6	385
			6510	3.0	17.6	17.0	385
			7900	4.5	21.5	20.8	380
			10300	6.5	28.0	27.1	380
			13200	9.0	34.5	33.4	395
			15600	11.5	38.3	36.9	420
			18100	13.5	38.8	37.2	490
			21000	16.0	39.5	37.7	560
			26500	20.5	41.0	38.7	680
			34300	28.0	43.1	40.1	860

ETHYL ALCOHOL

Test No.	Feed Rates		q/A	Vaporization	ΔT		h
	Liquid	Vapour			Measured	Corrected	
	lb/hr	lb/hr	Btu/hrft^2	lb/hr	F^o	F^o	Btu/hrft^{2}F^o
40	200	90.5	5300	0.5	11.8	11.3	470
			6450	2.5	14.3	13.7	470
			7890	3.5	17.2	16.5	480
			10400	6.0	22.2	21.3	490
			12900	8.0	26.5	25.4	510
			17800	12.5	32.8	31.3	570
			22100	15.0	37.7	35.8	620
41	200	39	5230	0.5	18.7	18.2	285
			6510	1.5	23.6	23.0	285
			7810	2.5	28.3	27.6	285
			10600	5.0	38.2	37.3	285
			13700	8.0	39.6	38.4	355
			16700	11.0	39.5	38.1	440
42	200	12	3880	0.5	14.5	14.2	275
			5390	1.5	20.3	19.8	270
			7660	4.5	28.7	28.0	275
			10400	6.0	34.0	33.1	315
43	100	42	1740	0	9.6	9.5	185
			2620	1.0	14.9	14.7	180
			3940	2.0	22.2	21.9	180
			5310	3.5	29.6	29.1	185
			6450	4.5	35.2	34.6	185
			7610	5.5	26.3	25.6	300
44	100	42	5240	3.0	29.1	28.6	185
			6950	6.0	26.5	25.9	270
			10200	8.5	24.8	23.9	430
			12900	11.0	26.4	25.3	510
			15400	13.5	27.0	25.7	600
			18200	16.0	27.6	26.0	700
			21600	19.5	27.9	26.0	830
			29500	27.0	29.6	27.0	1090

ETHYL ALCOHOL

Test No.	Feed Rates		q/A	Vaporization	ΔT		h
	Liquid	Vapour			Measured	Corrected	
	lb/hr	lb/hr	Btu/hrft^2	lb/hr	F^o	F^o	Btu/hrft^{2}F^o
45	100	69	5130	2.5	19.6	19.2	270
			7430	5.0	28.3	27.7	270
			9850	7.5	28.3	27.4	360
			12600	10.5	30.0	28.9	435
			15700	13.5	28.9	27.5	570
			21300	19.0	29.8	28.0	760
46	100	101	7740	4.5	18.3	17.6	440
			10200	7.0	23.6	22.7	450
			12900	9.5	29.1	28.0	460
			16100	12.5	32.3	30.9	520
			19100	16.5	31.6	30.0	640
			23000	20.0	32.6	30.6	750
			30400	27.5	32.4	29.8	1020
			39900	37.0	33.9	30.4	1310
SURFACE AGAIN BLACKENED BECAUSE OF OVERHEATING CAUSED BY ONSET OF FILM BOILING							
47	50	43	1720	0.5	9.8	9.7	180
			2710	1.0	15.3	15.1	180
			3920	2.5	21.8	21.5	180
			5240	3.5	28.5	28.0	185
			6450	4.5	35.3	34.7	185
			7660	6.5	25.4	24.7	310
			11200	9.0	25.8	24.8	450
			13200	12.0	26.7	25.6	520
			16000	14.5	27.5	26.1	610
			19000	17.5	28.6	27.0	700
			22200	20.5	28.9	27.0	820
48	20	0	1660	0	7.5	7.4	225
			2180	0.5	10.2	10.0	220
			2590	1.0	12.1	11.9	220
			3480	2.0	15.9	15.6	225
			4280	2.5	19.1	18.7	230
			5250	3.5	22.7	22.2	235
			6000	4.0	25.5	25.0	240
			6870	5.0	28.8	28.2	245

ETHYL ALCOHOL

Test No.	Feed Rates		q/A	Vaporization	ΔT		h
	Liquid	Vapour			Measured	Corrected	
	lb/hr	lb/hr	Btu/hrft^2	lb/hr	F^o	F^o	Btu/hrft^{2}F^o
49	50	100	3880	2.0	10.7	10.4	370
			5290	3.5	14.8	14.3	370
			7660	5.5	20.9	20.2	380
			10200	8.0	27.7	26.8	380
			12800	10.5	31.5	30.4	420
			15600	13.5	31.4	30.0	520
			18500	17.0	32.2	30.6	600
			21900	20.0	32.1	30.2	720
			26300	24.5	33.8	31.5	840
50	50	28	2600	1.0	16.4	16.2	160
			3890	2.5	24.0	23.7	165
			5350	3.5	32.6	32.1	165
			7670	5.5	42.8	42.1	180
			9150	8.0	26.7	25.9	350
			10400	9.0	27.4	26.5	390
			13100	11.5	28.1	27.0	480
			15900	14.5	28.9	27.5	580
			18400	17.0	29.6	28.0	660
HEATING WINDING FAILED. WINDING WAS REPAIRED BEFORE CONTINUING BUT BLACKENED HEATED SURFACE WAS NOT TOUCHED. IMMERSED THERMOCOUPLES WERE REPLACED.							
51	50	39	1770	0	10.3	10.1	175
		39	2630	1.0	15.2	15.0	175
		40	3890	2.0	21.9	21.6	180
		41	5390	3.5	28.9	28.4	190
		42	6860	5.0	24.5	23.9	290
		42	7900	6.5	25.5	24.8	320
		44	10600	8.0	25.7	24.8	430
		44	13600	10.5	26.9	25.7	530
		44	16200	14.5	28.2	26.8	600
		44	20100	18.5	29.5	27.7	730

ETHYL ALCOHOL

Test No.	Feed Rates		q/A	Vaporization	ΔT		h
	Liquid	Vapour			Measured	Corrected	
	lb/hr	lb/hr	Btu/hrft^2	lb/hr	F^o	F^o	Btu/hrft^{2}F^o
52	50	24.5	1690	0	10.5	10.4	165
			2680	1.0	16.7	16.5	165
			3890	2.0	24.0	23.7	165
			5420	3.0	32.2	31.7	170
			6250	3.5	34.9	34.4	180
			7610	5.0	28.5	27.8	275
			8590	6.0	25.9	25.2	340
			10300	7.5	25.6	24.7	420
			13100	9.5	25.9	24.8	530
			16200	14.5	27.5	26.1	620
			18900	17.0	28.4	26.8	700
			21500	20.0	29.4	27.5	780
53	50	72	1710	0	7.3	7.1	240
			2610	1.0	11.0	10.8	240
			3880	2.0	16.3	15.9	240
			5180	3.0	21.6	21.1	245
			6340	4.0	26.3	25.7	245
			8550	7.0	28.7	27.9	305
			10400	8.5	29.4	28.5	365
			13000	11.0	29.7	28.6	455
			16100	14.0	30.2	28.8	560
			18400	16.5	30.7	29.1	630
			22200	20.0	31.5	29.6	750
54	50	0	2780	1.0	17.1	16.8	165
			4080	2.0	25.3	24.9	165
			5450	3.5	33.0	32.5	170
			6350	4.0	37.7	37.1	170
			7290	5.5	20.0	19.4	375
			8260	6.5	21.3	20.6	400
			8300	6.5	20.6	19.9	415

ETHYL ALCOHOL

Test No.	Feed Rates		q/A	Vaporization	ΔT		h
	Liquid	Vapour			Measured	Corrected	
	lb/hr	lb/hr	Btu/hrft^2	lb/hr	F^o	F^o	Btu/hrft^{2}F^o
55	50	14	1740	0	10.6	10.4	165
			2640	1.0	16.2	16.0	165
			3840	2.0	23.4	23.1	165
			5210	3.5	31.1	30.6	170
			6360	4.5	37.3	36.7	175
			7540	5.5	42.5	41.8	180
			8850	7.5	21.7	20.9	425
			10500	9.0	23.3	22.4	470
			12000	10.5	24.3	23.3	510
			13400	12.0	25.3	24.1	560
			14200	12.5	25.6	24.4	580
			15300	13.5	26.3	25.0	610
			17500	16.0	27.3	25.8	680
56	50	56	2800	1.0	14.7	14.5	195
			4030	2.0	20.9	20.5	195
			5410	3.5	27.6	27.1	200
			7700	6.0	28.0	27.3	280
			10600	8.5	28.3	27.4	385
			13600	11.5	28.8	27.6	495
			16600	14.5	29.7	28.3	590
			19500	17.5	30.3	28.6	680
57	100	28	1790	0	10.6	10.4	170
			2680	0.5	16.2	16.0	170
			3940	1.5	23.5	23.2	170
			5420	3.5	32.2	31.7	170
			6430	4.5	37.8	37.2	175
			7600	6.0	27.5	26.8	285
			10300	9.0	27.6	26.7	385
			13400	12.0	27.9	26.7	500
			16200	14.5	28.5	27.1	600
			19500	18.0	29.3	27.6	710

ETHYL ALCOHOL

Test No.	Feed Rates		q/A	Vaporization	ΔT		h
	Liquid	Vapour			Measured	Corrected	
	lb/hr	lb/hr	Btu/hrft^2	lb/hr	F^o	F^o	Btu/hrft^{2}F^o
58	100	0	2660	1.0	15.9	15.7	170
			4030	2.0	24.3	24.0	170
			5440	3.5	32.6	32.1	170
			6510	4.5	38.5	37.9	170
			7560	6.0	23.1	22.4	340
			8130	6.5	23.4	22.7	360
			8790	7.5	23.6	22.8	385
			10700	9.0	24.1	23.2	460
59	100	40	2660	1.0	15.0	14.7	180
			3850	2.0	21.9	21.5	180
			5250	3.0	29.4	28.9	180
			6590	4.5	36.3	35.7	185
			10500	9.0	28.3	27.3	385
			13000	11.0	28.6	27.4	475
			15500	14.0	29.1	27.6	560
			20600	19.0	30.5	28.5	720
			24200	22.5	31.3	29.0	830
60	100	73	4060	2.0	14.5	14.1	290
			5440	3.5	19.3	18.8	290
			6620	4.5	23.7	23.1	285
			8100	6.0	28.7	27.9	290
			11100	9.5	30.1	29.1	380
			13800	12.0	30.2	28.9	480
			16800	15.0	30.9	29.3	570
			21700	20.0	31.9	29.8	730
61	100	138	2630	0.5	4.7	4.5	580
			3900	2.0	7.0	6.7	580
			5320	3.0	9.8	9.3	570
			6550	4.0	11.8	11.2	580
			7850	5.5	14.1	13.4	580
			10400	7.5	18.3	17.3	600
			13100	8.5	22.8	21.6	610
			15800	12.5	27.4	25.9	610
			18500	15.0	31.1	29.3	630
			21600	19.5	31.9	29.8	730
			25400	23.5	33.2	30.8	830
			29600	27.0	34.2	31.4	940

ETHYL ALCOHOL

Test No.	Feed Rates		q/A	Vaporization	ΔT		h
	Liquid	Vapour			Measured	Corrected	
	lb/hr	lb/hr	Btu/hrft^2	lb/hr	F^o	F^o	Btu/hrft^{2}F^o
62	50	144	5520	3.5	11.0	10.5	530
			8000	6.0	15.7	15.0	530
			10600	8.0	20.9	20.0	530
			13400	9.0	26.2	25.0	540
			16300	13.0	31.2	29.8	550
			18800	17.0	32.0	30.4	620
			21800	20.0	32.0	30.2	720
63	50	0	2790	1.0	16.9	16.7	165
			3960	2.0	24.5	24.2	165
			3980	2.5	24.6	24.3	165
			7410	6.5	21.7	21.1	350
			8150	7.0	22.0	21.3	380
			8690	8.0	22.1	21.3	410
64	100	13	2560	1.0	15.7	15.5	165
			3790	2.0	23.3	23.0	165
			5290	3.5	32.2	31.7	165
			9130	7.5	23.7	22.9	400
			10600	9.0	23.7	22.8	465
			12900	11.5	25.0	23.9	540
			15400	14.0	26.6	25.3	610
			18200	16.5	27.9	26.3	690
			20500	19.0	29.0	27.2	750
			22100	20.5	29.6	27.7	800
			24200	22.5	30.4	28.3	850
			25800	24.0	30.8	28.5	910
65	30	28	1810	1.0	9.8	9.6	190
			2670	2.0	14.4	14.2	190
			3860	3.0	20.5	20.2	190
			5250	4.5	27.1	26.6	200
			7920	7.5	23.0	22.3	355
			8550	8.0	23.7	23.0	370
			9300	8.5	24.1	23.3	400
			10600	10.0	24.8	23.9	445
			11800	11.5	25.5	24.5	480
			13500	13.0	26.3	25.1	540

ETHYL ALCOHOL

Test No.	Feed Rates		q/A	Vaporization	ΔT		h
	Liquid	Vapour			Measured	Corrected	
	lb/hr	lb/hr	Btu/hrft^2	lb/hr	F^o	F^o	Btu/hrft^{2}F^o
66	200	28	2710	0.5	10.5	10.3	265
			3960	1.5	15.5	15.2	260
			5470	3.0	21.6	21.1	260
			6560	3.5	25.9	25.3	260
			7920	5.0	31.0	30.3	260
67	30	57	2430	1.5	11.2	11.0	220
			3740	3.0	17.0	16.7	225
			5080	4.0	22.3	21.9	230
			7760	6.5	32.4	31.7	245
			8650	8.0	26.5	25.7	335
			9560	9.0	27.6	26.8	360
			10500	10.0	27.5	26.6	395
			12100	11.5	27.3	26.3	460
			13100	12.5	27.8	26.7	490
			14600	14.0	28.2	26.9	540
68	30	105	2620	2.0	7.2	7.0	375
			5300	4.5	14.7	14.2	375
			7630	6.0	21.1	20.4	375
			10500	9.0	25.3	24.4	430
69	30	0	1910	1.5	10.7	10.5	180
			2600	2.0	14.5	14.3	180
			3820	3.0	21.1	20.8	185
			5080	4.0	27.6	27.2	185
			7830	7.0	21.0	20.3	385
			8790	8.0	20.9	20.1	440
			9600	9.0	21.9	21.1	455
70	30	13	1880	1.0	10.4	10.2	185
			2560	2.0	14.2	14.0	185
			3860	3.0	21.2	20.9	185
			5140	4.0	27.8	27.4	190
			6920	6.5	23.3	22.7	305
			8000	7.5	21.7	21.0	380
			8770	8.0	22.6	21.8	400
			9800	9.0	22.9	22.0	445
			10800	10.0	23.5	22.6	480

ETHYL ALCOHOL

Test No.	Feed Rates		q/A	Vaporization	ΔT		h
	Liquid	Vapour			Measured	Corrected	
	lb/hr	lb/hr	Btu/hrft^2	lb/hr	F^o	F^o	Btu/hrft^{2}F^o
71	200	0	2710	1.0	10.4	10.2	265
			3980	2.0	15.5	15.2	260
			5620	3.5	23.2	22.7	250
			6460	4.0	25.5	24.9	260
			8060	4.5	31.2	30.5	265
			10900	6.5	26.7	25.8	420
			12800	8.5	27.2	26.1	490
			15900	11.5	26.8	25.4	630
			18300	14.0	27.4	25.8	710
72	75	0	2480	0.5	15.7	15.5	160
			3800	2.0	24.2	23.9	160
			5080	3.0	32.5	32.1	160
73	150	0	2320	1.0	10.8	10.6	220
			2740	1.0	13.0	12.8	215
			3800	1.5	18.8	18.5	205
			5310	3.0	26.1	25.6	205
74	200	50	3900	1.5	13.5	13.2	295
			5250	2.5	18.5	18.0	290
			6460	4.0	22.8	22.2	290
			8060	5.5	28.6	27.9	290
			11600	10.0	29.2	28.2	410
			13100	11.0	29.8	28.7	455
			15800	12.5	29.2	27.8	570
			18500	15.0	29.5	27.9	660
			21100	18.5	30.2	28.4	740
			25100	22.5	31.0	28.8	870
			29600	26.5	31.8	29.2	1000

ETHYL ALCOHOL

Test No.	Feed Rates		q/A	Vaporization	ΔT		h
	Liquid	Vapour			Measured	Corrected	
	lb/hr	lb/hr	Btu/hrft^2	lb/hr	F^o	F^o	Btu/hrft^{2}F^o
75	200	20	2560	0.5	9.8	9.6	265
			3910	2.0	15.4	15.1	260
			6400	4.0	25.5	24.9	260
			8030	5.0	31.8	31.1	260
			11600	8.0	22.8	21.8	530
			13600	10.5	23.5	22.3	610
			16200	14.5	24.6	23.2	700
			20800	17.0	25.4	23.6	880
			25000	22.0	26.0	23.8	1050
			29400	26.5	27.4	24.9	1180
76	200	68	8340	4.0	24.3	23.6	355
			10300	5.0	29.6	28.7	360
			12900	8.5	28.7	27.6	465
			15500	11.0	29.2	27.9	560
			18900	15.0	30.1	28.5	660
			22200	18.0	31.1	29.2	760
			26600	22.0	32.1	29.8	890
77	200	92	8030	5.0	17.4	16.7	480
			10500	6.5	21.9	21.0	500
			13000	9.5	26.1	25.0	520
			18200	15.5	30.9	29.3	620
			21000	18.5	31.7	29.9	700
			25500	22.5	32.7	30.5	840
78	200	14	10500	8.5	21.2	20.3	520
			14000	12.0	22.1	20.9	670
			19500	17.5	23.3	21.6	900
79	200	22	5150	2.5	20.0	19.6	265
			7780	5.0	29.7	29.0	270
			9380	7.0	26.0	25.2	370
			10200	8.0	26.5	25.6	400
			12200	10.0	27.0	25.9	470
			15800	13.0	26.3	24.9	640
			19500	16.5	27.3	25.6	760
			22800	20.0	28.1	26.1	870

ETHYL ALCOHOL

Test No.	Feed Rates		q/A	Vaporization	ΔT		h
	Liquid	Vapour			Measured	Corrected	
	lb/hr	lb/hr	Btu/hrft^2	lb/hr	F^o	F^o	Btu/hrft^{2}F^o
80	30	74	2630 3780 5320	2.0 3.0 4.5	10.3 14.9 20.3	10.1 14.6 19.8	260 260 270

METHYL ALCOHOL

Test No.	Feed Rates		q/A	Vaporization	ΔT		h
	Liquid	Vapour			Measured	Corrected	
	lb/hr	lb/hr	Btu/hrft^2	lb/hr	F^o	F^o	Btu/hrft^{2}F^o
81	100	0	2670	1.0	11.0	10.8	250
			3910	1.5	16.2	15.9	245
			5300	3.0	22.3	21.8	245
			6450	3.5	27.2	26.6	245
			7720	4.5	32.2	31.5	245
			8590	5.5	20.3	19.5	440
			9730	6.5	20.2	19.3	500
			11300	8.0	21.1	20.1	560
			13400	9.0	21.8	20.6	650
			15800	11.0	22.2	20.8	760
82	50	0	1770	1.0	8.0	7.8	225
			2600	1.5	11.7	11.5	225
			3860	2.0	17.5	17.2	225
			5330	3.5	23.9	23.4	230
			6470	4.0	28.8	28.2	230
			7700	5.5	20.4	19.7	390
			8770	6.5	19.8	19.0	460
			9690	7.0	20.2	19.3	500
			11300	8.5	20.2	19.2	590
			13200	9.5	20.5	19.3	680
			15000	11.0	21.3	20.0	750
83	75	0	1750	0.5	7.6	7.4	235
			2630	1.0	11.9	11.7	225
			3900	2.0	17.7	17.4	225
			5370	3.0	23.8	23.3	230
			6500	3.5	28.4	27.8	235
			7780	4.5	33.7	33.0	235
84	150	0	3420	1.5	11.1	10.8	315
			4410	2.0	14.8	14.4	305
			5300	2.5	18.3	17.8	300
			6620	3.5	22.4	21.8	305
			8370	4.5	28.5	27.8	300

METHYL ALCOHOL

Test No.	Feed Rates		q/A	Vaporization	ΔT		h
	Liquid	Vapour			Measured	Corrected	
	lb/hr	lb/hr	Btu/hrft^2	lb/hr	F^o	F^o	Btu/hrft^{2}F^o
85	60	0	1690	1.0	7.7	7.6	225
			2680	1.5	12.5	12.3	220
			3900	2.5	18.2	17.9	220
			5380	4.0	12.0	11.5	470
			6450	4.5	13.7	13.1	495
			7820	5.5	15.8	15.1	520
			10500	7.5	19.1	18.2	580
			13300	9.0	21.3	20.1	660
			14900	10.5	22.2	20.9	710
			16800	12.0	22.6	21.1	800
86	20	0	1700	1.0	6.5	6.3	270
			2640	1.5	9.8	9.6	275
87	30	0	1720	1.0	7.1	6.9	250
			2640	1.5	11.1	10.9	245
			3490	2.0	14.5	14.2	245
			3960	2.0	12.4	12.0	330
			6430	4.0	17.3	16.7	385
			7960	5.5	19.8	19.1	415
			9370	6.5	21.3	20.5	460
			10800	7.5	21.4	20.5	530
			13300	9.5	22.6	21.4	620
			15000	11.0	22.5	21.2	710
88	40	0	1710	0.5	7.4	7.2	235
			2140	1.0	9.5	9.3	230
			2720	1.0	12.0	11.8	230
			3300	2.5	14.8	14.5	230
			3850	3.0	17.2	16.9	230
			5320	4.5	23.4	22.9	235
			6260	5.5	27.4	26.8	235

METHYL ALCOHOL

Test No.	Feed Rates		q/A	Vaporization	ΔT		h
	Liquid	Vapour			Measured	Corrected	
	lb/hr	lb/hr	Btu/hrft^2	lb/hr	F^o	F^o	Btu/hrft^{2}F^o
89	15.5	0	1750	1.0	6.2	6.0	290
			2110	1.0	7.6	7.4	285
			2750	1.5	9.8	9.6	290
			3150	2.0	11.2	10.9	290
			3900	2.5	13.7	13.4	290
			5350	4.0	18.5	18.0	300
			6110	4.0	20.4	19.9	310
90	200	0	5260	1.5	14.6	14.1	370
			6400	2.5	18.5	17.9	360
			7700	3.5	22.5	21.8	355
			8770	4.5	25.4	24.6	355
			10200	5.0	30.0	29.1	350
			13200	8.0	27.9	26.7	495
			15500	10.0	23.5	22.1	700
			18000	11.5	24.4	22.8	790
			20700	14.0	23.9	22.1	940
			23400	16.0	24.8	22.7	1030
			26000	17.5	25.1	22.8	1140
91	200	17	3340	0.5	9.5	9.2	365
			4070	0.5	11.7	11.3	360
			5400	2.0	15.9	15.4	350
			6500	2.5	19.2	18.6	350
			7660	3.0	22.8	22.1	345
			9380	4.5	27.9	27.1	345
			18800	12.0	26.9	25.2	750
			21700	14.5	28.0	26.1	830
			25800	17.5	28.4	26.1	990
			30200	21.0	29.4	26.7	1130
92	236	0	5350	1.0	13.6	13.1	410
			6700	1.0	16.0	15.4	425
			7920	1.5	19.6	18.9	420
			8850	2.0	22.2	21.4	415
			10800	3.0	27.4	26.4	410

METHYL ALCOHOL

Test No.	Feed Rates		q/A	Vaporization	ΔT		h
	Liquid	Vapour			Measured	Corrected	
	lb/hr	lb/hr	Btu/hrft^2	lb/hr	F^o	F^o	Btu/hrft^{2}F^o
93	100	15	2700	0.5	11.3	11.1	245
			4050	1.5	16.9	16.5	245
			5320	2.5	22.0	21.5	250
			6410	3.5	26.2	25.6	250
			10600	7.0	26.1	25.2	420
			12500	8.0	26.1	25.0	500
			14900	10.0	26.4	25.1	590
			17800	12.5	26.9	25.3	700
			19900	14.0	26.9	25.1	790
			22200	16.0	26.7	24.7	900
			25100	18.0	27.3	25.1	1000
			29300	21.0	28.0	25.4	1150
94	100	50	2600	0.5	9.1	8.9	290
			3910	1.0	13.7	13.4	290
			5410	2.0	19.1	18.6	290
			6630	3.0	23.1	22.5	295
			7650	4.0	26.2	25.5	300
			9080	4.5	31.1	30.3	300
			13100	8.5	29.0	27.8	470
			19200	13.0	30.2	28.5	670
			22500	15.5	30.9	28.9	780
			25000	18.0	31.5	29.3	850
			29100	20.5	32.5	29.9	970
95	100	100	2660	0	4.7	4.5	590
			4020	1.0	7.0	6.6	610
			5360	2.0	9.3	8.8	610
			7530	3.5	13.0	12.3	610
			10200	5.5	17.7	16.8	600
			13100	7.0	21.6	20.4	640
			16100	9.5	25.8	24.4	660
			19100	11.5	29.8	28.1	680
			21900	13.5	33.7	31.8	690
			25000	17.0	33.8	31.6	790
			27200	18.5	34.4	32.0	850
			30100	21.0	35.2	32.5	930
			34400	24.5	36.0	33.0	1040

METHYL ALCOHOL

Test No.	Feed Rates		q/A	Vaporization	ΔT		h
	Liquid	Vapour			Measured	Corrected	
	lb/hr	lb/hr	Btu/hrft^2	lb/hr	F^o	F^o	Btu/hrft^{2}F^o
96	100	70	2660	0	6.6	6.4	415
			5180	2.0	12.8	12.3	420
			7620	3.5	18.9	18.2	420
			10300	5.5	25.2	24.3	425
97	100	37	2660	0	10.8	10.6	250
			3980	1.0	15.8	15.4	260
			5640	2.0	22.2	21.7	260
			6700	3.0	26.2	25.6	260
			8010	4.0	30.9	30.2	265
98	100	30	2680	0	11.1	10.9	245
			3910	1.0	16.1	15.8	250
			5440	2.0	22.4	21.9	250
			6530	3.0	26.4	25.8	255
			7900	3.5	31.0	30.3	260
			17100	11.5	28.0	26.5	640
			21600	15.0	29.4	27.5	780
			25800	18.0	30.4	28.1	920
			29000	20.5	30.9	28.3	1020
99	30	30	1620	1.0	6.0	5.9	275
			2610	1.5	10.0	9.8	265
			3770	2.5	14.4	14.1	270
			5120	3.0	19.1	18.7	275
100	30	31	4050	2.0	15.6	15.2	265
			5600	3.5	20.9	20.4	275
			6630	4.0	24.6	24.0	275
			11700	7.5	22.6	21.6	540
			13200	9.5	24.6	23.4	560
			15900	11.5	25.4	24.0	660
			18300	13.5	26.1	24.5	750

METHYL ALCOHOL

Test No.	Feed Rates		q/A	Vaporization	ΔT		h
	Liquid	Vapour			Measured	Corrected	
	lb/hr	lb/hr	Btu/hrft^2	lb/hr	F^o	F^o	Btu/hrft^{2}F^o
101	30	50	1850	1.0	6.2	6.0	310
			2660	1.5	8.9	8.7	305
			3890	2.0	12.9	12.6	310
			5490	3.5	17.9	17.4	315
			6610	4.0	21.6	21.0	315
			7850	5.0	25.0	24.3	320
			10100	7.0	23.2	22.3	455
			15500	11.0	24.0	22.6	690
102	30	50	2720	1.0	9.2	9.0	300
			6570	4.0	21.2	20.6	320
			10300	7.5	26.6	25.7	400
			13500	9.5	25.5	24.3	560
103	30	0	1940	1.0	8.0	7.8	250
			2660	1.5	11.0	10.8	245
			3820	2.0	15.9	15.6	245
			5430	3.5	22.0	21.5	250
			6800	4.0	27.0	26.4	255
104	30	40	1690	0.5	6.3	6.2	275
			2620	1.0	9.7	9.5	275
			3870	1.5	14.4	14.1	275
			5470	3.5	19.6	19.1	285
			6910	4.5	24.4	23.8	290
105	30	100	1760	0.5	3.3	3.2	550
			2710	1.5	5.1	4.9	550
			3910	2.0	7.4	7.1	550
			5450	3.0	10.5	10.0	540
			7570	4.5	14.4	13.7	550
106	30	70	1670	0.5	4.3	4.2	395
			2680	1.5	7.1	6.9	390
			4060	2.5	10.8	10.4	390
			5360	3.0	14.2	13.7	390
			6590	4.0	17.4	16.8	390

METHYL ALCOHOL

Test No.	Feed Rates		q/A	Vaporization	ΔT		h
	Liquid	Vapour			Measured	Corrected	
	lb/hr	lb/hr	Btu/hrft^2	lb/hr	F^o	F^o	Btu/hrft^{2}F^o
107	30	13	1960	1.0	7.6	7.4	265
			2630	1.5	10.4	10.2	260
			3840	1.5	15.2	14.9	260
			5310	3.0	20.9	20.4	260
			6450	4.0	25.3	24.7	260
			7780	5.0	30.1	29.4	265
			10400	7.5	20.1	19.2	540
			13300	10.0	22.8	21.6	620
			15700	11.5	23.3	21.9	720
			18600	13.5	24.2	22.6	820
108	30	84	1810	1.0	4.1	3.9	465
			2730	1.5	6.2	6.0	455
			4230	2.5	9.6	9.2	460
			6470	4.0	14.6	14.0	460
109	200	32	3980	0.5	10.6	10.2	390
			5340	1.5	14.4	13.9	385
			6760	2.5	18.7	18.1	375
			9230	4.0	25.6	24.8	375
110	200	70	3510	0	6.5	6.2	570
			4210	0	7.8	7.4	570
			5450	1.0	10.0	9.5	570
			7150	2.5	13.2	12.6	570
			10800	5.0	19.9	18.9	570
111	200	100	4150	0	5.7	5.3	780
			5300	0.5	7.4	6.9	770
			7600	2.5	10.4	9.7	780
			10300	4.5	14.0	13.1	790
			13100	6.0	17.5	16.3	800
			16400	8.5	21.2	19.7	830
			21800	12.0	27.3	25.4	860
			26200	17.0	32.2	29.9	880
			31500	21.0	35.9	33.1	950
			35800	24.0	36.9	33.7	1060

METHYL ALCOHOL

Test No.	Feed Rates		q/A	Vaporization	ΔT		h
	Liquid	Vapour			Measured	Corrected	
	lb/hr	lb/hr	Btu/hrft^2	lb/hr	F^o	F^o	Btu/hrft^{2}F^o
112	200	58	3400	0	7.6	7.3	465
			4030	0.5	9.1	8.7	465
			5400	1.5	12.1	11.6	465
			7720	3.0	17.3	16.6	465
			10300	5.0	22.6	21.7	475
113	200	50	3820	0	9.5	9.2	415
			5050	1.0	12.6	12.2	415
			6560	2.0	16.4	15.8	415
			7880	3.0	19.7	19.0	415
			10000	4.5	25.0	24.1	415
			13000	7.5	31.9	30.7	425
			16100	10.0	30.9	29.5	550
			19300	12.5	31.6	29.9	650
			22700	15.0	32.8	30.6	740
			29200	19.5	34.4	31.8	920
			35300	24.5	35.2	32.1	1100
			39700	27.5	35.9	32.4	1230
			47000	33.0	37.2	33.0	1430
114	200	30	5320	1.0	15.0	14.5	370
			6490	1.5	18.4	17.8	365
			7870	2.5	22.2	21.5	365
			10500	4.5	29.7	28.8	365
			19600	12.0	30.2	28.5	690
			24800	16.5	31.4	29.2	850
			28700	19.0	32.2	29.7	970
			33800	23.0	33.3	30.3	1120
			39100	27.0	34.2	30.7	1270
			43000	30.0	34.8	31.0	1390
115	200	0	5300	2.0	15.5	15.0	355
			6480	2.5	18.9	18.3	355
			8050	3.5	23.5	22.8	355
			10300	4.5	30.5	29.6	350
116	100	0	3900	2.0	16.3	16.0	245
			5440	3.0	22.7	22.2	245
			7050	4.0	29.0	28.4	250

Test No.	Feed Rates		q/A	Vaporization	ΔT		h
	Liquid	Vapour			Measured	Corrected	
	lb/hr	lb/hr	Btu/hrft^2	lb/hr	F^o	F^o	Btu/hrft^{2}F^o
117	100	0	2200	1.0	15.5	15.3	145
			2710	1.5	19.5	19.3	140
			3930	3.0	28.8	28.5	140
			5300	5.0	17.7	17.2	310
			6630	7.0	17.5	16.9	390
			7900	8.5	17.5	16.8	470
			9110	10.0	17.8	17.0	540
			10600	12.0	18.9	18.0	590
118	150	0	1760	1.5	11.0	10.8	165
			2620	2.5	16.3	16.1	165
			3980	3.5	24.4	24.1	165
119	75	0	1620	1.0	12.5	12.4	130
			1940	1.5	15.2	15.0	130
			2680	2.0	21.3	21.1	125
			3930	3.5	30.6	30.3	130
120	60	0	1590	0.5	12.0	11.9	135
			2050	1.0	16.0	15.8	130
			2660	1.5	20.8	20.6	130
121	40	0	1720	1.0	12.7	12.6	135
			2190	1.5	16.4	16.2	135
			2720	2.0	20.2	20.0	135
			3480	2.5	25.5	25.2	140
122	20	0	1600	1.0	9.9	9.8	165
			2160	1.5	13.4	13.2	165
			2660	2.0	16.4	16.2	165
			3440	3.0	20.9	20.6	170
			4060	4.0	23.9	23.5	175
123	200	0	2680	2.0	12.6	12.4	215
			3510	3.0	16.6	16.3	215
			4270	4.0	20.1	19.7	215

iso-PROPYL ALCOHOL

Test No.	Feed Rates		q/A	Vaporization	ΔT		h
	Liquid	Vapour			Measured	Corrected	
	lb/hr	lb/hr	Btu/hrft^2	lb/hr	F°	F°	Btu/hrft^{2}F°
124	170	0	2470	2.0	13.8	13.6	180
			3280	3.0	18.3	18.0	180
			4030	4.0	22.7	22.4	180
125	125	0	1720	1.5	12.3	12.2	140
			2610	2.0	18.7	18.5	140
			3540	3.0	25.2	24.9	140
			4230	4.0	29.4	29.0	145
126	100	0	2250	2.0	17.2	17.0	130
			2740	2.5	21.0	20.8	130
127	100	0	1710	1.5	13.3	13.2	130
			2720	2.5	20.0	19.8	135
128	84	0	1690	1.5	13.0	12.9	130
			2090	2.0	16.0	15.8	130
			2730	2.5	20.7	20.5	135
129	20	0	1810	1.0	11.3	11.1	165
			2770	2.0	17.4	17.2	160
			3840	3.5	23.3	23.0	165
130	50	0	1700	1.0	13.2	13.1	130
			2200	1.5	17.0	16.8	130
			2690	2.0	21.0	20.8	130
			3540	3.0	27.3	27.0	130
131	30	0	1690	1.0	11.8	11.7	145
			2140	1.5	14.9	14.7	145
			2740	2.5	19.3	19.1	145
			3520	3.0	24.3	24.0	145
132	100	49	1620	0	10.2	10.1	160
			2160	0.5	13.8	13.6	160
			2680	1.5	17.3	17.1	155
			3510	2.5	22.8	22.5	155
			4410	3.5	28.4	28.0	160

iso-PROPYL ALCOHOL

Test No.	Feed Rates		q/A	Vaporization	ΔT		h
	Liquid	Vapour			Measured	Corrected	
	lb/hr	lb/hr	Btu/hrft^2	lb/hr	F^o	F^o	Btu/hrft^{2}F^o
133	100	74	1620	0.5	7.9	7.8	210
			2160	1.0	10.6	10.4	210
			2590	1.5	12.6	12.4	210
			3700	2.5	18.0	17.7	210
			4550	3.5	21.6	21.2	215
			5520	5.0	25.5	25.0	220
134	100	115	1680	0.5	4.8	4.7	360
		115	2200	1.0	6.3	6.1	360
		115	2810	1.5	8.1	7.9	355
		115	4130	3.0	11.9	11.5	360
		119	6160	5.5	17.0	16.5	375
		121	8220	8.0	21.8	21.1	390
135	100	15	1650	0.5	12.5	12.4	135
			2110	1.5	16.0	15.8	135
			2670	2.0	20.0	19.8	135
			3500	3.0	25.4	25.1	140
136	100	90	1730	0	6.3	6.2	280
			2170	0.5	8.0	7.8	280
			2800	1.5	10.4	10.2	275
			3900	2.5	14.4	14.1	275
			5130	4.0	19.1	18.7	275
137	100	62	1670	0	9.6	9.5	175
			2300	0.5	13.4	13.2	175
			3120	1.5	18.3	18.0	175
			4350	3.0	25.5	25.1	175
138	100	156	2740	0.5	5.5	5.3	520
			3900	1.5	7.9	7.6	510
			5590	3.0	11.2	10.6	530
			7690	6.0	15.4	14.7	520
			9720	8.0	19.6	18.8	520

Test No.	Feed Rates		q/A	Vaporization	ΔT		h
	Liquid	Vapour			Measured	Corrected	
	lb/hr	lb/hr	Btu/hrft^2	lb/hr	F^o	F^o	Btu/hrft^{2}F^o
139	100	31	2270	1.0	17.0	16.8	135
			2720	2.0	21.6	21.4	130
			3780	3.5	27.6	27.3	140
			1580	0.5	11.9	11.8	135
140	100	39	1700	0.5	12.1	12.0	140
			2170	1.0	15.5	15.3	140
			2720	2.0	19.6	19.4	140
			3600	3.0	25.6	25.3	140
141	30	39	1440	1.5	10.2	10.1	145
			2200	2.0	15.3	15.1	145
			2740	3.0	19.1	18.9	145
			3640	4.0	24.7	24.4	150
142	30	46	1120	0.5	7.5	7.4	150
			1700	1.0	11.4	11.3	150
			2670	2.5	17.6	17.4	155
			3870	3.5	25.0	24.7	155
143	30	99	1120	0.5	4.4	4.3	260
			1690	1.0	6.8	6.7	255
			2200	1.5	8.7	8.5	260
			2770	2.5	11.0	10.8	255
			3900	3.5	15.8	15.5	250
			5240	5.0	21.0	20.5	255
144	30	76	1150	0.5	6.0	5.9	195
			1730	1.5	8.9	8.8	195
			2550	2.0	13.3	13.1	195
			3960	4.0	20.4	20.1	195
145	30	163	1320	1.0	3.2	3.1	425
			1730	1.5	4.2	4.0	430
			2160	1.5	5.2	5.0	430
			2880	2.5	6.9	6.6	435
			3840	3.5	9.3	9.0	430
			5350	5.5	12.6	12.1	440

Iso-PROPYL ALCOHOL

Test No.	Feed Rates		q/A	Vaporization	ΔT		h
	Liquid	Vapour			Measured	Corrected	
	lb/hr	lb/hr	Btu/hrft^2	lb/hr	F^o	F^o	Btu/hrft^{2}F^o
146	30	60	1180	1.0	7.1	7.0	170
			1730	1.5	10.2	10.0	175
			2190	2.0	12.4	12.2	180
			2870	2.5	15.8	15.6	185
147	30	60	1740	1.5	10.4	10.2	170
			2680	2.5	16.0	15.8	170
			3890	4.0	22.6	22.3	175
			1100	0.5	6.6	6.5	170
148	30	28	1120	0.5	7.8	7.7	145
			1700	1.5	11.8	11.7	145
			2310	2.0	15.9	15.7	145
			2730	2.5	18.8	18.6	145
			3420	3.5	23.2	22.9	150
149	30	127	1320	1.0	4.0	3.9	340
			1720	1.5	5.3	5.2	330
			2160	2.0	6.6	6.4	340
			2720	2.5	8.4	8.2	330
			3760	3.5	11.6	11.3	335
			5140	5.0	15.8	15.4	335
			6690	7.0	20.4	19.8	340
150	50	32	1710	1.0	13.2	13.1	130
			2200	1.5	16.9	16.7	130
			2620	2.0	20.2	20.0	130
			3440	3.0	26.0	25.7	135
			1290	0.5	9.9	9.8	130
151	50	61	1300	0.5	8.5	8.4	155
			1740	1.0	11.3	11.1	155
			2260	1.5	14.6	14.4	155
			2740	2.0	17.6	17.4	160
			3560	3.0	22.6	22.3	160

iso-PROPYL ALCOHOL

Test No.	Feed Rates		q/A	Vaporization	ΔT		h
	Liquid	Vapour			Measured	Corrected	
	lb/hr	lb/hr	Btu/hrft^2	lb/hr	F^o	F^o	Btu/hrft^{2}F^o
152	50	103	1220	0	4.9	4.8	255
			1750	1.0	7.0	6.8	260
			2570	2.0	10.2	10.0	255
			3580	3.0	13.9	13.6	265
			4970	4.5	19.0	18.6	265
153	50	170	1590	0.5	3.7	3.6	440
			2210	1.0	5.1	4.9	450
			2710	2.0	6.3	6.1	445
			3500	3.0	8.2	7.9	445
			4930	4.5	11.4	11.0	450
154	50	140	1530	0.5	4.4	4.3	350
			2090	1.0	6.0	5.8	360
			2700	2.0	7.7	7.5	360
			3820	3.0	11.0	10.7	360
			5350	5.0	15.0	14.5	370
155	50	82	1320	0.5	6.8	6.7	195
			1750	1.0	9.1	8.9	195
			2620	2.0	13.6	13.4	195
			3630	3.0	18.7	18.4	200
156	50	50	1210	0.5	8.9	8.8	140
			1730	1.0	12.6	12.5	140
			2600	2.0	18.9	18.7	140
			3680	3.0	25.9	25.6	145
157	50	42	1220	0.5	9.3	9.2	135
			1740	1.0	13.3	13.1	135
			2630	2.0	20.0	19.8	135
158	200	39	2320	0.5	9.9	9.7	240
			2700	1.0	11.7	11.5	235
			3410	2.0	14.8	14.5	235
			4620	3.5	20.0	19.6	235

iso-PROPYL ALCOHOL

Test No.	Feed Rates		q/A	Vaporization	ΔT		h
	Liquid	Vapour			Measured	Corrected	
	lb/hr	lb/hr	Btu/hrft^2	lb/hr	F^o	F^o	Btu/hrft^{2}F^o
159	200	96	1750	0	4.8	4.6	380
			2070	0.5	5.6	5.4	380
			2610	1.5	7.2	7.0	375
			3890	2.5	10.6	10.3	380
			5300	4.5	14.3	13.8	385
			7700	7.5	20.0	19.3	400
160	200	82	1720	0.5	5.6	5.5	315
			2700	1.5	8.8	8.6	315
			4010	3.0	13.0	12.7	315
			6600	6.0	21.1	20.5	320
161	200	138	1750	0	3.3	3.1	560
			2820	1.5	5.3	5.1	550
			4380	3.5	8.3	7.9	550
			6580	6.0	12.4	11.8	560
			9700	10.5	17.7	16.9	570
162	200	68	1710	0	6.3	6.2	275
			2670	1.0	9.9	9.7	275
			3980	2.5	14.6	14.3	280
			6210	5.5	22.6	22.1	280
163	200	58	1800	0.5	7.1	6.9	260
			2680	1.5	10.6	10.4	260
			3980	3.0	15.9	15.6	255
			6130	5.5	24.3	23.8	260
164	200	47	1750	0.5	7.3	7.1	245
			2610	1.5	11.0	10.8	240
			3790	2.5	15.8	15.5	245
			5650	4.5	23.6	23.1	245
165	200	30	2240	1.5	10.2	10.0	225
			2650	1.5	12.0	11.8	225
			3910	3.0	17.7	17.4	225
			4780	3.5	21.5	21.1	225

iso-PROPYL ALCOHOL

Test No.	Feed Rates		q/A	Vaporization	ΔT		h
	Liquid	Vapour			Measured	Corrected	
	lb/hr	lb/hr	Btu/hrft^2	lb/hr	F^o	F^o	Btu/hrft^{2}F^o
166	200	21	2160	1.0	10.0	9.8	220
			2750	1.5	12.6	12.4	220
			4000	3.0	18.3	18.0	220
167	150	97	1990	0.5	5.9	5.7	350
			2590	1.5	7.6	7.4	350
			4010	3.0	11.7	11.4	350
			5490	4.5	16.0	15.5	355
168	150	135	2620	1.5	5.6	5.4	485
			4030	3.0	8.6	8.2	490
			5430	4.5	11.6	11.1	490
			7120	6.5	15.0	14.4	495
			8800	8.5	18.3	17.5	500
			1770	0.5	3.8	3.6	490
169	150	84	1960	0.5	6.8	6.6	300
			2600	1.5	9.0	8.8	295
			3940	3.0	13.6	13.3	295
			5470	5.0	18.3	17.8	305
170	150	68	1850	0.5	7.8	7.6	245
			2680	1.5	11.4	11.2	240
			3880	3.0	16.3	16.0	245
			5310	4.5	22.0	21.5	245
171	150	54	1950	0.5	10.1	9.9	195
			2620	1.5	13.3	13.1	200
			3910	3.0	19.7	19.4	200
172	150	40	2040	1.0	11.7	11.5	180
			2730	1.5	15.8	15.6	175
			3980	3.0	22.6	22.3	180
173	150	28	1870	1.0	11.0	10.8	175
			2650	2.0	15.5	15.3	175
			3860	3.0	22.4	22.1	175

iso-PROPYL ALCOHOL

Test No.	Feed Rates		q/A	Vaporization	ΔT		h
	Liquid	Vapour			Measured	Corrected	
	lb/hr	lb/hr	Btu/hrft^2	lb/hr	F^o	F^o	Btu/hrft^{2}F^o
174	150	20	2070	1.0	12.2	12.0	170
			2680	1.5	15.8	15.6	170
			3930	3.0	23.0	22.7	175
175	150	0	1880	1.5	11.5	11.3	165
			2610	2.0	15.8	15.6	165
			3860	3.5	23.0	22.7	170
176	150	156	1950	0.5	3.6	3.4	570
			3280	2.0	6.0	5.7	580
			5400	4.5	10.0	9.5	570
			7430	7.0	13.7	13.1	570
177	170	156	1840	0.5	3.5	3.3	560
			2660	1.5	5.0	4.8	560
			4080	3.0	7.7	7.3	560
			6110	5.5	11.3	10.8	570
			8280	8.0	14.9	14.2	580
178	170	118	1870	0.5	4.8	4.6	410
			2630	1.5	6.7	6.5	410
			3960	3.0	10.0	9.7	410
			6250	5.0	15.2	14.7	420
179	170	58	1820	0.5	8.6	8.4	215
			2740	2.0	13.0	12.8	215
			4050	3.0	18.6	18.2	220
180	170	28	1890	1.0	10.4	10.2	185
			2720	2.0	14.9	14.7	185
181	170	98	1790	0.5	5.5	5.3	340
			2760	1.5	8.4	8.2	340
			4100	3.0	12.3	11.9	345
			6040	5.0	17.5	17.0	355
182	170	78	1890	0.5	7.0	6.8	280
			2650	2.0	10.0	9.8	270
			4510	4.0	16.3	15.9	285

iso-PROPYL ALCOHOL

Test No.	Feed Rates		q/A	Vaporization	ΔT		h
	Liquid	Vapour			Measured	Corrected	
	lb/hr	lb/hr	Btu/hrft^2	lb/hr	F^o	F^o	Btu/hrft^{2}F^o
183	170	0	2160	1.5	11.9	11.7	185
			2720	2.0	14.8	14.6	185
			3820	4.0	20.8	20.5	185
184	170	19	1940	1.0	10.9	10.7	180
			2670	2.0	14.8	14.6	185
			3800	3.5	20.7	20.4	185
185	170	41	1740	1.5	9.0	8.8	200
			2600	2.5	13.4	13.2	195
			3680	3.0	18.8	18.5	200
186	20	155	1690	1.0	4.0	3.9	435
			2120	1.5	5.0	4.8	440
			2730	2.5	6.6	6.4	430
187	20	109	1680	1.5	5.6	5.5	305
			2110	2.0	7.2	7.0	300
			2640	2.5	9.0	8.8	300
			3860	4.0	13.5	13.2	295
188	20	86	1520	1.0	6.6	6.5	235
			1790	1.5	7.8	7.6	235
			2110	2.0	9.1	8.9	235
			2670	2.5	11.5	11.3	235
			3880	4.0	16.5	16.2	240
189	20	69	1670	1.0	8.6	8.5	195
			2100	2.0	10.7	10.5	200
			2660	2.5	13.5	13.3	200
			3980	4.0	19.4	19.1	210
190	20	128	1690	1.5	4.9	4.8	345
			2120	2.0	6.2	6.0	355
191	20	32	1640	1.5	10.4	10.3	160
			2170	2.0	13.6	13.4	160
			2710	2.5	17.0	16.8	160
			3480	3.5	21.6	21.3	165

iso-PROPYL ALCOHOL

Test No.	Feed Rates		q/A	Vaporization	ΔT		h
	Liquid	Vapour			Measured	Corrected	
	lb/hr	lb/hr	Btu/hrft^2	lb/hr	F^o	F^o	Btu/hrft^{2}F^o
192	20	41	1590	1.5	9.7	9.6	165
			2090	2.0	12.7	12.5	165
			2710	3.0	16.4	16.2	165
193	20	54	1610	1.5	9.1	9.0	180
			2280	2.5	13.0	12.8	180
			3240	3.5	18.0	17.7	185
194	75	56	1630	1.0	11.1	11.0	150
			2160	1.5	14.5	14.3	150
			2660	2.5	17.9	17.7	150
			3740	3.5	25.0	24.7	150
195	75	144	1560	1.0	3.7	3.6	435
			2120	1.5	5.0	4.8	440
			2730	2.5	6.6	6.4	430
			3930	4.0	9.3	9.0	435
			5330	5.5	12.6	12.1	440
			7570	8.0	17.8	17.1	445
196	75	108	1560	1.0	5.2	5.1	305
			2110	1.5	7.0	6.8	310
			2720	2.0	8.9	8.7	315
			4100	4.0	13.3	12.9	315
197	75	80	1610	1.0	7.6	7.5	215
			2090	2.0	9.8	9.6	220
			2730	2.5	12.9	12.7	215
			3960	4.0	18.3	18.0	220
198	75	33	1620	1.0	12.7	12.6	130
			2200	2.0	17.4	17.2	130
			2830	2.5	22.4	22.2	130
			3760	3.5	28.9	28.6	125
199	75	46	1620	1.0	12.0	11.9	135
			2300	2.0	17.1	16.9	135
			2940	2.5	21.8	21.5	135

Iso-PROPYL ALCOHOL

Test No.	Feed Rates		q/A	Vaporization	ΔT		h
	Liquid	Vapour			Measured	Corrected	
	lb/hr	lb/hr	Btu/hrft^2	lb/hr	F^o	F^o	Btu/hrft^{2}F^o
200	75	20	1640	1.0	13.0	12.9	125
			2180	2.0	17.6	17.4	125
201	75	0	1630	1.5	12.9	12.8	125
			2080	2.0	16.7	16.5	125
			2630	2.5	21.2	21.0	125
			3660	3.5	28.9	28.6	130
202	100	0	1620	1.5	12.5	12.4	130
			2160	2.0	16.6	16.4	130
			2770	2.5	21.4	21.2	130
203	75	21	1620	1.0	12.6	12.5	130
			2220	2.0	17.6	17.4	130
			2650	2.5	20.9	20.7	130

WATER

Test No.	Feed Rates		q/A	Vaporization	ΔT		h
	Liquid	Vapour			Measured	Corrected	
	lb/hr	lb/hr	Btu/hrft^2	lb/hr	F^o	F^o	Btu/hrft^{2}F^o
204	100	0	2620	0.5	3.1	2.9	900
			3790	1.5	4.6	4.3	880
			5310	1.5	6.6	6.1	870
			7640	2.5	9.3	8.6	890
			9730	3.0	11.8	11.0	880
205	150	0	5170	1.5	5.5	5.1	1020
			6740	2.0	7.1	6.5	1040
			8730	2.5	9.2	8.4	1040
206	201	0	5230	1.0	5.0	4.5	1160
			6800	1.5	6.5	5.9	1150
			8770	2.5	8.4	7.6	1150
207	264	0	5730	0.5	4.4	3.9	1470
			7120	1.0	5.6	5.0	1430
			8810	2.0	7.2	6.4	1380
208	370	0	7990	1.0	5.0	4.3	1860
			9550	1.0	6.3	5.5	1740
209	75	0	2710	1.0	3.4	3.2	850
			3420	1.0	4.4	4.1	840
			5180	1.5	6.6	6.2	840
			7400	2.5	9.4	8.8	840
			9070	3.0	11.6	10.8	840
210	50	0	2670	0.5	3.4	3.2	830
			3500	1.0	4.5	4.2	830
			5130	1.5	6.5	6.1	840
			7470	2.0	9.4	8.8	850
211	30	0	2680	0.5	3.0	2.8	960
			3580	1.0	4.0	3.7	970
			5190	1.5	5.8	5.4	960
			7720	3.0	8.6	7.9	980

WATER

Test No.	Feed Rates		q/A	Vaporization	ΔT		h
	Liquid	Vapour			Measured	Corrected	
	lb/hr	lb/hr	Btu/hrft^2	lb/hr	F^o	F^o	Btu/hrft^{2}F^o
212	20	0	2620	0.5	2.6	2.4	1090
			3400	1.0	3.3	3.0	1130
			5300	1.5	5.1	4.6	1150
			7900	2.5	7.6	6.9	1150
213	40	0	3280	1.0	4.0	3.7	890
			5330	1.5	6.6	6.1	880
			7900	2.5	9.6	8.9	890
214	60	0	3350	0.5	4.2	3.9	860
			5120	1.0	6.6	6.2	830
			6850	1.5	8.8	8.2	840
215	60	23	3840	0.5	4.6	4.3	890
			5280	1.0	6.3	5.8	910
			6770	2.0	8.0	7.4	910
			8770	2.5	10.4	9.6	910
216	60	49	3450	0.5	3.4	3.1	1110
			4170	1.0	4.1	3.7	1130
			5660	1.5	5.6	5.1	1110
			8020	2.0	8.0	7.3	1100
217	60	42	3440	0.5	3.7	3.4	1010
			5510	1.5	6.0	5.5	1000
			8040	2.5	8.6	7.9	1020
218	60	0	3480	0.5	4.4	4.1	850
			5500	1.5	7.0	6.5	850
			6970	2.0	8.9	8.3	840
219	60	38	3560	0.5	4.0	3.7	960
			5350	1.0	6.0	5.5	970
			7040	1.5	7.9	7.3	960
220	60	32	3470	0.5	4.1	3.8	910
			5330	1.0	6.3	5.8	920
			6900	1.5	8.1	7.5	920

WATER

Test No.	Feed Rates		q/A	Vaporization	ΔT		h
	Liquid	Vapour			Measured	Corrected	
	lb/hr	lb/hr	Btu/hrft^2	lb/hr	F^o	F^o	Btu/hrft^{2}F^o
221	60	12	3430	1.0	4.2	3.9	880
			5310	1.5	6.5	6.0	890
			6950	2.0	8.4	7.8	890
222	60	48	3440	0.5	3.4	3.1	1110
			5840	1.5	5.8	5.3	1110
223	125	0	3400	1.0	3.9	3.6	950
			5460	1.5	6.3	5.8	940
			6950	2.0	8.0	7.4	940
224	232	0	6470	0.5	5.7	5.1	1270
			7850	1.5	6.9	6.2	1270
			8650	2.0	7.7	6.9	1260
225	320	0	5260	1.0	3.6	3.1	1700
			6700	1.0	4.6	4.0	1680
			7690	0.5	5.3	4.6	1680
			8680	1.0	6.0	5.2	1670
226	370	0	5490	0.5	3.4	2.9	1890
			6750	1.0	4.2	3.6	1880
			8250	0.5	5.2	4.5	1830
			9720	1.0	6.2	5.4	1800
227	20	0	3510	1.0	3.4	3.1	1130
			5290	1.5	5.1	4.6	1150
			6480	2.0	6.3	5.7	1140
228	20	34	2580	0.5	2.4	2.2	1170
			3410	1.0	3.2	2.9	1170
			5060	1.5	4.8	4.4	1150
			7580	2.0	7.1	6.4	1180
229	20	50	2670	0.5	2.3	2.1	1270
			3400	1.0	2.9	2.6	1310
			5170	1.5	4.4	4.0	1290
			7770	2.5	6.6	5.9	1310

WATER

Test No.	Feed Rates		q/A	Vaporization	ΔT		h
	Liquid	Vapour			Measured	Corrected	
	lb/hr	lb/hr	Btu/hrft^2	lb/hr	F^o	F^o	Btu/hrft^{2}F^o
230	20	46	2870	0.5	2.5	2.3	1250
			3600	1.0	3.3	3.0	1200
			5570	1.5	5.0	4.5	1240
231	20	10	2720	0.5	2.6	2.4	1130
			4060	1.0	3.9	3.5	1160
232	60	0	3520	1.0	4.4	4.1	860
			5290	1.5	6.7	6.2	850
			6910	2.0	8.8	8.2	850
			8510	2.5	10.6	9.9	860
			10500	3.0	13.1	12.2	860
			12400	3.5	14.8	13.7	910
			14500	4.5	17.4	16.1	900
			16600	5.5	19.1	17.7	940
			19400	7.0	21.3	19.6	990
			24800	8.5	16.8	14.6	1700
			28000	10.0	17.6	15.2	1850
			34900	13.0	19.4	16.4	2130
			43100	16.0	21.4	17.7	2440
			50000	18.0	22.8	18.5	2700
233	232	0	5490	1.0	4.8	4.3	1280
			8770	1.5	7.8	7.0	1250
			11600	2.5	10.3	9.3	1250
			13700	3.5	12.0	10.8	1270
			16300	4.0	13.6	12.2	1340
			21400	6.5	17.3	15.4	1390
			25800	8.5	20.5	18.3	1410
			31100	9.5	23.0	20.3	1530
			37100	12.5	24.6	21.4	1730
			43600	15.0	26.7	22.9	1900
			50000	17.5	28.5	24.2	2070

WATER

Test No.	Feed Rates		q/A	Vaporization	ΔT		h
	Liquid	Vapour			Measured	Corrected	
	lb/hr	lb/hr	Btu/hrft^2	lb/hr	F^o	F^o	Btu/hrft^{2}F^o
234	30	0	3430	0.5	3.8	3.5	980
			6910	2.0	7.7	7.1	970
			10300	3.0	11.5	10.6	970
			13300	4.0	14.8	13.6	980
			16000	5.0	17.4	16.0	1000
			20700	6.5	21.7	19.9	1040
			24600	8.0	24.6	22.5	1100
			29500	10.5	26.5	23.9	1240
			37200	13.0	28.8	25.6	1450
			41100	15.0	29.7	26.1	1580
235	320	0	7270	1.5	5.2	4.6	1580
			8810	0.5	6.2	5.4	1630
			11000	1.0	7.7	6.7	1640
			13400	2.0	9.6	8.4	1600
236	370	0	7740	1.0	4.9	4.2	1840
			10600	1.5	7.0	6.1	1740
			14000	2.0	9.4	8.2	1710
237	60	0	8340	2.5	10.3	9.6	870
			11600	3.5	13.0	12.0	970
			14100	4.5	14.9	13.6	1040
			17100	5.5	17.5	16.0	1070
			21600	8.0	20.9	19.0	1140
			25900	9.5	22.7	20.4	1270
			30600	11.0	24.3	21.6	1420
			37600	13.5	26.1	22.8	1650
			42800	15.5	27.6	23.9	1790
238	232	43	5240	0.5	4.2	3.7	1420
			8640	2.0	6.9	6.1	1420
			12000	3.0	9.6	8.6	1400
239	232	36	5310	1.0	4.6	4.1	1300
			8410	2.0	7.2	6.5	1290
			12300	3.5	10.6	9.5	1300
240	232	14	6150	1.0	5.4	4.9	1260
			10400	2.5	9.1	8.2	1270

ETHYL ALCOHOL
(Extended Period Reproducibility Check)

Test No.	Feed Rates		q/A	Vaporization	ΔT		h
	Liquid	Vapour			Measured	Corrected	
	lb/hr	lb/hr	Btu/hrft^2	lb/hr	F^o	F^o	Btu/hrft^{2}F^o
241	200	0	3490	2.5	13.5	13.2	265
			3890	3.0	15.1	14.8	265
			5430	4.0	21.4	20.9	260
			8470	6.5	33.3	32.6	260
242	100	0	1860	1.0	10.8	10.6	175
			2700	1.5	15.7	15.5	175
			3930	2.5	22.9	22.6	175
			5420	4.5	22.3	21.8	250
			6480	5.5	22.3	21.7	300
			7600	6.5	23.4	22.7	335
			9700	9.0	22.6	21.8	445
243	50	0	2710	1.5	16.7	16.5	165
			3820	2.5	23.6	23.3	165
			1810	1.0	11.1	10.9	165
244	30	0	1790	1.0	10.1	9.9	175
			2730	2.0	15.4	15.2	180
			4130	3.0	22.9	22.5	185
			5190	4.0	28.7	28.3	185
245	100	41	3430	2.5	18.1	17.8	195
		42	5040	4.0	26.4	26.0	195
		45	7600	7.0	29.5	28.8	265
		46	10300	9.5	31.8	30.9	335
		46	13400	12.5	33.4	32.2	415
		47	16600	15.5	33.9	32.5	510
		47	20500	19.5	34.9	33.1	620
		47	26100	24.5	36.2	33.9	770
246	100	80	3460	1.5	11.0	10.7	325
			5440	3.5	17.3	16.8	325
			8030	6.0	25.7	25.0	320
			13100	11.5	33.0	31.9	410
			17100	15.5	34.5	33.0	520
			21800	20.0	35.5	33.7	650
			26500	24.5	36.7	34.4	770

ETHYL ALCOHOL
(Extended Period Reproducibility Check)

Test No.	Feed Rates		q/A	Vaporization	ΔT		h
	Liquid	Vapour			Measured	Corrected	
	lb/hr	lb/hr	Btu/hrft^2	lb/hr	F^o	F^o	Btu/hrft^{2}F^o
247	100	20	2570	1.0	14.9	14.7	175
			3980	2.0	23.0	22.7	175
			5520	3.5	31.1	30.6	180
			7080	5.5	27.4	26.8	265
248	100	20	4100	2.0	23.6	23.2	175
			6950	5.5	27.5	26.9	260
			10300	8.5	29.8	28.9	355
			14800	13.0	30.7	29.4	500
			21500	19.5	33.1	31.2	690

CHLOROFORM

Test No.	Feed Rates		q/A	Vaporization	ΔT		h
	Liquid	Vapour			Measured	Corrected	
	lb/hr	lb/hr	Btu/hrft^2	lb/hr	F^o	F^o	Btu/hrft^{2}F^o
249	50	0	1490	3.5	9.3	9.2	160
			1860	4.5	11.7	11.5	160
			2640	7.0	16.7	16.5	160
			3760	10.5	23.7	23.4	160
250	30	0	1480	4.0	8.7	8.6	170
			1790	4.5	10.6	10.4	170
			2660	7.5	15.4	15.2	175
251	30	0	1290	3.5	7.5	7.4	175
			1720	4.5	9.9	9.8	175
			2650	6.5	14.7	14.5	185
252	50	0	1250	2.5	8.5	8.4	150
			1710	3.5	11.5	11.4	150
253	100	0	1600	3.0	9.9	9.8	165
			2090	6.0	12.5	12.3	170
254	200	0	1210	1.5	5.2	5.1	235
			1790	3.0	8.0	7.8	230
			2710	6.0	12.2	12.0	225
			3990	9.5	18.4	18.1	220
			5420	14.0	25.2	24.7	220
			6780	18.0	31.6	31.0	220
255	300	0	1700	2.5	6.1	6.0	285
			2610	5.5	9.4	9.2	285
			3890	8.5	14.5	14.2	275
			5280	11.5	19.8	19.3	275
			6560	15.0	24.8	24.2	270
256	140	0	1390	3.0	7.5	7.4	190
			1700	3.5	9.1	9.0	190
			2560	6.5	13.9	13.7	185
			3870	10.5	21.1	20.8	185
257	70	0	1200	2.0	8.4	8.3	145
			1770	4.0	12.1	11.9	150

CHLOROFORM

Test No.	Feed Rates		q/A	Vaporization	ΔT		h
	Liquid	Vapour			Measured	Corrected	
	lb/hr	lb/hr	Btu/hrft^2	lb/hr	F^o	F^o	Btu/hrft^{2}F^o
258	40	0	1220	2.5	7.7	7.6	160
			1700	4.0	10.7	10.6	160
			2650	7.0	16.4	16.2	165
259	100	0	1340	2.5	8.4	8.3	160
			1740	4.0	11.0	10.8	160
			2580	6.5	16.4	16.2	160
			3910	10.5	24.3	24.0	165
260	63	0	1320	3.0	9.1	9.0	145
			1750	4.0	12.0	11.8	150
			2680	7.0	17.9	17.7	150
261	240	0	1610	2.5	6.5	6.4	250
			2460	5.0	10.2	10.0	245
			3720	9.0	15.4	15.1	245
262	74	0	1290	2.5	8.7	8.6	150
			1740	4.0	11.7	11.5	150
			2720	7.0	18.3	18.1	150
263	33	0	1230	3.0	7.5	7.4	165
			1790	4.5	10.6	10.4	170
			2790	7.5	16.1	15.9	175
264	100	94	1290	1.5	6.9	6.8	190
			1760	2.5	9.4	9.2	190
			2660	5.0	14.1	13.9	190
			3870	9.5	20.6	20.3	190
265	100	210	1240	1.5	3.5	3.4	365
			1720	3.0	5.0	4.9	350
			2690	6.0	7.6	7.4	365
			5320	14.0	15.4	14.9	360
266	100	131	1310	2.0	5.6	5.5	240
			1720	3.0	7.4	7.3	235
			2780	6.0	12.0	11.8	235
			5300	14.0	23.0	22.5	235

CHLOROFORM

Test No.	Feed Rates		q/A	Vaporization	ΔT		h
	Liquid	Vapour			Measured	Corrected	
	lb/hr	lb/hr	Btu/hrft^2	lb/hr	F$^\circ$	F$^\circ$	Btu/hrft^{2}F$^\circ$
267	100	67	1220	1.5	7.2	7.1	170
			1720	3.0	10.0	9.9	175
			2670	6.0	15.6	15.4	175
			4260	11.0	24.8	24.4	175
268	100	39	1230	1.5	7.5	7.4	165
			1730	3.0	10.4	10.3	170
			2610	6.0	15.6	15.4	170
			3960	10.0	23.4	23.1	170
269	100	21	1230	1.5	7.6	7.5	165
			1710	3.0	10.7	10.6	160
			2680	6.0	16.6	16.4	165
270	100	178	1290	2.0	4.3	4.2	310
			1750	3.0	5.8	5.6	315
			2640	6.0	8.8	8.6	310
			4960	13.0	16.6	16.2	305
271	100	250	1230	1.5	3.0	2.9	425
			1750	3.0	4.3	4.1	425
			2600	6.0	6.4	6.2	420
			5210	13.5	12.8	12.3	425
272	40	99	1230	2.5	6.8	6.7	185
			1740	4.0	9.5	9.3	185
			2670	7.0	14.6	14.4	185
			3910	11.0	21.1	20.8	190
			5220	15.0	27.4	26.9	195
273	40	178	1100	2.5	4.2	4.1	270
			1740	4.0	6.6	6.4	270
			2560	7.0	9.7	9.5	270
			5180	15.0	18.8	18.3	280
274	40	132	1270	3.0	6.2	6.1	210
			1710	4.0	8.4	8.3	205
			2670	7.0	12.9	12.7	210

CHLOROFORM

Test No.	Feed Rates		q/A	Vaporization	ΔT		h
	Liquid	Vapour			Measured	Corrected	
	lb/hr	lb/hr	Btu/hrft^2	lb/hr	F^o	F^o	Btu/hrft^{2}F^o
275	40	252	1230	2.5	3.6	3.5	350
			1810	4.5	5.1	4.9	370
			2660	7.0	7.6	7.4	360
			3940	11.0	11.2	10.9	360
276	40	62	1220	2.5	7.4	7.3	170
			1710	4.0	10.2	10.1	170
			2640	7.0	15.6	15.4	170
			3730	10.5	21.8	21.5	175
277	40	40	1270	3.0	7.9	7.8	165
			1790	4.5	11.0	10.8	165
			2680	7.0	16.2	16.0	165
			3890	11.0	23.4	23.1	170
278	40	211	1240	2.5	4.1	4.0	310
			1780	4.5	5.9	5.7	310
			2680	5.5	8.8	8.6	310
			4060	11.5	13.4	13.0	310
279	70	100	1230	2.0	7.2	7.1	175
			1670	3.5	9.7	9.6	175
			2650	6.5	15.5	15.3	175
			3900	10.5	22.6	22.3	175
280	70	178	1220	2.0	4.5	4.4	280
			1730	3.5	6.4	6.2	280
			2590	6.5	9.6	9.4	275
			3930	10.5	14.5	14.2	275
			5210	14.5	19.1	18.6	280
281	70	134	1230	2.0	5.9	5.8	210
			1750	4.0	8.2	8.0	220
			2610	5.5	12.3	12.1	215
			4380	15.0	20.9	20.5	215
282	70	250	1280	2.5	3.5	3.4	380
			1750	4.0	4.8	4.6	380
			2760	7.0	7.5	7.3	380
			4300	12.0	11.6	11.2	385

CHLOROFORM

Test No.	Feed Rates		q/A	Vaporization	ΔT		h
	Liquid	Vapour			Measured	Corrected	
	lb/hr	lb/hr	Btu/hrft^2	lb/hr	F^o	F^o	Btu/hrft^{2}F^o
283	70	210	1280	2.5	4.1	4.0	320
			1730	3.5	5.5	5.3	325
			2580	6.5	8.2	8.0	320
			3780	10.0	12.0	11.7	325
284	70	68	1280	2.5	8.2	8.1	160
			1740	4.0	11.0	10.8	160
			2610	6.5	16.4	16.2	160
			3880	10.5	24.2	23.9	165
285	70	42	1280	2.5	8.5	8.4	150
			1740	3.5	11.5	11.3	155
			2740	7.0	17.9	17.7	155
286	140	41	1290	2.0	6.7	6.6	195
			1800	3.5	9.5	9.3	195
			2820	6.5	14.8	14.6	195
287	140	100	1230	1.5	5.7	5.6	220
			1750	3.0	8.1	7.9	220
			2710	6.0	12.6	12.4	220
			3930	10.0	18.4	18.1	215
288	140	178	1230	0	3.9	3.8	325
			1750	1.5	5.4	5.2	335
			2590	4.0	8.1	7.9	330
			4030	8.5	12.6	12.2	330
289	140	140	1200	0	4.6	4.5	265
			1760	1.5	6.7	6.5	270
			2680	4.5	10.1	9.9	270
			3910	8.5	14.9	14.6	270
290	140	63	1180	0	6.1	6.0	195
			1720	1.5	8.9	8.8	195
			2630	4.5	13.6	13.4	195
			3960	8.5	20.3	20.0	200

CHLOROFORM

Test No.	Feed Rates		q/A	Vaporization	ΔT		h
	Liquid	Vapour			Measured	Corrected	
	lb/hr	lb/hr	Btu/hrft^2	lb/hr	F^o	F^o	Btu/hrft^{2}F^o
291	140	257	1320	0.5	3.1	3.0	440
			1770	2.0	4.1	4.0	445
			2740	4.5	6.4	6.2	445
292	140	212	1250	0.5	3.4	3.3	380
			1710	2.0	4.7	4.6	375
			2640	5.0	7.2	7.0	380
			4050	9.0	11.1	10.7	380
293	240	98	1630	2.0	5.9	5.8	280
			2600	5.0	9.6	9.4	275
			3890	9.0	14.7	14.4	270
294	240	176	1600	2.0	4.1	4.0	400
			2560	5.0	6.8	6.6	390
			3940	9.0	10.6	10.3	385
295	240	135	1600	1.5	5.2	5.1	315
			2590	5.0	8.5	8.3	310
			3910	9.0	12.9	12.6	310
296	240	205	1630	2.0	4.0	3.9	420
			2700	5.0	6.6	6.4	425
			4030	9.5	9.8	9.4	430
297	240	151	1600	1.5	4.7	4.6	350
			2640	5.0	7.9	7.7	345
			4080	9.5	12.3	11.9	345
298	240	247	1640	2.0	3.6	3.5	470
			2770	5.0	6.1	5.9	470
			4050	9.5	8.9	8.5	480
299	240	66	1230	0.5	4.9	4.8	255
			1730	1.5	6.8	6.6	260
			2530	4.0	10.2	10.0	255
			3890	7.5	15.6	15.3	255

CHLOROFORM

Test No.	Feed Rates		q/A	Vaporization	ΔT		h
	Liquid	Vapour			Measured	Corrected	
	lb/hr	lb/hr	Btu/hrft^2	lb/hr	F^o	F^o	Btu/hrft^{2}F^o
300	240	40	1630	0.5	6.6	6.5	250
			2610	4.0	10.6	10.4	250
			3890	8.5	16.1	15.8	245
301	30	41	1280	3.5	7.6	7.5	170
			1750	4.5	10.3	10.1	175
			2540	7.0	14.7	14.5	175
302	30	100	1230	3.0	6.3	6.2	200
			1770	4.5	9.2	9.0	195
			2720	7.5	13.9	13.7	200
303	30	67	1200	3.0	6.7	6.6	180
			1700	4.5	9.5	9.4	180
			2780	8.0	15.3	15.1	185
304	30	178	1210	3.0	4.4	4.3	280
			1800	4.5	6.6	6.4	280
			2670	7.5	9.7	9.5	280
305	30	210	1210	3.0	3.8	3.7	325
			1700	4.5	5.4	5.3	320
			2710	7.5	8.6	8.4	325
306	30	256	1200	3.0	3.3	3.2	375
			1830	5.0	5.0	4.8	380
			2570	7.0	7.0	6.8	380
			3960	11.5	10.8	10.5	380
307	30	140	1280	3.0	5.8	5.7	225
			1700	5.0	7.7	7.6	225
			2640	8.0	11.9	11.7	225
308	54	100	1240	2.5	7.1	7.0	175
			1750	4.0	9.9	9.7	180
			2630	7.0	15.1	14.9	175

CHLOROFORM

Test No.	Feed Rates		q/A	Vaporization	ΔT		h
	Liquid	Vapour			Measured	Corrected	
	lb/hr	lb/hr	Btu/hrft^2	lb/hr	F^o	F^o	Btu/hrft^{2}F^o
309	54	182	1270	2.5	4.9	4.8	265
			1800	4.0	6.9	6.7	270
			2640	7.0	10.1	9.9	265
			4130	11.0	15.6	15.2	270
310	54	140	1240	2.5	6.0	5.9	210
			1700	4.0	8.3	8.2	210
			2660	7.0	12.8	12.6	210
311	54	210	1210	2.5	4.1	4.0	300
			1760	4.0	6.0	5.8	305
			2720	7.0	9.1	8.9	305
			4450	12.5	15.0	14.6	305
312	54	253	1210	2.5	3.4	3.3	365
			1710	4.0	4.8	4.7	365
			2690	5.0	7.6	7.4	365
			4010	11.0	11.3	10.9	370
313	54	66	1220	2.5	7.9	7.8	155
			1780	4.5	11.2	11.0	160
			2750	7.5	17.2	17.0	160
314	54	40	1200	2.5	8.0	7.9	150
			1800	4.5	11.9	11.7	155
315	54	0	1290	2.5	9.0	8.9	145
316	54	0	1230	2.5	8.4	8.3	150
			1680	4.0	11.4	11.3	150
			2540	6.5	17.2	17.0	150
317	200	100	1240	1.0	5.0	4.9	255
			1690	2.5	6.7	6.6	255
			2670	5.5	10.6	10.4	255
			3940	9.5	15.9	15.6	255

CHLOROFORM

Test No.	Feed Rates		q/A	Vaporization	ΔT		h
	Liquid	Vapour			Measured	Corrected	
	lb/hr	lb/hr	Btu/hrft^2	lb/hr	F^o	F^o	Btu/hrft^{2}F^o
318	200	178	1240	1.0	3.6	3.5	355
			1740	2.5	5.0	4.8	360
			2610	5.0	7.6	7.4	355
			3840	9.5	11.0	10.7	360
319	200	136	1230	0.5	4.4	4.3	285
			1750	2.0	6.3	6.1	285
			2700	4.5	9.7	9.5	285
320	200	211	1230	1.0	3.2	3.1	400
			1750	2.5	4.6	4.4	400
			2570	5.0	6.7	6.5	395
			4100	10.0	10.7	10.3	400
321	200	260	1210	0.5	2.8	2.7	450
			1750	2.0	4.1	3.9	450
			2710	5.0	6.3	6.1	445
			4190	10.0	9.7	9.3	445
322	200	67	1230	0.5	5.3	5.2	235
			1720	2.5	7.4	7.3	235
			2670	5.5	11.5	11.3	235
			3930	9.0	17.1	16.8	235
323	200	38	1200	0.5	5.2	5.1	235
			1750	2.0	7.7	7.5	235
			2640	5.0	11.7	11.5	230
324	200	191	1210	1.0	3.3	3.2	380
			1760	2.5	4.7	4.5	390
			2730	5.0	7.4	7.2	380
325	140	191	1260	1.5	3.7	3.6	350
			1710	3.0	5.0	4.9	350
			2690	6.0	8.0	7.8	345
326	200	151	1210	1.0	4.0	3.9	310
			1760	2.5	5.9	5.7	310
			2700	5.0	9.0	8.8	310
			4170	9.5	13.5	13.1	320

CHLOROFORM

Test No.	Feed Rates		q/A	Vaporization	ΔT		h
	Liquid	Vapour			Measured	Corrected	
	lb/hr	lb/hr	Btu/hrft^2	lb/hr	F^o	F^o	Btu/hrft^{2}F^o
327	140	256	1270	1.5	3.0	2.9	440
			1810	3.5	4.3	4.1	440
			2730	6.0	6.5	6.3	435
328	200	0	1290	1.5	5.7	5.6	230
			1760	2.5	7.9	7.7	230
			2760	6.0	12.4	12.2	225
			4010	9.5	18.4	18.0	225
329	300	100	1750	0	5.9	5.7	305
			2670	1.0	9.2	9.0	300
330	300	174	2590	2.0	6.8	6.6	390
			3930	7.0	10.4	10.1	390
331	300	136	2690	2.5	8.3	8.1	335
			3930	7.0	12.4	12.1	325
332	300	209	1780	0	4.3	4.1	435
			2670	3.0	6.4	6.2	430
			4060	7.5	9.7	9.3	440
333	300	253	2620	2.0	5.7	5.5	480
			3960	6.0	8.6	8.3	480
334	300	146	1760	0	5.1	4.9	360
			2800	3.0	8.2	8.0	350
335	300	65	1770	0.5	6.4	6.2	285
			2640	4.0	9.6	9.4	280
			3820	7.0	14.1	13.8	280
336	300	38	1760	1.0	6.4	6.2	285
			2620	3.5	9.6	9.4	280

APPENDIX II

PHYSICAL PROPERTIES OF THE TEST LIQUIDS

WATER 212°F			Source of data*
ρ_L	59.8	lb/ft^3	(1)
ρ_V	0.037	lb/ft^3	Calculated from data of (15), checked by (16)
μ_L	0.685	lb/hr ft	(6), confirmed by data of (17)
μ_V	0.0307	lb/hr ft	(7)
c	1.01	Btu/lb F°	(8), confirmed by data of (18)
k	0.394	Btu/hr ft F°	(26), confirmed by data of (19)
λ	971	Btu/lb	(15)
σ	0.00403	lb force/ft	(10)
Pr	1.76	dimensionless	Calculated from above data, confirmed by data of (20)
$\frac{(\nu^2/g)^{1/3}}{k}$	1.73×10^{-4}	(Btu/hr ft^2 F°)$^{-1}$	Calculated from above data

*References for this Appendix are given on pages A64-65.

CHLOROFORM 143°F			Source of data
ρ_L	88.1	lb/ft^3	(2)
ρ_V	0.281	lb/ft^3	(16)
μ_L	0.94	lb/hr ft	Graphical extrapolation of data of (14), (21), (23)
μ_V	0.0278	lb/hr ft	Graphical interpolation between data of (22), (24)
c	0.244	Btu/lb F°	(25)
k	0.063	Btu/hr ft F°	Extrapolations of data of (27), (33)
λ	106	Btu/lb	(9)
σ	0.001147	lb force/ft	(11)
Pr	3.64	dimensionless	Calculated from above data
$\frac{(\nu^2/g)^{1/3}}{k}$	10.3 x 10^{-4}	(Btu/hr ft^2 F°)$^{-1}$	Calculated from above data

METHYL ALCOHOL 148°F			Source of data
ρ_L	46.9	lb/ft^3	(4)
ρ_V	0.0761	lb/ft^3	(4), checked by (16)
μ_L	0.80	lb/hr ft	Graphical extrapolation of data of (14), (21), (23)
μ_V	0.0269	lb/hr ft	Graphical interpolation between data of (22), (24)
c	0.644	Btu/lb F°	(25)
k	0.108	Btu/hr ft F°	Extrapolation of data of (29), checked against high-temperature data of (31), good agreement with extrapolations of data of (27), (28), (30)
λ	473	Btu/lb	(9)
σ	0.00130	lb force/ft	(11)
Pr	4.77	dimensionless	Calculated from above data
$\frac{(\nu^2/g)^{1/3}}{k}$	8.21×10^{-4}	(Btu/hr ft^2 F°)$^{-1}$	Calculated from above data

ETHYL ALCOHOL 173°F			Source of data
ρ_L	46.0	lb/ft^3	(3)
ρ_V	0.103	lb/ft^3	(5), checked by (16)
μ_L	1.08	lb/hr ft	Graphical extrapolation of data of (21), (23)
μ_V	0.0247	lb/hr ft	Graphical extrapolation of data of (22), (24)
c	0.780	Btu/lb F°	(25)
k	0.0893	Btu/hr ft F°	Extrapolations of data of (29), (30), checked against high-temperature data of (31)
λ	368	Btu/lb	(9)
σ	0.00120	lb force/ft	(12)
Pr	9.68	dimensionless	Calculated from above data
$\frac{(\nu^2/g)^{1/3}}{k}$	12.6 x 10^{-4}	(Btu/hr ft^2 F°)$^{-1}$	Calculated from above data

iso-PROPYL ALCOHOL 180°F			Source of data
ρ_L	45.8	lb/ft^3	(2)
ρ_V	0.135	lb/ft^3	(16)
μ_L	1.22	lb/hr ft	Graphical extrapolation of data of (21), (23)
μ_V	0.0225	lb/hr ft	Graphical extrapolation of data of (22), (24)
c	0.832	Btu/lb F°	(25)
k	0.0751	Btu/hr ft F°	Extrapolations of data of (30), (32)
λ	287	Btu/lb	(9)
σ	0.00115	lb force/ft	(13)
Pr	13.5	dimensionless	Calculated from above data
$\frac{(\nu^2/g)^{1/3}}{k}$	15.9 x 10^{-4}	(Btu/hr ft^2 F°)$^{-1}$	Calculated from above data

REFERENCES FOR APPENDIX II

(1) "International Critical Tables", 1928, Vol. III, p.26, (McGraw-Hill, New York).

(2) "International Critical Tables", ibid, Vol. III, p.28.

(3) "International Critical Tables", ibid, Vol. III, p.27.

(4) "International Critical Tables", ibid, Vol. III, p.237.

(5) "International Critical Tables", ibid, Vol. III, p.238.

(6) "International Critical Tables", ibid, Vol. IV, p.10.

(7) "International Critical Tables", ibid, Vol. V, p.4.

(8) "International Critical Tables", ibid, Vol. V, p.113.

(9) "International Critical Tables", ibid, Vol. V, p.138.

(10) "International Critical Tables", ibid, Vol. IV, p.447.

(11) "International Critical Tables", ibid, Vol. IV, p.448.

(12) "International Critical Tables", ibid, Vol. IV, p.449.

(13) "International Critical Tables", ibid, Vol. IV, p.450.

(14) "International Critical Tables", ibid, Vol. V, p.11.

(15) Callendar, H.L., "Abridged Steam Tables", Fourth Edition, 1939, (Edward Arnold, London).

(16) Calculation from gas laws using compressibility factor data from Hougen, O.A., Watson, K.M., and Ragatz, R.A., "Chemical Process Principles", Vol. 2, Second Edition, 1959, p.582, (Wiley, New York).

(17) Wellman, E.J., "A Survey of the Thermodynamic and Physical Properties of Water", M.Sc. Thesis in Mechanical Engineering, Purdue University, 1950, (available as U.S.A.E.C. Report No. NP-5300, 1950), p.39.

(18) Wellman, E.J., ibid, p.31.

(19) Wellman, E.J., ibid, p.35.

(20) Wellman, E.J., ibid, p.42.

(21) Reid, C.E., and Sherwood, T.K., "The Properties of Gases and Liquids", 1958, pp.210-213, (McGraw-Hill, New York).

(22) Reid, C.E., and Sherwood, T.K., ibid, pp.191-193.

(23) Hodgman, C.D. (Editor), "Handbook of Chemistry and Physics", Forty-first Edition, 1960, pp.2182-2187, (Chemical Rubber Publishing Co., Cleveland, Ohio).

(24) Hodgman, C.D., ibid, pp.2188-2192.

(25) Perry, J.H. (Editor), "Chemical Engineers' Handbook", Third Edition, 1950, p.228 (McGraw-Hill, New York).

(26) McAdams, W.H., "Heat Transmission", Third Edition, 1954, p.484, (McGraw-Hill, New York).

(27) Mason, H.L., Tr. A.S.M.E., 76, 817-820 (1954).

(28) Bates, O.K., Hazzard, G., and Palmer, G., Ind. Eng. Chem., Anal. Edition, 10, 314-318 (1938).

(29) Riedel, L., Chem. Ing.-Tech., 23, 465-469 (1951).

(30) Sakiadis, B.C., and Coates, J., A.I.Ch.E. Jl., 1, 275-288 (1955).

(31) Scheffy, W.J., and Johnson, E.F., Jl. of Chem. Eng. Data, 6, 245-249 (1961).

(32) Kharbanda, O.P., Chem. and Process Engineering, 35, 385-387 (1954).

(33) Bates, O.K., Hazzard, G., and Palmer, G., Ind. Eng. Chem., 33, 375-376 (1941).

APPENDIX IIA

PHYSICAL PROPERTIES OF THE ADDITIONAL TEST LIQUIDS OF STAKER

Property	Units	Water 150°F	n-Butanol 237°F	Ethyl Acetate 168°F
ρ_L	lb/ft^3	61.2	46.3	52.2
ρ_V	lb/ft^3	0.0103	0.145	0.190
μ_L	lb/hr ft	1.06	0.97	0.65
μ_V	lb/hr ft	0.027	0.024	0.021
σ	lb force/ft	0.0045	0.00113	0.00117

Source of Data : Appendix I, Staker, R., Ph.D. Thesis, University of Adelaide (1959).

APPENDIX III

TYPICAL CALCULATIONS OF HEAT TRANSFER COEFFICIENTS AND EXPERIMENTAL CONDITIONS

Consider Test Run No. 17 which includes both falling film and the nucleate boiling conditions, and has readings carried out at low, medium, and high temperature differences and heat fluxes.

Run No. 17

Brass tube, 1.000 in. O.D. x 18 in. long

Test liquid - Ethyl Alcohol

Liquid feedrate = 50 lb/hr

Vapour feedrate = 132 lb/hr

First reading

Heat input = 154 watts (calibrated wattmeter)

= 525 Btu/hr

Losses = nil (jacket winding adjusted accordingly)

Axial conduction - negligible (see Appendix IV)

Tube surface area = $\pi \times \frac{1}{12} \times \frac{18}{12} = 0.393$ ft^2

$\therefore$ Heat flux = $\frac{525}{0.393} = 1340$ Btu/hr ft^2

Liquid feed temperature $\equiv$ 2.934 mV

Calibration correction = +0.006 mV

$\therefore$ Corrected liquid feed temperature $\equiv$ 2.940 mV

Vapour temperature $\equiv$ 3.193 mV

$\therefore$ Subcooling of liquid feed below saturation temperature

$\equiv$ 253 μV

But 23 μV $\equiv$ 1 F^{o} (chromel-alumel thermocouples)

$\therefore$ Subcooling = 11.0 F^{o}

$\therefore$ Preheat required = liquid feedrate x specific heat x subcooling

= 50 x 0.78 x 11

= 429 Btu/hr

The test thermocouples are located $2\frac{7}{8}$ in. from the bottom.

$\therefore$ Input to test point = $\frac{15\frac{1}{2}}{18}$ x 525

= 441 Btu/hr

$\therefore$ Input for evaporation = 441 - 429 = 12 Btu/hr

$\therefore$ Vaporization = $\frac{12}{368}$ lb/hr - negligible

$\therefore$ Local liquid flowrate, L = 50 lb/hr

Local vapour flowrate, V = 132 lb/hr

		Calibrn. Corrn.	
Surface thermocouple readings	3.258 mV	+3 μV	= 3.261 mV
	3.256	+3 μV	= 3.259
	3.241	+18 μV	= 3.259

$\therefore$ Average surface temperature $\equiv$ 3.260 mV

Vapour temperature $\equiv$ 3.193 mV

$\therefore$ Temperature difference, ΔT $\equiv$ 67 μV

= 2.9 F^{o}

But wall thermocouples are immersed 1/16 in. below the surface.

$\therefore$ Immersed thermocouple correction (see Appendix IV) $= \frac{q/A}{k/\Delta x} = \frac{1340}{11500} = 0.1\ F^o$ (rounded)

$\therefore$ Corrected $\Delta T = 2.8\ F^o$

$\therefore$ Heat transfer coefficient, $h = \frac{q/A}{\Delta T} = \frac{1340}{2.8}$

$= 479$ Btu/hr ft^2 F^o

$= 480$ Btu/hr ft^2 F^o (rounded)

This heat transfer coefficient is h_{LV}, determined for L = 50 lb/hr and V = 132 lb/hr.

The heat transfer coefficient due to liquid flow alone, for L = 50 lb/hr, is

$h_L = 165$ Btu/hr ft^2 F^o (from Figure 16)

$\therefore \frac{h_{LV}}{h_L} = \frac{480}{165} = 2.91$

These data are plotted in Figures 7A and 13.

Seventh reading

Heat input = 1525 watts

= 5200 Btu/hr

Losses - nil

Axial conduction - negligible

Heat flux = $\frac{5200}{0.393} = 13200$ Btu/hr ft^2

Liquid feed temperature $\equiv$ 2.946 mV

Calibration correction = +0.006 mV

Vapour temperature ≡ 3.200 mV

∴ Subcooling ≡ 248 μV ≡ 10.8 F°

Preheat required = 420 Btu/hr

Input to test point = $\frac{15\frac{1}{2}}{18}$ x 5200 = 4370 Btu/hr

∴ Input for vaporization = 4370 - 420 = 3950 Btu/hr

∴ Vaporization = $\frac{3950}{368}$ = 10⅞ lb/hr (rounded)

∴ Local liquid flowrate, L = 39½ lb/hr

Local vapour flowrate, V = 142½ lb/hr

Surface thermocouple readings	3.818	+3 μV	= 3.821 mV
	3.825	+3 μV	= 3.828
	3.807	+18 μV	= 3.825

∴ Temperature difference, ΔT ≡ 3.825 - 3.200 mV

= 27.2 F°

Immersed thermocouple correction = $\frac{13200}{11500}$ = 1.1 F° (rounded)

∴ Corrected ΔT = 26.1 F°

∴ Heat transfer coefficient, $h_{LV} = \frac{13200}{26.1}$ = 510 Btu/hr ft^2 F° (rounded)

The heat transfer coefficient for liquid flow alone, for L = 39½ lb/hr is

h_L = 174 Btu/hr ft^2 F°

∴ $\frac{h_{LV}}{h_L}$ = 2.93

These data are plotted in figures 7A and 13.

Twelfth reading (nucleate boiling conditions)

Heat input = 3600 watts

= 12,290 Btu/hr

Losses - nil

Axial conduction - negligible

$\therefore$ Heat flux = $\frac{12,290}{0.393}$ = 31,300 Btu/hr ft^2

Liquid feed temperature ≡ 2.945 mV

Calibration correction = +0.006 mV

Vapour temperature ≡ 3.200 mV

$\therefore$ Subcooling ≡ 249 mV ≡ 10.8 F^o

$\therefore$ Preheat required = 420 Btu/hr

Input to test point = $\frac{15\frac{1}{2}}{18}$ x 12290 = 10320 Btu/hr

$\therefore$ Input for vaporization = 10320 - 420 = 9900 Btu/hr

$\therefore$ Vaporization = $\frac{9900}{368}$ = 27 lb/hr (rounded)

$\therefore$ Local liquid flowrate, L = 23 lb/hr

Local vapour flowrate, V = 159 lb/hr

Surface thermocouple readings	4.23	+3 μV	= 4.23 mV
	4.27	+3 μV	= 4.27 mV
	4.26	+18 μV	= 4.28 mV

(Temperature oscillations were such that no greater accuracy of reading was warranted)

$\therefore$ Temperature difference, ΔT ≡ 4.26 - 3.200 mV

= 46.1 F^o

Immersed thermocouple correction $= \frac{31300}{11500} = 2.7\ F^{o}$ (rounded)

$\therefore$ Corrected $\Delta T = 43.4\ F^{o}$

$\therefore$ Heat transfer coefficient $= \frac{31300}{43.4} = 720$ Btu/hr $ft^2\ F^{o}$ (rounded)

APPENDIX IV

ESTIMATE OF AXIAL AND RADIAL CORRECTIONS

The thermal conductivities of the materials of construction and the dimensions for the test section are such that axial correction to heat flux and radial correction to temperature difference may be required.

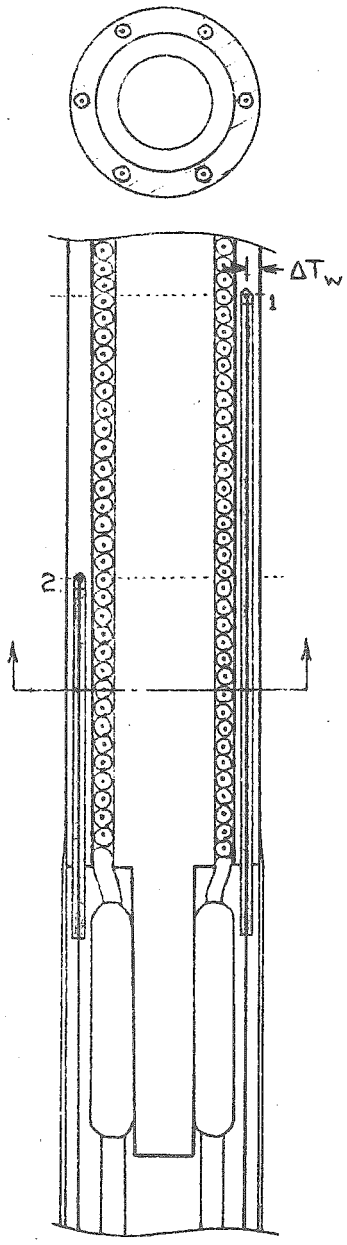

A cross-section of the test section at its lower end is shown opposite.

(1) is the test plane (i.e. three thermocouples distributed circumferentially, 120° apart).

(2) is a check plane (three thermocouples distributed circumferentially, 120° apart, each offset 60° from a thermocouple of plane (1)).

The ½ mm. stainless steel sheathed magnesia insulated thermocouples are located within 1/16 in. O.D., 0.020 in. I.D. copper sleeves inserted in holes drilled along the brass wall.

Planes (1) and (2) are located 2⅜ in. and 1¼ in. respectively from the lower end of the heated section.

Equivalent planes are located at the upper end of the 18 in. long heated test section.

AXIAL CORRECTION

A correction to radial heat flux at plane (1) for variation in axial heat flux cannot be obtained with the thermocouple distribution as shown.

In the absence of thermocouples located upstream of (1) at a distance equal to that of (2), an estimate can be obtained as follows:

1) Calculate the axial heat flux q_{1-2} between planes (1) and (2).
2) Calculate the axial heat flux at the middle of the test section using the thermocouple readings at plane (2) and at its equivalent at the feed end.
3) The difference between these axial heat fluxes gives the net axial heat flux over the length between the respective mid-points, i.e. over the length
$(9 - \frac{2\frac{7}{8} + 1\frac{1}{2}}{2}) = 6\frac{13}{16}$ in. $= 6.813$ in.
4) The net axial heat flux can be compared with the internal generation over the 6.813 in. length.

Estimation of axial heat flux between planes (1) and (2)

Consider the cross-section of the test section as shown in the figure on page A73.

The type of pyrotenax heating cable which was used has a conductor of Kumanal, the resistance of which does not

vary with temperature. Therefore, the rate of heat generation by the winding will be uniform over the whole wound length.

To a first approximation there will be the same temperature drop across the wall at points (1) and (2). Also, since there is no heat generation within the copper former, the temperature profile across it will be flat.

Therefore, the temperature difference between all corresponding points in planes (1) and (2) will be

$$(T_1 - T_2) = \Delta T_{1-2},$$

and the axial heat flux between planes (1) and (2) will be

$$q_{axial_{1-2}} = k_m A_m \frac{\Delta T_{1-2}}{\Delta x} .$$

For axial conduction, the presence of the pyrotenax winding and the thermocoax thermocouples may be ignored because of the relatively low thermal conductivity of the magnesia insulation.

For typical operating conditions (surface temperature approximately 200°F),

$$k_{copper} = 218 \text{ Btu/hr ft } F^o$$

$$k_{brass} = 60 \text{ Btu/hr ft } F^o$$

$\therefore k_m A_m = k_m A_m$ for the brass wall (excl. the drilled holes)

$+ k_m A_m$ for the copper thermocouple sleeves

$+ k_m A_m$ for the copper former for the pyrotenax winding

$$= 60\left[\frac{\pi}{4} \cdot \frac{1^2 - (\frac{3}{4})^2}{144} - 3\frac{\pi}{4}\left(\frac{1/16}{12}\right)^2\right] + 218 \cdot \frac{\pi}{4} \cdot (\frac{0.55}{12})^2$$

$$+ 3 \cdot 218 \cdot \frac{\pi}{4} \cdot \frac{(1/16)^2 - (0.020)^2}{144}$$

$$= 0.51 \text{ Btu/hr } (F^o/\text{ft}).$$

The distance between planes (1) and (2) is $1\frac{3}{8}$ inches.

$$\therefore q_{axial_{1-2}} = 0.51 \frac{\Delta T_{1-2}}{1\frac{3}{8}/12}$$

$$= 4.4\, \Delta T_{1-2} \text{ Btu/hr.}$$

The distance between plane (1) and the corresponding plane at the upper end is $12\frac{1}{4}$ in.

$k_m A_m$ for the middle of the test section (i.e. no thermocouples or sleeves) is 0.50 Btu/hr (F^o/ft).

$$\therefore q_{axial_{mid}} = 0.50 \frac{\Delta T_{mid}}{12\frac{1}{4}/12}$$

$$= 0.49\, \Delta T_{mid} \text{ Btu/hr.}$$

Consider data from Run No. 17, for which calculations are presented in Appendix III.

<u>First reading</u>

Thermocouple readings at plane (1) - the test "point".

	Calibr. corrn.		
3.258 mV	+3 μV	3.261 mV	
3.256	+3	3.259	3.260 average
3.241	+18	3.259	

Thermocouple readings at plane (2)

	Calibr. corrn.		
3.258 mV	+3 μV	3.261	
3.254	+3	3.257	3.258 average
3.249	+8	3.257	

Difference = 2 μV $\equiv$ $^{2}/_{23}$ F°

$\therefore$ $q_{axial_{1-2}}$ = 4.4 x $^{2}/_{23}$ = 0.4 Btu/hr (towards exit)

The procedure can be repeated for the six thermocouples at the entrance end of the test section (i.e. liquid preheating region).

Difference = 48 μV $\equiv$ 2.1 F°

$\therefore$ $q_{axial_{top}}$ = 4.4 x 2.1 = 9.2 Btu/hr (towards entrance)

An estimate of $q_{axial_{mid}}$ is obtained from T_1 and its equivalent at the upper end.

Difference = 22 μV $\equiv$ $^{22}/_{23}$ F°

$\therefore$ $q_{axial_{mid}}$ = 0.49 x $\frac{22}{23}$ $\simeq$ 0.5 Btu/hr (towards exit)

Thus the axial heat fluxes at three zones in the test section may be compared.

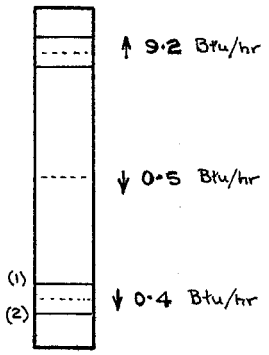

There is a net gain of 0.1 Btu/hr over the length between the reference points at which $q_{axial_{mid}}$ and $q_{axial_{1-2}}$ were determined.

The midpoint between the planes (1) and (2) is distant $6\frac{13}{16}$ in. from the midpoint of the test section.

The heat output from the pyrotenax winding over this length is

$$\frac{6\frac{13}{16}}{18} \times \text{total generation} = \frac{6\frac{13}{16}}{18} \times 525 = 200 \text{ Btu/hr.}$$

The net gain due to axial conduction is negligible in comparison to this internal generation over the same length.

Seventh reading

Difference between thermocouple readings (1) - (2) = 4 μV

$\equiv {}^{4}/_{23}$ F°

$\therefore q_{axial_{1-2}} = 0.7$ Btu/hr (towards exit)

Difference between upper thermocouples = 63 μV

$\therefore q_{axial_{upper}} = 12$ Btu/hr (towards exit)

Difference between (1) and its upper equivalent = 239 μV

$\therefore q_{axial_{mid}} = 5.1$ Btu/hr (towards exit)

$\therefore$ Gain over $6\frac{13}{16}$ in. = 5.1 - 0.7 = 4.4 Btu/hr.

Input over $6\frac{13}{16}$ in. = $\frac{6\frac{13}{16}}{18} \times 5210 = 1970$ Btu/hr.

The net gain is negligible in comparison to this input over the same length.

Twelfth reading

Difference between thermocouple readings (1) - (2) = 30 μV

$\therefore q_{axial_{1-2}}$ = 5.8 Btu/hr (towards entrance)

Difference between upper thermocouples = 73 μV

$\therefore q_{axial_{upper}}$ = 14 Btu/hr (towards exit)

Difference between (1) and its upper equivalent = 110 μV

$\therefore q_{axial_{mid}}$ = 2.4 Btu/hr (towards entrance)

$\therefore$ Gain over $6\frac{13}{16}$ in. length = 5.8 - 2.4 = 3.4 Btu/hr

Input over $6\frac{13}{16}$ in. length = 4600 Btu/hr.

The net axial heat flux is negligible in comparison to this input over the same length.

Note: The direction of $q_{axial_{1-2}}$ for the twelfth reading is contrary to what would be expected normally. For this reading intense nucleation was occurring over the lower part of the tube and partial dry wall conditions prevailed in the region of the thermocouple plane (2). Thus, temperatures were abnormally high at (2).

Further check calculations, similar to those for Run No. 17, have been carried out for a wide range of the remainder of the test runs. Errors were found to be significant only for runs at the lower vapour flowrates. In general, flux losses of 0-2% were encountered (cf. very small gains encountered for Run No. 17). The largest losses encountered were about 4%, usually at the lowest flux for a particular run, and were associated with relatively large

conduction towards the preheat zone.

The most common errors of $\leq 2\%$ are relatively small, and are of the same order as the effect of the uncertainties in the lengths, in the conductivities, and in the difference between thermocouple readings on which they are based. Therefore correction for axial losses is hardly justified, and the small uncertain error is better included with overall experimental errors.

For the later series of runs with methanol, isopropanol, water and with chloroform, larger external preheats were supplied, such that smaller preheats at the test section were required. Also, for the latter three liquids, much less emphasis was placed on high heat fluxes and on the nucleate boiling regime. For these conditions, which represent a large proportion of the readings which were taken, flatter temperature profiles were encountered in the region of the test point, such that axial flux corrections were unnecessary.

RADIAL TEMPERATURE CORRECTION

It has been shown above that the effect of axial conduction on the local heat flux may be neglected. Therefore, at any point heat may be assumed to flow in a direction perpendicular to the face of the heated tube at a rate equal to the rate of internal generation.

The thermocouples which indicate the surface temperature are buried in intimate contact with the brass tube, with the centre of the beads being located 1/16 in. below the surface.

The thermocouple beads are small (approximately 0.010 in.) so that it may be assumed that the temperature which is indicated is that sensed by the midpoint of the bead, located at the midpoint of the brass wall.

The true surface temperature is equal to the temperature indicated at the midpoint of the wall minus the temperature drop across 1/16 in. of brass.

The temperature drop across 1/16 in. of brass is given by

$$\Delta T = \frac{q/A}{k/\Delta x} = \frac{q/A}{k/\frac{1}{16 \times 12}} .$$

The thermal conductivity of brass does not vary greatly with temperature. A mean value of k will be used, based on an average operating temperature difference of 20 F°.

	Satn. Temp. °F	k_m, Brass Btu/hr ft F°	$k/\Delta x$ Btu/hr ft^2 F°
Water	212	60½	11600
Chloroform	143	59	11300
Methyl Alcohol	148	59	11300
Ethyl Alcohol	173	60	11500
iso-Propanol	180	60	11500

Typical calculations of correlations for the observed temperature differences are given in Appendix III.

e.g. Ethanol, Run No. 17, first reading

$q/A = 1340$ Btu/hr ft^2

$\Delta T_{observed} = 2.9\ F^o$

$\Delta T_{correction} = \frac{1340}{11500} = 0.1\ F^o$ (rounded)

$\therefore \Delta T_{true} = 2.9 - 0.1 = 2.8\ F^o$

i.e. a correction of approximately 3½% is required.

Note that

$$\Delta T_{correction} \propto q/A \propto h\Delta T$$

$$\therefore \frac{\Delta T_{correction}}{\Delta T} \times 100\% \propto \text{Percentage correction} \propto h$$

Results presented in Appendix I show that corrections to temperature difference of up to 19% have been necessary (Run No. 232).

APPENDIX V

REPLOTS OF RESULTS OF PREVIOUS WORKERS

The results of the analyses of Rohsenow et al. (71) and of Dukler (30,31,32) are replotted on pages A84-92 (i.e. Figures A1-A9) to provide bases for discussion in Section 2.2.2.4. (Rohsenow et al.) and Section 2.2.3. (Dukler).

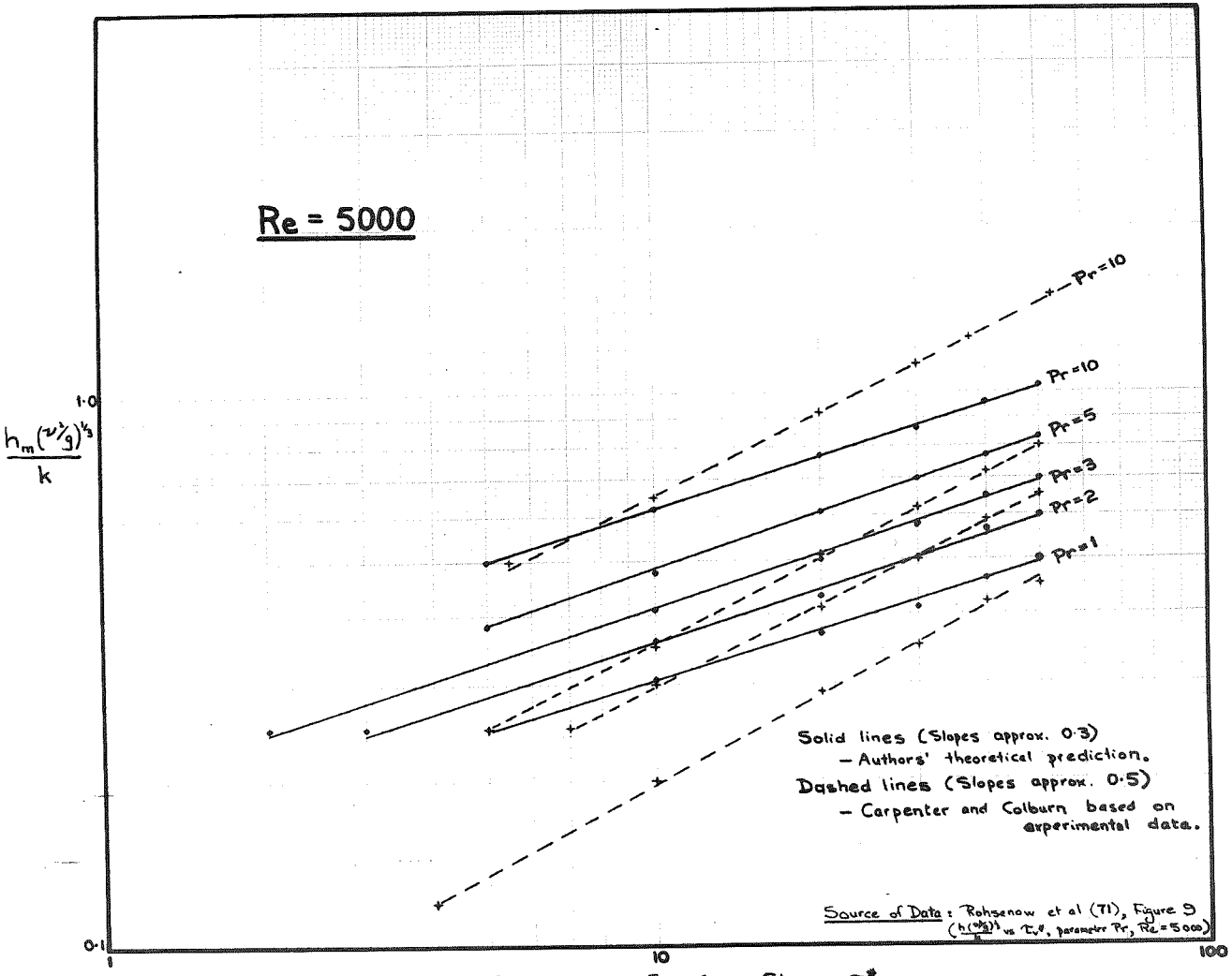

Figure A1 REPLOT OF DATA OF ROHSENOW ET AL (71)

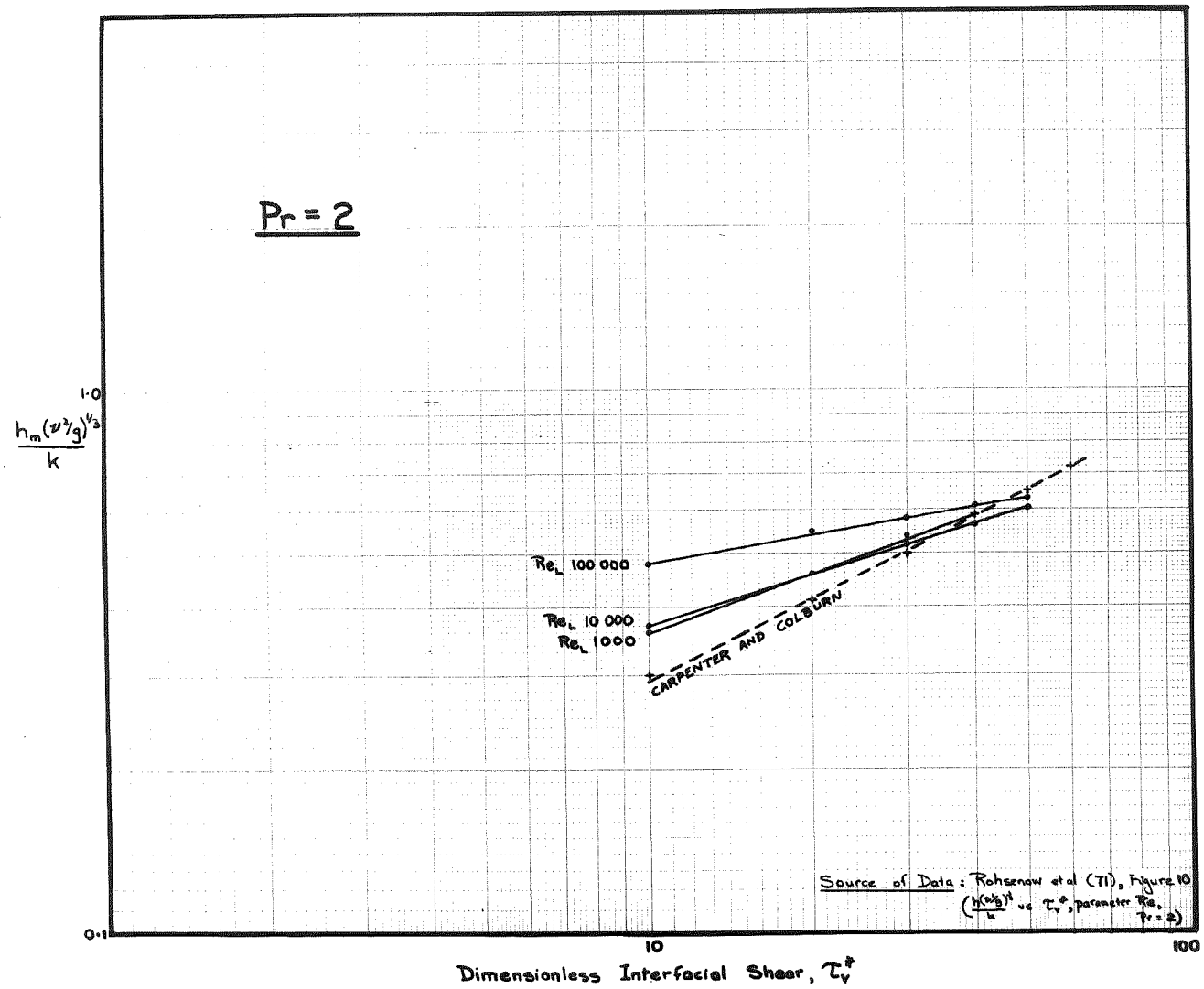

Figure A2 REPLOT OF DATA OF ROHSENOW ET AL (71)

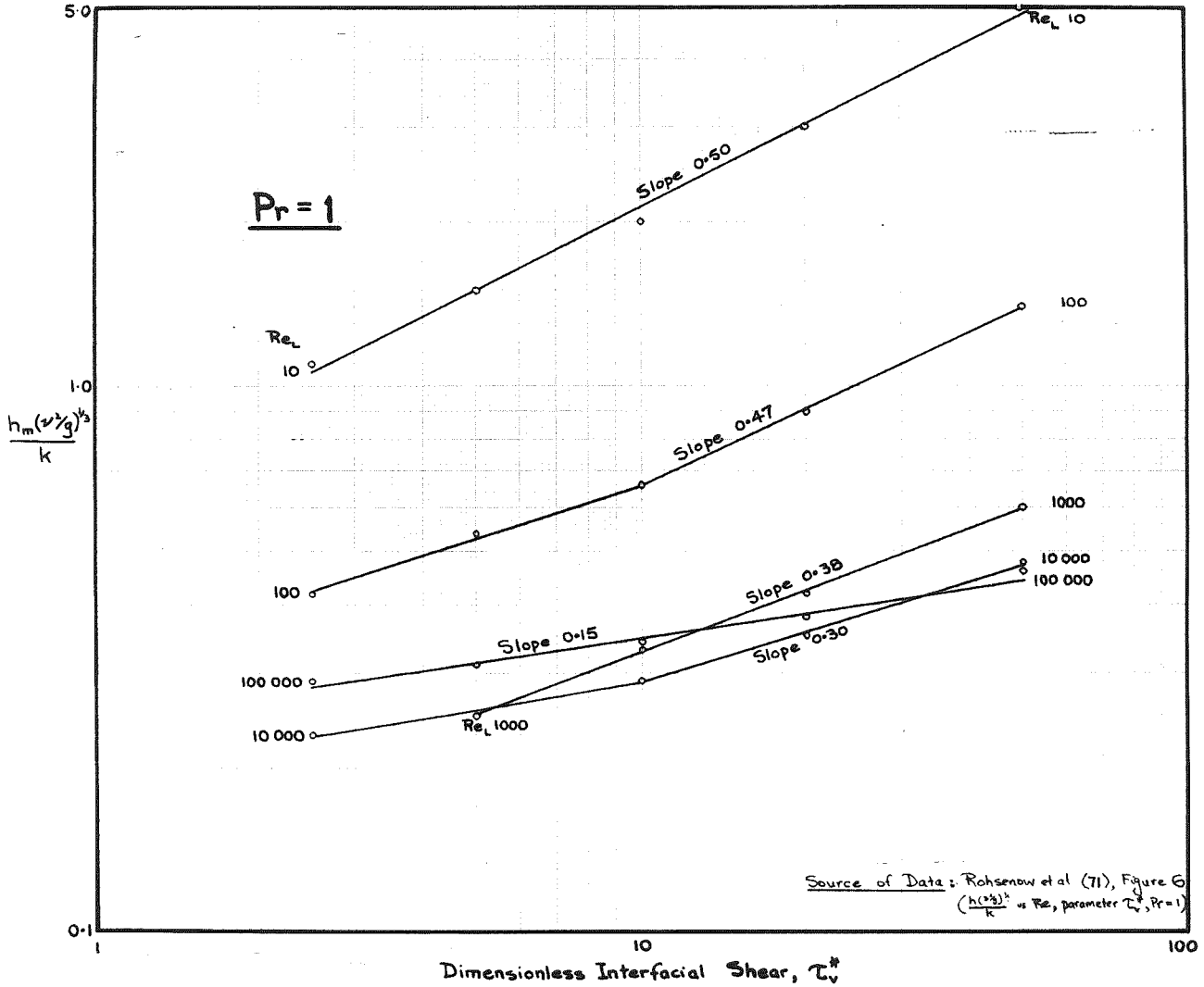

Figure A3 REPLOT OF DATA OF ROHSENOW ET AL (71)

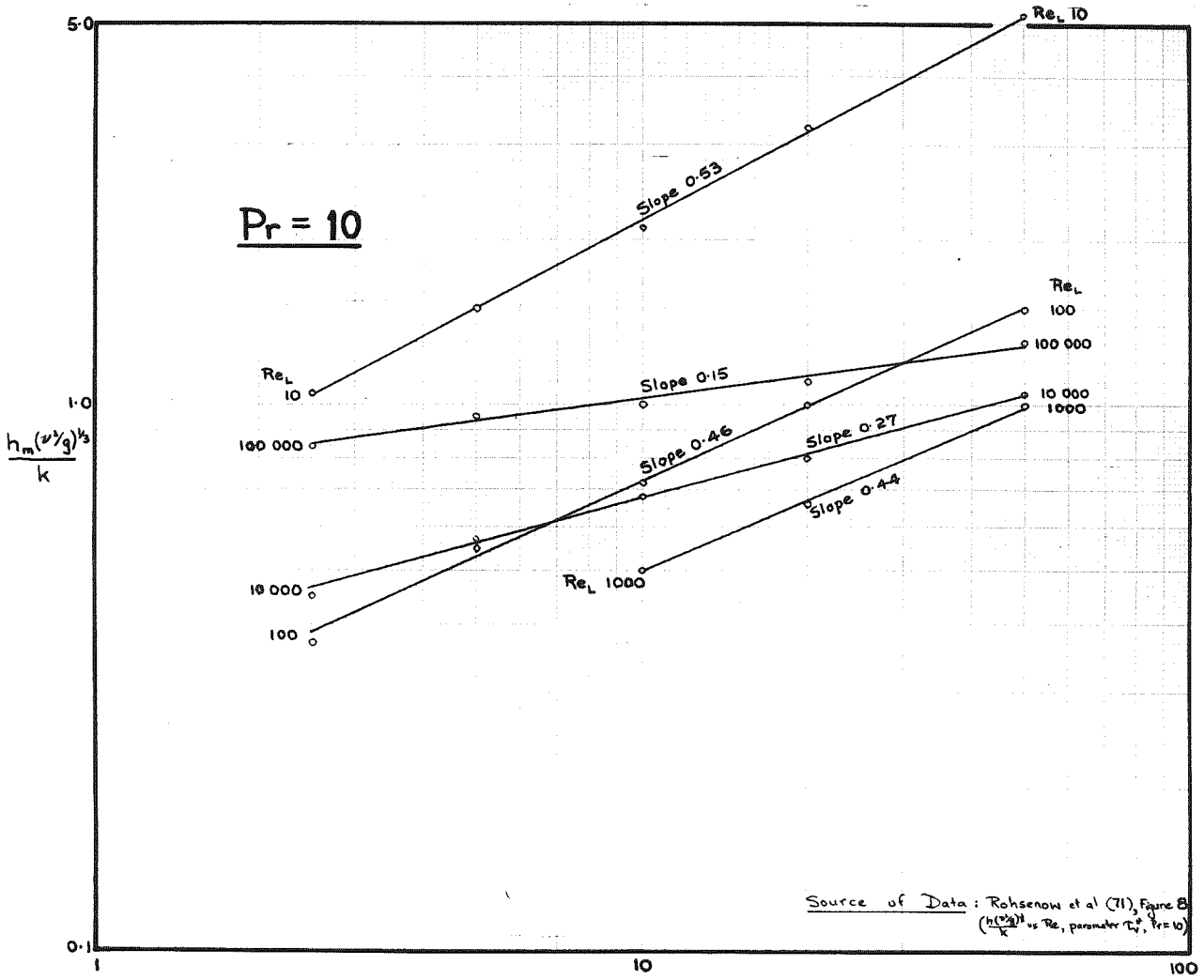

Figure A4 REPLOT OF DATA OF ROHSENOW ET AL (71)

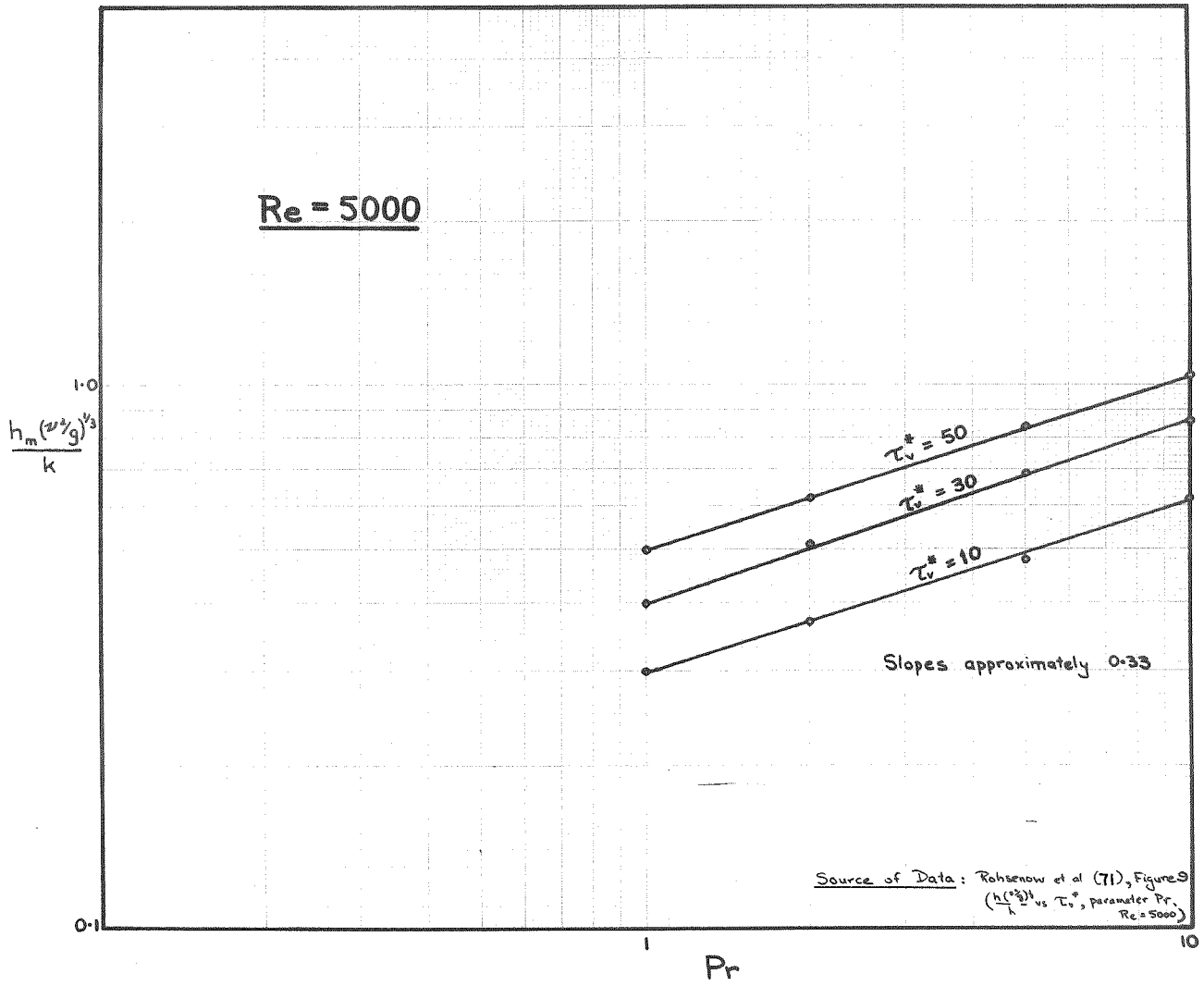

Figure A5 REPLOT OF DATA OF ROHSENOW ET AL (71)

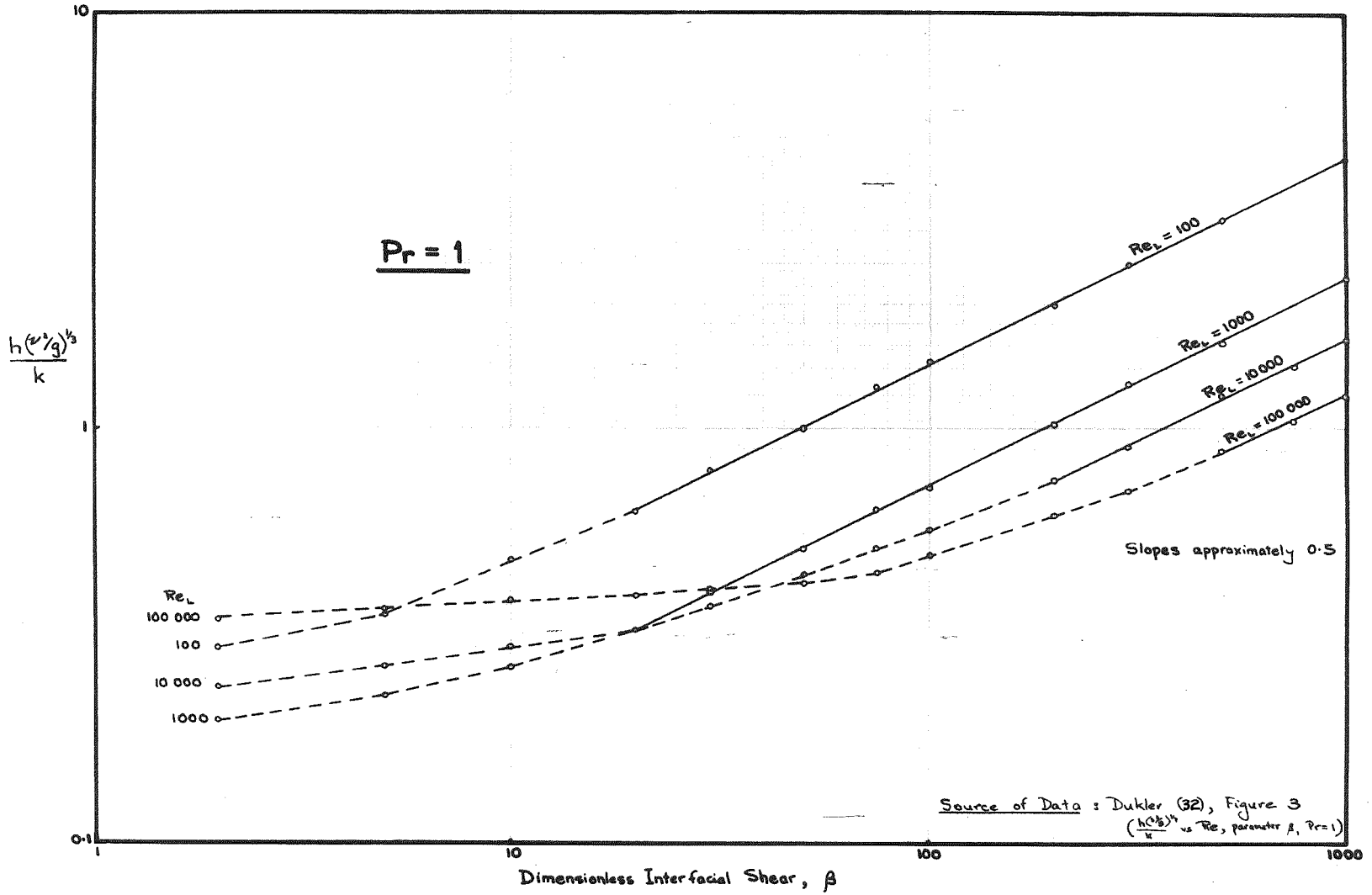

Figure A6

REPLOT OF DATA OF DUKLER (32)

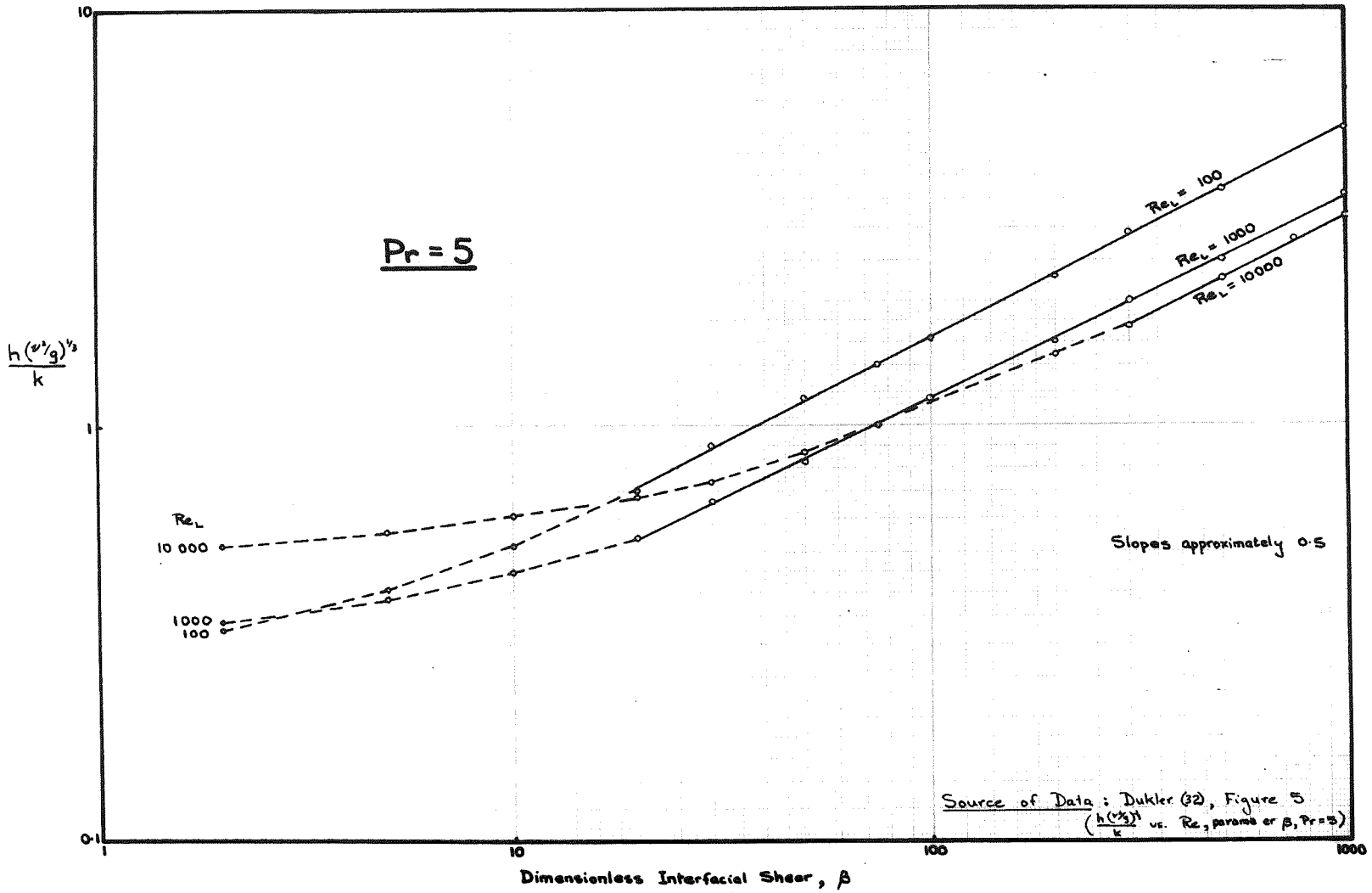

Figure A7 REPLOT OF DATA OF DUKLER (32)

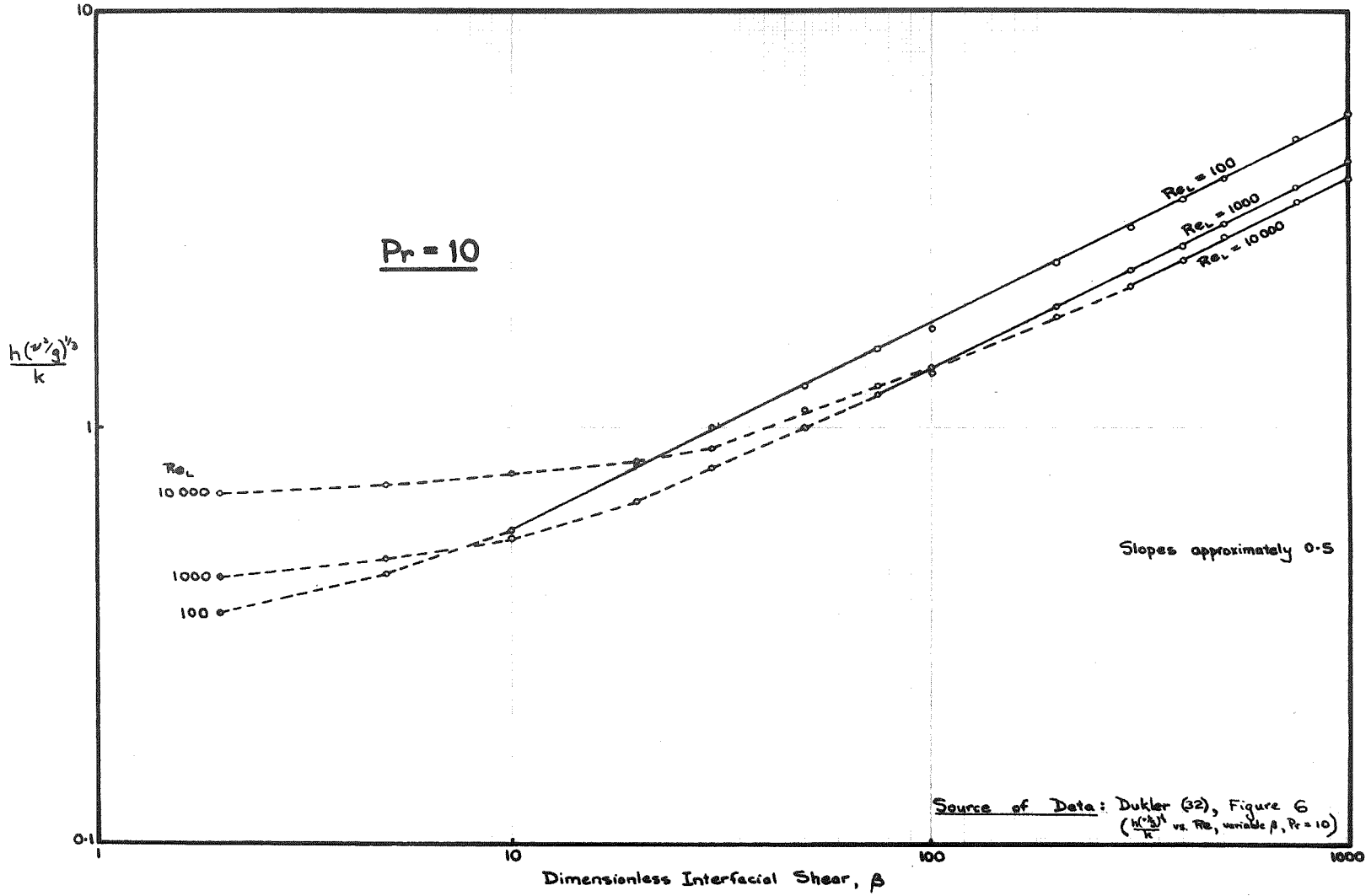

Figure A8

REPLOT OF DATA OF DUKLER (32)

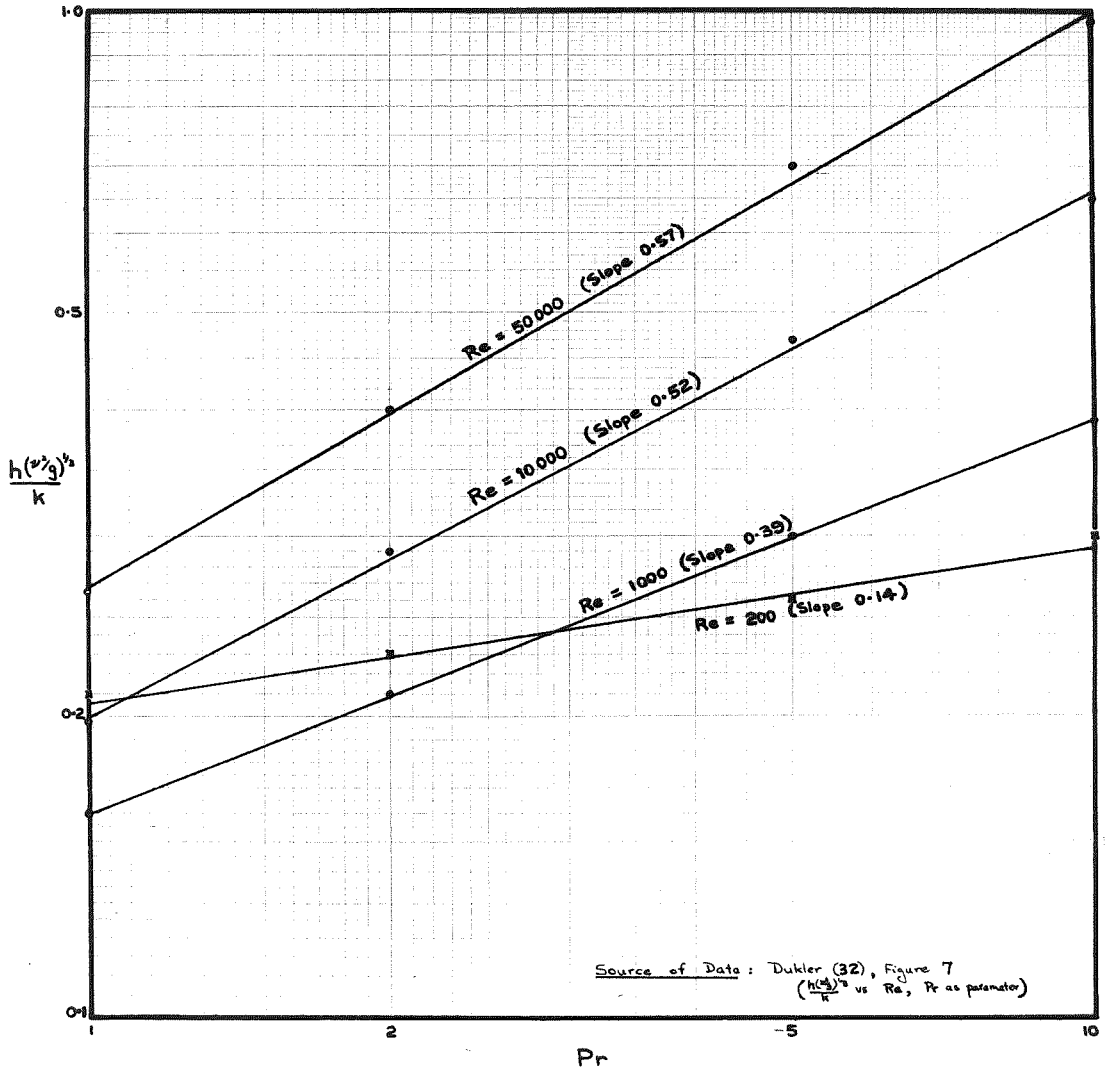

Figure A9 REPLOT OF DATA OF DUKLER (32)

REFERENCES

(1) Allen, J.M., Brit. Chem. Eng., 8, 192 (1963), i.e. abstract of Ph.D. Thesis, Manchester College of Science and Technology (1962).

(2) Armstrong, C., Bell, N.R., and Murray, H.D., Manufacturing Chemist, 28, 263-68 (1957).

(3) Asbjornsen, O.A., Chem. Eng. Sci., XIV, 211-226 (1961).

(4) Bankoff, S.G., A.I.Ch.E. Jl., 8, 1, 63-5 (1962).

(5) Bankoff, S.G., Chem. Eng. Progress Symposium Series, 55, No. 29, 87-94 (1959).

(6) Bates, O.K., Hazzard, G., and Palmer, G., Ind. Eng. Chem. (Anal. Edn.), 10, 6, 314-318 (1938).

(7) Bays, G.S., and McAdams, W.H., Ind. Eng. Chem., 29, 11, 1240-6 (1937).

(8) Belkin, H.H., MacLeod, A.A., Monrad, C.C., and Rothfus, R.R., A.I.Ch.E. Jl., 5, 2, 245-8 (1959).

(9) Benjamin, T.B., Jl. Fluid Mechanics, 2, 554-574 (1957).

(10) Bennett, J.A.R., Collier, J.G., Pratt, H.R.C., and Thornton, J.D., Trans. Instn. Chem. Engrs., 39, 113-126 (1961).

(11) Bergelin, O.P., Kegel, P.K., Carpenter, F.G., and Gazley, C., Heat Transfer and Fluid Mechanics Institute, published by A.S.M.E. (1949), pp.19-28.

(12) Brauer, H., V.D.I.-Forschungsheft No. 457 (1956).

(13) Brauer, H., Kaltetechnik, 9, 274-9 (1957).

(14) Bressler, R., V.D.I.-Z., 100, 630-8 (1958).

(15) Brotz, W., Chem.-Ing.-Tech., 26, 470-8 (1954).

(16) Carpenter, F.G., and Colburn, A.P., Proceedings of General Discussion on Heat Transfer, I.Mech.E. and A.S.M.E., London (1951), pp.20-26.

(17) Clegg, M.J., Ph.D. Thesis, University of Adelaide, to be presented.

(18) Clegg, M.J., personal communication, Univ. of Adelaide (1963).

(19) Colburn, A.P., Ind. Eng. Chem., 26, 4, 432-4 (1934).

(20) Colburn, A.P., Tr.A.I.Ch.E., XXIX, 174-210 (1933).

(21) Colburn, A.P., Proceedings of General Discussion on Heat Transfer, I.Mech.E. and A.S.M.E. (1951), pp.1-11.

(22) Collier, J.G., Discussion following reference (65), Trans. Instn. Chem. Engrs, 38, 320-1 (1960).

(23) Cooper, C.M., Drew, T.B., and McAdams, W.H., Ind. Eng. Chem., 26, 4, 428-31 (1934).

(24) Corcoran, W.H., and Sage, B.H., A.I.Ch.E. Jl., 2, 2, 251-8 (1956).

(25) Corty, C., and Foust, A.S., Chem. Eng. Progress Symposium Series, 51, No. 17, 1-12 (1955).

(26) Coston, M.M., and Lindsey, E.E., Chem. Eng. Progress, 52, 2, 49-52 (1956).

(27) Dedert, W.G., and Moore, J.G., Ind. Eng. Chem., 55, 6, 57-60 (1963).

(28) Deissler, R.G., NACA TR 1210 (1955).

(29) Dengler, C.E., and Addoms, J.N., Chem. Eng. Progress Symposium Series, 52, 18, 95-104 (1956).

(30) Dukler, A.E., Chem. Eng. Progress, 55, 10, 62-67 (1959).

(31) Dukler, A.E., Chem. Eng. Progress Symposium Series, 56, No. 30, 1-10 (1960).

(32) Dukler, A.E., Petro/Chem. Engr., 33, 9, 52-54 (1961) 33, 11, 46-53 (1961).

(33) Dukler, A.E., ARS Jl., 31, 86-87 (1961).

(34) Dukler, A.E., and Bergelin, O.P., Chem. Eng. Progress, 48, 11, 557-563 (1952).

(35) Forster, H.K., and Greif, R., Tr. A.S.M.E., 81, Series C (Jl. of Heat Transfer), 43-53 (1959).

(36) Foust, A.S., et al., "Principles of Unit Operations", Wiley, New York (1960), Chapter 13.

(37) Friedman, S.J., and Miller, C.O., Ind. Eng. Chem., 33, 7, 885-891 (1941).

(38) Garwin, L., and Kelly, E.W., Ind. Eng. Chem., 47, 3, 392-5 (1955).

(39) Gill, L.E., and Hewitt, G.F., U.K.A.E.A. Report No. AERE-R 3935 (H.M.S.O., London, 1962).

(40) Grigull, U., Forsch. Gebiete Ingenieurw., 18, 1, 10-12 (1952).

(41) Grimley, S.S., Trans. Instn. Chem. Engrs., 23, 228-35 (1945).

(42) Heartinger, D.J., Dissertation Abs., 21, 1490-1 (1960), i.e. abstract of D.Sc. Thesis, Univ. Washington (1960).

(43) Hershman, A., Dissertation Abs., 21, 1491-2 (1960), i.e. abstract of Ph.D. Thesis, Univ. Illinois (1960).

(44) Hewitt, G.F., U.K.A.E.A. Report No. AERE-R 3680 (H.M.S.O., London, 1961).

(45) "International Critical Tables", Vol. V, p. 227, McGraw-Hill, New York (1928).

(46) Jackson, M.L., A.I.Ch.E. Jl., 1, 2, 231-240 (1955).

(47) Jakob, M., "Heat Transfer", Vol. 1, Wiley, N.Y. (1949).
"Heat Transfer", Vol. 2, Wiley, N.Y. (1957).

(47a) Jakob, M., ibid., Vol. 1, pp. 661-680.

(47b) Jakob, M., ibid., Vol. 1, pp. 675-680.

(47c) Jakob, M., ibid., Vol. 1, p. 677.

(47d) Jakob, M., ibid., Vol. 2, pp. 356-365.

(47e) Jakob, M., ibid., Vol. 2, p. 368.

(47f) Jakob, M., ibid., Vol. 1, pp. 636-7.

(48) Kapitsa, P.L., Zhur. Eksper. Teor Fiz., 18, 1, 3-18 (1948).

(49) Karetnikov, U.P., Zhur. Tekh. Fiz., XXIV, 2, 193-199 (1954).

(50) von Karman, T., Tr. A.S.M.E., 61, 705-710 (1939).

(51) Kelly, E.J., Chem. Eng. Progress, 48, 12, 589-93 (1952).

(52) Kern, D.Q., "Process Heat Transfer", McGraw-Hill, N.Y. (1959), pp. 104-5.

(53) Keville, J.F., Preprint No. 18, Second National Heat Transfer Conference, A.I.Ch.E.-A.S.M.E., Chicago (1958).

(54) Keville, J.F., Chem. Eng. Progress, 54, 10, 83-84 (1958).

(55) Kirkbride, C.G., Ind. Eng. Chem., 26, 4, 425-428 (1934).

(56) Kramers, H., van Cappelle, A.E.F., and van der Schraaf, E.E., De Ingenieur, 67, 8, 9-15 (1955).

(57) Lacey, P.M.C., Hewitt, G.F., and Collier, J.G., U.K.A.E.A. Report No. AERE-R 3692 (1962).

(58) Leidenfrost, W., Naturwissenschaften, 43, 465-6 (1956).

(59) Lin, C.S., Moulton, R.W., and Putnam, G.L., Ind. Eng. Chem., 45, 3, 636-640 (1953).

(60) McAdams, W.H., "Heat Transmission", Third edition, McGraw-Hill, N.Y. (1954).

(60a) McAdams, W.H., ibid., p. 333.

(60b) McAdams, W.H., ibid., p. 337.

(60c) McAdams, W.H., ibid., p. 219.

(60d) McAdams, W.H., ibid., p. 245.

(60e) McAdams, W.H., ibid., p. 470.

(60f) McAdams, W.H., ibid., pp. 466-7.

(60g) McAdams, W.H., ibid., pp. 477-8.

(61) McAdams, W.H., Drew, T.B., and Bays, G.S., Tr. A.S.M.E., 62, 627-31 (1940).

(62) McNelly, M.J., Ph.D. Thesis, Univ. of London (1955).

(63) Mickley, H.S., Sherwood, T.K., and Reed, C.E., "Applied Mathematics in Chemical Engineering", Second Edition, McGraw-Hill, N.Y. (1957), pp. 53-55.

(64) Moore, J.G., and Hesler, W.E., Chem. Eng. Progress, 59, 2, 87-92 (1963).

(65) Norman, W.S., and McIntyre, V., Trans. Inst. Chem. Engrs., 38, 301-7 (1960).

(66) Nusselt, W., Z. Ver. Deut. Ing., 60, 27, 541-6 (1916) 60, 28, 569-75 (1916).

(67) Nusselt, W., Z. Ver. Deut. Ing., 67, 9, 206-210 (1923).

(68) Penman, T.O., Ph.D. Thesis, Univ. of Adelaide (1962).

(69) Pratt, H.R.C. and Thornton, J.D., Proc. Int. Conf. on Peaceful Uses of At. Energy, Geneva (1958), 2, 813-18.

(70) Richkov, A.I., and Pospelov, V.K., Khim Prom., 5, 426-9 (1959).

(71) Rohsenow, W.M., Webber, J.H., and Ling, A.T., Tr. A.S.M.E., 78, 1637-43 (1956).

(71A) Martinelli, R.C., Tr. A.S.M.E., 69, 947-59 (1947).

(72) Rowe, P.N., The Chemical Engineer, No. 166, 69-74 (1963).

(73) Saveanu, Th., Ibanescu, I., and Vasiliu, M., Chem. Abs., 58, 8, 7623h (1963), i.e. abstract of Rev. Chim. (Bucharest), 13, 589-92 (1962).

(74) Seban, R.A., Tr. A.S.M.E., 76, 299-303 (1954).

(75) Seban, R.A., Tr. A.S.M.E., 78, 1642 (1956).

(76) Sexauer, T., Forsch. Ing.-Wes., 10, 5, 286-96 (1939).

(77) Shibuya, I., Report of the Inst. of High Speed Mechanics, Tohoku Univ., 1, 17-25 (1950).

(78) Sinek, J.R., Dissertation Abstr., 23, 1, 177 (1962), and Chem. Abstr., 58, 7, 6465gh (1963), i.e. abstracts of Ph.D. Thesis, Univ. Michigan (1962).

(79) Sinek, J.R., and Young, E.H., Chem. Eng. Progress, 58, 12, 74-80 (1962).

(80) Staker, R., Ph.D. Thesis, Univ. of Adelaide (1959).

(81) Stirba, C., and Hurt, D.M., A.I.Ch.E. Jl., 1, 2, 178-184 (1955).

(82) Tailby, S.R., and Portalski, S., Trans. Instn. Chem. Engrs., 38, 324-30 (1960).

(83) Vieth, W.R., Porter, J.H., and Sherwood, T.K., Ind. Eng. Chem. Fundamentals, 2, 1, 1-3 (1963).

(84) Westwater, J.W., "Advances in Chemical Engineering", Volume 1, pp. 2-76, Academic Press, N.Y. (1956).

(85) Wilke, W.W., VDI-Forschungsheft No. 490 (1962).

(86) Wilke, W.W., Kaltetechnik, 13, 339-345 (1961).

(87) Wilkes, J.O., and Nedderman, R.M., Chem. Eng. Sci., 17, 177-187 (1962).

(88) Yih, C-S., Proc. Second U.S. Congress Appl. Mech. (A.S.M.E., New York, 1955), pp. 623-8.

(89) Yih, C-S., The Physics of Fluids, 6, 3, 321-34 (1963).

(90) Zhivaikin, L.Y., International Chem. Eng., 2, 3, 337-341 (1962).

(91) Zhivaikin, L.Y., and Volgin, B.V., Translation of Zhur. Prik. Khim., 34, 6, 1236-1243 (1961), published by Consultants Bureau Inc., March 1962, pp. 1178-84.